Universidade de Aveiro Departamento de Engenharia Civil
2011

Inês Osório de Castro Meireles

Hidráulica dos descarregadores em degraus: estudo experimental-numérico-teórico

Hydraulics of stepped chutes: experimental-numerical-theoretical study

Universidade de Aveiro Departamento de Engenharia Civil
2011

Inês Osório de Castro Meireles

Hidráulica dos descarregadores em degraus: estudo experimental-numérico-teórico

Hydraulics of stepped chutes: experimental-numerical-theoretical study

Dissertação apresentada à Universidade de Aveiro para cumprimento dos requisitos necessários à obtenção do grau de Doutor em Engenharia Civil, realizada sob a orientação científica do Doutor Jorge de Saldanha Gonçalves Matos, Professor Auxiliar do Departamento de Engenharia Civil e Arquitectura do Instituto Superior Técnico da Universidade Técnica de Lisboa e a co-orientação do Doutor Armando Baptista da Silva Afonso, Professor Associado Convidado do Departamento de Engenharia Civil da Universidade de Aveiro

Apoio financeiro da FCT no âmbito do projecto PTDC/ECM/108128/2008 e da bolsa SFRH/BD/38003/2007.

Financially supported by FCT in the framework of the project PTDC/ECM/108128/2008 and of the grant SFRH/BD/38003/2007.

Apoio financeiro da Fulbright/FLAD

Financially supported by Fulbright/FLAD

Ao Tuca e à Gui

Entre o sono e sonho,
Entre mim e o que em mim
É o quem eu me suponho
Corre um rio sem fim.
Passou por outras margens,
Diversas mais além,
Naquelas várias viagens
Que todo o rio tem.
Chegou onde hoje habito
A casa que hoje sou.
Passa, se eu me medito;
Se desperto, passou.

E quem me sinto e morre
No que me liga a mim
Dorme onde o rio corre -
Esse rio sem fim.

Fernando Pessoa

o júri

presidente

Prof. Doutor Joaquim Arnaldo Carvalho Martins
professor catedrático da Universidade de Aveiro

Prof. Doutor José Manuel Pinto Ferreira Lemos
professor catedrático aposentado da Faculdade de Engenharia da Universidade do Porto

Prof. Doutor Paulo Jorge de Melo Matias Faria de Vila Real
professor catedrático da Universidade de Aveiro

Prof. Doutor Fabián Alejandro Bombardelli
assistant professor of the University of California

Prof. Doutor Armando Baptista da Silva Afonso
professor associado convidado da Universidade de Aveiro

Prof. Doutor Jorge de Saldanha Gonçalves Matos
professor auxiliar do Instituto Superior Técnico da Universidade Técnica de Lisboa

Prof. Doutor José Alfeu Almeida de Sá Marques
professor auxiliar da Faculdade de Ciências e Tecnologia da Universidade de Coimbra

Prof. Doutor Carlos Daniel Borges Coelho
professor auxiliar da Universidade de Aveiro

agradecimentos

acknowledgements

Ao Prof. Jorge Saldanha Matos, do Instituto Superior Técnico (IST), pela sua orientação, por me ter incutido o gosto pela investigação e pela excelência, por me ter guiado nestes 8 anos iniciados com a minha dissertação de mestrado e por me ter ensinado o que sei hoje de investigação experimental.

Ao Prof. Armando Silva Afonso, da Universidade de Aveiro, pela sua co-orientação, pela grande abertura a colaborações nacionais e internacionais e pelo apoio estratégico, sempre presente.

To Prof. Fabián Bombardelli, from the University of California at Davis (UCDavis), USA; for his supervision during my stays at Davis, for introducing me to turbulence and computational fluid dynamics, for investing in me as his own student and treating me as a friend.

À Universidade de Aveiro pela dispensa de serviço docente.

Ao Prof. Armando Silva Afonso e ao Prof. Carlos Coelho, que me substituíram.

Ao Prof. Claudino Cardoso, presidente do conselho directivo do Departamento de Engenharia Civil da UA, pelos meios que disponibilizou para a realização desta tese e pela aposta que em mim depositou.

To UCDavis for the two periods of 6 months as Visiting Scholar.

À Fulbright e à Fundação Luso-Americana para o Desenvolvimento, pelo financiamento da deslocação à UCDavis em 2007/2008, e à Fundação para a Ciência e a Tecnologia, pelo apoio financeiro no âmbito do projecto PTDC/ECM/108128/2008 e da bolsa SFRH/BD/38003/2007, que permitiram a conclusão desta tese e financiaram as deslocações à UCDavis em 2010.

Ao Laboratório Nacional de Engenharia Civil (LNEC) pelo acolhimento e enquadramento no Núcleo de Recursos Hídricos e Estruturas Hidráulicas (NRHEH) para realizar investigação experimental no âmbito desta tese.

Ao Eng. João Soromenho Rocha, Chefe do NRHEH, pela supervisão do estágio no LNEC. Aos Engs Lúcia Couto, Teresa Viseu, Elsa Alves, João Fernandes e Sílvia Amaral por me enquadrarem no NRHEH. Aos Srs Guilhermino Lisboa, João Andrade Pereira e João Santos, pela disponibilidade para proceder às alterações da instalação experimental. Sendo esta dissertação fruto da continuação dos trabalhos de mestrado, ao Eng. Falcão de Melo, à data Chefe do NRHEH do LNEC e meu co-orientador, pelo apoio que me permitiu realizar a maioria dos ensaios experimentais apresentados nesta tese e ao Eng. João Palma, investigador principal do Núcleo de Sistemas Electrotécnicos do LNEC, pelo apoio à resolução de problemas surgidos durante a utilização da sonda de detecção de bolhas de ar e do tubo de Pitot modificado.

To Prof. Bassam Younis, from UCDavis, for giving me the opportunity to attend to his course in computational river mechanics, to Vitor Sousa for working with me in the assigned projects, and to both, for the interesting paper that we wrote together.

Ao Prof. José Carlos Pereira, do Departamento de Engenharia Mecânica (DEM) do IST, por me ter permitido assistir à sua disciplina de mecânica dos fluidos computacional. Ao Eng. Pedro Neto e ao Prof. José Manuel Chaves Pereira, também do DEM, pelo apoio na utilização do programa computacional StarCCM e à Engª Sílvia Amaral e à Engª Marina Filonovich, doutorandas do IST e da Universidade Nova de Lisboa, respectivamente, pelos trabalhos de grupo que realizámos nesse âmbito.

To Prof. Hubert Chanson, from the University of Queensland, Australia, for his enthusiastic support, in particular during the "International Junior Researcher and Engineer Workshop on Hydraulic Structures" in Portugal, in 2006, and for his kind review of my first journal paper in stepped spillways, in co-authorship with Prof. Jorge Matos.

To Eng. Kathy Frizell, from the USBR, USA, for her always prompt help with the experimental investigation and for the co-authorship in a conference paper.

To Schnabel Engineering, in particular to Eng. Greg Paxson, for providing interesting information and photographs of stepped spillways.

À EDIA, em particular ao Eng. Hemetério Monteiro e ao Eng. Morim de Oliveira, por me facultarem acesso à barragem de Pedrógão durante a descarga de 2010 e pelos dados disponibilizados; às Engªs Teresa Viseu e Sílvia Amaral, do LNEC, pelas informações facultadas relativas ao projecto da mesma barragem, e a Hugo Amaral, pelas fotografias tiradas à barragem de Pedrógão durante a descarga de 2010.

To Dr. Floriana Renna, research assistant at the Technical University of Bari, Italy, for the exchange of ideas and enjoyable months she spent working in Portugal in the framework of her PhD dissertation.
À Engª Ruth Lopes, aluna de doutoramento do IST, pela prontidão em ajudar sempre que as nossas investigações experimentais se cruzavam fisicamente.
Ao Eng. António Relvas, doutorado pelo IST, e à Engª Ana Margarida Ricardo, doutoranda do IST/EPFL (Suiça), pela ajuda com a bibliografia e à Sara Velha, pela ajuda preciosa na formatação dos gráficos.
To Fabián, Mike, Hsin-Ying, Rhodora, Ryann, Corvin, Pato, Carolina, Christina, Alan, Ana Christina, Elçin, Maria, Isabel, Beatriz, and Annie Caroll for becoming part of my life during my stays at Davis. I already miss you guys.
Ao Eng. Joaquim Macedo, ao Prof. Agostinho Benta, à Profª Fernanda Rodrigues e à Doutora Cristina Oliveira, colegas da Universidade de Aveiro, pelos bons momentos passados em Aveiro.

Aos meus pais, por terem feito de mim o que sou hoje e por serem o meu porto de abrigo.

Ao Tuca, pelas suas ideias entusiásticas e incansável energia para ver sempre mais além, de cujas conversas resultaram interessantes revisões da tese. Mas sobretudo, por ser o amor da minha vida.

À Gui, pelo seu amor e alegria e por me ensinar todos os dias o que é realmente importante na vida. Pela sua capacidade de adaptação a uma língua e cultura diferentes e pela sua paciência nas longas horas em que "a mamã está a trabalhar com o Fabián".

palavras-chave

descarregador em degraus, escoamento deslizante sobre turbilhões, escoamento mono-fásico, escoamento bi-fásico, bacia de dissipação de energia, ensaios experimentais, simulações numéricas, análise teórica, sonda de detecção de bolhas de ar, tubo de Pitot modificado, mecânica dos fluidos computacional (CFD), média de Reynolds das equações de Navier-Stokes (RANS).

resumo

O estudo de escoamentos turbulentos em descarregadores em degraus tem sido um desafio para os investigadores. A macro-rugosidade do leito, a ondulação da superfície livre, a intermitência da localização da secção inicial de entrada de ar e o escoamento bi-fásico a jusante da secção inicial de entrada de ar fazem com que a caracterização do escoamento deslizante sobre turbilhões em descarregadores em degraus não seja simples. Actualmente, é possível combinar técnicas de medição fiáveis com simulações numéricas e análise teórica.

Nesta dissertação, o estudo experimental baseia-se em resultados experimentais obtidos em duas instalações experimentais: a instalação A, do Laboratório Nacional de Engenharia Civil (*LNEC*), dotada de um descarregador em degraus com declive de 1V:0.75H e a instalação B, do Instituto Superior Técnico (*IST*), dotada de um descarregador em degraus com declive de 1V:2H. Uma sonda de ar, um tubo de Pitot modificado e vários hidrómetros permitiram o estudo do escoamento deslizante sobre turbilhões mono- e bi-fásico ao longo do descarregador em degraus da instalação A. Na bacia de dissipação de energia, a observação visual do escoamento foi auxiliada pelas leituras efectuadas em tomadas de pressão localizadas na soleira da bacia e pelas leituras da altura do escoamento efectuadas em réguas graduadas localizadas nas paredes da bacia. Na instalação B foram utilizados um tubo de Pitot e vários hidrómetros para estudar a região não arejada do escoamento deslizante sobre turbilhões no descarregador em degraus.

O estudo numérico é baseado em simulações numéricas da região não arejada do escoamento deslizante sobre turbilhões sobre descarregadores em degraus com o código comercial de CFD *FLOW-3D*® de modo a reproduzir as condições ensaiadas experimentalmente. As simulações beneficiaram da técnica de blocos múltiplos (*multi-block*) num sistema de coordenadas cartesianas, da determinação da superfície livre pelo método *TruVOF* e da utilização de dois modelos de turbulência: os modelos k-ε e *RNG* k-ε.

Por último, o estudo teórico consistiu em desenvolver um modelo simplificado 1D para determinar as características hidráulicas principais do trecho não arejado do escoamento deslizante sobre turbilhões em descarregadores em degraus. O modelo foi desenvolvido a partir das equações de Navier-Stokes, conjuntamente com resultados experimentais e numéricos.

Os resultados apresentados nesta dissertação contribuem para o conhecimento do escoamento deslizante sobre turbilhões em descarregadores em degraus, nomeadamente na região não arejada, na secção inicial de entrada de ar e na região arejada. A hidráulica dos dissipadores de energia a jusante de descarregadores em degraus, em particular das bacias tipo III do USBR, é também objecto de estudo.

Em relação à região não arejada do escoamento em descarregadores com declive acentuado, e com base em resultados experimentais e numéricos, são propostas expressões para estimar o desenvolvimento da altura equivalente de água, da espessura da camada limite, da concentração média de ar, do coeficiente de energia cinética, da dissipação de energia, do factor de resistência e do coeficiente n da fórmula de Manning. São ainda propostas expressões adimensionais para a energia cinética turbulenta e sua dissipação. Para declives moderados, são propostas expressões para estimar o

desenvolvimento da altura equivalente de água, do coeficiente de energia cinética e da energia específica residual. São ainda apresentados valores do expoente *1/N* da expressão adimensional da distribuição de velocidades, quer para descarregadores com declive acentuado quer com declive moderado.

Em conformidade com outros estudos centrados em escoamentos de parede e com derivações teóricas, para a região não arejada do escoamento em descarregadores em degraus de acentuado declive, observa-se que o factor de resistência depende da macro-rugosidade criada pelos degraus e da geometria da secção transversal e que o coeficiente *n* da fórmula de Manning aumenta com a rugosidade. A descrição estatística da turbulência do escoamento é igualmente explorada, contribuindo para o conhecimento da estrutura do escoamento. Observou-se que para números de Reynolds rugoso não superiores a 6.8×10^4 a energia cinética turbulência e a sua dissipação cumprem leis de semelhança. Estas expressões adimensionais estão de acordo com os resultados obtidos por outros autores para escoamentos completamente desenvolvidos em canais abertos e no escoamento em rios com leito de gravilha. Em acréscimo, a taxa de dissipação de energia, quer para descarregadores de declive acentuado quer de moderado declive, é baixa. Por último, observa-se que os valores da média temporal da concentração de ar entre 0 e 1 medidos na região não arejada do escoamento dizem respeito não só ao ar capturado entre ondas de água, na zona de ondulação da superfície livre, mas também ao ar emulsionado no escoamento, i.e., sob a forma de bolhas de ar, quando perto da secção média inicial de entrada de ar, devido à diferença entre localizações instantânea e média temporal.

Foram revistas metodologias e fórmulas para estimar a localização da secção inicial de entrada de ar e apresentadas expressões para estimar a concentração média de ar e a altura equivalente de água nessa secção.

Relativamente à região de escoamento arejado em descarregadores em degraus com declive acentuado, os resultados experimentais apresentados nesta dissertação permitiram estimar a influência da definição da superfície livre nos parâmetros hidráulicos da região do escoamento arejado e estimar a máxima elevação do escoamento nesta região do escoamento.

Com base nos resultados experimentais obtidos na bacia de dissipação de energia do tipo III do *USBR* localizada a jusante do descarregador em degraus da instalação A, observou-se que os perfis da altura piezométrica e da altura do escoamento tendem a seguir o perfil recomendado pelo *USBR* para bacias tipo III. A excepção ocorre à entrada da bacia, onde as alturas piezométricas apresentadas nesta dissertação excedem largamente as apresentadas pelo *USBR*. É ainda observado que, tal como entre as bacias tipo I e tipo III do *USBR*, o ressalto hidráulico estabiliza muito mais rapidamente numa bacia tipo III a jusante de um descarregador em degraus do que uma bacia tipo I a jusante do mesmo descarregador em degraus. Finalmente, observa-se que os blocos de amortecimento a colocar no descarregador não têm influência visível nos resultados da altura piezométrica nem da altura do escoamento ao longo da bacia.

Relativamente às simulações numéricas do escoamento não arejado, a proximidade entre resultados experimentais e numéricos permite validar o modelo teórico e a integração numérica usados no *FLOW-3D*®. As simulações desenvolvidas também mostraram que o modelo de turbulência k-ε permite representar as características do escoamento não arejado em descarregadores em degraus, uma vez que não foram observadas diferenças significativas entre as simulações com este modelo e com o modelo *RNG* k-ε. Finalmente, observou-se que o modelo de entrada de ar usado no *FLOW-3D*® é válido para estimar a localização da secção inicial de entrada de ar.

Por último, a proximidade entre os resultados obtidos da aplicação do modelo teórico desenvolvido no âmbito desta dissertação e os resultados experimentais indica que as hipóteses e simplificações consideradas no desenvolvimento do modelo são adequadas.

keywords

stepped chute, skimming flow, mono-phase flow, two-phase flow, stilling basin, experimental measurements, numerical simulations, theoretical analysis, conductivity probe, back-flushing Pitot tube, computational fluid dynamics (CFD), Reynolds Averaged Navier-Stokes equations (RANS).

abstract

The study of turbulent flows in stepped chutes has been a challenge for researchers. The macro-roughness of the bottom, the undulated free-surface, the intermittent inception point location and the two-phase flow downstream of the inception point do not make the characterization of the skimming flow in stepped chutes easy. At present, reliable measurement techniques can be combined with numerical simulations and theoretical analysis.

In this dissertation, the experimental study is based on data acquired in two laboratory models: model A, of the Laboratório Nacional de Engenharia Civil (*LNEC*), which has a stepped chute with slope of 1V:0.75H, and model B, of the Instituto Superior Técnico (*IST*), which has a stepped chute with slope of 1V:2H. A conductivity probe, a back-flushing Pitot tube and several point gauges allowed the investigation of the mono- and two-phase skimming flow down the stepped chute of model A. In the stilling basin, visual observation was helped by pressure taps installed along the floor of the basin and by rulers in the sidewalls of the channel. In model B, a Pitot tube and point gauges were used to study the non-aerated skimming flow region in the stepped chute.

The numerical study is based on numerical simulations of the non-aerated region of the skimming flow down stepped chutes with the CFD commercial code *FLOW-3D*® to reproduce the experimental conditions. The numerical runs benefited from the ability of using multi-block grids in a Cartesian coordinate system, from capturing the free-surface with the *TruVOF* method embedded in the code, and from the use of two turbulence models: the *k-*ε and the *RNG k-*ε models.

Finally, the theoretical study consisted in developing a simplified 1D model to predict the main hydraulic characteristics of the non-aerated skimming flow region in stepped chutes. Based on the Navier-Stokes equations, the model was developed with the help of experimental and numerical data.

The results presented in this dissertation contribute to the understanding of the skimming flow in stepped chutes, namely in the non-aerated flow region, the inception point and the aerated region. The hydraulics of energy dissipators downstream of stepped chutes, specifically *USBR* type III basins, is also studied.

Pertaining to the non-aerated flow region, and based in experimental and numerical data, expressions are proposed to estimate the development of the equivalent clear-water depth, the boundary layer thickness, the mean air concentration, the kinetic energy coefficient; the energy dissipation, the friction factor and Manning's *n*. Self-similarities of the turbulent kinetic energy and its dissipation for steep slopes are also proposed. For moderate slopes, expressions are proposed to estimate the development of the equivalent clear-water depth, the kinetic energy coefficient, and the residual specific energy. Values for the exponent *1/N* of the self-similar velocity distribution are also presented, respectively for steep and moderate slopes.

In agreement with other wall flow studies and theoretical derivations, for the non-aerated flow region of steep stepped chutes the friction factor is observed to depend on the steps macro-roughness and on the geometry of the cross-section and Manning's n is observed to increase with roughness. Turbulence statistics are equally explored for contributing to the knowledge of the flow structure. For roughness Reynolds numbers up to 6.8×10^4 the normalized turbulent kinetic energy and its dissipation are observed to be self-similar.

These self-similarities are in accordance with the findings of other authors for fully developed open channel flows and gravel bed river flows. In addition, the rate of energy dissipation, for both steep and moderate slope stepped channels, is observed to be small. At last, time-averaged local air concentration values between 0 and 1 measured in the non-aerated flow region are observed to not only pertain to entrapped air captured between water waves in the contorted free-surface but also to air bubbles present inside the flow (entrained air) when near the time-averaged inception point, due to the difference between instantaneous and time-averaged inception point location.

Existing methodologies and formulae for estimating the location of the inception point of air entrainment are revisited. Formulae for estimating the mean air concentration and the equivalent clear-water depth at that location are also presented.

Focused on the aerated region of steep stepped chutes, experimental data presented in this dissertation allowed to evaluate the influence of the definition of the free-surface in the hydraulic parameters of the aerated flow region and estimate the maximum flow bulking in this flow region.

Based on the experimental data collected in the *USBR* type III basin downstream of the steep stepped chute, in model A, the results show that the profiles of pressure head and flow depth tend to follow those recommended by the *USBR* for type III basins. The exception occurs at the entrance of the basin, where the pressure head values presented in this dissertation exceed largely those presented by the *USBR*. Is also observed that, as between *USBR* type I and III basins located downstream of conventional spillways, the hydraulic jump stabilizes much faster than in the type I basin downstream of a stepped chute of equal characteristics. Finally, the chute blocks are observed to have no influence in the pressure head and flow depth profiles along the basin.

In terms of numerical simulations of the non-aerated flow region, the excellent agreement between experimental and numerical data permitted to validate the selected theoretical model and numerical integration used in *FLOW-3D*®. The developed runs also showed that the use of a *k-*ε model allows for an accurate representation of the flow features in the non-aerated flow region of stepped channels, since no significant differences were observed in the simulations with this closure and the *RNG k-*ε model. One last important finding is that the air entrainment model used in *FLOW-3D*® is accurate to predict the location of the inception point of air entrainment.

At last, the good agreement between the results obtained with the developed theoretical model and experimental data indicates that the assumptions and simplifications considered in the model construction are adequate.

TABLE OF CONTENTS

1 INTRODUCTION

1.1 Motivation

1.2 Background

1.3 Objectives

1.4 Text organization

2 EXPERIMENTAL SET-UPS AND INSTRUMENTATION

2.1 Introduction

2.2 Experimental facility at LNEC

2.3 Experimental facility at IST

3 MATHEMATICAL MODEL

3.1 General mathematical model

3.2 Turbulence models

3.3 FAVOR^{TM} method

3.4 Boundary conditions

3.5 Finite volumes/finite differences method

3.6 Stability conditions

4 EXPERIMENTAL STUDY

4.1 On the prediction of the hydraulic parameters of the non-aerated skimming flow down steep stepped spillways

4.2 Measuring air entrainment and flow bulking in skimming flow over steeply sloping stepped chutes

4.3 Flow characteristics along USBR type III stilling basins downstream of steep stepped spillways

4.4 Skimming flow in the non-aerated region of stepped spillways over embankment dams

5 NUMERICAL STUDY

5.1 Laboratory measurements and multi-block numerical simulations of the mean flow and turbulence in the non-aerated skimming flow region of steep stepped spillways

5.2 Boundary-layer development, self-similar velocity profiles, and turbulence statistics in the non-aerated skimming flow region of steep stepped spillways

5.3 Predictors for the inception of air entrainment in flows on steep stepped spillways: an analysis

5.4 Experimental and numerical investigation of the non-aerated skimming flow on stepped spillways over embankment dams

6 THEORETICAL STUDY

6.1 Theoretical model of the mean flow in the non-aerated skimming flow region of steep stepped spillways

7 FINAL CONSIDERATIONS

7.1 Summary of the main conclusions and contributions

7.2 Suggestions for future research

APPENDIX

Chapter 1

Introduction

1.1 MOTIVATION

Stepped spillways have been used since ancient times but gained popularity recently, when non-conventional construction techniques like roller compacted concrete began to be used in dam engineering. Such technique drives naturally to a stepped downstream dam face which, when used as a spillway, increases the rate of energy dissipation when compared to a conventional solution. Different types of flows can be observed down a stepped surface, depending on discharge and steps configuration, but for the design discharge of stepped spillways over concrete or gravity dams, the main flow usually skims over the recirculation flow inside the steps cavities.

Because research in this topic has been lead mainly from a design approach, this thesis pretends also to contribute to the detailed mechanistic characterization of the skimming flow. In fact, the main features of the skimming flow (1. single- and two-phase flow; 2. flow in a channel with large roughness; and 3. channel with large slope) lead to complex mechanisms not completely known yet, interesting from the mechanics of fluids point of view.

Because in stepped spillways the appearance of air in the skimming flow occurs faster than in smooth spillways, the air-water flow region has been extensively studied through the last decades in detriment of the non-aerated region of the flow, for which studies are scarce and limited. However, for small dams and/or high design unit discharges, the non-aerated region can be dominant. Predicting tools of the main characteristics of the non-aerated flow region are therefore needed to characterize the flow and help in the design, revision and hydraulic rehabilitation of a wide variety of stepped chutes and spillways. Therefore, this dissertation presents a study of the skimming flow in stepped chutes, mostly focused on the non-aerated flow region.

Because the stepped profile increases the rate of energy dissipation in the spillway, the length of the required downstream energy dissipator is consequently reduced when compared to a conventional solution. Up to date, the effect of the chute steps on the flow characteristics of the required downstream energy dissipator remains practically unknown, despite its importance for the design of this kind of structures. A basin similar to the type III basin from the Bureau of Reclamation of the United States Department of the Interior (USBR) may be adequate downstream of stepped spillways with limited discharges and moderate velocities at the entrance of the basin. For this reason, the hydraulics of a basin similar to the USBR type III basin are studied in this dissertation.

In addition, studies focused on stepped spillways have been performed mainly experimentally, with the increased appearance of some recent numerical papers. However, to the best of my knowledge, none of them presented a detailed study of the skimming flow using an accurate numerical model. Therefore, detailed numerical simulations with the use of the commercial code *FLOW-3D*® are performed in the framework of this dissertation because, when validated, numerical tools can be a supplement to the available experimental tools for the analysis of the flow in stepped spillways, and for helping in the design of such structures.

Due to the complexity of the flow in stepped spillways, a theoretical model to predict the main hydraulic characteristics of the non-aerated flow is still missing. However, data from precise and

detailed experimental measurements and numerical simulations might help with the simplifications and assumptions in order to convert the equations to a tractable model. In this line of thought, a 1D theoretical model of the main flow, derived directly from the Navier-Stokes equation, is proposed in this dissertation.

In summary, this dissertation congregates detailed experimental, numerical and theoretical approaches to increase the knowledge on the mechanics of fluids of the skimming flow on stepped spillways in particular and on rough flows in channels with large slope in general, since the steps can be seen as a macro-roughness.

1.2 BACKGROUND

1.2.1 Introduction

A contextualization of stepped chute flows is presented in this subchapter, beginning with some examples of typical stepped spillways in roller compacted concrete (RCC) and embankment dams, and followed by a classification of the flow regimes in stepped chutes. Finally, a concise review of the most important experimental and numerical studies on the skimming flow regime is presented, with particular attention to the non-aerated flow region and downstream energy dissipators.

1.2.2 Examples of stepped spillways

RCC dams

The recent construction technique of RCC applied to dam engineering is closely linked to the significant increase of the number of stepped spillways in the last three decades. Such technique consists in disposing "dry" concrete (drier than conventional concrete) in layers of about 0.3 m, spreading the blend with asphalt-paving equipment, and then compacting it with rollers. The use of earthfill construction methods contributes to faster construction and reduced cost compared to conventional smooth spillways (e.g., Dunstan 1999, Chanson 2002). The placement method, by horizontal layers, forms naturally a stepped form on the sloped, downside face of the dam, which contributes to increase the flow energy dissipation when compared with smooth conventional spillways. With an increased interest in maintenance and rehabilitation of dams, this configuration facilitates also the access to the dam body, simplifying operations of maintenance and inspections of the dam body (Geringer and Officer 1995). Figure 1 shows the construction of Pedrógão dam, finished in 2005, which is the first RCC dam built in Portugal.

Figure 1 - Pedrógão dam construction: detail of the RCC layers placement and compaction.

Although the application of this technique to dam engineering was suggested in the early 40's (ICOLD 2000), the first RCC high dam was only built in 1963 (RCC DAMS 2005). Until 1990, 25 RCC high dams were built, increasing to 175 at the end of that century. At the end of 2005, around 250 high RCC dams were already built in the world and about 30% had stepped spillway (RCC DAMS 2005).

Table 1 presents the main hydraulic parameters of stepped spillways in some important RCC dams. The high differences in dam height (15 to 130 m) and maximum unit discharge (1 to 165 m^2/s) show the large field of application of stepped spillways in RCC dams. Figures 2 to 4 present some examples of stepped spillways in RCC dams.

Table 1 - Typical examples of steep stepped spillways around the world.

Name, Country, Year	Ref.	H_d (m)	θ (º)	b (m)	h (m)	$(q_w)_{max}$ (m^2/s)	L' (%)
Grindstone Canyon, USA, 1986	[GO]	34	53	30	0.3	1	12
De MistKraal, South Africa, 1986	[HD], [GO]	18	59	195	1	29	100
Zaaihoek, South Africa, 1986	[HD], [GO]	37	58	160	1	15.6	77
Upper Stillwater, USA, 1987	[HO]	61	72;59	183	0.6	11.6	44
Monksville, USA, 1987	[SO]	36.6	52	61	0.61	9.3	52
Lower Chase Creek, USA, 1987	[GO], [FR]	18	55	61	0.6	3.3	52
Les Olivettes, France, 1987	[GO]	31.5	53	40	0.6	6.6	48
Stagecoach, USA, 1988	[FR], [SJ]	43	51	17	0.6	3.6	22
Wolwedans, South Africa, 1990	[GE], [W&D]	70	63	77.25	1	12.4	36
Riou, France, 1990	[GO], [W&D]	19	59	105	0.6	1.1	24
Puebla de Cazalla, Spain, 1991	[ME], [W&D]	58.2	51	18	0.9	9	31
Choldocogania, France, 1991	[GO], [W&D]	32.5	50	13.5	0.6	2.1	20
Belén-Gato, Spain, 1991	[SJ], [W&D]	33.5	53	17.4	0.85	1.73	17
Caballar I, Spain, 1991	[SJ], [W&D]	14.8	53	17.4	0.85	1.73	38
Amatisteros III, Spain, 1991	[SJ], [W&D]	14.8	53	17.4	0.85	1.73	38

Belén-Caguella, Spain, 1992	[SJ]	31	53	17.4	0.85	13.5	79
Belén-Flores, Spain, 1992	[SJ]	27	53	17.4	0.85	1.73	21
Taung, South Africa, 1993	[GO]	50	53	35	0.6	6.1	29
New Victoria, Australia, 1993	[WA], [W&D]	35	72	130	0.6	5.4	44
Cenza, Spain, 1993	[SJ], [W&D]	49	53	58	0.6	3.47	19
Sierra Brava, Spain, 1994	[SJ], [W&D]	54	53	166	0.9	3.9	19
Petit Saut, French Guiana, 1994	[DU], [GO]	31	51	60	0.6	4	33
La Touche Poupart, France, 1994	[GO], [W&D]	33	53	35	0.6	6.1	43
Shuidong, China, 1994	[GX]	38	60	60	0.9	100.2	100
Atance, Spain, 1997	[W&D]	45	51	32	1.2	5.94	29
Boquerón, Spain, 1997	[ME], [SJ]	46	54	16	1.2	17.8	64
Randleman, USA, 1997	[TA]	31*	53	152.4	0.9	37.1	100
Nakasujigawa, Japan, 1998	[HS]	71.6	55	175	0.75	6.6	21
Tannur, Jordan, 2001	[W&D], [AI]	50	51	180	1.2	3.4	18
Dachaoshan, China, 2004	[GU], [GU2], [W&D]	115*	55	5x14	1.0	165	100
Pedrógão, Portugal, 2005	[ML]	29	51	301	0.6	39.9	100
Çine, Turkey, 2010	[DA], [W&D]	130*	50	150		17.2	

Note: H_d - spillway height; θ - spillway slope; b – spillway width; h - step height; $(q_w)_{max}$ – maximum discharge per unit width; L' – relative length of the spillway where non-aerated flow conditions would occur for the design discharge; * - dam height.

[AI] Airey (2004); [DA] Darama (2003); [DU] Dussard et al. (1992); [FR] Frizell (1992); [GE] Geringer (1995); [GO] Goubet (1992); [GU] Guo et al. (2003); [GU2] Guo et al. (2006); [GX] Guangtong and Xiankang (1995); [HD] Hollingworth and Druyts (1986); [HO] Houston (1987); [HS] Hakoishi and Sumi (2000); [ME] Mateos and Elviro (1992); [ML] Melo (2004); [SJ] Sánchez-Juny (2001); [SO] Sorensen (1985); [TA] Talbot, et al. (1997, Internet); [WA] Wark et al. (1991); [W&D] RCC Dams (2003).

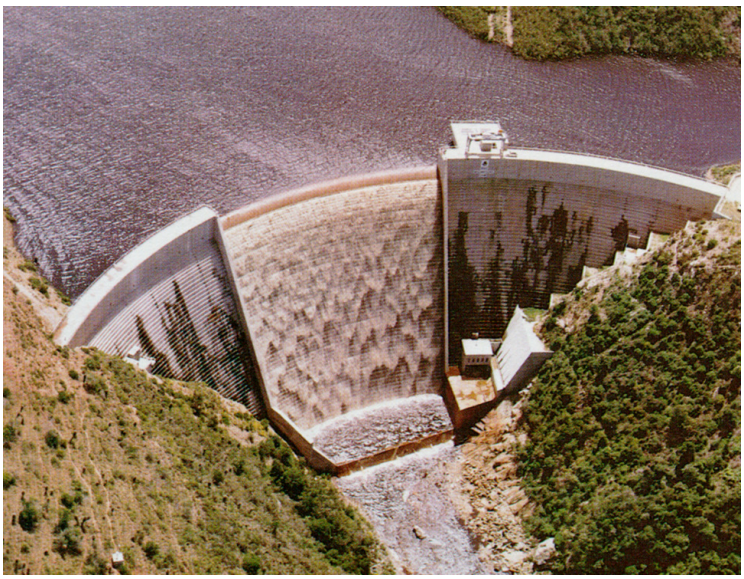

Figure 2 - Wolwedans Dam, South Africa (H_d = 70; θ = 60º; h = 1.0 m; q_{max} = 12.4 m^2s^{-1}). View of the downstream face of the dam (in Matos 1999).

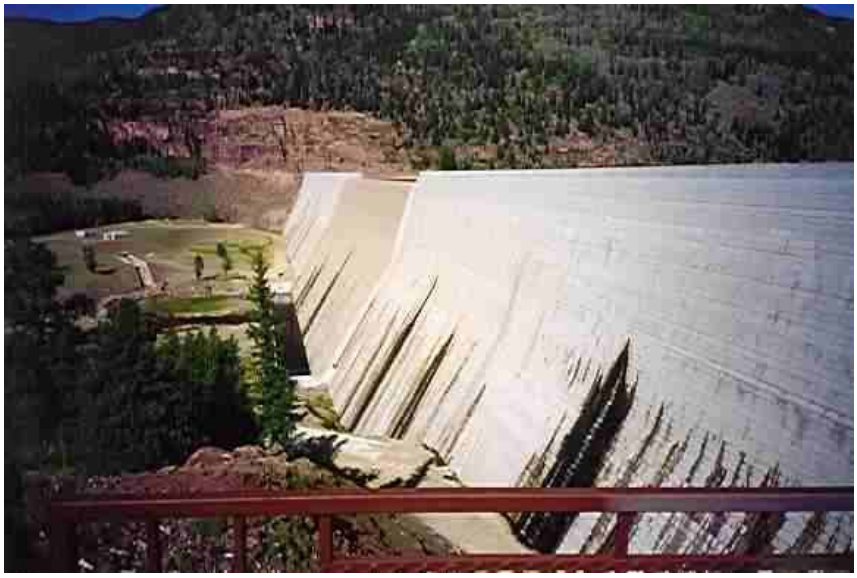

Figure 3 - Upper Stillwater Dam, USA (H_d = 61; θ = 72º, 59º; h = 0.6 m; q_{max} = 11.6 m^2s^{-1}). View of the downstream face of the dam (Photo: courtesy of J. Matos).

a) b)

Figure 4 - Pedrógão Dam, Portugal (H_d = 29 m; θ = 51º; h = 0.6 m; q_{max} = 39.9 m^2s^{-1}): a) view of the downstream face of the dam; b) detail of the crest.

Embankment dams

Recent re-evaluation of the design flood of several embankment dams around the world showed that many have inadequate spillway capacity, which can result in dam overtopping. The overtopping of embankment dams can cause the failure of the structure as a whole, unless a convenient protective system is considered. Safe overtopping protection methods are often an economical option when compared to providing additional conventional spillway capacity. These include grass-covered channels or embankments, geotextile and membranes, reno mattresses, riprap, gabions, concrete blocks, reinforced concrete slab, roller compacted concrete and soil

cement (Frizell 2004). In the USA, roller compacted concrete (RCC) construction technique started to be used in embankment dam rehabilitation in the early 80's and in 1998 58 dams were already rehabilitated (Hansen and Bass 1999), being in process or in perspective 72 more interventions in that year (Bass 2000). The overtopping protection with RCC has been adopted in some other countries, namely from South America (McLean and Hansen 1993).

Table 2 presents examples of several embankment dams rehabilitated with RCC, to allow dam overtopping, and respective hydraulic characteristics. The majority respects to small and medium size dams. In fact, 70% are up to 15 m high, from which 40% are smaller than 10 m. The unit discharges are mainly small, with values up to 10 m^2/s in 75% of the cases. The maximum head at the crest is, generally, smaller than 4.0 m, being smaller than 2.0 m in 50% of the presented cases.

Figures 5 to 7 present some examples of the variety of solutions for overtopping protection with RCC.

Table 2 – Typical examples of RCC embankment overtopping protection in the USA (adapted from McLean and Hansen 1993).

Dam (year of construction)	H_d (m)	$(q_w)_{max}$ (m^2/s)	θ (º)	h (m)	L' (%)
Brownwood Country Club (1984)	5.8	2.3	26.6	0.2	85
Comanche Trail (1988)	6.1	5.6	26.6	0.3	100
Bishop Creek n. 2 (1989)(1)	12.5	2.2	18.4	0.3	29
Goose Lake (1989)	10.7	0.8	45.0	0.5	30
Thompson Park n. 3 (1990)	9.1	2.8	14.0	0.3	38
Ringtown Nº 5 (1991)(2)	18.3	5.2	20.0	0.3	38
Ashton (1991)	18.3	11.3	33.7	0.6	91
Goose Pasture (1991)	19.8	8.8	18.4	0.3	49
Butler Reservoir (1992)	13.1	12.7	21.8	0.3	100
Lake Diversion (1993)(2)	25.9	29.4	20.0	0.2	96
Horsethief (1992)	19.8	1.6	26.6	0.3	18
Meadowlark Lake (1992)	8.5	11.0	18.4	0.3	100
Phillipsburg Dam n. 3 (1992)	6.1	1.3	26.6	0.3	52
North Potato Diversion (1992)(3)	10.7	31.6	11.3	0.6	100
Lima (1993)	16.5	5.7	26.6	0.6	53
Rosebud (1993)	10.1	5.1	26.6	0.3	84
Umberger (1993)	12.2	20.1	18.4	0.3	100

Note: (1) – new emergency spillway; (2) – combined principal and emergency spillway; (3) – new spillway.

H_d - spillway height; $(q_w)_{max}$ – maximum discharge per unit width; θ - spillway slope; h - step height; L' – relative length of the spillway where non-aerated flow conditions would occur for the design discharge.

Figure 5 - Brownwood Country Club Dam, Texas, USA (H_d = 5.8 m; θ = 26.6º - 1V:2H; h = 0.2 m; q_{max} = 2.3 m^2s^{-1}; h_{max}= 1.7 m). View of the RCC stepped spillway on the downstream face of the dam (in Matos and Meireles 2006).

Figure 6 - Goose Pasture Dam, Colorado, USA (H_d = 19.8 m; θ = 18.4º - 1V:3H; h = 0.3 m; q_{max} = 8.8 m^2s^{-1}; h_{max}= 3.0 m). View of the primary spillway (in operation) and of the emergency spillway, in RCC, on the downstream face of the dam (in Matos and Meireles 2006).

Figure 7 - Phillipsburg Nº 3 Dam, Pennsylvania, USA. View of the RCC stepped spillway on the downstream face of the dam; steps covered with earth and grass (in Matos and Meireles 2006).

1.2.3 Types of flows

For a certain stepped spillway, nappe flow, transition flow, and skimming flow occur with increasing discharge (e.g., Ohtsu and Yasuda 1997a,b, Matos 1999 and Pinheiro and Fael 2000, Chanson 2002).

Nappe flow is characterized by a succession of free falls with an air pocket at each step cavity and has been divided in three subtypes (e.g., Essery and Horner 1978, Peyras *et al.* 1991, 1992 and Matos and Quintela 1997): (1) *isolated nappe flow with fully developed hydraulic jump*; (2) *isolated nappe flow with partially developed hydraulic jump*; and (3) *partial nappe flow* or *nappe interference flow* (Fig. 8). Chanson (2002) gives a slightly different designation to the last subtype (*nappe flow without hydraulic jump)*. In the nappe flow, energy can be dissipated by three different processes: with the fragmentation of the jet in the air, when the jet impinges the step and, if applicable, in the hydraulic jump.

On skimming flow, the main stream skims over the step edges (designated pseudo-bottom) and a secondary flow occupies the cavities formed by the steps. This type of flow can be divided in (e.g., Chanson 1994a,b, 2002 and Matos 1999): (1) *wake-step interference*; (2) *wake-wake interference*; and (3) *recirculating cavity flow* (Fig. 9). In the skimming flow the energy is, in great extent, dissipated in the eddies developed in the step cavities. The eddies are maintained due to transference of shear stress from the adjacent flow (e.g., Morris 1955, 1961 *in* Sorensen 1985 and Rajaratnam 1990).

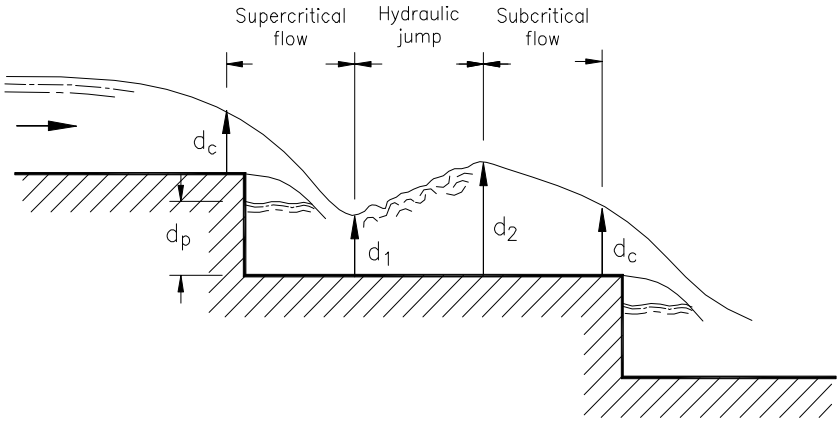

a) isolated nappe flow with fully developed hydraulic jump

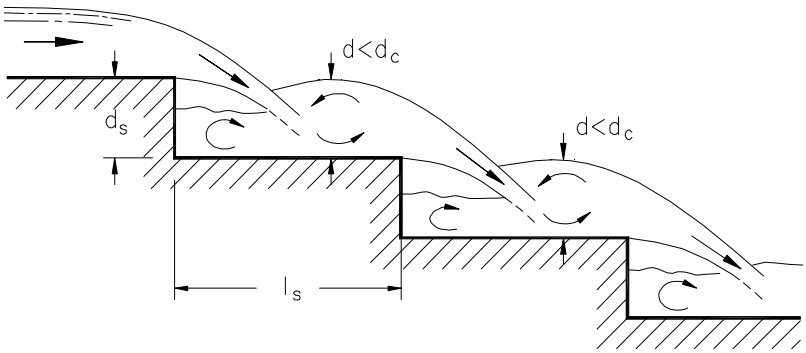

b) isolated nappe flow with partially developed hydraulic jump

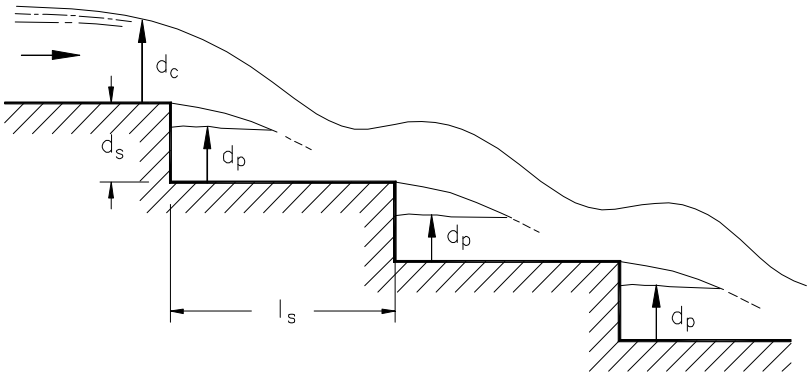

c) partial nappe flow or nappe interference flow

Figure 8 - Subtypes of nappe flow (adapted from Matos 1999).

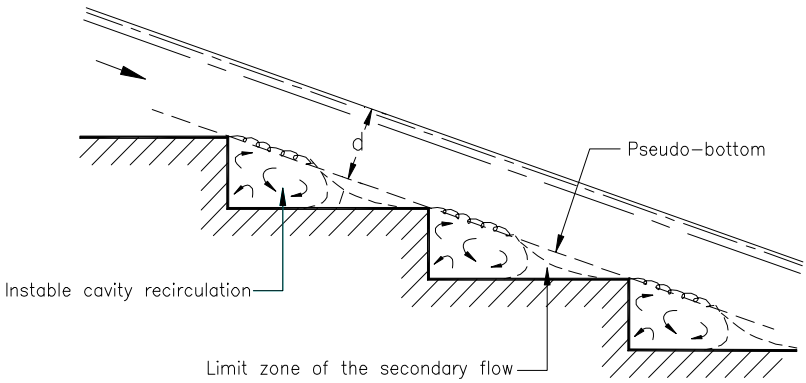

a) wake-step interference

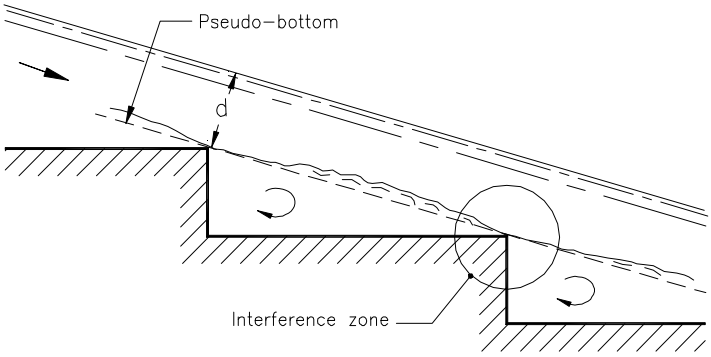

b) wake-wake interference

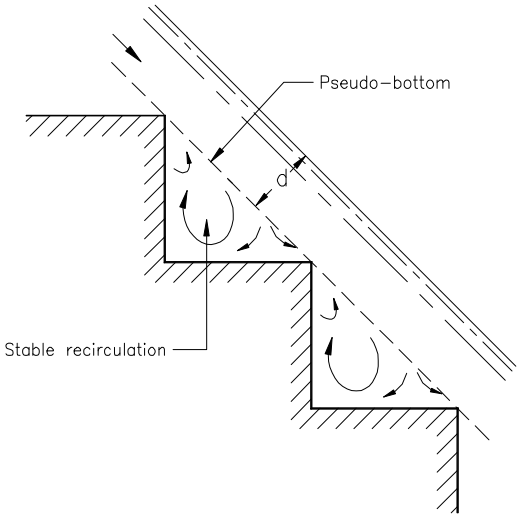

c) recirculating cavity flow

Figure 9 - Subtypes of skimming flow (adapted from Matos 1999).

Until the mid 90's, several authors considered a direct transition between nappe flow and skimming flow, with increasing flow, not making explicit reference to the transition flow (e.g., Stephenson 1988, Peyras *et al.* 1991 and Kells 1995). Although Ohtsu and Yasuda (1997a,b) proposed limits to define the zone of transition between nappe flow and skimming flow, transition flow has been already pointed in earlier studies (e.g., Essery and Horner 1978 and Elviro and Mateos 1995). More recently, several researchers (e.g., Elviro and Mateos 1995, Ohtsu and Yasuda 1997a,b, Haddad

1998, Matos 1999, Chamani and Rajaratnam 1999, André et al. 2001, André and Ramos 2003, Chanson and Toombes 2002, 2004, Meireles 2004, Renna 2004) established criteria and determined experimentally the conditions of end of the nappe flow and beginning of the transition flow and of end of the transition flow and beginning of the skimming flow. However, the definition of transition flow has not been consensual (Matos 2001). Ohtsu and Yasuda (1997a,b), Matos (1999), Fael (2000), Yasuda et al. (2001), André et al. (2001), Boes and Hager (2003b), André and Ramos (2003) and Meireles (2004) consider that the flow skims over some of the step edges and exhibits a nappe with an air pocket in the cavity on the remaining steps. Intense splashing and spray near the free-surface are features of this flow regime, as observed by Chanson and Toombes (2004). Matos (1999), Fael (2000), Yasuda et al. (2001), Boes and Hager (2003b), Chamani and Rajaratnam (1999), Chanson (2002), Chanson and Toombes (2004), among others, presented equations to define the flow regime limits. Considering any of these equations, the skimming flow is observed to occur for the design discharge of the presented examples of embankment dam and RCC stepped spillways from Tables 1 and 2, respectively.

1.2.4 Skimming flow characterization

In skimming flows down stepped chutes, the flow is initially smooth and glassy. The development of the boundary layer is observed along the *non-aerated flow region* and when the boundary layer is close to the free-surface the flow begins to exhibit an undulated pattern. At the *inception point of air entrainment* large quantities of air begin to entrain in the flow. Downstream, the *aerated flow region* can be divided in three different flow regions, respectively: a) partially developed aerated flow region, b) completely developed aerated flow region and c) uniform flow region.

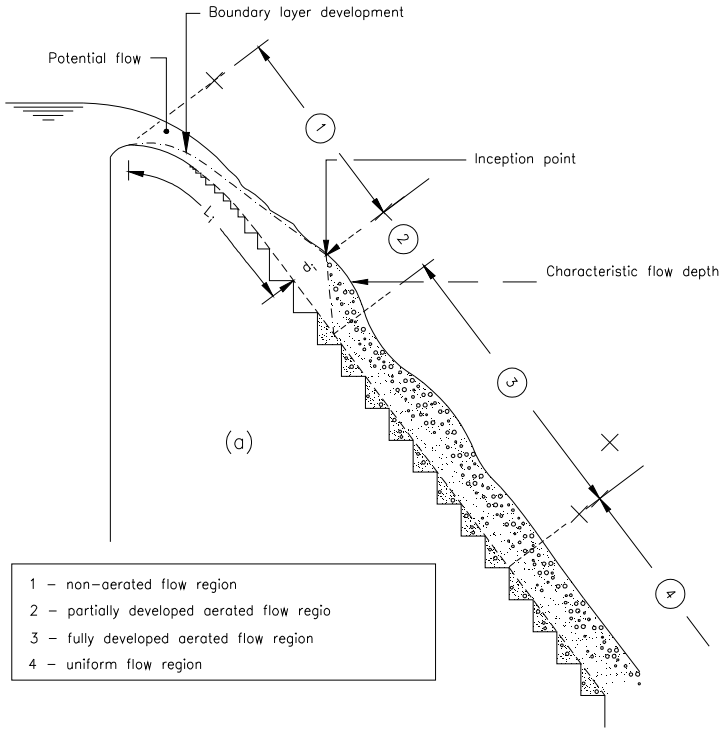

Figure 10 - Skimming flow regions (adapted from Matos 1999).

Non-aerated flow region

Studies on the non-aerated flow region are scarce. Chanson (2002) and Gonzalez and Chanson (2007) include the analysis of the non-aerated flow region, presenting results and methodologies to be applied to this region of the flow. André and Ramos (2003) and Cabrita (2007) acquired data in a stepped channel with slope typical of embankment dams and Meireles et al. (2006) presented data acquired in a steep stepped channel, nevertheless the data are not yet extensively analyzed nor published in peer reviewed journals. Amador et al. (2006, 2009) performed a detailed study on the non-aerated flow region of stepped spillways with precise Particle Image Velocimetry (PIV) instrumentation, focusing on the characterization of the flow in terms of water velocity, boundary layer thickness, equivalent clear-water depth, friction factor, energy dissipation, and turbulence statistics. However, this study is limited to one discharge and step height, corresponding to a small range of application.

Inception point

In stepped spillways, the inception point has been mainly located by visual observation, both in experimental models (e.g., Sorensen 1985; Tozzi 1992; Bindo et al. 1993; Mateos and Elviro 1997; Sánchez-Juny 2001; Chanson and Toombes 2002; Yasuda and Chanson 2003; Sanagiotto 2003; Dai Prá 2004; André 2004; Gonzalez 2005; Relvas and Pinheiro 2008; Bung 2009) and in prototypes (e.g., Amador et al. 2009). Fewer studies determined the location of the inception point as the intersection between the boundary layer and the flow profile (e.g., Matos 1999; Meireles 2004; Renna 2004; Amador et al. 2009) or as the position where the local air concentration at the pseudo-bottom reaches a certain value (e.g., Boes and Hager 2003a). However, theoretically more accurate methods to determine the inception point have been discussed for open channel flows in general, that were never applied to stepped spillways flows.

Aerated flow region

Ever since stepped spillways gained popularity, many experimental studies have been done in that topic, focused mainly in the characterization of the aerated flow region, regarding the study of air concentration and velocity distributions (e.g., Gaston 1995; Chamani and Rajaratnam 1999; Matos 1999; Matos 2000; Chanson 2002; Boes and Hager 2003a; Ohtsu et al. 2004; André 2004; Meireles 2004; Renna 2004; Gonzalez 2005; Gomes 2006; Felder and Chanson 2009), pressure field on the steps (e.g., Sánchez-Juny 2001; Yasuda and Ohtsu 2003; André 2004; Amador et al. 2009; Gomes 2006), gas transfer (e.g., Toombes and Chanson 2000; McKenna 2001; Bung 2009), friction factor (e.g., Matos 1999; Chamani and Rajaratnam 1999; Yasuda and Ohtsu 1999), and macro-roughness and non-conventional configurations (e.g., André 2004; Gonzalez 2005; Hunt et al. 2008; Relvas and Pinheiro 2008; Chinnarasri et al. 2008; Bung and Schlenkhoff 2010). Empirical models have been developed for predicting the main air-water flow properties along the chute by Hager and Boes (2000), Matos (2000), Boes and Hager (2003a, b), Meireles (2004), Renna (2004) and Ohtsu et al. (2004).

1.2.5 Stilling basins downstream of steep stepped chutes

In spite of the considerable number of studies on stepped spillways, only very few have been focused on the hydraulics of the energy dissipators located downstream of stepped spillways. Within this scope, several studies were centered in the application of the classical momentum equation to the hydraulic jump to determine the residual energy of the stepped spillway (e.g., Diez-Cascon et al. 1991, Tozzi 1992, 1994, Pegram et al. 1999). In this approach it is assumed that the specific energy of the flow at the toe of the chute is approximately equal to that at the upstream end of the jump. Later, Yasuda and Ohtsu (1999, 2003), Meireles (2004) and Meireles et al. (2005) applied the momentum equation taking this condition into account that the pressure distribution was non-hydrostatic at the upstream end of the hydraulic jump.

Meireles et al. (2005), Cardoso (2006), Cardoso (2007) and Cardoso et al. (2007) studied a simple hydraulic jump basin and a baffle basin. Expressions to determine pressure head along the basins have been proposed in both studies. Cardoso et al. (2007) also presented flow depths and compared jump and roller lengths with values for the classical USBR basins.

1.2.6 Numerical modeling of the skimming flow

The recent advances in computational codes and hardware technology allow for new opportunities to employ numerical solutions as a supplement to the available experimental tools for the analysis of flow in stepped spillways, and for helping in the design of such structures. The number of studies on computational fluid dynamics (CFD) focusing on hydraulic structures has increased notably in the last ten years (e.g., Unami et al. 1999; Song and Zhou 1999; Bombardelli et al. 2000; Savage and Johnson 2001; Chatila and Tabbara 2004; Savage et al. 2004; Higgs and Frizell 2004; Dargahi 2006; Ho et al. 2006; Ye et al. 2006; Paxson and Savage 2006; Johnson and Savage 2006; Bhuiyan and Hey 2007), but very few attempts have been made to simulate the skimming flow over moderate slope (Cheng et al. 2004a,b) and steep (Chen et al. 2002; Tabbara et al. 2005; Arantes 2007; Carvalho and Amador 2008) stepped spillways. Cheng et al. (2004a,b) studied the aerated flow, Tabbara et al. (2005) and Carvalho and Amador (2008) described the non-aerated flow region, and Chen et al. (2002) and Arantes (2007) were focused on the entire spillway flow. For the validation of any numerical code attention must be taken to the reliability of both, experimental and numerical results. However, the experimental data presented by Chen et al. (2002) and Tabbara et al. (2005) respect to relatively small facilities, with potential significant scale effects, and the devices used by Chen et al. (2002) to capture flow depth and velocity are not apt to be used downstream of the inception point (see Yasuda et al. 2004 and Chen et al. 2004 for more details). In terms of the considered solution schemes, Chen et al. (2002), Cheng et al. (2004a,b), and Arantes (2007) solved the flows of water and air altogether (which was defined as Partial Volume-of-Fluid (VoF) method in Bombardelli et al. 2001), Tabbara et al. (2005) employed a numerical strategy based on re-meshing each time step, corresponding to big efforts in terms of simulation time. In turn, Carvalho and Amador (2008) used a purported VoF method, but they did not report comparisons of numerical results with data of the free-surface. In addition, in Chen et al. (2002), Tabbara et al. (2005) and Arantes (2007) the simulations have been developed using

unstructured grids with good resolution near the walls but with a lower resolution near the free-surface, which might compromise the accuracy of the results.

1.3 OBJECTIVES

The aim of this dissertation is to contribute to increase the knowledge on the mechanics of fluids of the skimming flow on stepped chutes of moderate to steep slope and downstream energy dissipators. For that purpose, the combination of three different approaches, experimental, numerical and theoretical, will be considered. In this context, the main objectives of this dissertation are to contribute to the:

a) Mechanistic explanation of the non-aerated flow and inception point in stepped spillways in relation with turbulence intensities.

b) Characterization of the non-aerated flow, inception point and flow in downstream energy dissipators for design purposes and evaluation of the definition of free-surface for aerated flows.

c) Implementation and validation of a CFD code for the non-aerated flow and inception point.

d) Development of a theoretical model for the non-aerated flow.

To that end, this dissertation will be focused on the:

- Skimming flow on stepped chutes, namely with the:

  Evaluation of the main hydraulic characteristics of the non-aerated flow, including flow depth, boundary layer development, velocity profiles, flow resistance, turbulence statistics and energy dissipation, validation of existing methodologies and recommendation of new expressions.

  Analysis of the concepts of entrapped air, entrained air and undulation.

  Characterization of the flow at the inception point of air entrainment and evaluation of different existing methodologies to determine its location.

  Evaluation of the influence of the definition of the free-surface in the hydraulic parameters of the aerated region.

  Estimation of the maximum flow bulking in the aerated flow region.

- Energy dissipators located downstream of stepped chutes, specifically basins similar to USBR type III basins, with the:

  Evaluation of the pressure head and flow depth along the basin.

  Comparison between USBR type I and III basins and similar basins located downstream of stepped chutes.

  Evaluation of the effect of the chute blocks in the flow.

- Use of CFD codes to model stepped chute flows, namely with the validation of the commercial code *FLOW-3D®* to accurately reproduce the behavior of the flow in stepped spillways by comparing experimental and numerical results.

- Development of a 1D theoretical model of the main flow, derived directly from the Navier-Stokes equations, able to characterize the non-aerated flow region down stepped chutes, with the:

  Consideration of several assumptions and simplifications from the observation of experimental and numerical data.

  Comparison of the results with experimental data.

1.4 TEXT ORGANIZATION

This Ph.D. dissertation is composed by seven major chapters:

1) The first chapter provides the motivation of the present study, a brief introduction to the topic, and the objectives of the dissertation, along with the organization of the text.

2) The second chapter describes the experimental facilities and the instrumentation used to acquire the data analyzed in this dissertation: experimental facility at LNEC (in subchapter 2.1) and experimental facility at IST (in subchapter 2.2).

3) The third chapter describes the mathematical model, which is the base of the commercial CFD program used in Chapter 5 and of the theoretical model developed in Chapter 6.

4) In the forth chapter experimental data on stepped chutes are analyzed. Focused on the skimming flow in steep stepped spillways, subchapter 4.1 analyzes the main hydraulic parameters of the non-aerated flow region, subchapter 4.2 presents a new analysis of the flow in the aerated flow region related to the definition of free-surface and subchapter 4.3 is focused on the hydraulics of energy dissipators downstream of stepped chutes. At last, subchapter 4.4 analyzes the main hydraulic parameters of the non-aerated region of the skimming flow down stepped chutes with moderate slope.

5) In the fifth chapter experimental and numerical data are analyzed and compared. Pertaining to the non-aerated skimming flow region in steep stepped chutes, subchapter 5.1 presents a detailed analysis and comparison between experimental and numerical data, subchapter 5.2 extends this comparison to more data and presents new insights in terms of flow resistance and turbulence, and subchapter 5.3 respects to the analysis of predictors for the inception of air entrainment. Subchapter 5.4 presents a comparison between experimental and numerical data obtained in a stepped chute with moderate slope.

6) In the sixth chapter a theoretical model is developed to be applied to the non-aerated skimming flow region of stepped chutes of constant slope.

7) The seventh chapter presents the main conclusions of the present research in subchapter 7.1 and the ideas for future research in subchapter 7.2.

Each of the following subchapters written as articles starts with a cover page, giving a summary of the contents of the corresponding subchapter. Because these subchapter are written as articles, the necessary theoretical and experimental description is given and, therefore, part of this information may be repeated in several subchapters.

At last, an appendix is included containing the paper entitled "Prediction of the Asymptotic Water Depth in Rough Compound Channels", from B. Younis, V. Sousa and I. Meireles, published in the Journal of Irrigation and Drainage Engineering, ASCE, in April, 2009. This paper was developed in the framework of the course *Computational River Mechanics* of Prof. Bassam Younis, at UCDavis, USA attended in 2007/2008.

REFERENCES

Airey, M. (2004). Personal communication.

Amador, A., Sanchez-Juny, M., Dolz, J. (2006). "Characterization of the non-aerated flow region in a stepped spillway by PIV." J. Fluid Eng., ASME, 138(6), 1266-1273.

Amador, A., Sánchez-Juny, M. and Dolz, J. (2009). "Developing flow region and pressure fluctuations on steeply sloping stepped spillways." J. Hydr. Eng., ASCE, 135(12), 1092-1100.

André, M. and Ramos, P. (2003). "Hidráulica de descarregadores de cheia em degraus: aplicação a descarregadores com paredes convergentes." Graduate Research Report, IST, Lisbon, Portugal (in Portuguese).

André, S. (2004). "High velocity aerated flows over stepped chutes with macro-roughness elements." PhD thesis, EPFL, Lausanne, Switzerland.

André, S.; Boillat, J.-L.; Schleiss, A. J. (2001). "High velocity two-phase turbulent flow over macro-roughness steppes chutes: Focus on dynamic pressures". Proc. 2001 Intl. Symposium on Environmental Hydraulics.

Arantes, E. J. (2007). "Caracterização do escoamento sobre vertedouros em degraus via CFD." Ph.D. thesis, EESC/USP, São Carlos, Brazil (in Portuguese).

Bass, R. (2000). "Future RCC projects." Proc. Int. RCC Dams Seminar, K.D. Hansen (ed), Denver, USA.

Bhuiyan, A. B. M., and Hey, R. (2007). "Computation of three-dimensional flow field created by weir-type structures." Engineering Applications of Computational Fluid Mechanics, 1(4), 350-360.

Bindo, M., Gautier, J., and Lacroix, F. (1993). "The stepped spillway of M'Bali Dam." Water Power & Dam Const., 45(1), 35-36.

Boes, R. M. and Hager, W. H. (2003a). "Two phase flow characteristics of stepped spillways." J. Hydr. Eng., ASCE, 129(9), 661-670.

Boes, R. M. and Hager, W. H. (2003b). "Hydraulic design of stepped spillways." J. Hydr. Eng., ASCE, 129(9), 671-679.

Bombardelli, F. A., García, M. H., and Caisley, M. E. (2000). "2-D and 3-D numerical simulation of abrupt transitions in open-channel flows. Application to the design of canoe chutes." Proc. 4th. Int. Conf. on Hydroinformatics, IAHR, Iowa City, IA, USA. (In CD.)

Bombardelli, F. A., Hirt, C. W., and García, M. H. (2001). “Discussion on 'Computations of curved free surface water flow on spiral concentrators.' by Matthews et al.” J. Hydr. Eng., ASCE, 127(7), 629-631.

Bung, D. B. (2009). "Zur selbstbelüfteten gerinneströmung auf kaskaden mit gemässigter neigung." Ph.D. thesis, Bergische University of Wuppertal, Germany (in German).

Bung, D. B. and Schlenkhoff, A. (2010) "Self-aerated skimming flow on embankment stepped spillways - the effect of additional micro-roughness on energy dissipation and oxygen transfer" Proc. 1st European IAHR Congress, Edimburgh, UK. (In CD.)

Cabrita, J. (2007). “Caracterização do escoamento deslizante sobre turbilhões em descarregadores de cheias em degraus com paredes convergentes.” MSc. thesis, IST, Lisbon, Portugal (in Portuguese).

Cardoso, G. (2006). “Estudo do ressalto hidráulico em bacias de dissipação de energia a jusante de descarregadores de cheias em degraus.” Graduate Research Report, IST, Lisbon, Portugal (in Portuguese).

Cardoso, G. (2007). “Ressalto hidráulico em bacias de dissipação com acessórios a jusante de descarregadores de cheias em degraus. estudo experimental.” MSc. thesis, IST, Lisbon, Portugal (in Portuguese).

Cardoso, G., Meireles, I., and Matos, J. (2007). “Pressure head along baffle stilling basins downstream of steeply sloping stepped chutes.” Proc. 32th IAHR Congress, Venice, Italy. (In CD.)

Carvalho, R., and Amador, A. (2008). “Physical and numerical investigation of the skimming flow over a stepped spillway.” Proc. 3rd. IAHR Int. Symposium on Hydraulic Structures, Nanjing, China, 1767-1772. (In CD.)

Chamani, M. R., and Rajaratnam, N. (1999). “Characteristics of skimming flow over stepped spillways.” J. Hydr. Eng., ASCE, 125(4), 361-368.

Chanson, H. (1994a). “Hydraulic design of stepped cascades, channels, weirs and spillways.” Pergamon, UK.

Chanson, H. (1994b). “State of the art of hydraulic design of stepped chute spillways.” Hydropower & Dams, July, 33-42.

Chanson, H. and Toombes, L. (2002). “Experimental investigations of air entrainment in transition and skimming flows down a stepped chute.” Can. J. of Civil Eng., 29(1), 145–156.

Chanson, H. and Toombes, L. (2004). “Hydraulics of stepped chutes: the transition flow.” J. Hydr. Res., IAHR, 42(1), 43-54.

Chanson, H. (2002). “The hydraulics of stepped chutes and spillways.” Balkema, Lisse, The Netherlands.

Chatila, J., and Tabbara, M. (2004). “Computational modeling of flow over an ogee spillway.” Comp. & Struct., Elsevier, 82, 1805-1812.

Chen, Q., Dai, G., and Liu, H. (2002). “Volume of fluid model for turbulence numerical simulation of stepped spillway overflow.” J. Hydr. Eng., ASCE, 128(7), 683-688.

Cheng, X., Luo, L., and Zhao, W. (2004a). “Study of aeration in the water flow over stepped spillway.” Proc. World Water Congress 2004, ASCE, Salt Lake City, Utah, USA.

Cheng, X., Luo, L., Zhao, W., and Li, R. (2004b). “Two-phase flow simulation of aeration on stepped spillway.” Progress in Natural Science, 14(7), 626-630.

Chinnarasri, C., Donjadee, S. and Israngkura, U. (2008). “Hydraulic characteristics of gabion-stepped weirs.” J. Hydr. Eng., ASCE, 134(8), 1147-1152.

Dai Prá, M. (2004). "Características de escoamentos sobre vertedouros em degraus de declividade 1V:1H." M.Sc. thesis, UFRGS, Porto Alegre, Brazil (in Portuguese).

Darama, Y. (2003). “Hydraulics of the stepped spillway model of the Çine Dam”. Proc. 30th IAHR Congress, Theme D, IAHR, Thessaloniki, Greece, 703-710. (In CD.)

Dargahi, B. (2006). “Experimental study and 3D numerical simulations for a free-overflow spillway.” J. Hydr. Eng., ASCE, 132(9), 899-907.

Diez-cascon, J., Blanco, J.L., Revilla, J. and Garcia, R. (1991). “Studies on the hydraulic behavior of stepped spillways.” Water Power & Dam Construction, 43(9), 22-26.

Dunstan, M.R.H. (1999). “Recent developments in RCC dams.” Int. Journal on Hydropower & Dams, March, 40-45.

Dussard B.; Deschard, B. and Penel, F. (1992). “Petit Saut: an RCC dam in a wet tropical climate.” Water Power & Dam Construction, February, 30-32.

Elviro, G. and Mateos, I. (1995). “Spanish research into stepped spillways.” Int. J. Hydropower & Dams, 2(5), 61-65.

Essery, I. T. S. and Horner, M. W. (1978). “The hydraulic design of stepped spillways.” CIRIA, 33, 2nd edition, London, UK.

Fael, C. (2000). “Escoamento em quedas sucessivas: Ocorrência e dissipação de energia.” MSc. Thesis, Instituto Superior Técnico, Lisbon, Portugal (in Portuguese).

Felder, S., and Chanson, H. (2009). “Energy dissipation, flow resistance, and gas liquid interfacial area in skimming flows on moderate-slope stepped spillways.” Environmental Fluid Mechanics, 9(4), 427-441.

Frizell, K. H. (1992). “Hydraulics of stepped spillways for RCC dams and dam rehabilitation.” Proc. 3rd Specialty Conference in Roller Compacted Concrete, ASCE, San Diego CA, USA, 423-439.

Frizell, K. H. (2004). “Protection against overtopping in earthfill dams. Brief overview of technologies.” Proc. 1as Jornadas Técnicas Sobre Aliviaderos No Convencionales, SEPREM, Madrid, Spain.

Gaston, M. (1995). “Air entrainment and energy dissipation on a stepped block spillway. ” M.Sc. thesis, Colorado State University (CSU), Fort Collins, Colorado, USA.

Geringer, J. J. (1995). “The design and construction of RCC dams in Southern Africa.” Proc. Int. Symposium on RCC Dams, Santander, Spain, 1459-1495.

Geringer, J. J. and Officer, A. K. (1995). “Stepped spillway hydraulic research for RCC dams – Quo vadis?” Proc. Int. Symposium on RCC Dams, Santander, Spain, 549-563.

Gomes, J. F. (2006). “Campo de pressões: Condições de incipiência à cavitação em vertedouros em degraus com declividade 1V:0,75H.” Ph.D. thesis, UFRGS, Porto Alegre, Brazil (in Portuguese).

Gonzalez, C. (2005). “An experimental study of free-surface aeration on embankment stepped chutes.” Ph.D. thesis, University of Queensland, Brisbane, Australia.

Gonzalez, C. and Chanson, H. (2007). “Hydraulic design of stepped spillways and downstream energy dissipators for embankment dams.” Dam Engineering, 17(4), 223-244.

Goubet, A. (1992). “Evacuateurs de crues en marches d’escalier.” La Houille Blanche, 2/3, 159-162 (in French).

Guangtong, H. and Xiankang (1995). “The integral RCC dam design characteristics and optimization of its energy dissipater in Shuidong Hydropower Station”. Proc. Int. Symposium on RCC Dams, Santander, Spain, 405-412.

Guo, J., Liu, Z., Liu, J. and Lu, Y. (2003). “Field observation on the RCC stepped spillways with the flaring pier gate on the Dachaoshan project”. Proc. 30th IAHR Congress, Theme D, IAHR, Thessaloniki, Greece, 703-710. (In CD.)

Guo, J., Wu, Y., Zhang, D., Liu, J. and Sun, S. (2006). “Recent achievements on the hydraulic research in IWHR”. Proc. ISHS, IAHR, Ciudad Guayana, Venezuela, 54-ATO-G2102. (In CD.)

Haddad, A. A. (1998). “Water flow over stepped spillway. ” M.Sc. thesis, Politecnico di Bari, Bari, Italy.

Hager, W., and Boes, R. M. (2000). “Backwater and drawdown curves in stepped spillway flow.” Proc. 1st Int. Workshop on Hydraulics of Stepped Spillway, Zurich, Switzerland, A. A. Balkema Publisher, Rotterdam, The Netherlands, 129-136.

Hakoishi, N. and Sumi, T. (2000). “Hydraulic design of Nakasujigawa dam stepped spillway.” Proc. 1st Int. Workshop on Hydraulics of Stepped Spillway, Zürich, Switzerland, A.A. Balkema Publisher, Rotterdam, The Netherlands, 27-34.

Hansen, K.D. and Bass, R. (1999). “How old dams are reborn”. Intl. Water Power & Dam Construction, June, 40-45.

Higgs, J., and Frizell, K. W. (2004). “Investigation of the Lake Plant Pump Station - Lower Colorado River Authority.” Hydraulic Laboratory Report HL-2004-02, Denver Technical Center, Bureau of Reclamation, United States Department of the Interior, Denver, Colorado, December, 2004.

Ho, D. K. H., Cooper, B. W., Riddette, K. M., and Donohoo, S. M. (2006). "Application of numerical modelling to spillways in Australia." Dams and Reservoirs, Societies and Environment in the 21st Century, Berga et al. (Ed.), Taylor & Francis Group, London, UK.

Hollingworth, F. and Druyts, F. H. W. (1986). "Rollcrete: some applications to dams in South Africa." Water Power & Dam Construction, 38(1), 13-16.

Houston, K. L. (1987). "Hydraulic model studies of Upper Stillwater dam stepped spillway and outlet works." Report nº REC-ERC-87-6, U.S. Department of Interior, Bureau of Reclamation, Denver, USA.

Hunt, S. L., Kadavy, K. C., Abt, S. R., Temple, D. M. (2008) "Impact of converging chute walls for roller compacted concrete stepped spillways." J. Hydr. Eng., ASCE, 134(7), 1000-1003.

ICOLD (2000). "State-of-the-art of roller-compacted concrete dams". Bulletin CIRC 1599 (Draft), Version 4.1, Dec.

Johnson, M. C., and Savage, B. M. (2006). "Physical and numerical comparison of flow over ogee spillway in the presence of tailwater." J. Hydr. Eng., ASCE, 132(12), 1353-1357.

Kells, J. A. (1995). "Discussion on 'Comparison of energy dissipation between nappe and skimming flow regimes on stepped chutes.' by Chanson" J. Hydr. Res., IAHR, 33(1), 128-133.

Mateos, I. and Elviro, G. (1992). "The use of stepped spillways in energy dissipation". Proc. Intl Symposium on Dams and Extreme Floods. ICOLD, Spanish National Committee, Granada (Spain), 241-265.

Mateos, I. and Elviro, G. (1997). "Initiation of aeration in stepped spillways". Proc. 27th IAHR Intl Congress, Theme D, San Francisco, USA, 589-594. (In CD.)

Matos (1999). "Emulsionamento de ar e dissipação de energia do escoamento em descarregadores em degraus." Ph.D. thesis, IST, Lisbon, Portugal (in Portuguese).

Matos, J. (2000). "Hydraulic design of stepped spillways over RCC Dams." Proc. 1st Int. Workshop on Hydraulics of Stepped Spillway, Zürich, Switzerland, A.A. Balkema Publisher, Rotterdam, The Netherlands, 187-194.

Matos, J. (2001). "Discussion on 'Onset of skimming flow on stepped spillways.' by Chamani and Rajaratnam", J. Hydr. Eng., ASCE, 118(7), 519-521.

Matos, J. and Meireles, I. (2006). "Estudo detalhado sobre descarregadores de cheias em degraus de betão compactado por cilindros aplicado a barragens de betão e de aterro. Relatório final - Parte II: Barragens de aterro." Cehidro Report, Contract 2003/029/INAG, Lisbon, Portugal (in Portuguese).

Matos, J. and Quintela, A. (1997). "Escoamento em quedas sucessivas em descarregadores em degraus. Dissipação de energia". Simpósio sobre Aproveitamentos Hidroeléctricos, APRH, Lisbon, Portugal (in Portuguese).

McKenna, B. W. (2001). "Air-water gas transfer on stepped spillways." M.Sc. Thesis, Colorado State University, USA.

McLean, F. G. and Hansen, K. D. (1993). "Roller compacted concrete for embankment overtopping protection." Geotechnical Practice for Dam Rehabilitation, ASCE, New York, USA.

Meireles, M. (2004). "Caracterização do escoamento deslizante sobre turbilhões e energia específica residual em descarregadores de cheias em degraus." M.Sc. thesis, IST, Lisbon, Portugal (in Portuguese).

Meireles, I., Matos, J., and Melo, J. F. (2005). "Pressure head and residual energy in skimming flow on steeply sloping stepped spillways." Proc. 31th IAHR Congress, Theme D, 2654-2663, Seoul, South Korea. (In CD.)

Meireles, I., Matos, J. and Melo, J. F. (2006). "Skimming flow properties upstream of air entrainment inception on steeply sloping stepped chutes. " Proc. Intl Symposium on Hydraulic Structures, IAHR, Ciudad Guayana, Venezuela. (In CD.)

Melo, J. F. (2004). Personal communication.

Morris, H.M. (1955)*. "A new concept of flow in rough conduits." Transactions, ASCE, 120, 373-410.

Morris, H.M. (1961)*. "Design methods for flow in rough conduits." Transactions, ASCE, 126, Part 1, 454-490.

Ohtsu, I. and Yasuda, Y. (1997a). "Characteristics of flow conditions on stepped channels." Proc. 27th IAHR Congress, San Francisco, USA. (In CD.)

Ohtsu, I. and Yasuda, Y. (1997b). "Characteristics of flow conditions on stepped channels." Notes of the presentation to the 27th IAHR Congress, San Francisco, USA, courtesy of Youichi Yasuda.

Ohtsu, I., Yasuda, Y. and Takahashi, M. (2004). "Flow characteristics of skimming flows in stepped channels." J. Hydr. Eng., ASCE, 130(9), 860-869.

Paxson, G., and Savage, B. (2006). "Labyrinth spillways: comparison of two popular U.S.A. design methods and consideration of non-standard approach conditions and geometries." Proc. Int. Junior Researcher and Engineer Workshop on Hydraulic Structures, J. Matos and H. Chanson (Ed.), Report CH61/06, Div. of Civil Eng., The University of Queensland, Brisbane, Australia (ISBN 1864998687).

Pegram, G., Officer, A. and Mottram, S. (1999). "Hydraulics of skimming flow on modeled stepped spillways." J. Hydr. Eng., ASCE, 125(4), 361-368.

Peyras, L.; Royet, P. and Degoutte, G. (1991). "Ecoulement et dissipation sur les déservoirs en gradin de gabions." La Houille Blanche, 1, 37-47 (in French).

Peyras, L.; Royet, P. and Degoutte, G. (1992). "Flow and energy dissipation over gabion weirs." J. Hydr. Eng., ASCE, 118(5), 707-717.

Pinheiro, A. N. and Fael, C. S. (2000). “Nappe flow in stepped channels-occurrence and energy dissipation.” Proc. 1st Int. Workshop on Hydraulics of Stepped Spillway, Zürich, Switzerland, A.A. Balkema Publisher, Rotterdam, The Netherlands, 119-126.

Rajaratnam, N. (1990). “Skimming flow in stepped spillways.” J. Hydr. Eng., ASCE, 116(4), 587-591.

RCC Dams (2003). “Water Power & Dam Construction Yearbook 2003.” Water Power & Dam Construction, 239-245.

RCC DAMS (2005). “Water Power & Dam Construction Yearbook 2005. ” Water Power & Dam Construction, 284-293.

Relvas, A. T. and Pinheiro, A. N. (2008). "Inception point and air concentration in flows on stepped chutes lined with wedge-shaped concrete blocks." J. Hydr. Eng., ASCE, 134(8), 1042-1051.

Renna, F. (2004). “Caratterizzazione fenomenologica del moto di un fluido bifasico lungo scaricatori a gradini.” Ph.D. thesis, Politecnico di Bari, Cosenza, Italy (in Italian).

Sanagiotto, D. (2003). “Características do escoamento sobre vertedouros em degraus de declividade 1V:0,75H.” M.Sc. thesis, UFRGS, Porto Alegre, Brazil (in Portuguese).

Sánchez-Juny, M. (2001). “Comportamiento hidráulico de los aliviaderos escalonados en presas de hormigón compactado. análisis del campo de presiones.” Ph.D. thesis, UPC, Barcelona, Spain (in Spanish).

Savage, B. M., and Johnson, M. C. (2001). “Flow over ogee spillway: physical and numerical model case study.” J. of Hydr. Eng., ASCE, 127(8), 640-649.

Savage, B., Frizell, K., and Crowder, J. (2004). “Brains versus brawn: the changing world of hydraulic model studies.” Proc. 2004 Annual Conference, Association of State Dam Safety Officials (ASDSO). Phoenix, USA.

Song, C. C. S., and Zhou, F. (1999). “Simulations of free surface flow over spillway.” J. Hydr. Eng., ASCE, 125(9), 959-967.

Sorensen, R. (1985). “Stepped spillway hydraulic model investigation.” J. Hydr. Eng., ASCE, 111(12), 1461-1472.

Stephenson, D. (1988). “Stepped energy dissipators.” Proc. Int. Symp. on Hydraulics for High Dams, IAHR, Beijing, China, 1228-12-35.

Tabbara, M., Chatila, J., and Awwad, R. (2005). “Computational simulation of flow over stepped spillways.” Computers & Structures, Elsevier, 83, 2215-2224.

Talbot, J. R.; Robinson, K. M. and Kavady, K. C. (1997). “Hydraulic model study of a compacted concrete stepped spillway with converging chute walls.”. Proc. Association of State Dam Safety Officials Annual Conference, Pittsburg, USA, September. Accessed in 2004, July 30th to URL<http://www.pswcrl.ars.usda.gov/hydpubs/hpsum170.htm.

Toombes, L., and Chanson, H. (2000). “Air-water flow and gas transfer at aeration cascades: a comparative study of smooth and stepped chutes.” Proc. 1st Int. Workshop on Hydraulics of Stepped Spillway, Zürich, Switzerland, A.A. Balkema Publisher, Rotterdam, The Netherlands, 77-84.

Tozzi, M. J. (1992). “Caracterização/comportamento de escoamentos em vertedouros com paramento em degraus.” Ph.D. thesis, Escola Politécnica da Universidade de S. Paulo, Brazil (in Portuguese).

Tozzi, M. J. (1994). “Residual energy in stepped spillways”. Water Power & Dam Construction, May, 32-34.

Unami, K., Kawachi, T., Babar, M. M., and Itagaki, H. (1999). “Two-dimensional numerical model of spillway flow.” J. Hydr. Eng., ASCE, 125(4), 369-375.

Wark, R. J., Kerby, N. E. and Mann, G. B. (1991). “New Victoria dam project.” ANCOLD Bulletin, 88, August, 14-32.

Yasuda, Y. and Chanson, H. (2003). “Micro- and macro-scopic study of two-phase flow on a stepped chute.” Proc. 30th IAHR Intl Congress, Thessaloniki, Greece, 695-702. (In CD.)

Yasuda, Y. and Othsu, I. (1999). "Flow resistance in skimming flow stepped channels", Proc. 28th IAHR Congress, Theme B, B 14, Graz, Austria. (In CD.)

Yasuda, Y., and Ohtsu, I. (2003). “Effect of step cavity area on flow characteristics of skimming flows on stepped chutes.” Proc. 30th IAHR Int. Congress, Thessaloniki, Greece, 703-710. (In CD.)

Yasuda, Y., Takahashi, M. and Ohtsu, I. (2001). “Energy dissipation of skimming flows on stepped-channel chutes.” Proc. 29th IAHR Congress, Theme D, Beijing, China, 531. (In CD.)

Yasuda, Y., Takahashi, M., and Ohtsu, I. (2004). “Discussion of 'Volume of fluid model for turbulence numerical simulation of stepped spillway overflow.' by Chen et al.” J. Hydr. Eng., ASCE, 130(2), 170.

Ye, M., Wu, C., Chen, Y., and Zhou, Q. (2006). “Case study of an s-shaped spillway using physical and numerical models.” J. Hydr. Eng., ASCE, 132(9), 892-898.

*article not directly read.

Chapter 2

Experimental set-ups and instrumentation

2.1 INTRODUCTION

The present dissertation takes advantage of the large amount of data collected by Matos (1999), Meireles (2004) and Renna (2004) in a steep stepped channel located at the Laboratório Nacional de Engenharia Civil (LNEC), of data acquired by André and Ramos (2003) and Cabrita (2007) in a moderate slope stepped channel built at the Laboratório de Hidráulica e Recursos Hídricos of Instituto Superior Técnico (IST), and of data acquired in the framework of this dissertation in the stilling basin of the steep stepped channel in LNEC.

Subchapters 2.2 and 2.3 describe the LNEC experimental facility and the IST experimental facility, respectively. A description of the used instrumentation is also presented.

2.2 EXPERIMENTAL FACILITY AT LNEC

2.2.1 Experimental facility and instrumentation

The experimental facility assembled at the Water Resources and Hydraulic Structures Division of the National Laboratory for Civil Engineering (Laboratório Nacional de Engenharia Civil - LNEC), Portugal, is composed by an uncontrolled weir, a stepped channel, a horizontal stilling basin and a recirculation system (Figs 1 and 2).

The facility is supplied from an elevated reservoir by a pipe diameter 350 mm. The discharge is adjusted by a globe valve and the maximum allowed discharge is about 220 l/s. The volume flow rate was measured with the help of a Bazin weir located downstream of the stilling basin and tests were carried out for unit discharges ranging from 0.05 to 0.20 m^2/s, corresponding to the skimming flow regime.

The stepped channel is 2.90 m high (from crest to toe), 1.00 m wide and has a slope of 1V:0.75H (53 degrees from horizontal). The upstream end of the ogee crest is smooth, followed by variable size steps (two 0.5 cm, two 1.0 cm, five 2.0 cm and one 4.0 cm high) to adopt a profile identical to that proposed by the Waterways Experiment Station (WES), U. S. Army Corps of Engineers (Fig. 1). The design head is H_0 = 0.20 m and corresponds to a unit discharge, q_0, of 0.20 m^2/s for a discharge coefficient, C_0, equal to 0.5. (The stage discharge curve in a WES ogee crests is given by $Q_0 = C_0 b\sqrt{2g}H_0^{3/2}$, where b is the channel width and g is the acceleration of gravity.) This last value was obtained according to the results presented by Abecasis (1977) (in Quintela 1998) for WES ogee crests. Downstream, the constant slope region was tested for step heights, h, of 2, 4 and 8 cm.

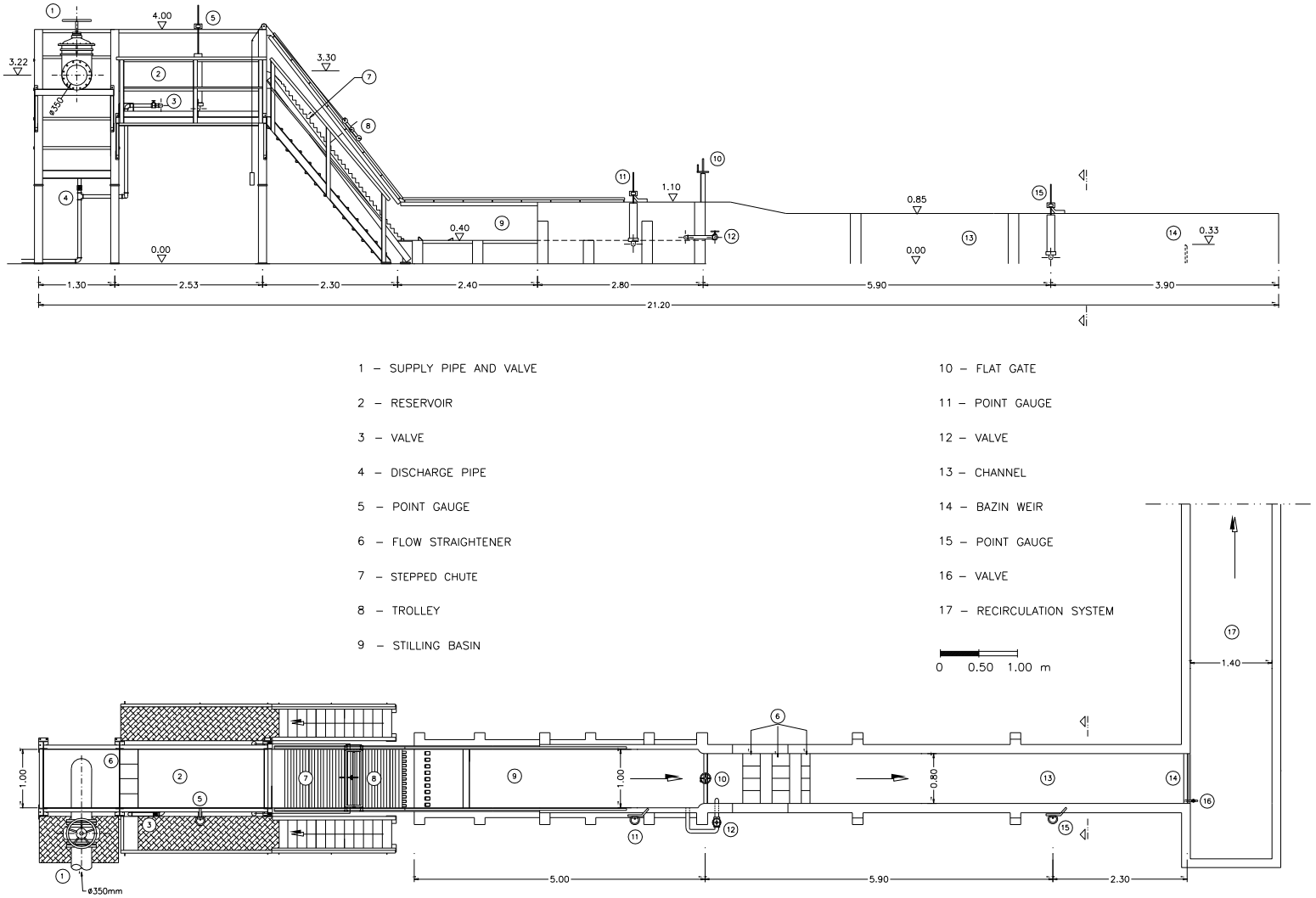

Figure 1 - Scheme of the experimental facility at LNEC for 0.04 m high steps (adapted from Matos 1999).

Figure 2 - Experimental facility at LNEC: stepped channel and stilling basin (view from downstream).

A conductivity probe and a back-flushing Pitot tube, both developed and calibrated by the U.S. Bureau of Reclamation, were used to measure local time-averaged air concentration and water velocity (Figs 3 and 4). The local air concentration, C, is defined herein as the volume of air devided by the total volume of air and water.

a) b)

Figure 3 - Instrumentation developed by the U.S. Bureau of Reclamation to measure air concentration: a) conductivity probe inside the non-aerated flow; b) electronic device for detection of air and computer showing the polarization curves.

a) b)

Figure 4 - Instrumentation developed by the U.S. Bureau of Reclamation to measure water velocity: a) differential pressure transducer; b) Pitot tube.

The work principle of the conductivity probe is based on the difference between electric resistivity of air and water. When any of the two 0.2 mm diameter platinum wires is in contact with air, the electric current is interrupted. Air concentration is then defined as the percentage of time any wire (or both simultaneously) is in contact with air, relatively to the total acquisition time. In the back-flushing Pitot tube, total and static pressure heads were measured through holes with diameters of 1.0 and 0.5 mm, respectively. Continuous back-flushing of the Pitot tube was provided in order to avoid an erroneous measurement of the water velocity with entrance of air in the Pitot tube. The static pressure and the total head ports of the Pitot tube were fed by water from a reservoir with constant head, where the back-flushing flow rate to each port was controlled by needle valves. The output signal of the instrumentation was scanned at 30 kHz for 90 s with a posterior filtration to 30 Hz, to save memory and facilitate storage. The instrumentation was mounted in a trolley and the accuracy for the vertical position was of 0.1 mm. The error in the longitudinal and transverse positions was estimated as being less than 5 mm and less than 1 mm, respectively.

In the smooth ogee crest, where the free-surface is observed to be virtually smooth, the water depth was measured in the chute centerline with the help of two point gauges located at the upstream end of the crest and immediately upstream of the first step of the spillway, respectively. Downstream, the equivalent clear-water depth data was obtained from

$$d = \int_0^{Y_\varphi} (1 - C)\, dy \qquad (1)$$

where Y_φ is the depth where the air concentration is φ%, assumed equal to 90% in the present study, as usually considered (e.g., Matos 2000; Chanson 2002; Boes and Hager 2003), and y is the transverse coordinate originating at the pseudo-bottom (the pseudo-bottom is defined as the surface tangent to consecutive step edges). The equivalent clear-water depth represents a fictitious flow depth which would exist if in presence of no free-surface waviness nor air bubbles inside the flow.

The water velocity was obtained from

$$V = \sqrt{\frac{2\,\Delta P}{\rho_w\,(1 - C)}} \qquad (2)$$

where ΔP is the difference between the total pressure head and the static pressure head, measured with the back-flushing Pitot tube and ρ_w is the water density. However, near the free-surface, the waves leave the instrumentation uncovered for some moments during the total time of acquisition. Due to the high frequency of the free-surface waves, as opposed to the time response of the back-flushing Pitot tube, it is not possible to obtain reliable velocity results in this zone (Matos et al. 2002).

Downstream of the stepped channel, the stilling basin is 5.00 m long and 1.00 m wide, with exception to the last 0.20 m where the width decreases gradually to 0.80 m. At the downstream end of the stilling basin a sluice gate allows for the definition of the hydraulic jump location inside the basin, and 40 piezometric taps connected to a piezometric panel allow pressure measurements. Figure 5 presents the location of the pressure taps in the floor of the stilling basin and Figure 6 shows a photograph of the piezometric panel.

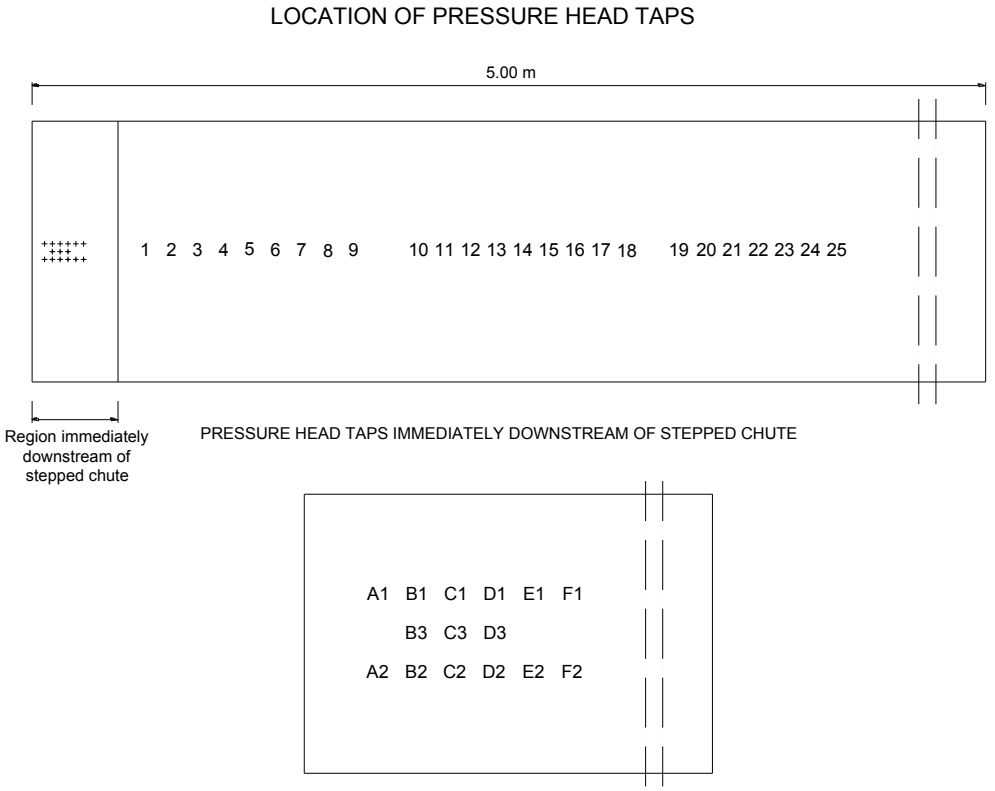

Figure 5 - Pressure head taps located in the stilling basin floor.

Figure 6 - Piezometric panel.

Appurtenances have been designed based on the USBR recommendations for type III basins (Figs 7 and 8). Calculations were done based in basin inflow conditions determined from empirical expressions developed by Meireles (2004) for stepped spillways.

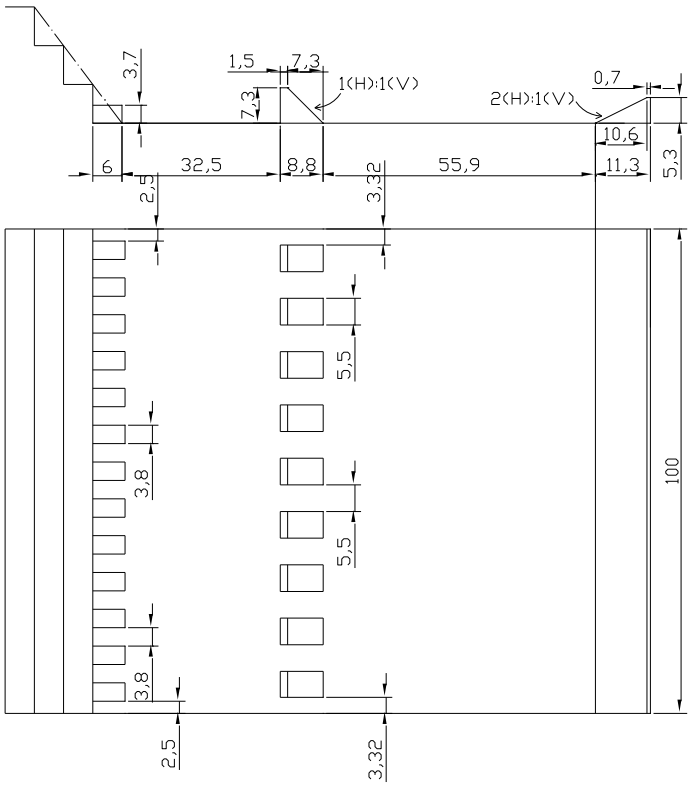

Figure 7 - Sketch of the stilling basin downstream of the stepped channel designed based on the USBR recommendations for type III basins (dimensions in cm).

a) b)

Figure 8 - Stilling basin downstream of the stepped channel designed based on the USBR recommendations for type III basins: a) general view; b) hydraulic jump for q_w = 0.140 m^2/s.

The piezometric taps were used to obtain pressure head values along the basin. Mean flow depths were measured by visual observation through the basin sidewall rulers.

Measurements along the stilling basin were collected for a range of discharges corresponding to the skimming flow regime over the approaching chute.

Further details of the facility and instrumentation can be obtained in Matos and Frizell (1997; 2000), Matos (1999), Meireles (2004) and Renna (2004).

2.2.2 Data

Experimental data presented and analyzed in this dissertation and pertaining to the steep stepped channel at LNEC were acquired by Matos (1999), Meireles (2004) and Renna (2004). At the stilling basin installed with appurtenances designed based on the USBR recommendations for type III basins, the data were acquired in the framework of this dissertation.

Table 1 presents a summary of the experimental conditions presented in this study pertaining to the steep stepped channel at LNEC.

Table 1 – Summary of the experimental conditions presented in this study pertaining to the steep stepped channel at LNEC.

Model	Slope (º)	h (m)	q_w (m^2/s)	d_c/h (-)	Ref.
A	53.1	0.02	0.100	5.0	Renna (2004)
			0.140	6.3	
			0.200	8.0	
B	53.1	0.04	0.050	1.6	Meireles (2004)
			0.080	2.2	Meireles (2004) & Present study
			0.100	2.5	Renna (2004) & Present study
			0.140	3.1	Meireles (2004) & Present study
			0.180	3.7	
			0.200	4.0	Renna (2004) & Present study
C	53.1	0.08	0.080	1.1	Matos (1999) & Present study
			0.100	1.3	
			0.140	1.6	
			0.180	1.9	
			0.200	2.0	

Note: h - step height; q_w – water discharge per unit width and d_c/h – critical depth normalized by the step height.

2.3 EXPERIMENTAL FACILITY AT IST

2.3.1 Experimental facility and instrumentation

The experimental facility assembled at the Laboratory of Hydraulics and Water Resources (LHWR), IST, Technical University of Lisbon, Portugal, was composed by an uncontrolled broad-crested weir, a stepped channel, a horizontal stilling basin and a recirculation system (Fig. 9 and 10). The original flume was used by Fael (2000) and further readapted for the subsequent studies of André and Ramos (2003) and Cabrita (2007).

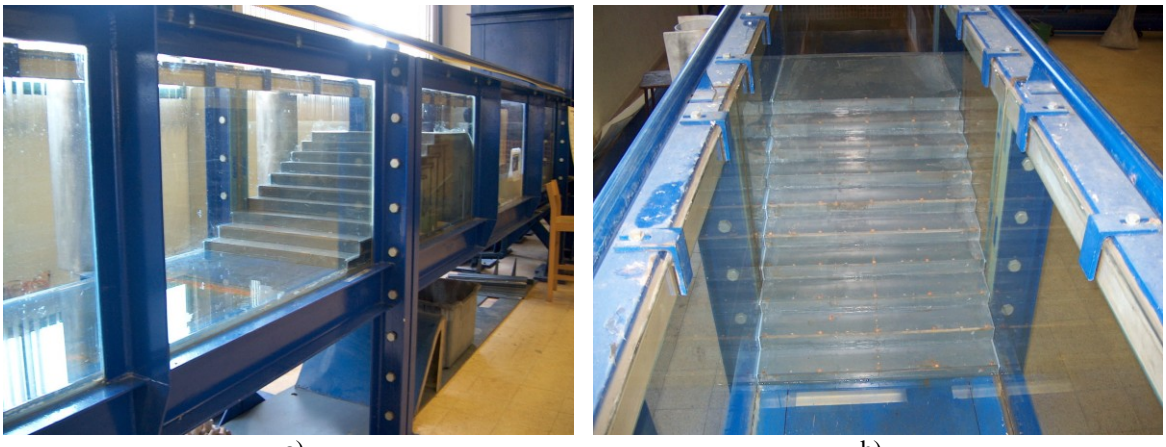

a) b)

Figure 9 - Experimental facility at IST: stepped channel with steps 0.05 m high (André and Ramos 2003).

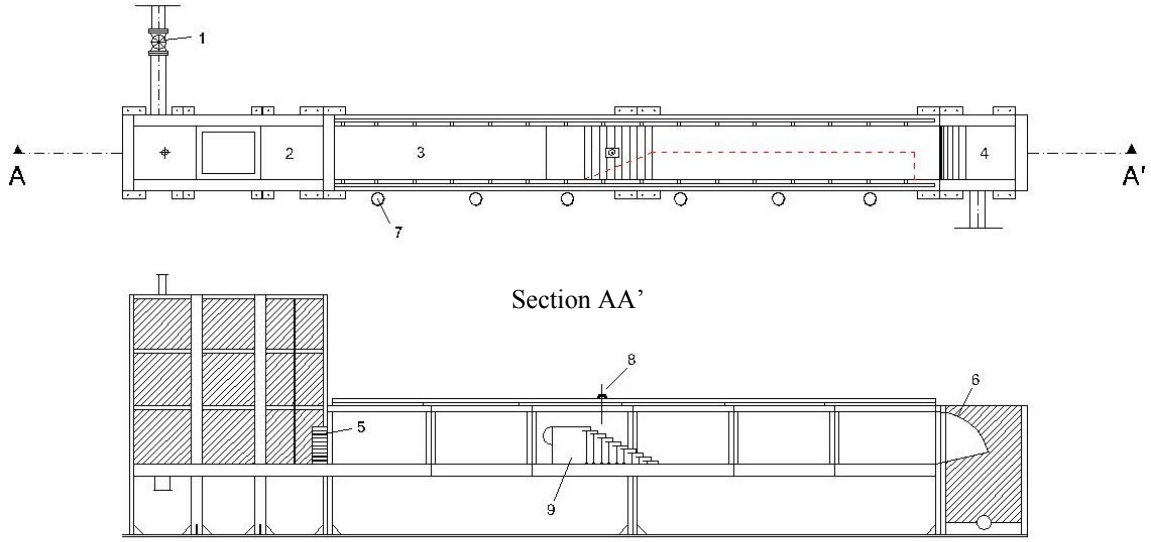

Figure 10 - Experimental facility at IST: scheme of the broad-crested weir, stepped channel for steps 0.05 m high, stilling basin and recirculation system (adapted from André and Ramos 2003).

The tested straight rectangular channel is 0.70 m wide and contains the broad-crested weir and the stepped channel, PVC made. The weir is 0.5 m long, 0.5 m high and incorporates a semi-circular upstream corner to reduce flow separation at the entrance. From the hydraulic point of view, the weir is long enough to be classified as broad-crested (Chow 1959; Hager and Schwalt 1994), ensuring that critical flow conditions occur at the crest for all measured flow rates. The chute has a slope of 1V:2H (26.6º from horizontal) and the data presented herein respects to step heights (h) of 0.025 and 0.050 m.

The experimental facility is fed from the general reservoir of the LHWR and the discharge was measured with an electromagnetic flowmeter installed in the supply pipe, diameter 200 mm (Fig. 11). The discharge is adjusted by a globe valve and the maximum allowed discharge is about 75 l/s. Tests were carried out for unit discharges ranging from 0.03 to 0.08 m^2/s, corresponding to the skimming flow regime.

The channel ends in a bottom-hinged flap gate allowing for the definition of the water depth at the stilling basin downstream of the stepped channel.

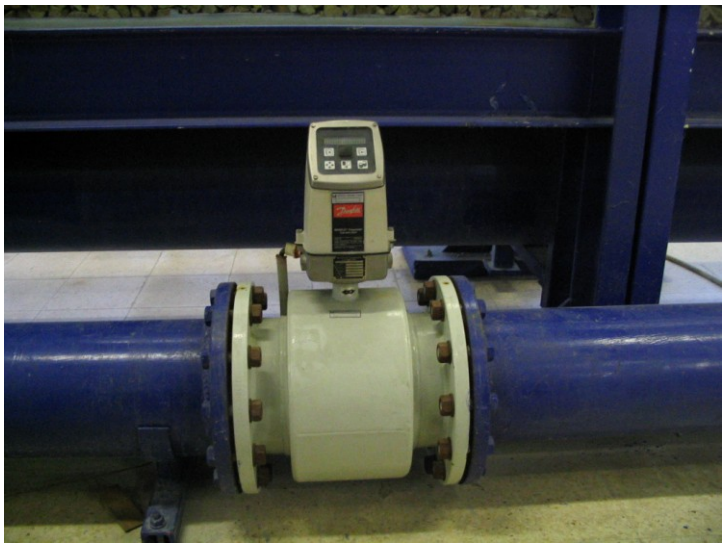

Figure 11 - Electromagnetic flowmeter (André and Ramos 2003).

A Prandtl-Pitot tube with 8 mm external diameter (Fig. 12) and a point gauge with a reading accuracy of ± 0.1 mm (Fig. 13) were respectively used for measuring velocity and equivalent clear-water depths at several cross sections, in the non-aerated flow region. The instrumentation was mounted in a trolley and the error in the longitudinal, transverse and vertical positions were estimated as being less than 5.0, 1.0 and 0.1 mm, respectively. The discharge obtained from the flowmeter was compared to that obtained experimentally from the integration of the velocity profile. In practically all tests, the relative differences were found to be lower than 8%, and the average value was lower than 5%. Flow depth was also determined by visual observation of rulers fixed in both sidewalls of the chute.

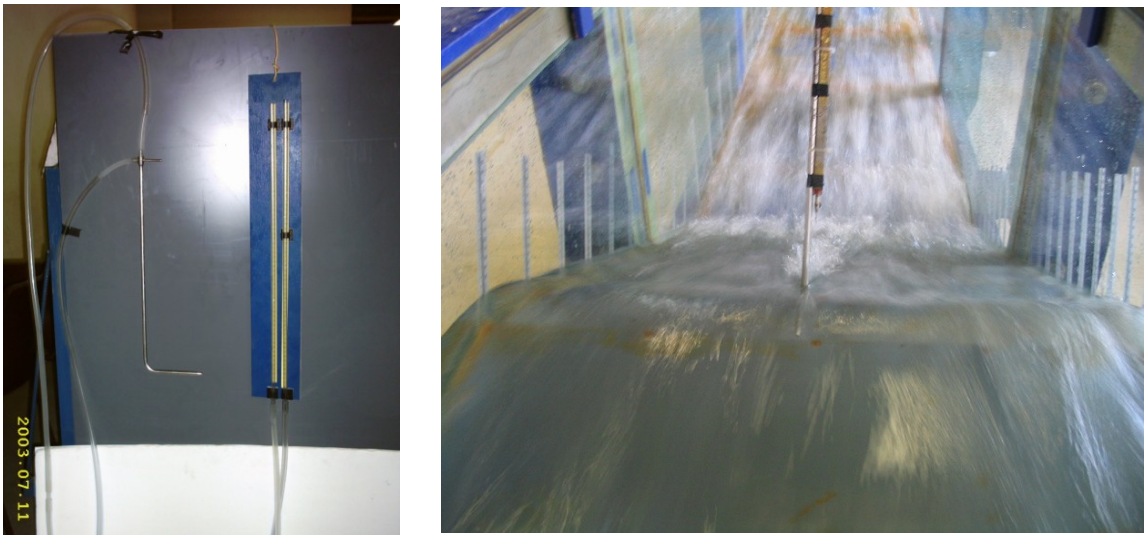

a) b)

Figure 12 - Instrumentation for velocity measurements (Prandtl-Pitot tube): a) Prandtl-Pitot tube and system for measuring total and piezometric heads (André and Ramos 2003); b) during data acquisition in the chute (Cabrita 2007).

a) b)

Figure 13 - Instrumentation for water depth measurements (André and Ramos 2003).

Further details of the facility and instrumentation can be obtained in André and Ramos (2003) and Cabrita (2007).

2.3.2 Data

In Fael (2000) the study was focused on the nappe flow which is out of the framework of the present dissertation. Experimental data presented and analyzed in this dissertation and pertaining to the moderate slope stepped channel at IST were acquired by André and Ramos (2003) and Cabrita (2007).

Table 2 presents a summary of the experimental conditions presented in this study pertaining to the moderate slope stepped channel at IST.

Table 2 – Summary of the experimental conditions presented in this study pertaining to the moderate slope stepped channel at IST.

Model	Slope (°)	h (m)	q_w (m^2/s)	d_c/h (-)	Ref.
D	26.6	0.025	0.03-0.07	1.8-3.2	André and Ramos (2003)
E	26.6	0.050	0.04-0.08	1.1-1.7	André and Ramos (2003) & Cabrita (2007)

Note: h - step height; q_w – water discharge per unit width; and d_c/h – critical depth normalized by the step height.

REFERENCES

Abecasis (1977). “The behaviour of spillway crests under flows higher than the design flow.” Proc. 19th IAHR Congress, Baden-Baden, Vol. 4, 559-566.

André, M. and Ramos, P. (2003). “Hidráulica de descarregadores de cheia em degraus: aplicação a descarregadores com paredes convergentes.” Graduate Research Report, IST, Lisbon, Portugal (in Portuguese).

Boes, R. M. and Hager, W. H. (2003). “Two phase flow characteristics of stepped spillways.” J. Hydr. Eng., ASCE, 129(9), 661-670.

Cabrita, J. (2007). “Caracterização do escoamento deslizante sobre turbilhões em descarregadores de cheias em degraus com paredes convergentes.” MSc thesis, IST, Lisbon, Portugal (in Portuguese).

Chanson, H. (2002). “The hydraulics of stepped chutes and spillways.” Balkema, Lisse, The Netherlands.

Chow, V. T. (1959). “Open-channel hydraulics.” McGraw-Hill, New York, USA.

Fael, C. (2000). “Escoamento em quedas sucessivas: ocorrência e dissipação de energia.” MSc thesis, IST, Lisbon, Portugal (in Portuguese).

Hager, W. and Schwalt, M. (1994). “Broad crested weirs.” J. of Irrigation and Drainage Eng., ASCE, 120(1), 13-26.

Matos (1999). "Emulsionamento de ar e dissipação de energia do escoamento em descarregadores em degraus." Ph.D. thesis, IST, Lisbon, Portugal (in Portuguese).

Matos, J. (2000). “Hydraulic design of stepped spillways over RCC dams.” Proc. 1st Int. Workshop on Hydraulics of Stepped Spillway, Zürich, Switzerland, A.A. Balkema Publisher, Rotterdam, The Netherlands, 187-194.

Matos, J., and Frizell, K. W. (1997). “Air concentration measurements in highly turbulent aerated flow”. Proc. 27th IAHR Congress, Theme D, Vol. 1, San Francisco, USA, S. S. Y. Wang and T. Carstens (eds.), 149-154.

Matos, J. and Frizell, K. H. (2000). “Air concentration and velocity measurements on self-aerated flow down stepped chutes.” Proc. ASCE 2000 Conference, Minneapolis, USA.

Matos, J., Frizell, K. H., André, S., and Frizell, K. W. (2002). “On the performance of velocity measurement techniques in air-water flows”. Proc. EWRI/IAHR Joint Conference on Hydraulic Measurements & Experimental Methods, ASCE, Estes Park, USA. (In CD.)

McKenna, B. W. (2001). “Air-water gas transfer on stepped spillways.” M.Sc. thesis, Colorado State University, USA.

Meireles, M. (2004). “Emulsionamento de ar e dissipação de energia do escoamento em descarregadores em degraus.” M.Sc. thesis, IST, Lisbon, Portugal (in Portuguese).

Quintela, A. (1998). “Hidráulica. ” 6th edition, Fundação Calouste Gulbenkian eds (in Portuguese).

Renna, F. (2004). “Caratterizzazione fenomenologica del moto di un fluido bifasico lungo scaricatori a gradini.” Ph.D. thesis, Politecnico di Bari, Cosenza, Italy (in Italian).

Chapter 3

Mathematical model

3.1 GENERAL MATHEMATICAL MODEL

The mathematical model is based upon the mixture equations for an air-water flow. Buscaglia et al. (2002), Bombardelli (2003, 2004), Bombardelli et al. (2007), and Bombardelli and Jha (2009) are followed in employing equations for a dilute mixture. The equations can be obtained via two consecutive averaging procedures (Crowe et al. 1998; Prosperetti and Tryggvason 2007): 1) an ensemble averaging, which basically addresses the bubble-to-bubble distance, and b) a turbulence averaging, which addresses turbulence scales larger than the inter-bubble distance (Bombardelli 2004). Length scales of turbulence range from the Kolmogorov length scale to the largest scales of the flow (dictated by the flow depth or width; see Gioia and Bombardelli 2002). It is believed that the length and time scales associated with the ensemble average are smaller than the intermediate to large scales pertaining to turbulence (Buscaglia et al. 2002; Bombardelli 2004; Bombardelli et al. 2007; Bombardelli and Jha 2009). Consequently, it is believed that the ensemble average represents only scales of the order of the bubble-to-bubble distance. Other authors have interpreted the ensemble average assuming that it considers all length scales (Drew and Passman 1999). Considering the hypothesis that the ensemble average does not consider all length scales, it is understood that an additional turbulence (time) average of the equations is necessary, to account for the intermediate and large scales of turbulence (see also Hrenya and Sinclair 1997; and discussion in Chapter 8 of Prosperetti and Tryggvason 2007 on the nature of the averaging procedures). The models have naturally the single-phase flow as a special case.

The mixture equations for a 3-D dilute and incompressible flow are as follows:

$$\frac{\partial u_{m_i}}{\partial x_i} = 0 \tag{1}$$

$$\rho_0 \left[\frac{\partial u_{m_i}}{\partial t} + \frac{\partial \left(u_{m_i} u_{m_j} \right)}{\partial x_j} \right] = -\frac{\partial p}{\partial x_i} + \mu \frac{\partial^2 u_{m_i}}{\partial x_j{}^2} - \rho_0 B_i \tag{2}$$

where u_{m_i} and u_{m_j} are the velocity components in the directions x_i and x_j; ρ_0 is the reference density; t is the time coordinate; p is the pressure, μ is the dynamic viscosity and B_i are the body forces components in the direction x_i. In the present problem, the body forces account only for gravity.

A transport equation for the air that entrains at the free-surface is also integrated in the mathematical model, as presented below

$$\frac{\partial C}{\partial t} + \nabla \cdot \left[\left(\underline{u}_m + \underline{W}_s \right) C \right] = \nabla \cdot \left(\underline{\underline{D}} \cdot \nabla C \right) \tag{3}$$

where C is the volumetric concentration of air; $\underline{W}_s$ is the slip-velocity vector (which points in the positive vertical direction); and $\underline{\underline{D}}$ denotes the air-diffusivity tensor.

To quantify the effect of turbulence, the parameters u_{m_i} and p are decomposed into mean and fluctuating parts, $u_{m_i} = \overline{u_{m_i}} + u'_{m_i}$ and $p_m = \overline{p_m} + p'_m$, where the overbars stand for mean and the primes for fluctuation. The mean quantities are defined as

$$\overline{u_{m_i}} = \frac{1}{\Delta t}\int_{t_0}^{t_1} u_{m_i}\, dt \quad , \quad \overline{p} = \frac{1}{\Delta t}\int_{t_0}^{t_1} p\, dt \tag{4}$$

and the averaging time $t_1 - t_0$ is long compared with the time scale of the turbulent motion (Rodi 1984). The subsequent averaged mixture equations are as follows

$$\frac{\partial \overline{u_{m_i}}}{\partial x_i} = 0 \tag{5}$$

$$\rho_0\left[\frac{\partial \overline{u_{m_i}}}{\partial t} + \frac{\partial\left(\overline{u_{m_i}}\,\overline{u_{m_j}}\right)}{\partial x_j}\right] = \rho_0 B_i + \mu\frac{\partial^2 \overline{u_{m_i}}}{\partial x_j{}^2} - \frac{\partial \overline{p}}{\partial x_i} - \frac{\partial \overline{u_{m_i}'u_{m_j}'}}{\partial x_j} \tag{6}$$

where $\overline{u_{m_i}}$ and $\overline{u_{m_j}}$ are the time–averaged mixture velocity components in the directions x_i and x_j; $\overline{p}$ is the time–averaged, modified pressure (Buscaglia et al. 2002; Rodi 1984); and u_{m_i}' and u_{m_j}' are the fluctuating mixture velocity components in the directions x_i and x_j. $-\rho\overline{u_{m_i}'u_{m_j}'}$ represent, physically, the transport of momentum due to the turbulent motion, acting as additional stresses on the fluid, being called Reynolds stresses. Although the equations are still exact, no more form a closed set, because of these additional unknown terms. Therefore, a turbulence model must be taken into account.

At last, the averaged transport equation for the air which is entrained at the free-surface is as follows:

$$\frac{\partial C}{\partial t} + \nabla\cdot\left[\left(\underline{\overline{u}}_m + \underline{W}_s\right)C\right] = \nabla\cdot\left(\underline{\underline{D}}\cdot\nabla C\right) \tag{7}$$

3.2 TURBULENCE MODELS

Turbulence can be defined as an unsteady and unpredictable flow with eddying motion, whose eddies have a wide spectrum of sizes. The large eddies extract kinetic energy from the mean motion, which is passed from scale to scale, until the viscous effects take place and dissipate the energy. The scale of these elements goes typically from the order of the flow domain extent until 10^{-3} times smaller (Rodi 1984).

In order to detect all the scales, in a numerical simulation, the grid has to be smaller than the smallest scale, which in three dimensions, implies at list 10^9 grid points to cover the entire domain (Rodi 1984). Direct Numerical Simulation (DNS) solves numerically all the relevant length scales of turbulence for what no turbulence modeling is needed. However, due to storage and simulation

time limitations, this resolution of the exact Navier-Stokes equations is still restricted to low Reynolds number flows. Contrarily to DNS, Large Eddy Simulation (LES) computes the large scales directly and models the small scales or the subgrid scales, solving the flow at a fraction of the cost of DNS, although still computationally demanding in most practical situations. (Note that, because turbulent kinetic energy is essentially obtained from the large scale turbulent motion, the resolution for large scales is the most important.) Comparing to LES, the Reynolds Average Navier-Stokes equations (RANS) resolve a smaller range of scales, modeling the others. However, the closure problem must be solved. In that regard, turbulence is treated using the Boussinesq model concept, which considers the Reynolds stresses to be proportional to the gradient of mean velocity, as follows (Rodi 1984):

$$-\rho_0 \overline{u_{m_i}' u_{m_j}'} = \mu_T \left(\frac{\partial \overline{u_{m_i}}}{\partial x_j} + \frac{\partial \overline{u_{m_j}}}{\partial x_i} \right) - \frac{2}{3} \rho_0 k \delta_{ij} \tag{8}$$

$$\mu_T = \rho_0 \, C_\mu \, \frac{k^2}{\varepsilon} \tag{9}$$

where μ_T is the eddy dynamic viscosity; and C_μ is a coefficient. k denotes in turn the turbulent kinetic energy (TKE), defined in this context as: $k = 1/2 \left(\overline{u_{m_i}' u_{m_i}'} \right)$; and ε is the dissipation rate of TKE. At last, δ_{ij} is the Kronecker delta ($\delta_{ij} = 1$ for $i = j$ and $\delta_{ij} = 0$ for $i \neq j$). (The Boussinesq model concept or eddy viscosity concept considers μ_T isotropic, since only one value is presented for all the different Reynolds stresses. Despite not completely true, was proved to be successful in many applications.)

Turbulence models based in the RANS can be divided in models of first-order closure (zero-, one- or two-equations models) and models of higher order. For the models of first-order closure, the main difference between models of different number of equations resides in the use or not of transport equations to determine the eddy viscosity. In the models of higher order, exact transport equations are derived for $\overline{u_{m_i}' u_{m_j}'}$, being obtained turbulence correlations of the next higher order which are then modeled to be obtained a closed system. The usual two-equations models, widely used, were proposed assuming several drastic assumptions to make the equations tractable and applicable to the most general hydraulic situations. However, for particular situations, some more complicated models have been proposed, for instance, to account for low Reynolds numbers, nonisotropic eddy viscosity or to be applied to flows were the mean-flow quantities vary very little in the vertical direction. Fig. 1 presents a resume of the most known turbulence models.

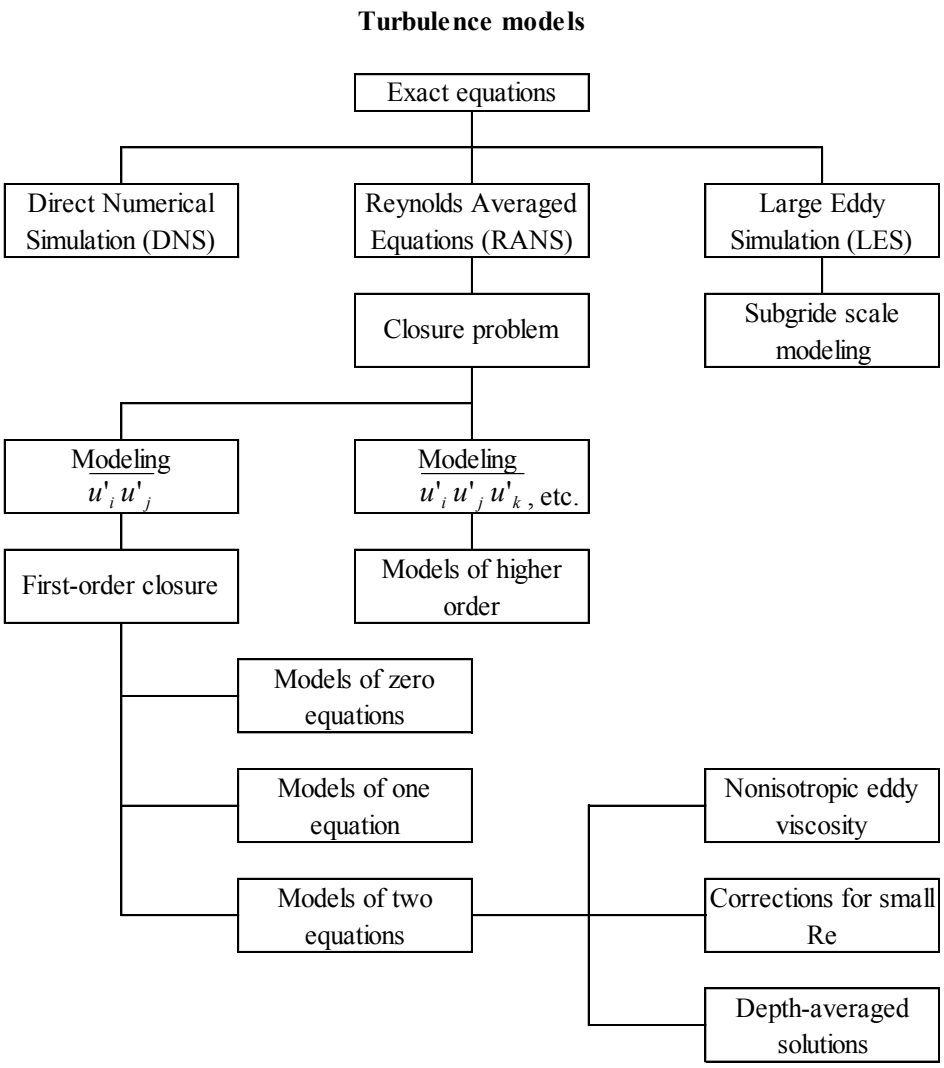

Figure 1 - Turbulence models (adapted from Garcia 1996).

Some more detail is given to the two-equations $k-\varepsilon$ (Harlow and Nakayama 1967, Launder and Spalding 1972) and *Renormalization Group* (*RNG*) $k-\varepsilon$ (Yakhot and Orszag 1986, Yakhot and Smith 1992) models, which will be used in Chapter 5. In each of these models, transport equations for k and ε are considered, which are, for high Reynolds numbers and assuming isotropic eddy viscosity, as follows

$$\underbrace{\rho_0\left[\frac{\partial k}{\partial t}\right.}_{\text{rate of change}}+\underbrace{\left.\overline{u_{m_j}}\frac{\partial k}{\partial x_j}\right]}_{\text{convective transport}}=\underbrace{\frac{\partial}{\partial x_j}\left(\frac{\mu_T}{\sigma_k}\frac{\partial k}{\partial x_j}\right)}_{\text{diffusive transport}}+\underbrace{\mu_T\left(\frac{\partial\overline{u_{m_i}}}{\partial x_j}+\frac{\partial\overline{u_{m_j}}}{\partial x_i}\right)\frac{\partial\overline{u_{m_i}}}{\partial x_j}}_{\text{production of shear}}+G-\underbrace{\rho_0\varepsilon}_{\text{viscous dissipation}} \qquad (10)$$

$$\underbrace{\rho_0\left[\frac{\partial \varepsilon}{\partial t}\right.}_{\text{rate of change}}+\underbrace{\left.\overline{u_{m_j}}\frac{\partial \varepsilon}{\partial x_j}\right]}_{\text{convective transport}}=\underbrace{\frac{\partial}{\partial x_j}\left(\frac{\mu_T}{\sigma_\varepsilon}\frac{\partial \varepsilon}{\partial x_j}\right)}_{\text{diffusive transport}}+$$

$$\underbrace{C_{1\varepsilon}\frac{\varepsilon}{k}\left[\mu_T\left(\frac{\partial \overline{u_{m_i}}}{\partial x_j}+\frac{\partial \overline{u_{m_j}}}{\partial x_i}\right)\frac{\partial \overline{u_{m_i}}}{\partial x_j}+C_{3\varepsilon}G\right]-\rho_0 C_{2\varepsilon}\frac{\varepsilon^2}{k}}_{\text{generation - destruction}} \tag{11}$$

where G is the buoyancy term and σ_k, σ_ε, $C_{1\varepsilon}$, $C_{2\varepsilon}$ and $C_{3\varepsilon}$ are constants. Table 1 presents the default values of the corresponding constants for each model (Isfahani and Brethour 2009). The transport equation of the turbulent kinetic energy is a balance between the rate of change of k in respect to time, the convective transport due to the mean flow motion, the diffusive transport due to the fluctuation of velocity and pressure, the production of k due to transfer of kinetic energy from the mean flow, and the dissipation of k into heat, due to viscosity. The buoyancy term respects to production or destruction of k due to buoyancy forces, when in buoyant flows. Similarly, the transport of turbulent kinetic energy dissipation respects to a balance between rate of change, convection, diffusion, generation and destruction. The main difference between both models is that in the $k-\varepsilon$ model the constants are obtained experimentally and in the RNG $k-\varepsilon$ model are derived explicitly, which makes RNG *k-ε* turbulence model more accurate (Flow Science 2008).

Table 1 – Values of the constants of the $k-\varepsilon$ and RNG *k-ε* models.

Constants	k-ε model	RNG k-ε model
C_μ	0.09	0.085
σ_k	1.00	0.72
σ_ε	1.30	0.72
$C_{1\varepsilon}$	1.44	1.42
$C_{2\varepsilon}$	1.92	function of k, ε and shear rate
$C_{3\varepsilon}$	0.20	0.20

3.3 FAVOR™ METHOD

FAVOR™ method, acronym for Fractional Area/Volume Obstacle Representation (Hirt and Sicilian 1985), is used by *FLOW-3D*® to represent obstacles by means of fractional areas and volumes in a fixed orthogonal grid. In each cell of the grid, volume fraction is defined as the ratio of the volume that is open to fluid to the total volume of the cell and, at each of the six faces of the cell, an area fraction is defined as the ratio of the open area to the total area (Wei 2005).

The main difference between the mixture and turbulence model equations already presented and those by *FLOW-3D*® is that the last are formulated with area and volume porosity functions of the

FAVOR™ method. The mixture equations for a 3-D dilute flow presented in the beginning of this chapter are, taking into account the FAVOR™ method, as follows:

$$\frac{\partial\left(A_j u_{m_j}\right)}{\partial x_j} = \frac{RSOR}{\rho_0} \tag{12}$$

$$\rho_0\left[\frac{\partial u_{m_i}}{\partial t} + \frac{1}{V_F}\frac{\partial\left(Au_m\right)_i u_{m_j}}{\partial x_j}\right] = -\frac{\partial p}{\partial x_i} + \rho_0 G_i + \rho_0 f_i - \rho_0 b_i - \frac{RSOR}{V_F} u_{m_i} \tag{13}$$

where A_i and A_j are the fractional areas open to the flow in the directions x_i and x_j; V_F is the fractional volume open to the flow; $RSOR$ is a mass source (e.g., with application in cases dealing with porous objects); G_i are body accelerations; f_i are viscous accelerations; b_i are losses due to porosity; and the last term is a source of mass. Considering variable dynamic viscosity, viscous accelerations are given by the expression below:

$$\rho_0 V_F f_i = ws_i - \frac{\partial\left(A_j \tau_{ij}\right)}{\partial x_j} \tag{14}$$

where ws_i are the wall stresses and τ_{ij} are the Reynolds stresses given by:

$$\tau_{ij} = -2\mu\, e_{ij} \tag{15}$$

where

$$e_{ij} = \frac{1}{2}\left(\frac{\partial u_i}{\partial x_j} + \frac{\partial u_j}{\partial x_i}\right) \tag{16}$$

The equations for the turbulent kinetic energy and for the turbulent kinetic energy dissipation of the $k-\varepsilon$ and RNG $k-\varepsilon$ models are described in *FLOW-3D*® as

$$\rho_0\left[\frac{\partial k}{\partial t} + \frac{\left(\overline{u_m} A\right)_j}{V_F}\frac{\partial k}{\partial x_j}\right] = P + Diff + G - \rho_0\varepsilon \tag{17}$$

$$\rho_0\left[\frac{\partial \varepsilon}{\partial t} + \frac{\left(\overline{u_m} A\right)_j}{V_F}\frac{\partial \varepsilon}{\partial x_j}\right] = \frac{C_{1\varepsilon}\varepsilon}{k}\left(P + C_{3\varepsilon}\cdot G\right) + DDif - \rho_0 C_{2\varepsilon}\frac{\varepsilon^2}{k} \tag{18}$$

where

$$P = \underline{\underline{\tau}} : \nabla u_m \tag{19}$$

$$Diff = \frac{1}{V_F}\frac{\partial}{\partial x_j}\left(\mu_T\left(A\nabla k\right)_j\right) \tag{20}$$

$$DDif = \frac{1}{V_F}\frac{\partial}{\partial x_j}\left(\mu_T \left(A\nabla\varepsilon\right)_j\right) \tag{21}$$

where $\underline{\underline{\tau}}$ denotes de Reynolds stresses tensor.

3.4 BOUNDARY CONDITIONS

The mathematical model equations are valid within a domain Ω which includes the flow in the stepped chute and the stilling basin, and is limited by the incoming flow in the tank, the outgoing flow downstream of the stilling basin, the solid boundary in the spillway, and the free-surface. The location of the free-surface is a priori unknown, involving the need to calculate that location each time step, starting from an initial condition.

The *TruVOF* method (embedded in *FLOW-3D*®; see Hirt and Nichols 1981) is used to capture the free-surface. *TruVOF* is a donor-acceptor algorithm and employs three key elements (Bombardelli et al. 2001). The first element is constituted by the definition and use of the F function, which depicts the fractional volume of fluid occupying each cell; its value ranges from zero (no fluid in the volume) to one (cell completely filled with fluid). The free-surface is defined to be located at a position pertaining to intermediate values of the fractional volume in the cells. A value of $F = 0.5$ is usually employed for that purpose (Flow Science 2008). The second element is the use of an appropriate advection numerical method for the equation governing the transport of the Volume-of-Fuid (VoF) function (Eq. (12)) that is designed to ensure a small numerical diffusion of the free-surface. At each time step, the function F is obtained by solving the following equation:

$$\frac{\partial F}{\partial t} + \nabla\cdot\left(\underline{\bar{u}}_m\ F\right) = 0 \tag{22}$$

in the entire domain (Ferziger and Peric 2002). Finally, an important third element is the application of boundary conditions at the free-surface.

Unlike in other methods published recently (see Matthews et al. 1999; 2001, for example), the flow and transport equations are solved only in cells with liquid, because the gas is assumed to possess negligible inertia. The gas is considered only able of applying a normal pressure on a liquid surface. Once the free-surface location is defined each time step, the model is numerically solved within the water domain limited by the free-surface while the air outside the free-surface does not participate of the "active volumes" of the computation. The *TruVOF* method enjoys the following advantages: a) minimum storage of information, since only one variable, F, has to be stored; b) adequate (small) computational cost; and c) good accuracy for fine meshes.

FLOW-3D® deals with different types of boundary conditions: a) rigid wall with slip; b) rigid wall with no-slip (imposed through a wall shear stress); c) specification of fixed velocities or pressures; d) symmetry planes; e) continuative "outflow" boundaries; f) periodic boundaries; g) outflow boundaries that minimize wave reflections; h) boundary values obtained from previous calculation using grid overlay (GO) procedure; i) inter-block boundaries.

A *rigid wall* has the characteristics of impenetrability, which corresponds to no normal velocities. For a *no-slip* type, the tangential velocity is also zero. For a solid boundary the *rigid wall with no-slip* is applicable (Rodi 1984). *Specified velocity* or *pressure* boundary conditions can be considered for both inflow and outflow types of grid boundaries. The inflow boundary condition for pressure can be considered either as a static pressure condition (where the pressure at the inlet is assumed static) or a stagnation pressure condition (where the inflow is considered to have total or stagnation pressure). In a *symmetry plane* the shear stress is zero and the flux of properties across the boundary is not allowed. When a boundary condition is not specified, *FLOW-3D*® considers by default a symmetry plane. Because of its particular characteristics, the free-surface could be classified as *rigid wall* or *symmetry plane*. In *FLOW-3D*®, it is treated as a *symmetry plane*. *Continuative "outflow" boundaries* are used when it is needed to consider the flow exiting the computational domain and the establishment of a boundary condition with physical meaning is not possible. This boundary condition has no physical basis and consequently should only be used when no other option is available. *Periodic boundaries* assume cells in one boundary of the domain to have the same characteristics as the cells of the opposite boundary. This boundary has especial application in waves. For wave propagation problems, a specific outflow boundary condition can be used. The speed and direction of waves approaching the boundary are determined and then the boundary conditions are set in a way that allows the waves to propagate with minimization of reflections. When a simulation is restarted and the grid is modified the *Grid Overlay (GO) procedure* is used to transfer the restart data from the old to the new grid. This is done considering the boundaries like fixed velocity boundaries. When part of the new grid has no correspondence in the old grid the *GO* boundaries are treated as fixed velocity boundaries and the initial conditions are considered. *Inter-block* boundaries permit to transfer data between grid blocks when a multi-block domain is considered. Finally, two types of boundary conditions, Neuman and Dirichlet, can be used to solve the Poisson equation for pressure (Barkhudarov 2004). For the Neumann type only velocity is passed between grids while in the Dirichlet type only pressure is passed between grids. A mixture of the two types can be used. By default, *FLOW-3D*® considers a weigh of 75% for the pressure and 25% for the velocity.

For the turbulence statistics, the boundary conditions for a solid wall make use of the usual "wall functions". "Wall functions" are universal functions that permit to describe the velocity profile close to the wall, in the viscous sublayer of a boundary layer (e.g., Olsen 2000, Ferziger and Peric 2002). Otherwise, CFD programs would have to spend a large amount of cells near the surface to resolve the velocity gradients at the wall. These equations are as follows (Pope 2000; Ferziger and Peric 2002; Chung 2006)

$$k\big|_w = \frac{u_*^{\,2}}{\sqrt{c_\mu}};\ \varepsilon\big|_w = \frac{u_*^{\,3}}{(\kappa\ y_1)} \tag{23}$$

where u_* is the wall-friction (shear) velocity, obtained iteratively by the use of the semi-logarithmic velocity law, κ is the von-Kármán constant, and y_1 is the normal distance perpendicular to the wall (Flow Science 2008). The steps developed to compute u_* and the

turbulence statistics at the wall are: a) determination of the direction normal to the wall in the wall volume; b) the cell-centered flow velocity at the wall volume is decomposed into parallel (uparallel) and perpendicular (uperpendicular) components; c) the average distance to the wall, y_1, is calculated as half of the volume width in the direction normal to the wall; d) u_* is computed using uparallel and y_1 in an iterative way.

3.5 FINITE VOLUMES/FINITE DIFFERENCES METHOD

In *FLOW-3D*® the equations previously described are solved using finite volumes/finite differences approximations. The domain is divided into cells of a structured Cartesian grid with dimensions δx_i, δy_j and δz_k. In each cell, all the variables are center-located, except the velocities, that are located at the cells faces. Fractional areas of the *FAVOR*^{TM} method are also positioned at the cells faces. The numerical method is first-order accurate with respect to time and space.

All the terms in the equations are computed explicitly, i.e., using the current time level values of the local variables, except the pressure term, treated considering a semi-implicit formulation, with pressures and velocities coupled implicitly. Momentum equations use time-advanced pressures and the continuity equation uses time-advanced velocities. As an example, the mixture equations for momentum for the finite volumes/finite differences approximation are:

$$\left(u_m\right)_{i,j,k}^{n+1} = \left(u_m\right)_{i,j,k}^{n} + \delta t^{n+1}\left[-\frac{p_{i+1,j,k}^{n+1} - p_{i,j,k}^{n+1}}{\left(\rho_0 \delta x\right)_{i+\frac{1}{2},j,k}^{n}} + G_x - FUX - FUY - FUZ + VISX - BX - WSX\right] \tag{24}$$

$$\left(v_m\right)_{i,j,k}^{n+1} = \left(v_m\right)_{i,j,k}^{n} + \delta t^{n+1}\left[-\frac{p_{i,j+1,k}^{n+1} - p_{i,j,k}^{n+1}}{\left(\rho_0 \delta y\right)_{i,j+\frac{1}{2},k}^{n}} + G_y - FVX - FVY - FVZ + VISY - BY - WSY\right] \tag{25}$$

$$\left(w_m\right)_{i,j,k}^{n+1} = \left(w_m\right)_{i,j,k}^{n} + \delta t^{n+1}\left[-\frac{p_{i,j,k+1}^{n+1} - p_{i,j,k}^{n+1}}{\left(\rho_0 \delta z\right)_{i,j,k+\frac{1}{2}}^{n}} + G_z - FWX - FWY - FWZ + VISZ - BZ - WSZ\right] \tag{26}$$

where, e.g., for the direction in the x-coordinate,

$$\left(\rho_0 \delta x\right)_{i+\frac{1}{2},j,k}^{n} = \frac{\left(\rho_{0_{i,j,k}}^{n} \delta x_i + \rho_{0_{i+1,j,k}}^{n} \delta x_{i+1}\right)}{2} \tag{27}$$

$u^n_{i,j,k}$ is the velocity component, at the middle of the $i+1/2$ cell-face, at time level n; δx is the cell spacing; G_x congregates gravitational, rotational, and general non-inertial accelerations; FUX is the momentum advection term; $VISX$ is the viscous acceleration; BX is the flow loss for a baffle normal to the x-direction; WSX is the viscous wall acceleration; and δt is the increment in time. It should be noticed that, because the code does not allow fractional indexes, by convention, all fractional indexes are decreased to the nearest whole integer. Consequently, the velocity component u at $i+1/2$, located on the cell-face between cells (i,j,k) and $(i+1,j,k)$ is denoted by $u^n_{i,j,k}$. See Flow Science (2008) for more details.

Pertaining to the pressure term, the semi-implicit formulation requires the use of an iterative technique for the equations to be solved. *FLOW-3D®* offers three different techniques: i) a successive over-relaxation (SOR); ii) modified Alternating-Direction-Implicit scheme (SADI); and iii) the general minimum residual method (GMRES). SOR and SADI are stationary iterative methods, i.e., in each iteration are performed the same operations on the current iteration vector, contrarily, GMRES is a nonstationary iterative method, having iteration-dependent coefficients (Barrett et al. 1994). GMRES is the most recent method to be implemented in *FLOW-3D®* and is highly accurate and efficient for a wide range of problems, although consumes more memory than the SOR or SADI methods. SOR is simple and works well for many problems but can be extremely slow to converge in some situations. It occurs, for instance, when one cell dimension is much larger than the others. In this case, SADI can be used considering a more implicit solution method in the direction of smaller cell sizes (Flow Science 2008).

3.6 STABILITY CONDITIONS

FLOW-3D® has several stability conditions to avoid numerical instabilities, all pertaining to the time-step size. However, it must be said that, by default, *FLOW-3D®* sets the time step automatically and that this is the recommending option for achieving optimal results.

Time-step must always satisfy the following criteria:

i) The fluid should not flow across more than one computational cell in one time-step:

$$\delta t < CON \cdot \min\left(\frac{V_F \delta x_i}{A_x u}; \frac{V_F \delta y_j}{A_y v}; \frac{V_F \delta z_k}{A_z w}\right) \tag{28}$$

where CON is a factor considered to take into account the most adverse situation. CON is usually equal to 0.45.

ii) When the ratio between open face area and volume is high the AVRCK algorithm decreases automatically this ratio by adjusting slightly the mesh/obstacle arrangement in order to avoid small time steps.

iii) The surface waves should not propagate more than one computational cell in one time-step:

$$\delta t < 0.5 \frac{\min\left(\delta x_i ; \delta y_j\right)}{\sqrt{\delta z_k \cdot ACCZ}} \tag{29}$$

where $ACCZ$ is the acceleration applied to the fluid in a normal direction to the free-surface if z is the normal direction to the surface. Similar limits have to be imposed to the other directions for the cells with free-surface.

iv) Limit of the time step when a non-zero value of the dynamic viscosity is used:

$$\delta t = \frac{0.25}{\max\left[RM \cdot \frac{\mu}{\rho}\left(\frac{1}{\delta x_i^{\,2}} + \frac{1}{\delta y_j^{\,2}} + \frac{1}{\delta z_k^{\,2}} \right) \right]} \tag{30}$$

where RM is a factor to take into account all the types of diffusional processes of the dynamic viscosity.

v) Limit of the time-step when the surface tension is considered:

$$\delta t^2 < \frac{DSM \cdot \rho_0}{16\sigma \cdot DSSX} \tag{31}$$

where

$$DSM = \min\left(\delta x_i ; \delta y_j ; \delta z_k\right) \tag{32}$$

$$DSSX = \max\left(\frac{1}{\delta x_i^{\,2}} + \frac{1}{\delta y_j^{\,2}} ; \frac{1}{\delta x_i^{\,2}} + \frac{1}{\delta z_k^{\,2}} ; \frac{1}{\delta y_j^{\,2}} + \frac{1}{\delta z_k^{\,2}} \right) \tag{33}$$

vi) Limit of the time-step pertaining to the relative amount of donor-cell and centered differencing used for the momentum advection terms:

$$\delta t \cdot \max\left(\frac{|u|}{\delta x_i} ; \frac{|v|}{\delta y_j} ; \frac{|w|}{\delta z_k} \right) < \alpha \le 1.0 \tag{34}$$

where α is a parameter of the approximation method used to calculate the momentum advection terms.

REFERENCES

Barkhudarov, M. R. (2004). "Multi-block gridding technique for Flow-3D." Flow Science Technical Notes, Flow Science, Inc., TN59, available online.

Barrett, R.; Berry, M.; Chan, T.F.; Demmel, J.; Donato, J.; Dongarra, J.; Eijkhout, V.; Pozo, R.; Romine, C.; and Van der Vorst, H. (1994). "Templates for the solution of linear systems building blocks for iterative methods." 2nd Edition, SIAM, Philadelphia, PA, available online.

Bombardelli, F. A. (2003). “Characterization of coherent structures from parallel, les computations of wandering effects in bubble plumes.” Proc. 2003 World Water and Environmental Resources Congress, Environmental & Water Resources Institute (EWRI), ASCE, Philadelphia, PA, USA, P. Bizier and P. DeBarry (Ed.). (In CD.)

Bombardelli, F. A. (2004). “Turbulence in multiphase models for aeration bubble plumes.” Ph.D. thesis. University of Illinois at Urbana-Champaign.

Bombardelli, F. A., and Jha, S. K. (2009). “hierarchical modeling of dilute, suspended-sediment transport in open channels.” Environ. Fluid Mech., 9(2), 207-230.

Bombardelli, F. A., Buscaglia, G. C., Rehmann, C. R., Rincón, L. E., and García, M. H. (2007). “Modeling and scaling of aeration bubble plumes: A two-phase flow analysis.” J. Hyd. Res., IAHR, 45(5), 617-630.

Bombardelli, F. A., Hirt, C. W., and García, M. H. (2001). “Discussion on ‘Computations of curved free surface water flow on spiral concentrators’, by Matthews et al.” J. Hydr. Eng., ASCE, 127(7), 629-631.

Buscaglia, G. C., Bombardelli, F. A., and García, M. H. (2002). “Numerical modeling of large scale bubble plumes accounting for mass transfer effects.” Int. J. Multiphase Flow, 28, 1763-1785.

Chung, T. J. (2006). “Computational fluid dynamics.” Cambrigde University Press, USA.

Crowe, C., Sommerfeld, M., and Tsuji, Y. (1998). “Multiphase flows with droplets and particles.” CRC Press, USA.

Drew, D. A., and Passman, S. L. (1999). “Theory of multicomponent fluids.” Springer, Vol. 135 of Applied Mathematical Sciences.

Ferziger, J. H., and Peric, M. (2002). “Computational methods for fluid dynamics.” Springer.

Flow Science, Inc. (2008). FLOW-3D User’s Manual, Version 9.3, Los Alamos, New Mexico, USA.

Garcia, M.H. (1996). “Hidrodinámica ambiental.” Colección Ciencia y Técnica, Centro de Publicaciones Universidad Nacional del Litoral, Argentina (in Spanish).

Gioia, G., and Bombardelli, F. A. (2002). “Scaling and similarity in rough channel flows.” Phys. Rev. Lett., 88(1), 014501.

Harlow, F.H., and Nakayama, P.I. (1967). “Turbulence transport equations.” Phys. of Fluids, 10, 2323.

Hirt, C. W., and Nichols, B. D. (1981). “Volume of Fluid (VOF) method for the dynamics of free boundaries.” J. Comp. Physics, 39, 201-225.

Hirt, C. and Sicilian, J. (1985). “A porosity technique for the definition of obstacles in rectangular cell meshes. ” Proc. Fourth Int. Conf. Ship Hydro., National Academy of Science, Washington, DC, USA.

Hrenya, C. M., and Sinclair, J. L. (1997). “Effects of particle-phase turbulence in gas-solid flows.” AIChE J., 43(4), 853-869.

Isfahani, A. H. G. and Brethour, J. M. (2009). “On the implementation of two-equation turbulence models in Flow-3D.” Flow Science Technical Notes, Flow Science, Inc., TN86, available online.

Launder, B. E., and Spalding, D. B. (1972). “Lectures in mathematical models of turbulence.” Academic Press.

Matthews, B. W., Fletcher, C. A. J., Partridge, A. C., and Vasquez, S. (1999). “Computations of curved free surface water flow on spiral concentrators.” J. Hydr. Eng., ASCE, 125(11), 1126-1139.

Matthews, B. W., Fletcher, C. A. J., Partridge, A. C., and Vasquez, S. (2001). “Computations of curved free surface water flow on spiral concentrators. Closure” J. Hydr. Eng., ASCE, 127(7), 631-631.

Olsen, N.R.B., and Kjellesvig, H.M. (1998). “Three-dimensional numerical flow modelling for estimation of spillway capacity.” J. Hyd. Res., IAHR, 36(5), 775-784.

Pope, S. B. (2000). “Turbulent flows.” Cambridge University Press, UK.

Prosperetti, A., and Tryggvason, G. (2007). “Computational methods for multiphase flow.” Cambridge Press, UK.

Rodi, W. (1984). “Turbulence models and their application in hydraulics.” State-of-the-Art Paper, IAHR.

Wei, G. (2005). “A fixed-mesh method for general moving objects in fluid flow.” Int. J. Modern Physics B, World Scientific Publishing Company.

Yakhot, V., and Orszag, S. A. (1986). “Renormalization group analysis of turbulence. I. Basic theory.” J. Scientific Computing, 1(1), 3-51.

Yakhot, V., and Smith, L. M. (1992) “The renormalization group, the E-Expansion, and the derivation of turbulence model.” J. Scientific Computing. 3, 35.

Chapter 4

Experimental study

4.1 ON THE PREDICTION OF THE HYDRAULIC PARAMETERS OF THE NON-AERATED SKIMMING FLOW DOWN STEEP STEPPED SPILLWAYS

This subchapter concerns to experimental results obtained in the 1V:0.75H slope stepped channel of LNEC and is focused on the hydraulic characteristics of the skimming flow in the non-aerated region.

ABSTRACT 4.1-1

1. INTRODUCTION 4.1-1

2. EXPERIMENTAL SET-UP 4.1-5

3. FLOW PROPERTIES AT THE INCEPTION POINT 4.1-8

4. FLOW PROPERTIES UPSTREAM OF THE INCEPTION POINT 4.1-13

   4.1. Air concentration 4.1-13

   4.2. Boundary layer development 4.1-15

   4.3. Velocity distribution 4.1-17

   4.4. Characteristic flow depths 4.1-18

   4.5. Energy dissipation 4.1-22

5. FINAL REMARKS 4.1-25

REFERENCES 4.1-26

ON THE PREDICTION OF THE HYDRAULIC PARAMETERS OF THE NON-AERATED SKIMMING FLOW DOWN STEEP STEPPED SPILLWAYS

ABSTRACT

Traditionally, the aerated flow region has been considered to dominate a large extension of the stepped spillway when comparing to the developing boundary layer flow region, instigating research to mainly focus in the aerated flow region. Conversely, in several stepped spillways the non-aerated region occupies a large portion of the spillway, for the design flow discharge. To have a better understanding of the non-aerated flow region of steep stepped spillways on roller compacted concrete (RCC) or concrete dams where is expected to exist a large portion of non-aerated flow, an experimental study was conducted in a large physical model constructed in the National Laboratory of Civil Engineering, Lisbon, Portugal. The concepts of entrapped and entrained air concentration are explored and an overview on the currently used inception point location methodologies is presented, culminating with new proposed equations to predict location, equivalent clear-water depth and mean air concentration at this section. Empirical and theoretical expressions to predict the mean air concentration, boundary layer development, velocity profiles, equivalent clear-water depth, and energy dissipation are presented, fostered by the proximity to experimental data. The energy dissipation is observed to be higher than in smooth spillways, although much smaller than reported for the aerated flow region of stepped spillways.

Keywords: experimental study, stepped spillway, non-aerated flow, conductivity probe, back-flushing Pitot tube, inception point, entrapped air concentration, entrained air concentration, energy dissipation.

---

1. INTRODUCTION

Generally, stepped spillways can be effective to dissipate more energy than smooth spillways and to promote entrainment of air in the flow, contributing to reduce cavitation risk and to increase oxygenation of the downstream water body. With an increased interest in maintenance and rehabilitation of dams, this configuration can also allow inspections of the dam body.

For a certain stepped spillway, nappe, transition, and skimming flows occur sequentially with increasing discharge. However, the typical design discharge of roller compacted concrete (RCC)

and concrete dams leads to the skimming flow regime, so that the majority of studies has been focused in this type of flow and present study makes no exception.

Because of the macro-roughness created by the steps, turbulence is enhanced and the entrainment of air occurs more upstream than in smooth spillways. In fact, the region of non-aerated flow has been considered negligible and studies have been focused mainly in the aerated region, regarding the experimental study of air concentration and velocity distributions (e.g., Chamani and Rajaratnam 1999; Matos 2000; Chanson 2002; Boes and Hager 2003; Ohtsu et al. 2004; André 2004; Meireles 2004; Renna 2004; Gonzalez 2005), pressure field on the steps (e.g., Sánchez-Juny 2001; Yasuda and Ohtsu 2003; André 2004; Amador et al. 2009; Gomes 2006), gas transfer (e.g., Toombes and Chanson 2000; McKenna 2001; Bung 2009), and macro-roughness and non-conventional configurations (e.g., André 2004; Gonzalez 2005; Hunt et al. 2008; Relvas and Pinheiro 2008; Chinnarasri et al. 2008; Bung and Schlenkhoff 2010). Recently, studies focused on numerical simulations started also to appear (e.g., Chen et al. 2002; Tabbara et al. 2005).

In presence of high discharges and/or small dams, the boundary layer cannot have enough distance to fully develop and the entrainment of air may not take place. Table 1 presents examples of several steep dams around the world, and the correspondent hydraulic characteristics. The last column respects to the percentage of the spillway that is subjected to the non-aerated flow, for the design discharge, for what the inception point was calculated with the formulation proposed by Chanson (2002). It is shown that the number of dams where the non-aerated region is important is not negligible and is even observed that in 3 of the 27 presented dams the aerated flow never takes place.

The need to increase the design specific discharge for new spillways and to update the probable maximum flood for existing spillways magnifies the importance of the non-aerated flow region, even if just a small number of studies was focused on this region, as summarized in Table 2.

A detailed analysis of the existing studies revealed the following features/issues:

i) Although the conference paper of Meireles et al. (2006) already explores the non-aerated region, it does not focus on the inception point, development of the boundary layer or variability of the exponent $1/N$ of the velocity power law and only one empirical methodology is presented to determine the equivalent clear-water depth. In contrast, present study does not only explore all these points but also presents a broader range of data (extended to one more step height and two more discharges).

ii) Amador et al. (2006, 2009) performed a detailed study on the non-aerated region of stepped spillways with precise Particle Image Velocimetry (PIV) instrumentation. However, this study just pertains to one single discharge and step height, corresponding to a small range of application, in opposition to the present study. In addition, a comparison between different methodologies to determine equivalent clear-water depth, specific energy, boundary layer development or the hydraulic characteristics of the inception point is not performed. Finally, the phenomenon of undulation is not described, nor the concepts of entrained/entrapped air concentration or characteristic depths.

Table 1 - Non-aerated region of several steep stepped spillways around the world.

Dam nº	Name, Country, Year	Ref.	H_d (m)	θ (º)	b (m)	h (m)	q_{max} (m^2/s)	% spillway non-aerated
1	Grindstone Canyon, USA, 1986	[GO]	34	53	30	0.3	1	12
2	De MistKraal, South Africa, 1986	[HD], [GO]	18	59	195	1	29	100
3	Zaaihoek, South Africa, 1986	[HD], [GO]	37	58	160	1	15.6	77
4	Upper Stillwater, USA, 1987	[HO]	61	73	183	0.6	11.6	44
5	Monksville, USA, 1987	[SO]	36.6	52	61	0.61	9.3	52
6	Lower Chase Creek, USA, 1987	[GO], [FR]	18	55	61	0.6	3.3	52
7	Les Olivettes, France, 1987	[GO]	31.5	53	40	0.6	6.6	48
8	Wolwedans, South Africa, 1990	[GE], [W&D]	70	63	77.25	1	12.4	36
9	Riou, France, 1990	[GO], [W&D]	19	59	105	0.6	1.1	24
10	Puebla de Cazalla, Spain, 1991	[ME], [W&D]	58.2	51	18	0.9	9	31
11	Choldocogania, France, 1991	[GO], [W&D]	32.5	50	13.5	0.6	2.1	20
12	Belén-Gato, Spain, 1991	[SJ], [W&D]	33.5	53	17.4	0.85	1.73	17
13	Caballar I, Spain, 1991	[SJ], [W&D]	14.8	53	17.4	0.85	1.73	38
14	Amatisteros III, Spain, 1991	[SJ], [W&D]	14.8	53	17.4	0.85	1.73	38
15	Belén-Cagüella, Spain, 1992	[SJ]	31	53	17.4	0.85	13.5	79
16	Belén-Flores, Spain, 1992	[SJ]	27	53	17.4	0.85	1.73	21
17	Taung, South Africa, 1993	[GO]	50	53	35	0.6	6.1	29
18	New Victoria, Australia, 1993	[WA], [W&D]	35	72	130	0.6	5.4	44
19	Cenza, Spain, 1993	[SJ], [W&D]	49	53	58	0.6	3.47	19
20	Sierra Brava, Spain, 1994	[SJ], [W&D]	54	53	166	0.9	3.9	19
21	Petit Saut, French Guiana, 1994	[DU], [GO]	31	51	60	0.6	4	33
22	La Touche Poupart, France, 1994	[GO], [W&D]	33	53	35	0.6	6.1	43
23	Atance, Spain, 1997	[W&D]	45	51	32	1.2	5.94	29
24	Randleman, USA, 1997	[MD]	31	53	152.4	0.9	37.1	100
25	Nakasujigawa, Japan, 1998	[HS]	71.6	55	175	0.75	6.6	21
26	Tannur, Jordan, 2001	[W&D], [AI]	50	51	180	1.2	3.4	18
27	Pedrógão, Portugal, 2005	[ML]	29	51	301	0.6	39.9	100

Note: H_d - spillway height; θ - spillway slope; b – spillway width; h - step height; q_{max} – maximum unit discharge; % spillway – percentage of the total length of the spillway subjected to the non-aerated region flow.

[AI] Airey (2004); [DU] Dussard *et al.* (1992); [FR] Frizell (1992); [GE] Geringer (1995); [GO] Goubet (1992); [HD] Hollingworth and Druyts (1986); [HO] Houston (1987); [HS] Hakoishi and Sumi (2000); [ME] Mateos and Elviro (1992); [ML] Melo (2004); [SJ] Sánchez-Juny (2001); [SO] Sorensen (1985); [WA] Wark *et al.* (1991); [W&D] RCC Dams (2003) and [MD] Mujib dam (30/07/2004, Internet).

Table 2 - Summary of investigations on the non-aerated region of stepped spillways.

Author (year)	Slope (V/H)	q_w (m^2/s)	h (m)	Obs.
Meireles et al. (2006)	1:0.75	0.05-0.20	0.04 & 0.08	Present empirical relations based on experimental data for different step heights and discharges. (conference paper)
Amador et al. (2006), (2009)	1:0.8	0.11	0.05	Present theoretical expressions applied to experimental data for a unique situation of step height and discharge.
Chanson (2002), Gonzalez & Chanson (2007)				Not exclusively focused on the non-aerated region; present theoretical expressions applied to experimental data of different authors for a wide range of angles and conditions.
Meireles & Matos (2009)	1:2	0.03-0.08	0.025 & 0.05	Present empirical relations based on experimental data for different step heights and discharges.
Carvalho & Amador (2008)	1:0.8	0.11	0.05	Present a comparison between experimental and numerical data. (conference paper)
Bombardelli et al (2010)	1:0.75	0.18	0.04	Present a comparison between experimental and numerical data.
Present study	1:0.75	0.05-0.20	0.02, 0.04 & 0.08	Presents theoretical expressions and empirical relations based on experimental data for different step heights and discharges.

Note: q_w – water discharge per unit width; h - step height.

iii) Chanson (2002) and Gonzalez and Chanson (2007), although not exclusively focused on the non-aerated region, discuss some results and methodologies to be applied to this region of the flow. However, the presented exponent of the velocity power law was obtained for a slope typical of embankment dams, the expression for predicting the boundary layer development is only based in data obtained at the inception point, and no comparison is performed between different methodologies to determine the inception point location and the equivalent clear-water depth along the non aerated region.

iv) Meireles and Matos (2009) is focused only on slopes typical of embankment dams in opposition to present study, focused on steep slopes typical of concrete dams. Moreover, the study does not compare different methodologies to determine the inception point and the equivalent clear-water depth and specific energy in the non aerated region. At last, nothing is said about the undulated flow.

v) The conference paper of Carvalho and Amador (2008) is focused in the comparison between the experimental results presented in Amador et al. (2006, 2009) and new numerical results.

vi) Bombardelli et al. (2010) is mainly focused in the comparison of some of the experimental data presented in the present study and new numerical results. The exponent of the velocity power law and the expression for the boundary layer development are presented for a limited number of data, comparing to the present study, and results of only one step height and discharge are presented for the inception point.

It is thus understood that more work is needed to understand completely the non aerated flow down steep stepped spillways. Present study pretends to help researchers and engineers in understanding the behavior of the non-aerated flow down steep stepped spillways and to give tools to quantitatively determine the main hydraulic parameters.

The paper is organized as follows. In Section 2 is presented the experimental set-up. Sections 3 and 4 show experimental results and flow properties at the inception point and in the non-aerated flow region, respectively. Finally Section 5 presents a discussion on the application of present study results.

2. EXPERIMENTAL SET-UP

A physical model investigation was conducted in the National Laboratory of Civil Engineering (LNEC), Portugal, in a stepped chute 2.90 m high (from crest to toe), 1.00 m wide and with a slope of 1V:0.75H (53 degrees from horizontal) (Figs 1 and 2). The crest shape fits the WES standard spillway profile and is composed by an upstream smooth region followed by 10 increasing size steps (Fig. 1). Downstream, the constant slope region was tested for step heights, h, of 2, 4 and 8 cm and unit discharges, q_w, ranging from 0.05 to 0.20 m^2/s, corresponding to the skimming flow regime (Table 3). The volume flow rate was measured with the help of a Bazin weir located downstream of the stilling basin. Further details can be found in Matos (1999), Meireles (2004) and Renna (2004).

A conductivity probe and a back-flushing Pitot tube, both developed and calibrated by the U.S. Bureau of Reclamation, were used to measure local time-averaged air concentration, C, and water velocity, u, at several step edges of the non-aerated flow region. Although present study is focused in the non-aerated region of the flow, the air concentration data were used to estimate the equivalent clear-water depth, d, and the velocity, due to the unsteady motion of the free-surface and boundary layer. Due to the waviness and turbulent nature of the flow, in the non-aerated flow region C refers to the entrapped air in the contorted free-surface and, near the inception point, can also denote the presence of air bubbles inside the flow (entrained air), due to the difference between instantaneous and averaged inception point locations (Bombardelli et al. 2010). The concept of entrapped air concentration as air captured between water waves in opposition to entrained air concentration as air bubbles inside the water body is clearly defined in Wilhelms and Gulliver (2005). The work principle of the conductivity probe is based on the difference between electric resistivity of air and water. When any of the two 0.2 mm diameter platinum wires is in contact with air, the electric current is interrupted. Air concentration is then defined as the percentage of time any wire (or both simultaneously) is in contact with air, relatively to the total acquisition time. In the back-flushing Pitot tube, total and static pressure heads were measured through holes with diameters of 1.0 and 0.5 mm, respectively. Continuous back-flushing of the Pitot tube was provided in order to avoid an erroneous measurement of the water velocity with entrance of air in the Pitot tube. The static pressure and the total head ports of the Pitot tube were fed by water from a reservoir with constant head, where the back-flushing flow rate to each port was controlled by needle valves. The output signal of the instrumentation was scanned at 30 kHz

for 90 s with a posterior filtration to 30 Hz, to save memory and facilitate storage. Further details can be found in Matos and Frizell (1997, 2000). The instrumentation was mounted in a trolley and the accuracy for the vertical position was of 0.1 mm. The error in the longitudinal and transverse positions was estimated as being less than 5 mm and less than 1 mm, respectively.

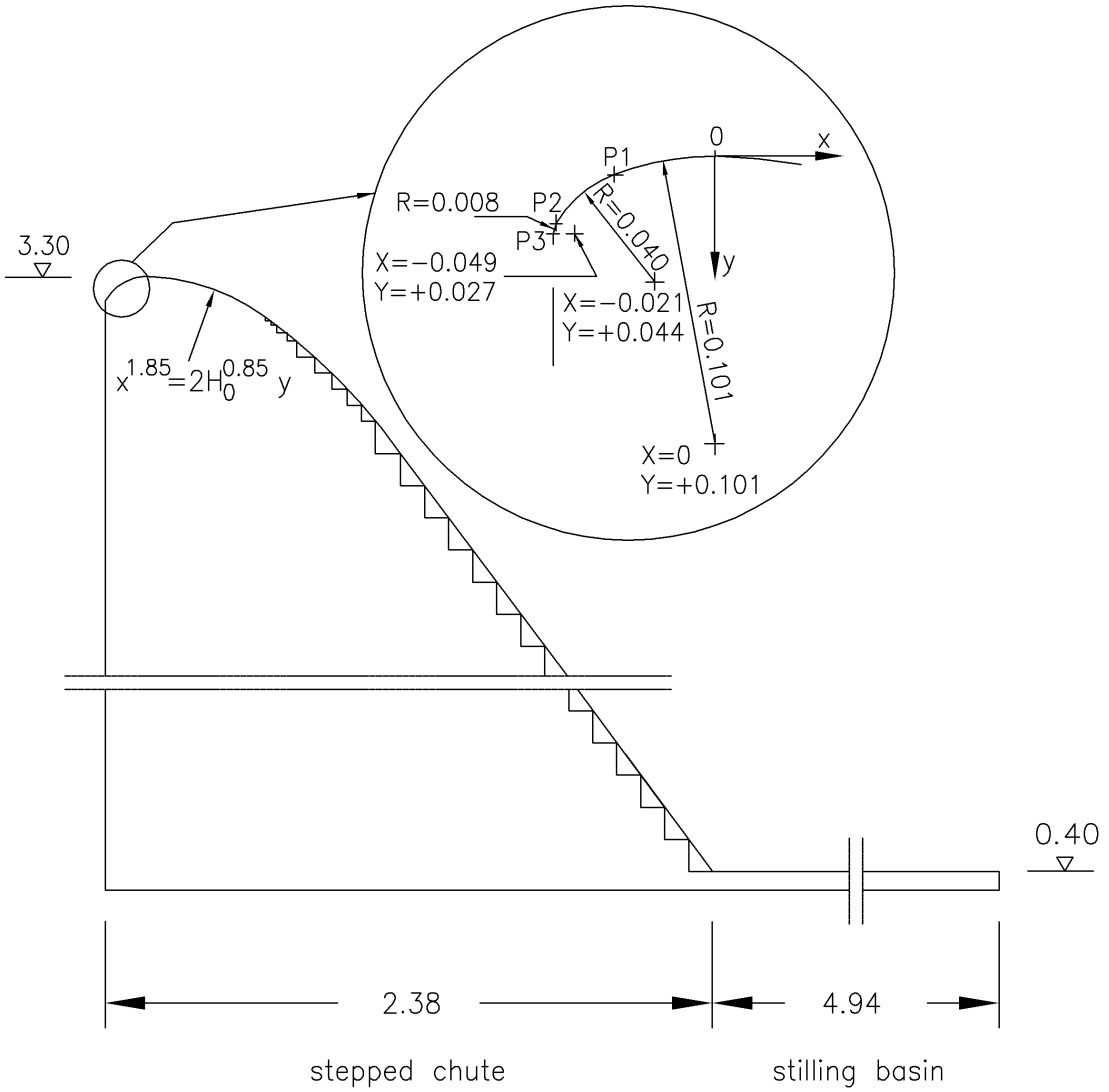

Figure 1 - Dimensional scheme of the experimental facility.

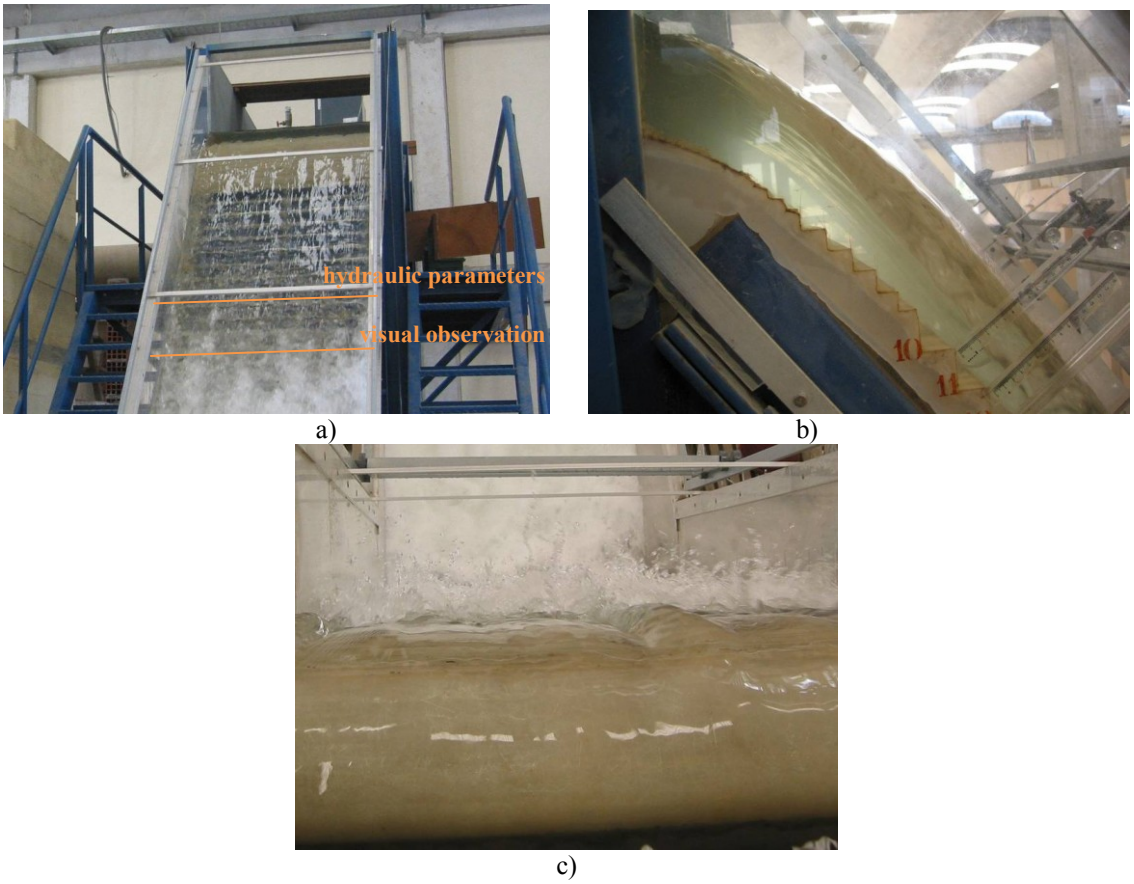

Figure 2 - Experimental facility in operation: a) front view of the flow with non-uniform entrance of air, highlighting the difficulties in predicting the inception point location; b) right sidewall view of the smooth and glassy non-aerated flow near the spillway crest; and c) view from the crest to downstream, revealing an highly contorted 3D non-aerated flow and a complex splashing aerated flow.

In the smooth ogee crest, where the free-surface is observed to be virtually smooth, the water depth was measured in the chute centerline with the help of two point gauges located at the upstream end of the crest and immediately upstream of the first step of the spillway, respectively. Downstream, clear-water depth data was obtained from

$$d = \int_0^{Y_\varphi} (1 - C)\, dy \qquad (1)$$

where Y_φ is the depth where the air concentration is φ%, assumed equal to 90% in the present study, as usually considered (e.g., Matos 2000; Chanson 2002; Boes and Hager 2003), and y is the transverse coordinate originating at the pseudo-bottom (the pseudo-bottom is defined as the surface tangent to consecutive step edges). The equivalent clear-water depth represents a fictitious flow depth which would exist if in presence of no free-surface waviness nor air bubbles inside the flow.

Velocity was obtained from:

$$V = \sqrt{\frac{2\,\Delta P}{\rho_w\,(1 - C)}} \qquad (2)$$

where ΔP is the difference between the total pressure head and the static pressure head, measured with the back-flushing Pitot tube and ρ_w is the water density. However, near the free-surface, the waves leave the instrumentation uncovered for some moments during the total time of acquisition. Due to the high frequency of the free-surface waves, as opposed to the time response of the back-flushing Pitot tube, it is not possible to obtain reliable velocity results in this zone (Matos et al. 2002). Because in the non-aerated flow high values of the air concentration correspond to the free-surface wavy region (see 4.1 air concentration and Fig. 5), in each velocity profile, only results corresponding to local air concentrations smaller than 0.7-0.8 are presented in this study (see Matos and Frizell 1997 for details). This limitation has direct impact in the determination of the boundary layer thickness near the inception point and, consequently, in locating the inception point.

A check on the reliability of experimental data was done by comparing the volume flow rate measured at the Bazin weir with the correspondent value obtained from the integration of the velocity profiles. Relative differences smaller than 8.8% (average of 5.5%) were obtained.

Table 3 - Summary of the experimental conditions presented in this study.

Model	h (m)	q_w (m^2/s)	d_c/h (-)	Ref.
A	0.02	0.100	5.0	[RE]
		0.140	6.3	
		0.200	8.0	
B	0.04	0.050	1.6	[ME]
		0.080	2.2	
		0.100	2.5	[RE]
		0.140	3.1	[ME]
		0.180	3.7	
		0.200	4.0	[RE]
C	0.08	0.080	1.1	[MA]
		0.100	1.3	
		0.140	1.6	
		0.180	1.9	
		0.200	2.0	

Note: h - step height; qw – water discharge per unit width and dc/h – critical depth normalized by the step height.
[MA] Matos (1999); [ME] Meireles (2004); [RE] Renna (2004).

3. FLOW PROPERTIES AT THE INCEPTION POINT

According to Wood (1991), in the non-aerated flow region close to the spillway crest, boundary layer grows from the spillway floor up to the free-surface, at the so called inception point, where entrainment of air initiates. In consonance, although the inception point of air entrainment depends not only on the full development of the boundary layer but also on the balance of disturbing turbulence forces and stabilizing gravity and surface tension forces, last approach is considered sufficiently accurate for design purposes (Volkart 1980), with the benefit of no need for turbulence

analysis. From this section, flow is aerated and highly turbulent, which contributes to an efficient energy dissipation. In comparison with smooth spillways, the boundary layer growth is faster in stepped spillways due to the macro-roughness generated by the steps. Chanson (2002) refers to a rate 2.8 times larger. The entrainment of air occurs closer to the spillway crest and the risk of erosion by cavitation decreases.

Due to turbulence, for a specific cross-section, the boundary layer thickness and the water depth fluctuate between a low and a high values. (For smooth spillways, instantaneous values of boundary layer thickness can vary between 0.4 and 1.2 times the mean temporal value (Wood 1991).) Because of the unsteadiness of the free-surface and boundary layer, air can instantaneously start to entrain upstream or downstream of the mean temporal inception point of air entrainment, which makes the process of determining its location hard. The difficulty in defining the averaged location of the inception point is the reason for the inexistence of an univocal criteria among authors. Criteria can be divided in two groups, the first is based on visual observation and the second is based on the evaluation of hydraulic parameters, such as velocity and air concentration. Inception point has been mainly located by visual observation (e.g., Sorensen 1985; Tozzi 1992; Bindo et al. 1993; Sanchez-Juny 2001; Chanson and Toombes 2002; Yasuda and Chanson 2003; Sanagiotto 2003; Dai Prá 2004; Gonzalez 2005; Relvas and Pinheiro 2008; Bung 2009). In opposition, Amador et al. (2009) estimate location and flow characteristics at the inception point of stepped spillways from analysis on the boundary layer and velocity profiles in similarity to Cain and Wood (1981), for smooth spillways; and Boes and Hager (2003) define inception point as the cross-section where the air concentration at the pseudo-bottom formed by the step edges equals 0.01.

Present study adopts the classical definition of inception point (the cross-section where the boundary layer reaches the free-surface) to determine its location. Due to instrumentation limitations (see details in chapter 2 Experimental set-up), near the free-surface the instrumentation can return unreliable velocity values (and consequently unreliable boundary layer values) being required another criterion to help determining the inception point location. From observation of air concentration profiles, the inception point is considered located in the cross-section where the time-averaged air concentration is different from zero immediately bellow the waviness zone, although at the pseudo-bottom is virtually null. Using this criterion, the air concentration at the pseudo-bottom is equal to zero, at the inception point, increasing rapidly and reaching the pseudo-bottom in a short distance. Fig. 3a presents air concentration profiles at the inception point, $L/L_i = 1.0$ (when no data was available in this precise location, data obtained in the nearest upstream cross-section was considered) where L is the streamwise coordinate originating at the upstream end of the spillway and L_i is the streamwise coordinate at the inception point. The position of the inception point was also determined by means of visual observation, to allow a comparison between methodologies. In this case, inception point was considered located at the vertical edge immediately upstream of the step concavity where the presence of bubbles is permanent in the entire cross-section (example in Fig. 2a, although locating inception point is a dynamic process and a photo is instantaneous), which is in accordance with the methodology of Mateos and Elviro

(1997). When comparing both approaches, visual observation drives to higher lengths of the non-aerated flow region (15, 20 and 30% higher for steps 8, 4 and 2 cm high, respectively). The corresponding air concentration profiles have large quantities of air at the pseudo-bottom (Fig. 3a), which reveals that the process started upstream. This difference in methodologies results occurs because visual observation does not allow to identify zones near the free-surface where a small quantity of air is already present inside the flow (Matos 1999).

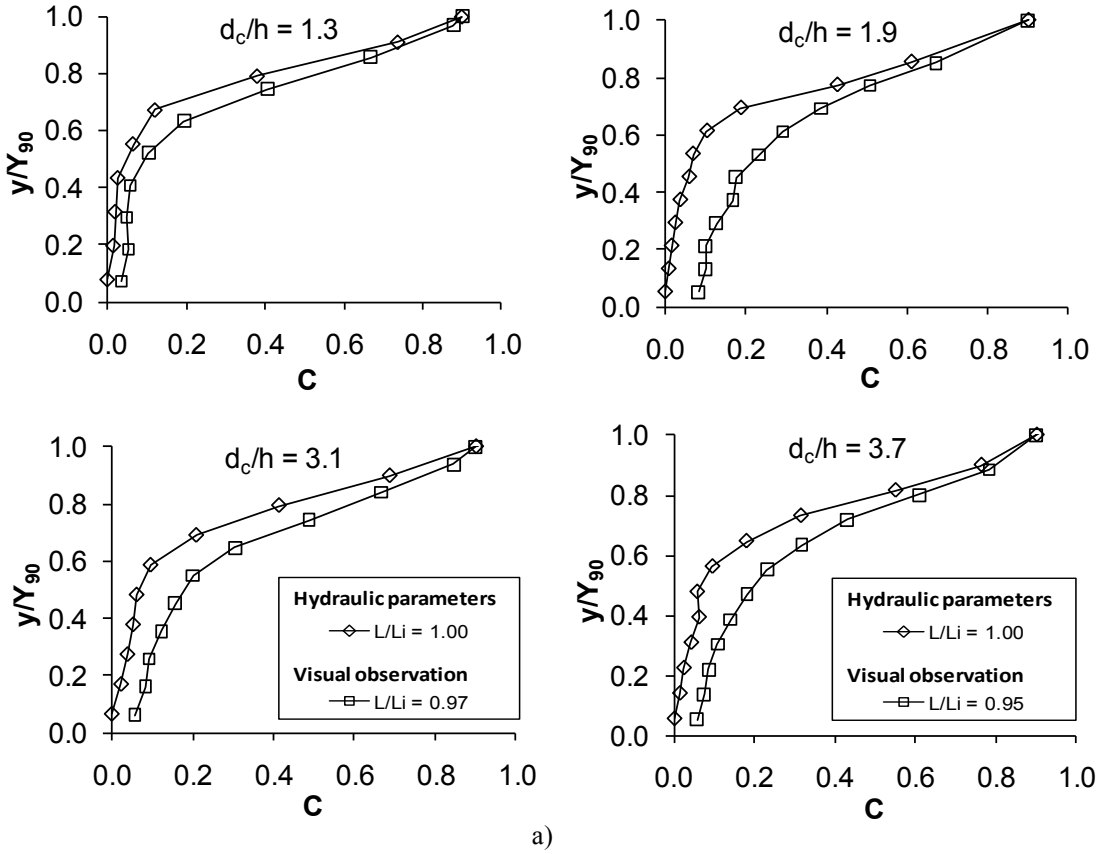

a)

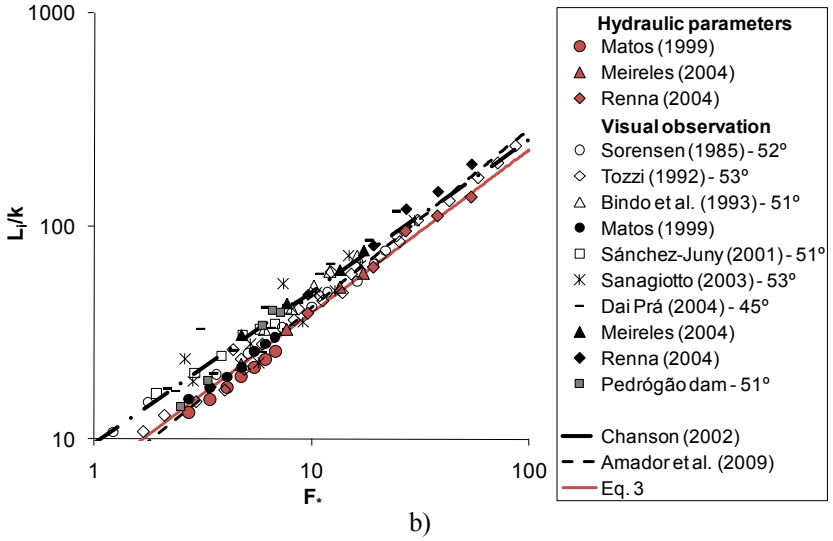

b)

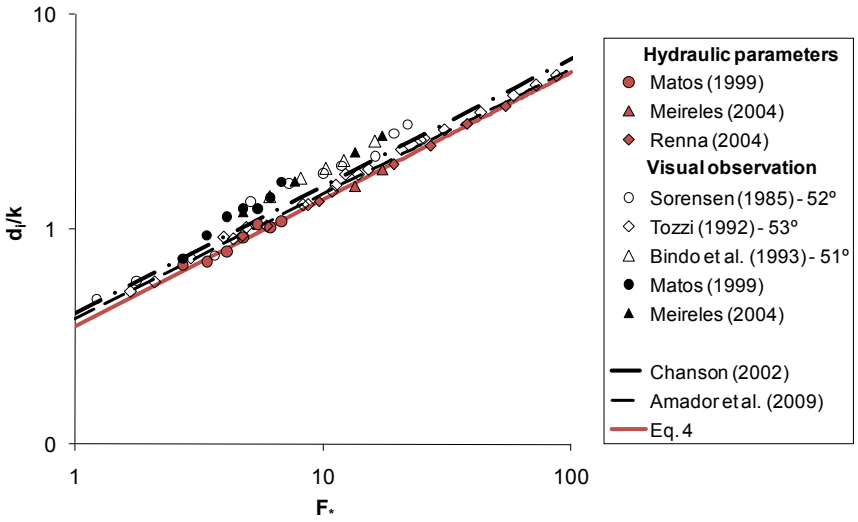

c)

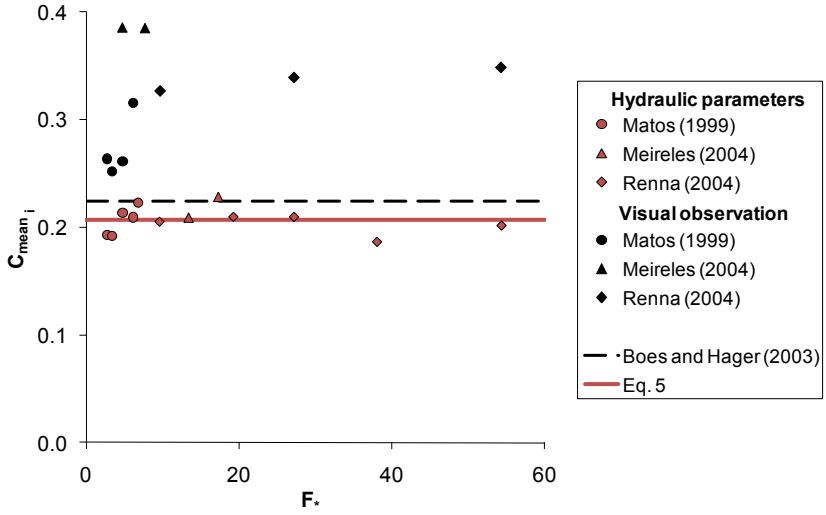

d)

Figure 3 - Flow properties at the inception point: a) air concentration distribution ($L/L_i \neq 1.0$ indicates that no experimental data is available at the inception point; alternatively, the closest upstream experimental air concentration profile was taken into account); b) location; c) equivalent clear-water depth; d) mean air concentration (mean air concentration values, obtained with the conductivity probe, correspond to cross-sections where the inception point was located using hydraulic parameters and by visual observation, respectively).

Cain and Wood (1981) referred that, in smooth spillways, the inception point location is primarily a function of discharge and roughness. These authors observed that it also depends on the spillway geometry, namely the crest type, although to a lesser extent. In this sense, new expressions are presented to determine the main flow properties at the inception point down steep stepped spillways with an ogee crest profile (Fig. 3):

$$\frac{L_i}{k} = 6.753 \left(F_*\right)^{0.765} \quad (3)$$

$$\frac{d_i}{k} = 0.354 \left(F_*\right)^{0.591} \quad (4)$$

$$C_{mean_i} = 0.207 \quad (5)$$

where d_i is the clear-water flow depth at the inception point, C_{meani_i} is the mean air concentration at the inception point, k is the roughness height perpendicular to the pseudo-bottom ($k = h\cos\theta$, where θ is the spillway slope) and F_* is the roughness Froude number, defined as $F_* = q_w \Big/ \sqrt{g \sin\theta\, k^3}$, being g the acceleration of gravity. The mean air concentration, C_{mean}, is defined as $C_{mean} = \int_0^{Y_\varphi} C dy \Big/ Y_\varphi$.

Fig. 3b presents inception point location data of several authors, obtained from different criteria and for different configurations (e.g., spillway slope and step height), although all pertaining to steep stepped spillways. It is observed that visual observation returns higher values of L_i than from the observation of the velocity and air concentration profiles. Data obtained in the Pedrógão dam, during a flood in 2010 (Fig. 4), is in agreement with the other results obtained in laboratory, suggesting the inexistence of scale effects in this parameter for the modeled situations. The entire set of data of the present study is represented by a single expression, in accordance to Boes and Hager (2003) who also observed the location of the inception point to be much more dependent on the critical depth, or unit discharge, than on the step height.

In Fig. 3c equivalent clear-water depth data at the inception point is also presented. Data obtained by visual observation returns slightly higher values, both because the beginning of the bulking aerated zone is already captured, and also because, by visual observation, a mixture depth is read instead of the equivalent clear-water depth (Matos et al. 2000 and Boes and Hager 2003).

Figure 4 - Stepped spillway of Pedrógão dam (Portugal) during a small flood in January 15th, 2010 (courtesy of Hugo Amaral).

The expressions of Chanson (2002), Boes and Hager (2003) and Amador et al. (2009) are also reported in Figs 3b and c. Chanson (2002) proposed his expressions based on a large number of experimental data obtained mainly by visual observation in experimental models and prototypes.

As expected, they return overestimated inception point location and equivalent clear-water depth values. The equation of Boes and Hager (2003) for the location of the inception point returns results close to those obtained in the present study, due to the proximity in criteria. Because a pressurized intake was used, these researchers developed an analytical solution for backwater and drawdown curves to calculate the inception point location for a crested spillway, and although Chanson (2006) argues that pressurized intake inflows return inception points located significantly upstream than uncontrolled chutes, similar results are observed between the uncontrolled chute of present study and the pressurized intake tested by Boes and Hager (2003). The equations of Amador et al. (2009) have been derived from data acquired with the highly accurate PIV instrumentation for one discharge, q_w = 0.11 m^2/s, and step height, h = 5 cm, corresponding to F_* = 7.2. Although obtained with the use of different instrumentation and by different methodologies, expressions of Amador et al. (2009) and of the present study are fairly similar for the tested range of Froude numbers, thanks to the adopted criteria, both based mainly on velocity profile observations. Because data of Amador et al. (2009) pertain to a single Froude number, present study's data allow to extend the range of validity of the expression proposed by these researchers to a wide range of Froude numbers.

Because of the unsteadiness in the boundary layer and water depth, at the inception point the mean air concentration is significantly higher than zero. In the present study, the mean air concentration at the inception point is similar for all tested step heights and discharges, being best predicted by 0.207 (Fig. 3d). The equation proposed by Boes and Hager (2003) (which returns $\overline{C}_i$ = 0.224 for the tested slope), just slightly overestimates the experimental data of this study, which is in accordance to the slight difference in criteria. Because overestimated air concentration profiles are observed when the inception point is located by visual observation (Fig. 3a), data of the mean air concentration are also overestimated (Fig. 3d).

4. FLOW PROPERTIES UPSTREAM OF THE INCEPTION POINT

4.1. AIR CONCENTRATION

In the non-aerated region, and far from the inception point, the air concentration profiles have a characteristic shape, as illustrated in the left side graphs of Fig. 5. At the pseudo-bottom and in a long extension of the profile, no air concentration is registered in opposition to the upper part of the profile, where a fast increase in air concentration is observed, corresponding to air entrapped in the free-surface wavy zone. Close to the inception point (right side graphs of Fig. 5) in addition to the phenomenon described above, entrained air is also captured due to the unsteadiness of the inception point location and consequently, at the wavy zone, higher values than those presented in the right-side graphs of Fig. 5 are registered and immediately below the wavy zone air concentration values different from zero are now captured.

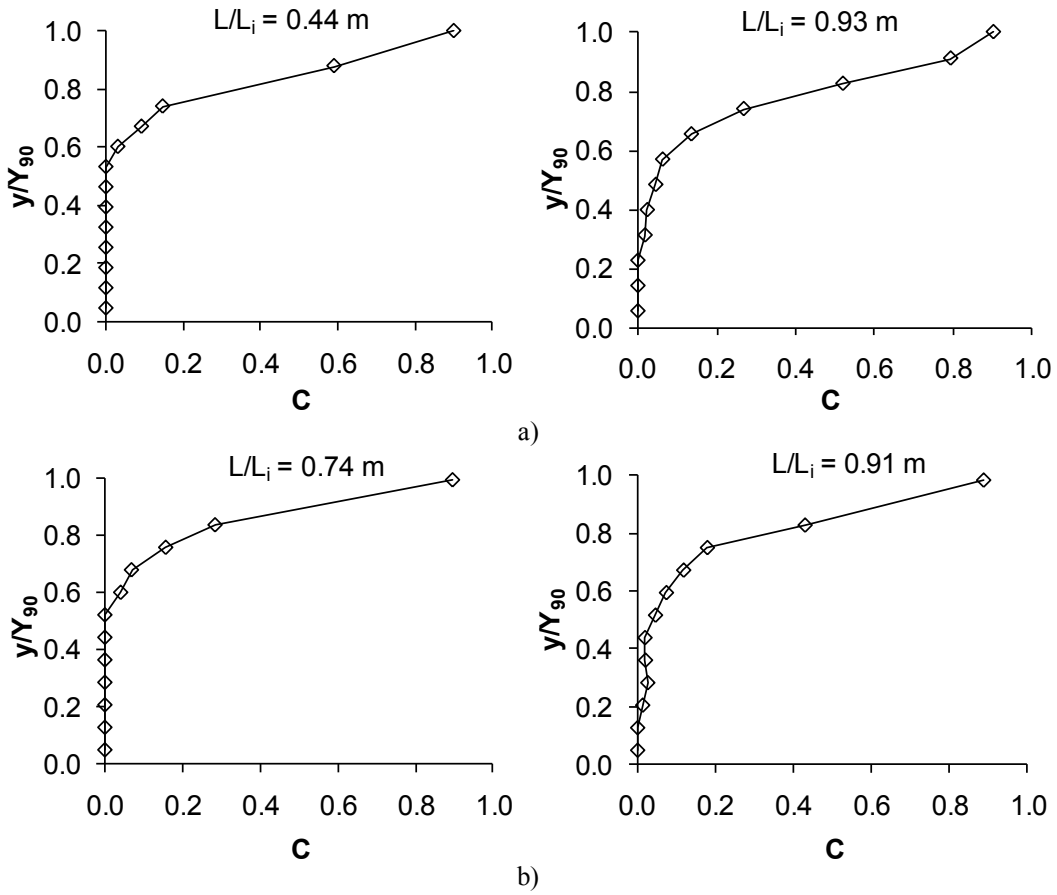

Figure 5 - Air concentration distribution profiles: a) for h = 4 cm and q_w = 180 m^2/s; and b) for h = 8 cm and q_w = 180 m^2/s.

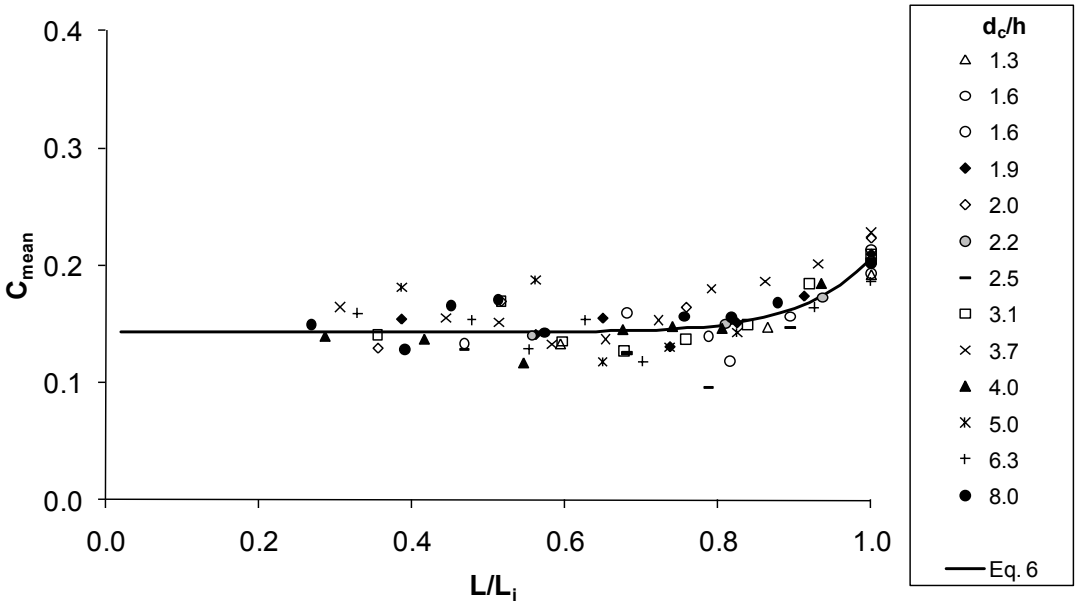

Figure 6 - Development of the mean air concentration: experimental data and Eq. 6.

Fig. 6 presents results of the mean air concentration downstream of the ogee crest, showing that the entrapped mean air concentration is practically constant in the region where the spillway has constant slope until $L/L_i \sim 0.8$, regardless of the normalized critical depth d_c/h, and increases in the vicinity of the inception point, reaching a value approximately equal to 0.2. This behaviour can be predicted, for $0.3 < L/L_i \leq 1.0$, by

$$C_{mean} = 0.143 + 0.0628\left(\frac{L}{L_i}\right)^{10.8} \quad (6)$$

The mean air concentration increases near the inception point, both because of the unsteadiness of the location of the inception point, and because of the increase in waviness near this location, due to turbulence. In fact, air is expected to entrain when the (turbulent) boundary layer reaches the free-surface, then, when close to the inception point, turbulence is already felt very close to the free-surface causing deformations of the surface (waves), that will originate the phenomenon of incorporation of air inside the flow.

4.2. BOUNDARY LAYER DEVELOPMENT

Boundary layer thickness, δ, is customarily defined as the perpendicular distance from the bottom of a channel to the point where the velocity is 0.99 times the potential velocity. Several experimental studies focused in the boundary layer development in smooth spillways (e.g., Bauer 1954 and Cain and Wood 1981) referred that it primarily depends on distance and roughness. Likewise, several researchers (e.g., Tozzi 1992, Chanson 2002 and Amador et al. 2009) considered the growth of the boundary layer down stepped spillways dependent on distance and on the macro-roughness formed by the steps (in similarity to the roughness of the material, but at a higher scale). Tozzi's equation was developed based on data acquired in a stepped chute model with a slope of 1V:0.75H making use of the fact that, at the inception point, water depth and boundary layer thickness overlap, for what no velocity analysis is needed. Latter, Chanson (2002) considered the same approach, based on his expressions to determine location and water depth at the inception point. Contrarily, Amador's equation was developed from the observation of the velocity profiles. In the present study, and in agreement with Amador, data was obtained from observation of the velocity profiles and, at the inception point, from the equivalent clear-water depth measurements. The subsequent expression is proposed for $1.3 < d_c/h < 8.0$, where d_c/h is the critical depth normalized by the step height (Fig. 7):

$$\frac{\delta}{L} = 0.114\left(\frac{L}{k}\right)^{-0.311} \quad (7)$$

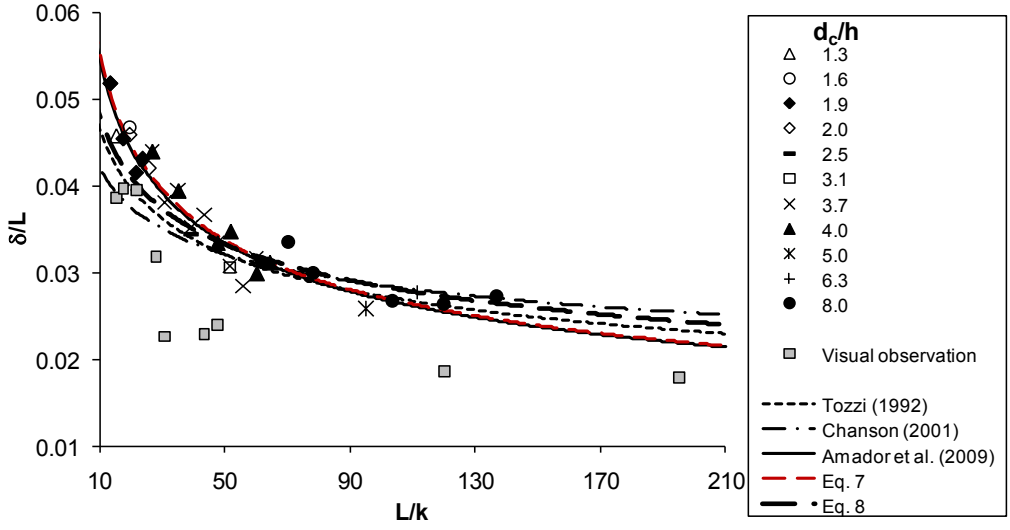

a)

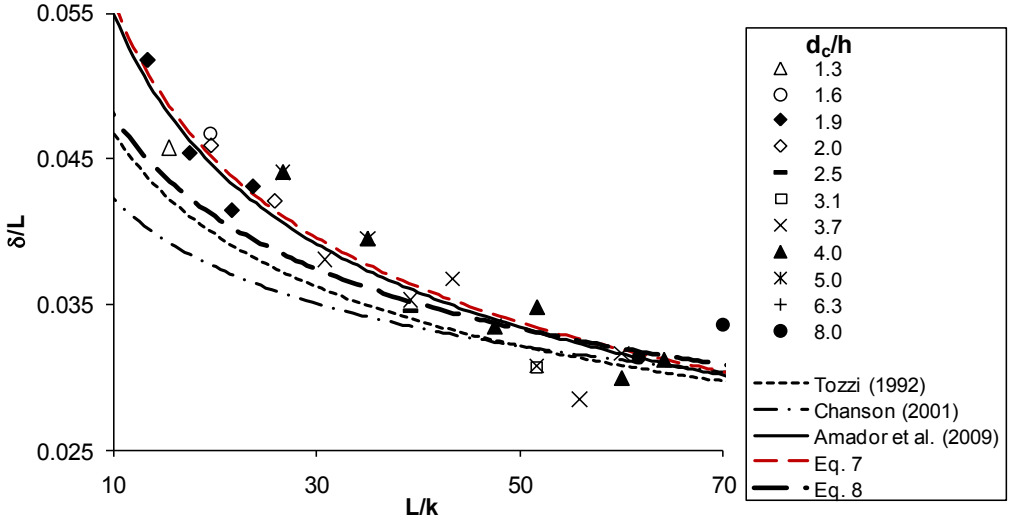

b)

Figure 7 - Development of the boundary layer: a) comparison between experimental data and equations of the type $\delta/L = a(L/k)^{-b}$ with coefficients proposed by different authors; b) detail for L/k < 70.

From Fig. 7, is possible to observe how slightly the boundary layer thickness is affected by d_c/h, explaining the tremendous proximity to Amador's expression, even if it was based only on data for one discharge and step height. Subsequently, presented experimental data allows to extend the validity of Amador's expression to $10 < L/k < 140$, since it was determined from data in the range $15 < L/k < 25$. For comparison purpose, the methodology of Tozzi and Chanson was also followed, considering data of the equivalent clear-water depth obtained at the inception point, located by visual observation (these data are presented in grey, in Fig. 7, and did not contribute to the regression above). It is observed a certain detachment from the other data of this study because of the methodology used to determine the inception point location.

Following Tozzi (1992) and Chanson (2002), the following expression for the development of the boundary layer was obtained from Eqs 3 and 4

$$\frac{\delta}{L} = 0.0810\left(\frac{L}{k}\right)^{-0.227} \qquad (8)$$

returning a curve slightly above Tozzi's equation. Although Eq. 8 is already obtained, indirectly, from data at the inception point obtained from the observation of hydraulic parameters (in opposition to visual observation), because of the difficulties in defining the inception point location, the authors consider Eq. 7 physically more meaningful and accurate. The difference between this last equation and Chanson's and Tozzi's expressions may then rely on the difference of methodologies to locate the inception point. In addition, Chanson's expression was obtained taking into account data obtained for different chute configurations (e.g., slope and type of crest), which might contribute to increase the difference.

4.3. VELOCITY DISTRIBUTION

The normalized velocity profile in non-aerated flows over stepped spillways may be expressed by a power law

$$\frac{V}{V_{max}} = \left(\frac{y}{\delta}\right)^{1/N} \qquad 0 < y/\delta < 1 \qquad (9)$$

where V_{max} is the free-stream velocity and $1/N$ is an exponent. The coefficient N was estimated equal to 5.0, by Chanson (2002), based on 1V:2.9H stepped chute data acquired by Ohtsu and Yasuda (1997), and 5.1 by Meireles and Matos (2009) for a 1V:2H stepped model. A lower value, equal to 3.0, was suggested by Amador et al. (2009) for a 1V:0.8H steep stepped model. In the present study, 66 velocity profiles were used to determine N (Fig. 8a). Although singular velocity profiles (examples in Fig. 8b) correspond to $2.3 \leq N \leq 4.3$ (Fig. 8c), an overall value of $N = 3.4$, with a correlation coefficient of 0.98, was obtained, in agreement with Amador et al. (2009).

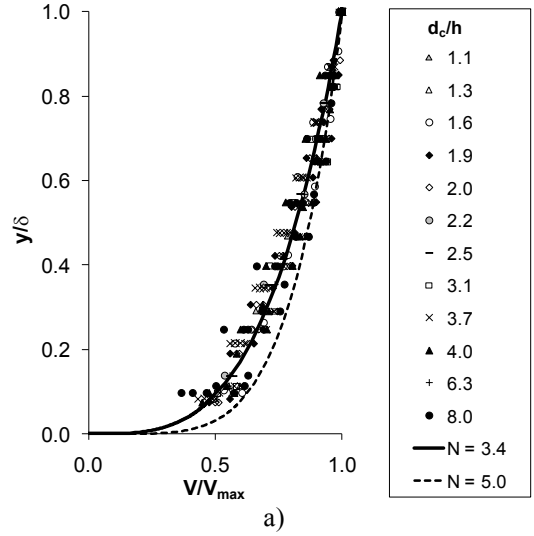

a)

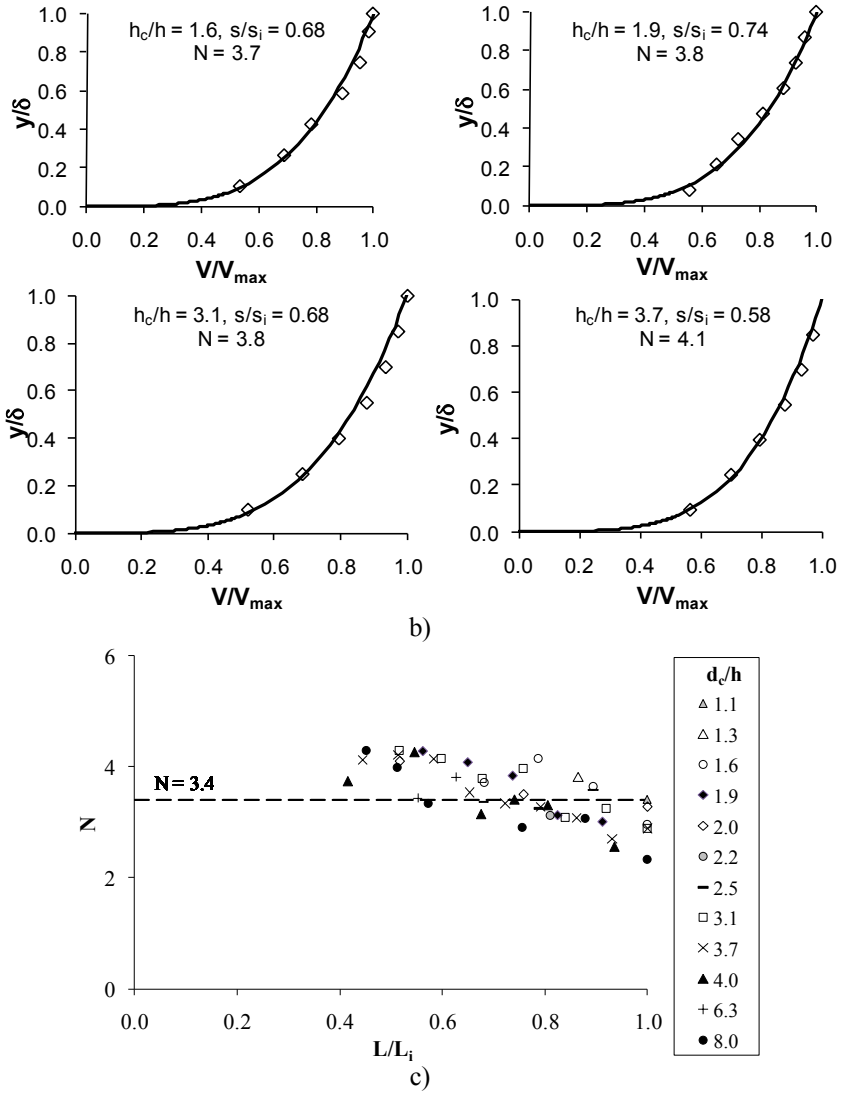

Figure 8 - Normalized velocity distribution upstream of the point of inception: a) comparison between experimental data and the power law for N = 3.4; b) comparison of experimental data at several cross-sections and its adjustment to the power law; and c) power law exponent result's for each tested velocity profile.

4.4. CHARACTERISTIC FLOW DEPTHS

Fig. 9 presents the development of the characteristic flow depths where the air concentration is 90, 95 and 99%, respectively Y_{90}, Y_{95} and Y_{99}, normalized by the equivalent clear-water depth. If the free-surface was smooth and the inception point had a constant location, they would all collapse in the value of the equivalent clear-water depth. Far from the inception point, results pertain uniquely to the frequency and amplitude of the waves. Observing Fig. 9, can be concluded, for instance, that the waves are around 1.5 times the equivalent clear-water depth and the highest waves are not prone to occur with high frequency. In fact, in a non-aerated flow, an air concentration of φ% does not stand for a flow mixture of air and water but for a wavy water flow for what, as high is the time-averaged air concentration, the less number of times the water attained that depth during the

global time of acquisition. These observations have direct implications in the design of the spillway sidewalls. For design purposes, the sidewalls can be 1.8 times the equivalent clear-water depth.

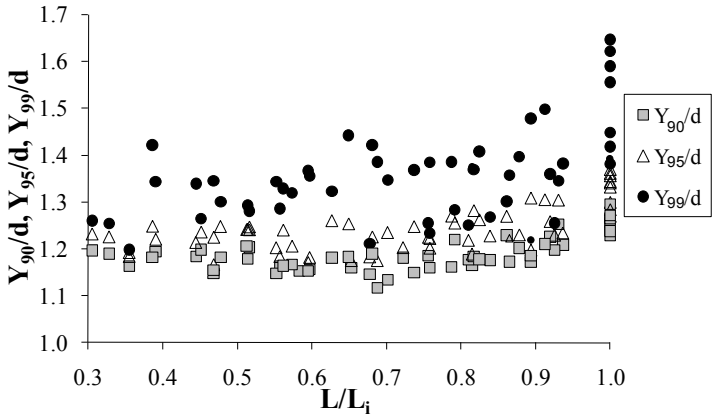

Figure 9 - Development of the characteristic flow depths Y_{90}, Y_{95} and Y_{99}.

For the gathered experimental data, normalized equivalent clear-water depth d/d_i is practically independent of dc/h and depends strongly on L/L_i (Fig. 10a). (d and L were normalized with experimental results of d_i and L_i, obtained from the observation of the velocity and air concentration profiles.) Fig. 10 presents also data of several other authors: Tozzi (1992) and Sanagiotto (2003) (Fig. 10b), for the slope of 1V:0.75H, plus Amador et al. (2009) (Fig. 10c), for 1V:0.8H, and Dai Prá. (2004) (Fig. 10d), for 1V:1H, where d and L were normalized with results of d_i and L_i obtained from Eqs 3 and 4. All the data ($0.44 \leq d_c/h \leq 19.34$) tend to collapse in (Fig.10):

$$\frac{d}{d_i} = 1.17 - 0.252\frac{L}{L_i} + \frac{0.0845}{L/L_i} \qquad (10)$$

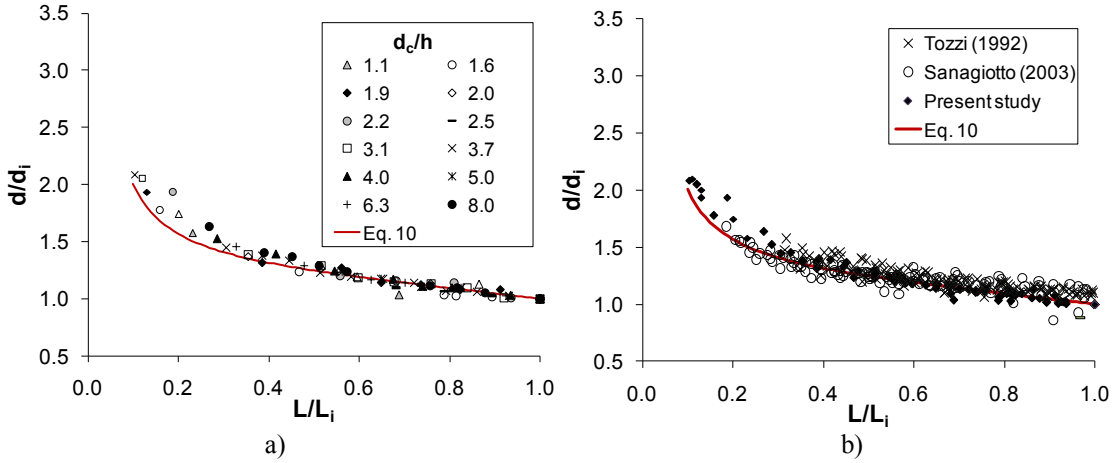

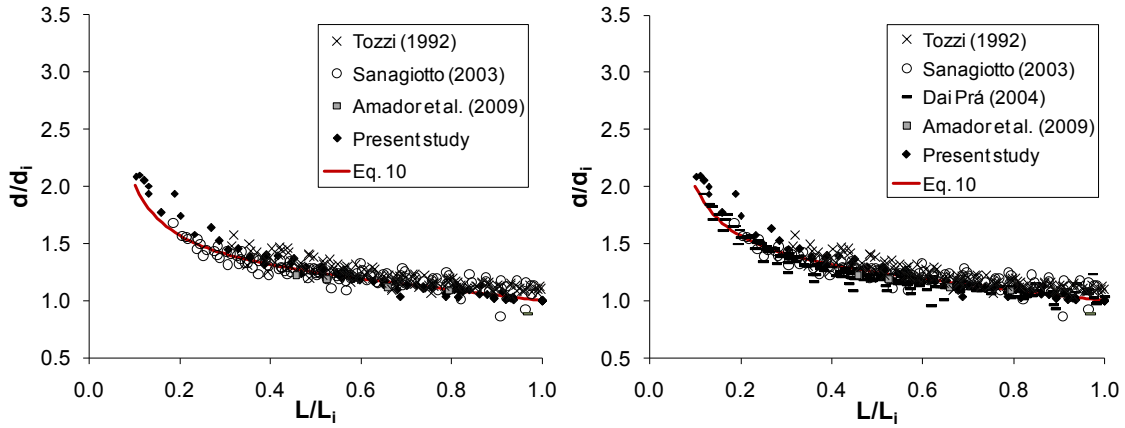

Figure 10 - Normalized equivalent clear-water depth development: comparison between experimental data and Eq. 10. Data of Amador et al. (2009) obtained from digitalization.

When applying Eq. 10, Eqs 3 and 4 should be used to determine the location of the point of inception of air entrainment and respective equivalent clear-water depth.

Theoretically, assuming the power law velocity distribution, the continuity equation results in (e.g., Chanson 2002)

$$q_w = V_{max} * \left(d - \frac{\delta}{N+1} \right) \quad (11)$$

where the free-stream velocity is given by

$$V_{max} = \sqrt{2g\left(H_{max} - z_0 - d\cos\theta\right)} \quad (12)$$

H_{max} is the upstream total head and z_0 is the vertical coordinate (from the downstream end of the stepped chute, positive sign upwards). If the definition of displacement thickness is considered and a power law velocity distribution is assumed, Eq. 11 is also obtained. (The displacement thickness δ_1 is the distance by which a surface would have to be moved in an ideal fluid flow to give the same discharge as in a real fluid, calculated for a two-dimensional flow by $\delta_1 = \int_0^{\delta} \left(1 - V/V_{max}\right) dy$ (Rouse 1959).)

For each tested discharge, water depth can be determined iteratively from Eq. 11, where the free-stream velocity and the boundary layer thickness are determined from Eqs 12 and 7, respectively, and N is assumed equal to 3.4. Where the spillway has variable slope, the vertical coordinate (z_0) and the water depth perpendicular to the bottom ($d\cos\theta$) are calculated considering the curvature of the bottom.

Fig. 11 presents a comparison between experimental data, the empirical relation and the theoretical methodology. Both methodologies return an overall good prediction of the data. As a curiosity, when Eq. 8 is considered to predict the boundary layer growth, differences in the results of Eq. 11 are imperceptible, showing that relatively large changes in the prediction of δ produce negligible changes in the equivalent clear-water depth.

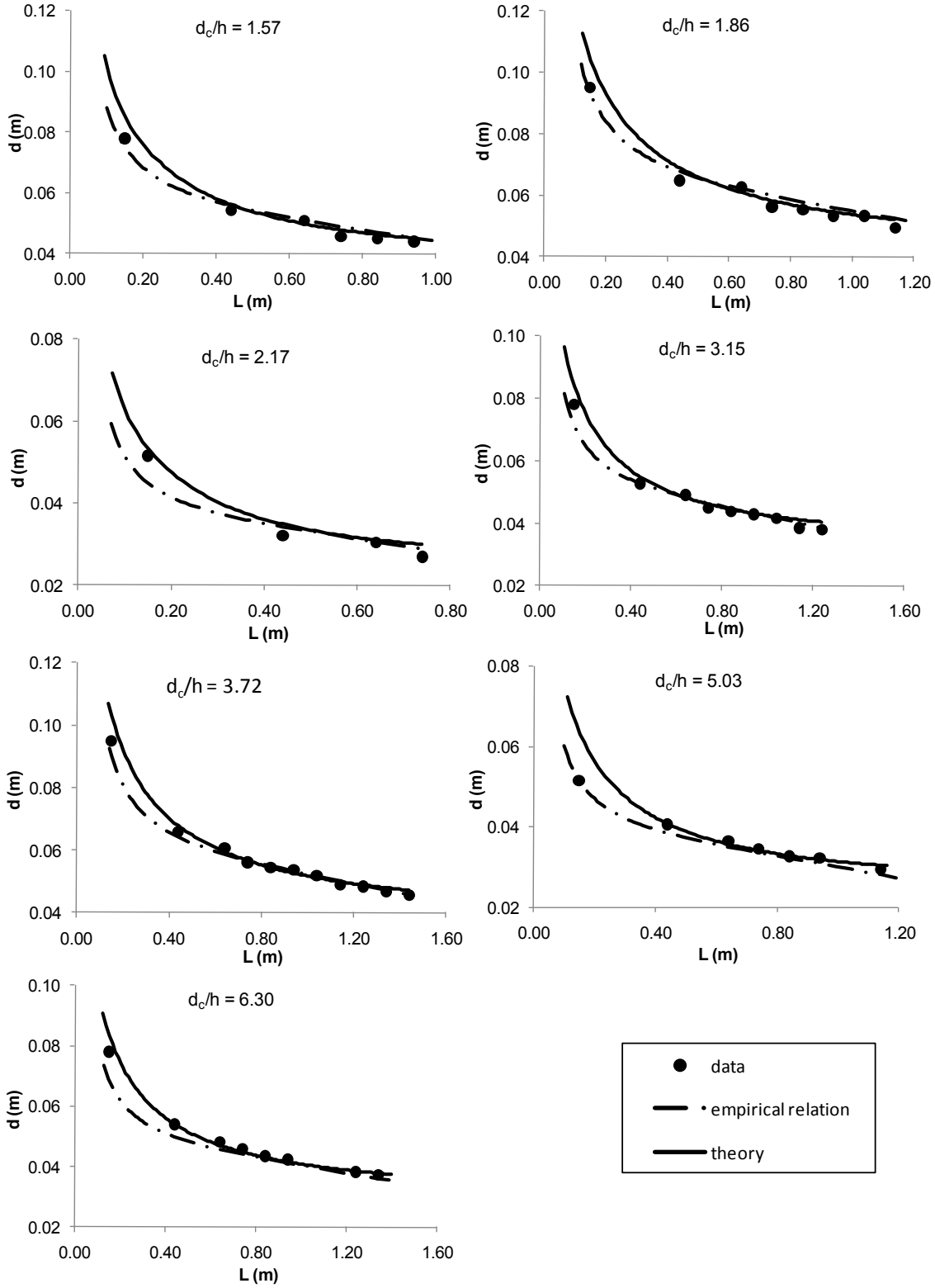

Figure 11 - Equivalent clear-water depth development: comparison between experimental data and different methodologies.

4.5. ENERGY DISSIPATION

In a steep stepped spillway of slope θ, considering gradually varying streamlines, the specific energy, H, can be calculated by

$$H = d\cos\theta + \alpha\frac{{q_w}^2}{d^2(2g)} \quad (13)$$

where α is the kinetic energy correction coefficient, which is, by definition

$$\alpha = \frac{\int_0^d V^3 dy}{{V_{mean}}^3 d} \quad (14)$$

Considering the velocity power law, the kinetic energy correction coefficient can be given by

$$\alpha = \left(\frac{V_{\max}}{(q_w/d)}\right)^3 \frac{1}{d}\left[\left(\frac{N}{N+3}\right)\delta + (d-\delta)\right] \quad (15)$$

Considering the energy principles described by Rouse (1946), and the concept of energy thickness, δ_3, Campbell et al. (1965) determined the head loss in the developing flow region from

$$\Delta H = \frac{\delta_3 U^3}{2gq_w} \quad (16)$$

In analogy to the displacement thickness, the energy thickness can be defined as the distance by which the surface would have to be moved in an ideal fluid flow to give the same flux of kinetic energy as in a real fluid. For a two-dimensional flow, the energy thickness is given by (Rouse 1959)

$$\delta_3 = \int_0^\delta \frac{V}{V_{\max}}\left(1 - \frac{V^2}{{V_{\max}}^2}\right)dy \quad (17)$$

which, considering the velocity power law, can be replaced by

$$\delta_3 = \delta\left[\left(1+\frac{1}{N}\right)^{-1} - \left(1+\frac{3}{N}\right)^{-1}\right] \quad (18)$$

The specific energy is thus obtained from

$$H = H_{\max} - \Delta H \quad (19)$$

where $H_{\max}$ is the maximum specific energy at any section along the chute.

Based on the experimental data obtained in the present study, the kinetic energy coefficient is computed from Eq. 15 and presented in Fig. 12 as a function of the dimensionless distance from the crest L/L_i. For $0.36 \leq L/L_i \leq 1.00$ the kinetic energy coefficient can be predicted by:

$$\alpha = 1 + 0.189 \left(\frac{L}{L_i} \right)^{1.28} \qquad (20)$$

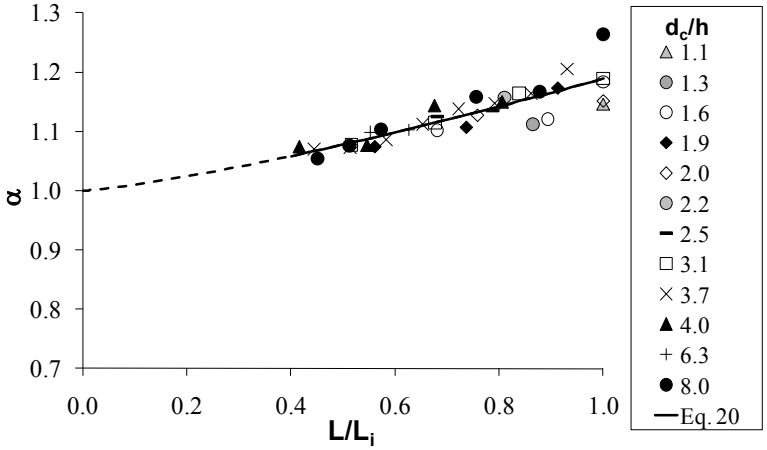

Figure 12 - Development of the kinetic energy coefficient: comparison between experimental data and Eq. 20.

Fig. 13 presents results of the specific energy obtained from Eq. 13, considering experimental results of the equivalent clear-water depth and the kinetic energy coefficient. Along with experimental data are also presented results of the two methodologies described above. In the first methodology, where the specific energy is computed with Eq. 13, Eqs 10 and 20 are used to compute the equivalent clear-water depth and the kinetic energy coefficient and Eqs 3 and 4 are used to determine the location and equivalent clear-water depth at the inception point. The second methodology considers Eq. 19 with Eqs 7, 16 and 18 to determine the boundary layer thickness, the energy loss and the energy thickness, respectively, considering N = 3.4.

The normalized specific energy, H_r/H_{max}, is computed and presented in Fig. 14 along with the following simple empirical equation

$$\frac{H_r}{H_{max}} = 1 - 0.315 \cdot \left(\frac{L}{L_i} \right) \qquad (21)$$

where the residual specific energy, H_r, is the specific energy at the downstream end of the spillway. Is observed a much smaller rate of energy dissipation than usually reported for stepped spillways with aerated flow condition, revealing that air contributes strongly to dissipate energy. However, results are in the range of the results obtained by Meireles and Matos (2009) and Hunt and Kadavy (2010) for the developing region of the skimming flow down stepped spillways with slope typical of embankment dams. In agreement with Hunt and Kadavy (2010), a linear variation is observed, for what a linear development is proposed for Eq. 21. Although higher rates of dissipation are observed in the non-aerated region of stepped spillways than in smooth spillways,

attention must be taken to the smaller amount of dissipation, when comparing with highly aerated flows, in the design of downstream energy dissipators.

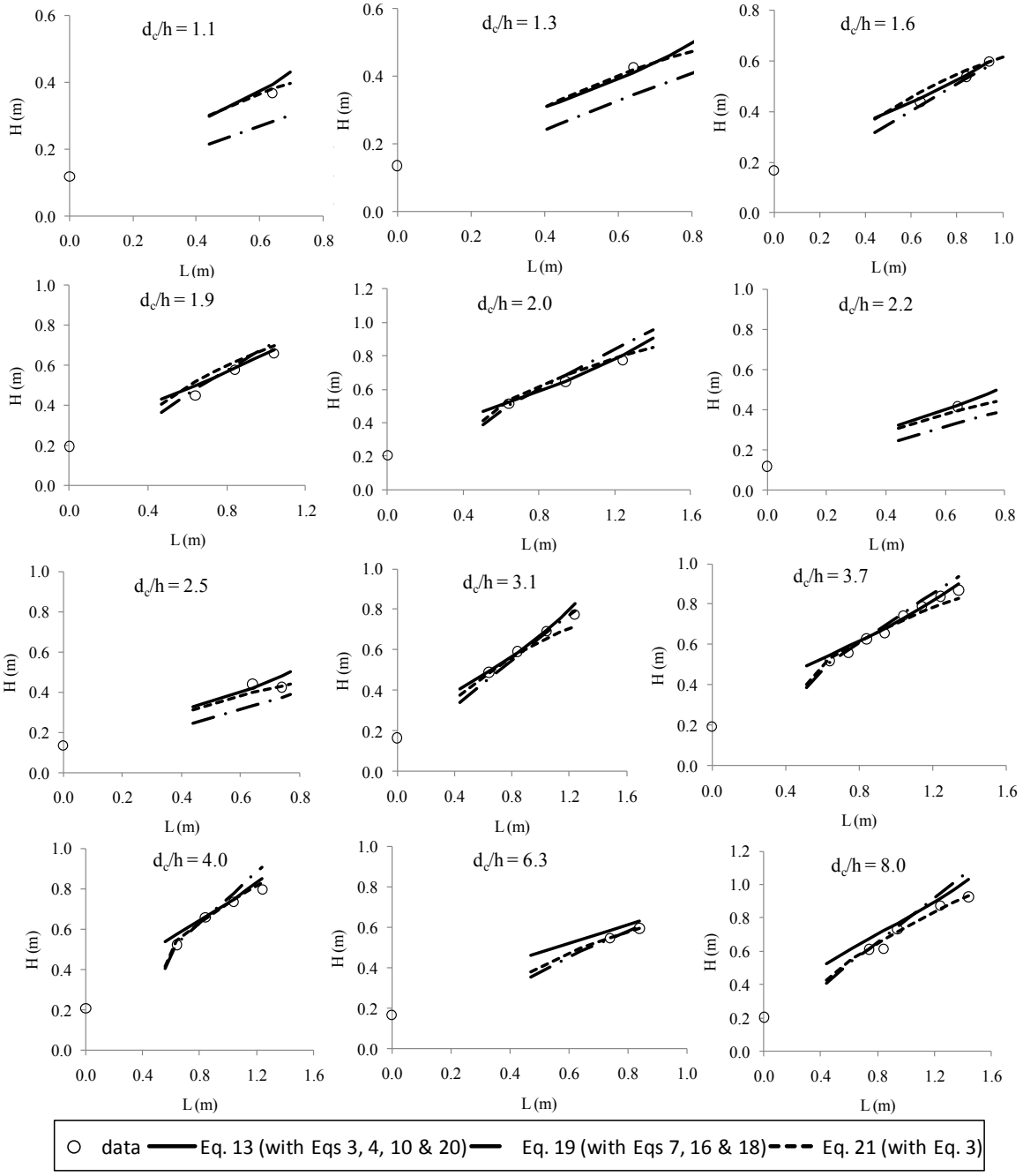

Figure 13 - Development of the specific energy: comparison between experimental data and Eqs 13 (with Eqs 3, 4, 10 and 20) and 19 (with Eqs 7, 16 and 18).

Results from Eq. 21 are also presented in Fig. 13. All the three methodologies presented in this figure give around the same level of agreement, being Eq. 21 of very simple and direct application for design purposes. The concept of energy loss described by Campbell et al. (1965) was used in some recent studies. Castro-Orgaz et al. (2010) apply the concept to the developing flow of a round-nosed broad-crested weir and Amador et al. (2009) apply to the developing flow of a steep stepped spillway, whose results are in close agreement with those of the present study.

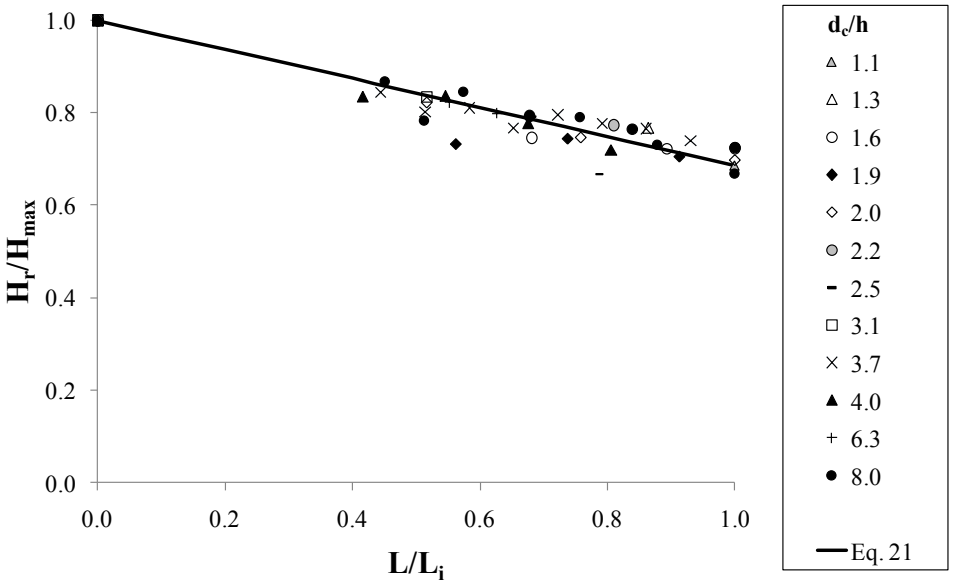

Figure 14 - Rate of energy dissipation: experimental data and Eq. 21.

5. FINAL REMARKS

A detailed and extensive experimental study focused on the non aerated region of the flow down steep stepped spillways was undertaken. The corresponding results have applicability in concrete or RCC dam stepped spillways of small dimension or subjected to high unit discharges.

A comparison between a broad range of data pertaining to the inception point and obtained from different methodologies is performed. Visual observation is observed to return values of the non aerated region length, L_i, up to 30% higher than considering the more accurate methodology based in the observation of hydraulic parameters. New expressions for determining the location at and the water depth and mean air concentration in the inception point from observation of hydraulic parameters are proposed. A comparison between visually observed inception point locations obtained both in experimental facilities and in prototype suggests the inexistence of scale effects for the corresponding modelled results.

Data acquired in the non aerated region allowed to characterize this region in terms of boundary layer development, characteristic depths, velocity, energy dissipation and entrapped air concentration. Boundary layer thickness data obtained from different methodologies and different expressions are presented and analyzed. Is observed a visible difference in results obtained considering different methodologies for locating the inception point and an expression obtained following the most accurate methodology is proposed. The concepts of entrained and entrapped air, along with undulation of the free-surface, are discussed and data from the characteristic depths Y_{90}, Y_{95} and Y_{99} are presented with the intention to help in the design of the spillway sidewalls. In fact, in the non aerated region, air concentrations between 0 and 1 respect to the waviness of the flow. For design purposes, the sidewalls are proposed to be 1.8 times the equivalent clear-water depth. Equivalent clear-water depth can be obtained from the presented theoretical or empirical expressions, returning similar results. For a certain discharge, the mean water velocity can be

obtained from the proposed water depth expressions and the velocity profiles can be well reproduced by a power law with $N = 3.4$. In fact, although experimental data of the power law exponent are observed to vary along the non aerated region, the scatter does not allow to observe a clear tendency and an overall exponent of 1/3.4 is suggested. Finally, different methodologies are presented to determine energy dissipation and a simple empirical expression is proposed for design purposes. The rate of energy dissipation is observed to be smaller than observed in stepped spillways subjected to highly aerated flows, which is in agreement with other studies presented in the literature for slopes typical of embankment dams.

ACKNOWLEDGMENTS Inês Meireles was Visiting Scholar at the University of California, Davis, for two periods of 6 months in 2007/2008 (supported by Fulbright/FLAD) and in 2009/2010 (supported by the Portuguese National Science Foundation - FCT) and is currently supported by FCT, Grant No. SFRH/BD/38003/2007. The financial support granted by FCT, though Project PTDC/ECM/108128/2008 and the support granted by the National Laboratory of Civil Engineering (LNEC), Lisbon, are also gratefully acknowledged.

REFERENCES

Airey, M. (2004). Personal communication.

Amador, A., Sanchez-Juni, M., Dolz, J. (2006). "Characterization of the non-aerated flow region in a stepped spillway by PIV." J. Fluid Eng., ASME, 138(6), 1266-1273.

Amador, A., Sánchez-Juny, M. and Dolz, J. (2009). "Developing flow region and pressure fluctuations on steeply sloping stepped spillways." J. Hydr. Eng., ASCE, 135(12), 1092-1100.

André, S. (2004). "High velocity aerated flows over stepped chutes with macro-roughness elements." Ph.D. thesis, EPFL, Lausanne, Switzerland.

Bauer, W. J. (1954). "Turbulent boundary layer on steep slopes." Transaction, ASCE, Vol. 119, 1212-1233.

Bindo, M., Gautier, J., and Lacroix, F. (1993). "The stepped spillway of M'Bali dam." Water Power & Dam Const., 45(1), 35-36. ou será 1999?

Boes, R. M. and Hager, W. H. (2003). "Two phase flow characteristics of stepped spillways." J. Hydr. Eng., ASCE, 129(9), 661-670.

Bombardelli, F. A., Meireles, I. and Matos, J. (2010). "Laboratory measurements and multi-block numerical simulations of the mean flow and turbulence in the non-aerated skimming flow region of steep stepped spillways." Env. Fluid Mechanics, Springer (published online).

Bung, D. B. (2009). "Zur selbstbelüfteten gerinneströmung auf kaskaden mit gemässigter neigung. " Ph.D. thesis, Bergische University of Wuppertal, Germany (in German).

Bung, D. B. and Schlenkhoff, A. (2010) "Self-aerated skimming flow on embankment stepped spillways - the effect of additional micro-roughness on energy dissipation and oxygen transfer." Proc. 1st European IAHR Congress, Edimburgh, UK. (In CD.)

Cain, P. and Wood, I. R. (1981). "Measurements of self-aerated flow on a spillway." J. Hydr. Eng., ASCE, 107(HY11), 1407-1424.

Campbell, F. B., Cox, R. G., and Boyd, M. B. (1965). "Boundary layer development and spillway energy loss." J. Hydr. Div., 91(3), 149–163.

Carvalho, R., and Amador, A. (2008). "Physical and numerical investigation of the skimming flow over a stepped spillway." Proc. 3rd IAHR Intl Symposium on Hydraulic Structures, Nanjing, China, 1767-1772. (In CD.)

Castro-Orgaz, O., Giráldez, J. V., and Ayuso, J. L. (2010). "Critical depth relationships in developing open-channel flow." J. Hydr. Eng., ASCE, 136(3), 175-178.

Chamani, M. R., and Rajaratnam, N. (1999). "Characteristics of skimming flow over stepped spillways." J. Hydr. Eng., ASCE, 125(4), 361-368.

Chanson, H. (2002). "The hydraulics of stepped chutes and spillways." Balkema, Lisse, The Netherlands.

Chanson, H. (2006). "Hydraulics of skimming flows on stepped chutes: The effects of inflow conditions?." J. Hydr. Res., 44(1), 51–60.

Chanson, H. and Toombes, L. (2002). "Experimental investigations of air entrainment in transition and skimming flows down a stepped chute." Can. J. Civil Eng., 29(1), 145–156.

Chen, Q., Dai, G., and Liu, H. (2002). "Volume of fluid model for turbulence numerical simulation of stepped spillway overflow." J. Hydr. Eng., ASCE, 128(7), 683-688.

Chinnarasri, C., Donjadee, S. and Israngkura, U. (2008). "hydraulic characteristics of gabion-stepped weirs." J. Hydr. Eng., ASCE, 134(8), 1147-1152.

Dai Prá, M. (2004). "Características de escoamentos sobre vertedouros em degraus de declividade 1V:1H. " M.Sc. thesis, UFRGS, Porto Alegre, Brazil (in Portuguese).

Dussard B., Deschard, B. and Penel, F. (1992). "Petit Saut: an RCC dam in a wet tropical climate." Water Power & Dam Construction, February, 30-32.

Frizel, K. H. (1992). "Hydraulics of stepped spillways for RCC dams and dam rehabilitation." Proc. 3rd Specialty Conference in Roller Compacted Concrete, ASCE, San Diego, USA, 423-439.

Geringer, J. J. (1995). "The design and construction of RCC dams in Southern Africa." Proc. Int. Symposium on RCC Dams, Santander, Spain, 1459-1495.

Gomes, J. F. (2006). "Campo de pressões: condições de incipiência à cavitação em vertedouros em degraus com declividade 1V:0,75H." Ph.D. thesis, UFRGS, Porto Alegre, Brazil (in Portuguese).

Gonzalez, C. (2005). “An experimental study of free-surface aeration on embankment stepped chutes.” Ph.D. thesis, University of Queensland, Brisbane, Australia.

Gonzalez, C., and Chanson, H. (2007). “Hydraulic design of stepped spillways and downstream energy dissipators for embankment dams.” Dam Engineering, XVII(4), 223-244.

Goubet, A. (1992). “Evacuateurs de crues en marches d’escalier.” La Houille Blanche, 2/3, 159-162 (in French).

Hakoishi, N. and Sumi, T. (2000). “Hydraulic design of Nakasujigawa dam stepped spillway.” Proc. 1st Int. Workshop on Hydraulics of Stepped Spillway, Zürich, Switzerland, A.A. Balkema Publisher, Rotterdam, The Netherlands, 27-34.

Hollingworth, F. and Druyts, F. H. W. (1986). “Rollcrete: some applications to dams in South Africa.” Water Power & Dam Construction, 38(1), 13-16.

Houston, K. L. (1987). “Hydraulic model studies of Upper Stillwater dam stepped spillway and outlet works.” Report nº REC-ERC-87-6, U.S. Department of Interior, Bureau of Reclamation, Denver, USA.

Hunt, S. L., and Kadavy, K. C. (2010). “Energy dissipation on flat-sloped stepped spillways: part 1. upstream of the inception point.” Transactions, ASABE, 53(1), 103-109.

Hunt, S. L., Kadavy, K. C., Abt, S. R., Temple, D. M. (2008) "Impact of converging chute walls for roller compacted concrete stepped spillways." J. Hydr. Eng., ASCE, 134(7), 1000-1003.

Mateos, I. and Elviro, G. (1992). “The use of stepped spillways in energy dissipation.” Proc. Intl Symposium on Dams and Extreme Floods. ICOLD, Spanish National Committee, Granada (Spain), 241-265.

Mateos, I. and Elviro, G. (1997). “Initiation of aeration in stepped spillways.” Proc. 27th IAHR Intl Congress, Theme D, San Francisco, USA, 589-594. (In CD.)

Matos (1999). "Emulsionamento de ar e dissipação de energia do escoamento em descarregadores em degraus." Ph.D. thesis, IST, Lisbon, Portugal (in Portuguese).

Matos, J. (2000). “Hydraulic design of stepped spillways over RCC dams.” Proc. 1st Int. Workshop on Hydraulics of Stepped Spillway, Zürich, Switzerland, A.A. Balkema Publisher, Rotterdam, The Netherlands, 187-194.

Matos, J., and Frizell, K. W. (1997). “Air concentration measurements in highly turbulent aerated flow”. Proc. 27th IAHR Congress, Theme D, Vol. 1, San Francisco, USA, S. S. Y. Wang and T. Carstens (eds.), 149-154.

Matos, J. and Frizell, K. H. (2000). “Air concentration and velocity measurements on self-aerated flow down stepped chutes.” Proc. ASCE 2000 Conference, Minneapolis, USA.

Matos, J., Sánchez, M., Quintela, A., and Dolz, J. (2000). ‘‘Air entrainment and safety against cavitation damage in stepped spillways over RCC dams.’’ Proc. 1st Int. Workshop on Hydraulics

of Stepped Spillway, Zürich, Switzerland, A.A. Balkema Publisher, Rotterdam, The Netherlands, 69–76.

Matos, J., Frizell, K. H., André, S., and Frizell, K. W. (2002). "On the performance of velocity measurement techniques in air-water flows." Proc. EWRI/IAHR Joint Conference on Hydraulic Measurements & Experimental Methods, ASCE, Estes Park, USA (CD-ROM).

McKenna, B. W. (2001). "Air-water gas transfer on stepped spillways." M.Sc. Thesis, Colorado State University, USA.

Meireles, M. (2004). "Emulsionamento de ar e dissipação de energia do escoamento em descarregadores em degraus." M.Sc. thesis, IST, Lisbon, Portugal (in Portuguese).

Meireles, I., and Matos, J. (2009). "Skimming flow in the non-aerated region of stepped spillways over embankment dams." J. Hydr. Eng., ASCE, 135(8), 685-689.

Meireles, I., Matos, J. and Falcão-de-Melo, J. (2006). "Skimming flow properties upstream of air entrainment inception on steeply sloping stepped chutes." Proc. Intl Symposium on Hydraulic Structures, IAHR, Ciudad Guayana, Venezuela. (In CD.)

Melo, J. F. (2004). Personal communication.

Mujib dam (2004, July 30). Lahameyer International, Consulting Engineering. Internet: URL< http://www.lahameyer.de/e/units/gw/mujib.pdf

Ohtsu, I., and Yasuda, Y. (1997). "Characteristics of flow conditions on stepped channels." Proc. 27th. IAHR Congress, San Francisco, Theme D, 583-588. (In CD.)

Ohtsu, I., Yasuda, Y. and Takahashi, M. (2004). "Flow characteristics of skimming flows in stepped channels." J. Hydr. Eng., ASCE, 130(9), 860-869.

RCC Dams (2003). "Water Power & Dam Construction Yearbook 2003." Water Power & Dam Construction, 239-245.

Relvas, A. T. and Pinheiro, A. N. (2008). "Inception point and air concentration in flows on stepped chutes lined with wedge-shaped concrete blocks" J. Hydr. Eng., ASCE, 134(8), 1042-1051.

Renna, F. (2004). "Caratterizzazione fenomenologica del moto di un fluido bifasico lungo scaricatori a gradini." Ph.D. thesis, Politecnico di Bari, Cosenza, Italy (in Italian).

Rouse, H. (1946). "Elementary mechanics of fluids", John Wiley & Sons, Inc., New York, USA.

Rouse, H. (1959). "Advanced mechanics of fluids", John Wiley & Sons, Inc., New York, USA.

Sanagiotto, D. (2003). "Características do escoamento sobre vertedouros em degraus de declividade 1V:0,75H." M.Sc. thesis, UFRGS, Porto Alegre, Brazil (in Portuguese).

Sánchez-Juny, M. (2001). "Comportamiento hidráulico de los aliviaderos escalonados en presas de hormigón compactado. análisis del campo de presiones." Ph.D. thesis, UPC, Barcelona, Spain (in Spanish).

Sorensen, R. (1985). “Stepped spillway hydraulic model investigation.” J. Hydr. Eng., ASCE, 111(12), 1461-1472.

Tabbara, M., Chatila, J. and Awwad, R. (2005). “Computational simulation of flow over stepped spillways.” Computers & Structures, Elsevier, 83 (2005), 2215-2224.

Toombes, L., and Chanson, H. (2000). “Air-water flow and gas transfer at aeration cascades: a comparative study of smooth and stepped chutes.” Proc. 1st Int. Workshop on Hydraulics of Stepped Spillway, Zürich, Switzerland, A.A. Balkema Publisher, Rotterdam, The Netherlands, 77-84.

Tozzi, M. J. (1992). “Caracterização/comportamento de escoamentos em vertedouros com paramento em degraus.” Ph.D. thesis, Escola Politécnica da Universidade de S. Paulo, Brazil (in Portuguese).

Wark, R. J., Kerby, N. E. and Mann, G. B. (1991). “New Victoria dam project.” ANCOLD Bulletin, 88, August, 14-32.

Wilhelms, S. C. and Gulliver, J. S. (2005). “Bubbles and waves description of self-aerated spillway flow.” J. Hydr. Res., 43(5), 522–531.

Wood, I. R. (1991). “Free-surface air entrainment on spillways”. Air entrainment in free-surface flows, Ed. Ian R. Wood, IAHR, Hydraulic Structures Design Manual nº 4, Hydraulic Design Considerations, Balkema, pp. 55-84.

Yasuda, Y. and Chanson, H. (2003). “Micro- and macro-scopic study of two-phase flow on a stepped chute.” Proc. 30th IAHR Congress, Thessaloniki, Greece, 695-702. (In CD.)

Yasuda, Y. and Ohtsu, I. (2003). “Effect of step cavity area on flow characteristics of skimming flows on stepped chutes.” Proc. 30th IAHR Congress, Thessaloniki, Greece, 703-710. (In CD.)

4.2 MEASURING AIR ENTRAINMENT AND FLOW BULKING IN SKIMMING FLOW OVER STEEPLY SLOPING STEPPED CHUTES

Sub-chapter 4.2 was published in the conference proceedings of the Hydraulic Measurements & Experimental Methods 2007, Lake Placid, September 2007. The authors are I. Meireles, J. Matos and K. Frizell.

This sub-chapter concerns to experimental results obtained in the 1V:0.75H slope stepped channel of LNEC and is focused on the hydraulic characteristics of the skimming flow in the aerated region.

ABSTRACT 4.2-1
1. INTRODUCTION 4.2-1
2. EXPERIMENTAL SET-UP 4.2-1
3. AIR ENTRAINMENT 4.2-2
4. FLOW BULKING 4.2-3
5. CONCLUSIONS 4.2-5
REFERENCES 4.2-5

MEASURING AIR ENTRAINMENT AND FLOW BULKING IN SKIMMING FLOW OVER STEEPLY SLOPING STEPPED CHUTES

ABSTRACT

Air entrainment and flow bulking along a steeply sloping stepped chute are analysed as a function of the characteristic depth used for defining the free-surface. The results of this investigation show that both the mean air concentration and the bulked depth may be considerably influenced by the definition of the free surface. They also show that the region in the vicinity of the point of inception may be the most critical concerning flow bulking, and consequently the chute sidewall design height. Empirical models are also presented for predicting the maximum flow bulking on the chute, as a function of the normalized critical depth.

---

1. INTRODUCTION

The evaluation of the air-water flow properties is particularly important on stepped spillways over RCC dams experiencing moderate unit discharges, because large quantities of air entrain upstream of the spillway toe.

On air-water flows down smooth and stepped chutes, the characteristic depth is usually defined as the perpendicular distance from the pseudo-bottom formed by the step edges where the air concentration is 90% (e.g. Ruff and Frizell 1994, Matos 2000, Chanson 2001, Boes and Hager 2003).

In the present paper, the research is focused on the air entrainment and flow bulking along the chute, as a function of the characteristic depth used for defining the free-surface.

2. EXPERIMENTAL SET-UP

Experimental tests were conducted on a steeply sloping stepped chute (1V:0.75H) assembled at the National Laboratory of Civil Engineering (LNEC), Lisbon. Even though tests were conducted for step heights (h) of 2, 4 and 8 cm (Renna, 2004), the present results apply only to those for which significant bulking occurred, namely 4 and 8 cm high steps (Meireles, 2004). All tests corresponded to the skimming flow regime, with unit discharges (q_w) ranging between 0.050 and 0.200 m^2/s.

Experimental measurements of air concentration were carried out with an air concentration probe (resistivity probe) developed by the U.S. Bureau of Reclamation. Further details on the instrumentation can be found in Matos and Frizell (1997).

3. AIR ENTRAINMENT

The local air concentration C is defined as the time-averaged value of the volume of air per unit volume of air and water. The mean (depth-averaged) air concentration is defined as

$$\overline{C}_{\varphi} = \int_{0}^{Y_{\varphi}} C \, dy \tag{1}$$

where y is measured perpendicular to the pseudo-bottom formed by the step edges and y_{φ} is the depth where the air concentration is φ%.

For the hydraulic design of stepped chutes, φ is typically 90%. Due to the significant flow bulking downstream of the point of inception (Figure 1), Y_{90} was found to underestimate considerably the maximum height of large air-water mass projections.

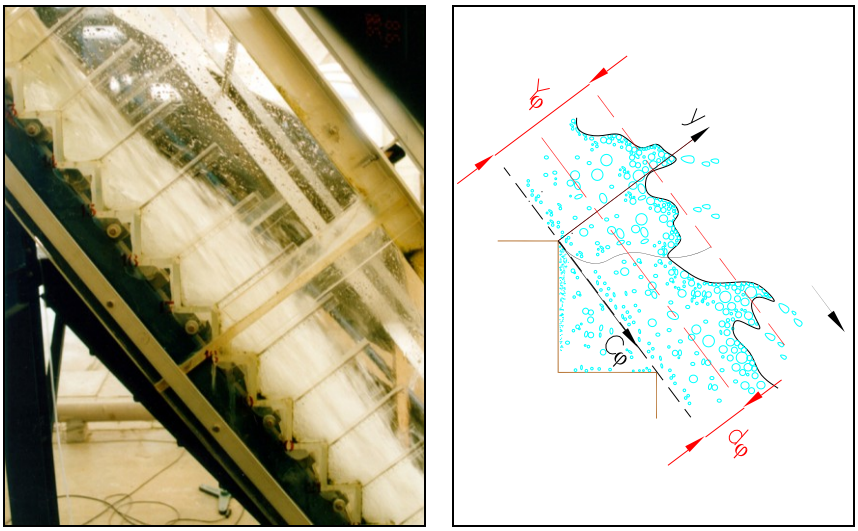

a) b)

Figure 1 - Flow bulking downstream of the inception point: a) photograph of the LNEC chute for h = 8 cm and q_w = 0.080 m²/s; b) definition sketch.

The present study is focused on the analysis of the flow properties considering characteristic depths based on air concentrations larger than 90% (e.g., air concentrations of 95% and 99%, the respective depths being Y_{95} and Y_{99}).

Figure 2 illustrates the mean air concentration along the chute, for different values of φ. Figure 2a) refers to both rapidly and gradually varied flow regions whereas Figure 2b) focus on the gradually varied flow. Both figures illustrate the influence of the parameter φ on the mean air concentration. The ratios $\overline{C}_{95}/\overline{C}_{90}$ and $\overline{C}_{99}/\overline{C}_{90}$ are on average equal to 1.1 and 1.3, respectively. The major differences occur in the vicinity of the inception point of air entrainment, where $\overline{C}_{95}/\overline{C}_{90}$ and

$\overline{C}_{99}/\overline{C}_{90}$ can attain 1.2 and 1.8, respectively. Far downstream, where the effect of flow bulking is mitigated, $\overline{C}_{95}/\overline{C}_{90}$ and $\overline{C}_{99}/\overline{C}_{90}$ decrease to 1.05 and 1.1, respectively.

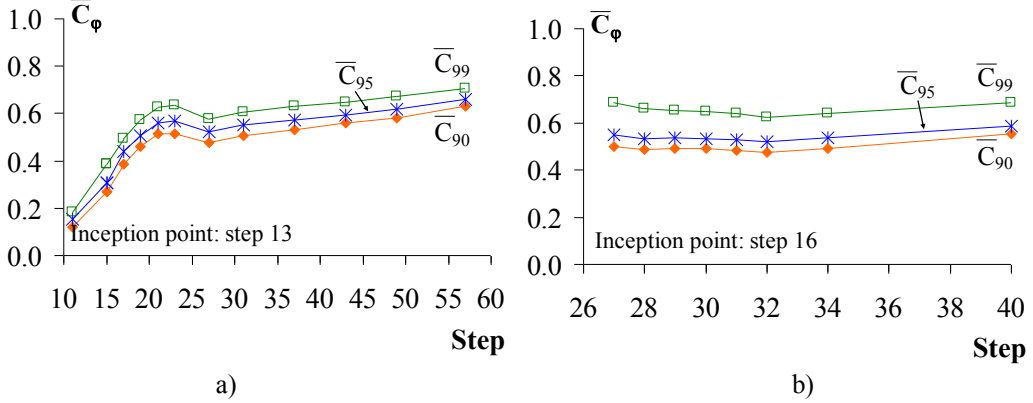

Figure 2 - Development of the mean air concentration: a) h = 4 cm and q_w = 0.050 m^2/s; b) h = 8 cm and q_w = 0.140 m^2/s.

4. FLOW BULKING

Due to air entrainment, the characteristic depths are significantly larger than the equivalent clear-water depth dφ defined as:

$$d_\varphi = \left(1 - \overline{C}_\varphi\right) Y_\varphi \qquad (2)$$

The differences obtained between Y_{90}, Y_{95} and Y_{99} were significant, particularly those between Y_{90} and Y_{99} for 8 cm high steps (Figure 3). The ratio Y_{95}/Y_{90} was approximately 1.1 for both step heights whereas Y_{99}/Y_{90} was significantly influenced by the step height. The average value of Y_{99}/Y_{90} was equal to 1.2 for 4 cm high steps and 1.4 for 8 cm high steps. The results are similar to those presented by Boes and Minor (2000), who obtained $Y_{95}/Y_{90} \approx 1.12$ and $Y_{99}/Y_{90} \approx 1.4$ on chute slopes ranging from 30 to 50 degrees.

Further the experimental results show that the region in the vicinity of the point of inception may be the most critical concerning flow bulking.

The clear-water depth is almost independent of the parameter φ, unlike as observed for the mean air concentration and the characteristic depths. The maximum observed differences were merely 2.8% between d_{95} and d_{90}, and 6.1% between d_{99} and d_{90}. Therefore, no major differences on the plots of d_{90}, d_{95} and d_{99} are noticed in Figure 3.

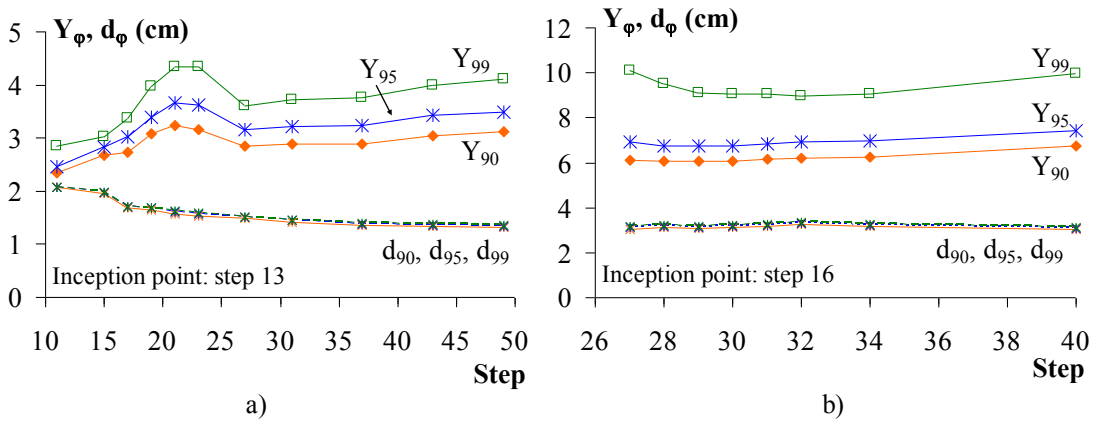

Figure 3 - Development of the characteristic depths: a) h = 4 cm and q_w = 0.050 m^2/s; b) h = 8 cm and q_w = 0.140 m^2/s.

The height of the chute sidewall (h_p) is usually based on the application of a safety factor (n) to Y_{90} (e.g. Boes and Minor 2000, Boes and Hager 2003, Ohtsu et al. 2004), namely as:

$$h_p = n\, Y_{90} \tag{3}$$

Ohtsu et al. (2004) suggested the use of n = 1.4, as per the experimental research by Boes and Minor (2000), based on the ratio Y_{99}/Y_{90}. Boes and Minor (2000) and Boes and Hager (2003) considered n = 1.2 for concrete dams with no concern of erosion and n = 1.5 for stepped emergency spillways on embankment dams prone to erosion.

The results of the present study show that the maximum relative characteristic depths $(Y_{95}/Y_{90})_{max}$ and $(Y_{99}/Y_{90})_{max}$ can be considerably larger than those proposed by other researchers, particularly for low normalized critical depths, d_c/h (Figure 4).

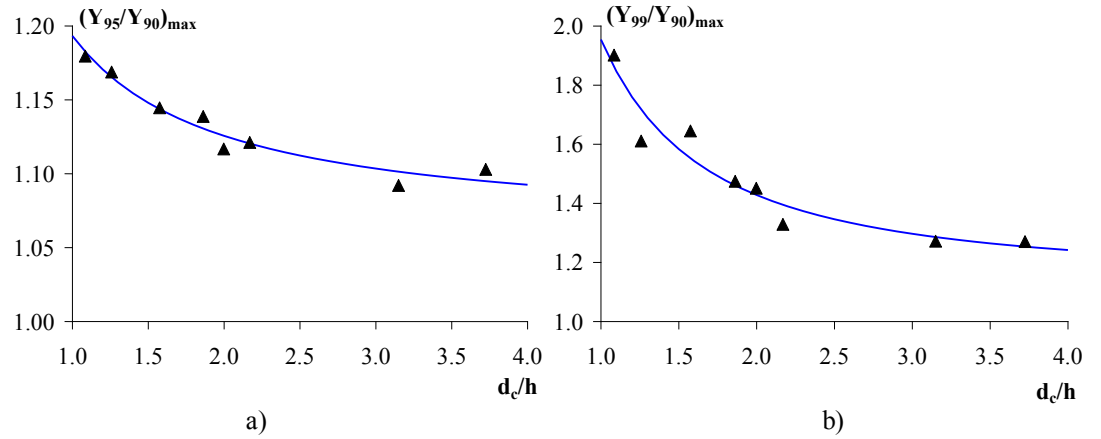

Figure 4 - Maximum normalized characteristic depths: a) $(Y_{95}/Y_{90})_{max}$; b) $(Y_{99}/Y_{90})_{max}$.

The maximum values of the ratios Y_{95}/Y_{90} and Y_{99}/Y_{90} may be obtained from:

$$\left(\frac{Y_{95}}{Y_{90}}\right)_{max} = 1.061 + 0.1322\left(\frac{d_c}{h}\right)^{-1.034} \tag{4}$$

$$\left(\frac{Y_{99}}{Y_{90}}\right)_{max} = 1.140 + 0.8143\left(\frac{d_c}{h}\right)^{-1.499} \quad (5)$$

Eq. (4) and (5) may be used for the chute sidewall design height of stepped chutes on typical RCC dam slopes, the latter if more restrictive conditions are required. The estimation of Y_{90} down the chute may be obtained from empirical models (e.g., Meireles 2004). Taking into account that aerated flow is not a well-mixed continuum (e.g., Falvey 1980, André 2004, Renna 2004, Wilhelms and Gulliver 2005), an accurate description of the intermittent wavy surface would also be of interest in future research.

5. CONCLUSIONS

The results of this investigation showed that both the mean air concentration and the bulked depth may be significantly influenced by the definition of the free surface. They also showed that the region in the vicinity of the point of inception may be the most critical concerning flow bulking. Empirical models were developed for estimating the maximum flow bulking as a function of the normalized critical depth, eventually providing a safer chute sidewall design.

ACKNOWLEDGMENTS The authors acknowledge the support granted by INAG (Project 2003/2029/INAG).

REFERENCES

André, S. (2004). "High velocity aerated flows over stepped chutes with macro-roughness elements." Ph.D. thesis, École Polytechnique Fédérale de Lausanne, Switzerland.

Boes, R. M. and Hager, W. H. (2003). "Hydraulic design of stepped spillways.", J. Hydr. Eng., ASCE, 129(9), 671-679.

Boes, R. M. and Minor, H. E. (2000). "Guidelines to the hydraulic design of stepped spillways." Proc. 1st International Workshop on Hydraulics of Stepped Spillway, Zurich, Switzerland, edited by H.-E. Minor and W.H. Hager, A.A. Balkema Publisher, Rotterdam, The Netherlands, 163-170.

Chanson, H. (2001). "The hydraulics of stepped chutes and spillways." Balkema, Lisse, The Netherlands.

Falvey, H. T. (1980). "Air-water flow in hydraulic structures." USBR Engrg. Monograph, No. 41, Denver, USA.

Matos, J. (2000). "Hydraulic design of stepped spillways over RCC dams." Proc. 1st International Workshop on Hydraulics of Stepped Spillway, Zurich, Switzerland, edited by H.-E. Minor and W.H. Hager, A.A. Balkema Publisher, Rotterdam, The Netherlands, 187-194.

Matos, J. and Frizell, K. (1997). "Air concentration measurements in highly turbulent aerated flow." Proc. 27th IAHR Congress, Theme D, Vol. 1, San Francisco, USA, edited by S.S.Y. Wang and T. Carstens, 149-154. (In CD.)

Meireles, I. (2004). "Caracterização do escoamento deslizante sobre turbilhões e energia específica residual em descarregadores de cheias em degraus." M.Sc. thesis, IST, Lisbon, Portugal (in Portuguese).

Ohtsu, I.; Yasuda, Y. and Takahashi, M. (2004). "Flow characteristics of skimming flows in stepped channels." J. Hydr. Eng., ASCE, 130(9), 860-869.

Wilhelms, S. and Gulliver, J. (2005). "Bubbles and waves description on self-aerated spillway flow." J. Hydr. Res., IAHR, 43(5), 522-531.

Renna, F. (2004). "Caratterizzazione fenomenologica del moto di un fluido bifasico lungo scaricatori a gradini." Ph.D. thesis, Politecnico di Bari, Cosenza, Italy (in Italian).

Ruff, J. F. and Frizell, K. H. (1994). "Air concentration measurements in highly-turbulent flow on a steeply-sloping chute." Proc. Hyd. Engrg. Conf., ASCE, Buffalo, N.Y., 999-1003.

4.3 FLOW CHARACTERISTICS ALONG USBR TYPE III STILLING BASINS DOWNSTREAM OF STEEP STEPPED SPILLWAYS

This sub-chapter 4.3 was published in the 3rd International Junior Researcher and Engineer Workshop on Hydraulic Structures. The authors are I. Meireles, J. Matos and A. Silva-Afonso.

This subchapter concerns to experimental results obtained in the stilling basin located downstream of the 1V:0.75H slope stepped channel of LNEC and is focused on the comparison between the hydraulics of USBR type III basins and of similar basins downstream of steep stepped spillways. To that end, and in analogy with Peterka (1958), mean pressure heads and flow depths were acquired.

ABSTRACT 4.3-1
1. INTRODUCTION.....4.3-1
2. EXPERIMENTAL SETUP 4.3-2
3. RESULTS AND DISCUSSION 4.3-3
4. CONCLUSIONS.....4.3-7
REFERENCES 4.3-7

FLOW CHARACTERISTICS ALONG USBR TYPE III STILLING BASINS DOWNSTREAM OF STEEP STEPPED SPILLWAYS

ABSTRACT

On a spillway chute, a stepped profile increases the rate of energy dissipation and consequently reduces the length of the required downstream energy dissipator when compared to a conventional solution. Up to date, the effect of the chute steps on the energy dissipator flow characteristics remains practically unknown, despite its importance for the design of this kind of structures. A USBR type III basin may be adequate downstream of stepped spillways with limited discharges and moderate velocities at the entrance of the basin. New measurements were acquired in a large-scale facility comprised by a steep stepped spillway followed by a stilling basin designed according to the USBR recommendations for type III stilling basins. Detailed flow characteristics along the basin were measured systematically for several flow rates. The results show that the profiles of pressure head and flow depth tend to follow those recommended by the USBR for type III basins. An exception occurs at the entrance of the basin, where the pressure head values are exceeded largely by the data presented in this study. With regard to the pressure head and flow depth in the basin, the chute blocks are observed to be dispensable.

Keywords: stepped spillway, USBR type III stilling basin, flow depth, pressure head.

---

1. INTRODUCTION

Stepped spillways have been used since ancient times (Chanson 2002). However, more recently they gained their popularity when non-conventional construction techniques like RCC (roller compacted concrete) began to be used in dam engineering. Such technique drives naturally to a stepped downstream dam face which, when used as a spillway, increases the rate of energy dissipation and consequently reduces the length of the required downstream energy dissipator when compared to a conventional solution. A USBR type III basin may be adequate downstream of stepped spillways with limited discharges and moderate velocities at the entrance of the basin.

For a given stepped spillway, and for the smaller discharges, a succession of free-falls, called nappe flow, is observed. For intermediate discharges, a transition flow occurs, and for higher discharges the main flow skims over the step edges. Although several experimental studies have been focused on the nappe and transition flows, research has been particularly intense for the skimming flow

because it is the type of flow which occurs for the design discharge of most steep stepped spillways. These studies were mostly focused on the non-aerated (e.g., Meireles et al. 2006, Amador et al. 2009, Meireles and Matos 2009) and aerated regions, particularly in the assessment of variables such as air concentration and velocity distribution (e.g., Matos 2000, Boes and Hager 2003, Meireles 2004, Renna 2004, Felder and Chanson 2009) or the pressure field on the steps (e.g., Sánchez-Juny 2001, Yasuda and Ohtsu 2003, André 2004, Amador et al. 2009, Gomes 2006), and in the characteristics of the inception point of air entrainment (e.g., Chanson 2002, Amador et al. 2009).

In spite of this considerable number of studies, only very few have been focused on the hydraulics of the energy dissipators located downstream of stepped spillways. Within this scope, several studies were centred in the application of the classical momentum equation to the hydraulic jump to determine the residual energy of the stepped spillway (e.g., Diez-Cascon et al. 1991, Tozzi 1992, 1994, Pegram et al. 1999). In this approach it is assumed that the specific energy of the flow at the toe of the chute is approximately equal to that at the upstream end of the jump. Later, Yasuda and Ohtsu (1999, 2003) and Meireles et al. (2005) applied the momentum equation taking into account that the pressure distribution was non-hydrostatic at the upstream end of the hydraulic jump. Meireles et al. (2005) and Cardoso et al. (2007) studied a simple hydraulic jump basin and a baffle basin, respectively. Expressions to determine mean pressure head along the basins have been proposed in both studies. Cardoso et al. (2007) also presented flow depths and compared jump and roller lengths with values for the classical USBR basins.

Notwithstanding these past studies, a systematic presentation of the main flow characteristics along USBR type III stilling basins downstream of steep stepped spillways has yet to be seen. The purpose of this study is to understand the behaviour of the flow along this type of structures by observing the experimental profiles of mean pressure head and flow depth, and by comparing the performance of:

- USBR type III basins downstream of stepped spillways for different discharges;
- USBR type III basins downstream of stepped spillways with the guidelines proposed by Peterka (1958) for USBR type III basins downstream of smooth spillways;
- USBR type III basins with simple hydraulic jump basins downstream of stepped spillways; and
- USBR type III basins with and without the initial chute blocks immediately downstream of stepped spillways.

2. EXPERIMENTAL SETUP

A facility assembled at the National Laboratory of Civil Engineering (LNEC), in Portugal, was used to conduct the experimental study. The installation comprises a stepped chute 2.90 m high, 1.00 m wide, with a slope of 1V:0.75H, 4 cm high steps, and a stilling basin 5.00 m long and 1.00 m wide, whose appurtenances have been designed according to the USBR recommendations for type III basins (Fig. 1). A total of 13 chute blocks and 9 baffle piers were installed equidistantly. Because of the stepped spillway surface, the chute blocks could not be installed in an

inclined plane, as recommended by the USBR for smooth chutes. However, in skimming flows, the modified chute blocks adopted in the present study are expected to behave similarly as the conventional chute blocks proposed by the USBR for smooth chutes.

Calculations were done based in basin inflow conditions determined from empirical expressions developed by Meireles (2004) for skimming flows over stepped spillways, leading to a 25% reduction in the basin length when comparing with a basin designed to be downstream of a similar smooth spillway.

The mean pressure head was obtained from 40 piezometric taps installed on the stilling basin floor and connected to a piezometric panel: 28 piezometric taps were located in the symmetry plane and 12 were located 3 cm apart from the centreline. In order to avoid the presence of air inside the piezometers tubing, a water cushion was imposed in the stilling basin prior to each experimental test, by closing the gate located at the downstream end of the stilling basin. Subsequently in all tests, the absence of air in the piezometers tubing was carefully checked. Mean flow depths were measured by visual observation through the basin sidewall rulers, corresponding to bulked depths, namely in the roller region.

Measurements along the stilling basin were collected for a range of discharges corresponding to the skimming flow regime over the approaching chute. In a typical prototype with 60 cm high steps (i.e., model scale of 1:15), the tested data refers to Froude numbers of about 8, velocities up to 18 m/s and unit discharges varying between 5 and 11 m^2/s, within the range of application of USBR type III basins. Self-aerated conditions were observed near the downstream end of the chute, with mean air concentrations approximately equal to 0.6.

For each discharge, Q_w, the stilling basin was tested for full conjugate tailwater depth (which is the conjugate depth of a free hydraulic jump), as recommended by Peterka (1958) for the design of USBR type III basins.

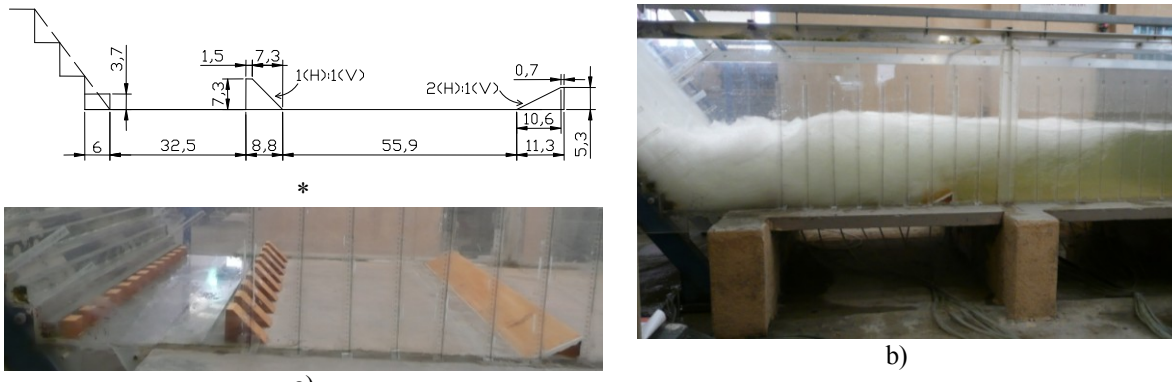

a) b)

Fig. 1 - USBR type III stilling basin downstream of the stepped chute: a) basin characteristics; b) hydraulic jump for Q_w = 140 l/s (dimensions in cm).

3. RESULTS AND DISCUSSION

New pressure distribution and flow depth data were collected for a USBR type III basin downstream of a stepped spillway (referred to as STEPPED type III basin for ease of use).

Profiles of mean pressure head, $P/(\rho_w g)$, and flow depth, d, in function of the distance from the intersection of the pseudo-bottom with the stilling basin, s, for the STEPPED type III basin are presented in Fig. 2. Overall the pressure head results are in accordance with the conclusions drawn by Meireles et al. (2005) for simple hydraulic jump stilling basins downstream of stepped chutes (STEPPED type I basins), in particular: (i) the pressure head along the stilling basin increases with discharge; and (ii) at the impact region, the pressure head is significantly larger than the corresponding value for an hydrostatic pressure distribution. It is also observed that for all of the tested discharges the minimum pressure head occurs downstream of the baffle piers, around s = 50 cm, but is still much higher than the atmospheric pressure. Similarly, as with the pressure head, the flow depth along the stilling basin also increases with discharge. At the upstream end of the basin, where the flow is chaotic and highly turbulent, flow depth increases rapidly after which it decreases and stabilizes to a constant value at the end of the hydraulic jump. This pattern was observed for all of the tested discharges. Interestingly, in Fig. 2 a), the location of the maximum value of the pressure head seems to be independent of the discharge. Its value seems to increase with this parameter while the minimum pressure head appears to stabilize in value and position, since they have the same value for the two highest discharges. On the other hand, the rate of growth of the maximum value of the flow depth with discharge seems to be faster for smaller discharges (Fig. 2 b). Its position moves downstream with this parameter. However, the small number of tests may not allow to generalize these conclusions. Attention must be drawn to the possibility that the position of the piezometric taps may not have allowed to capture the minimum value of the pressure head along the basin.

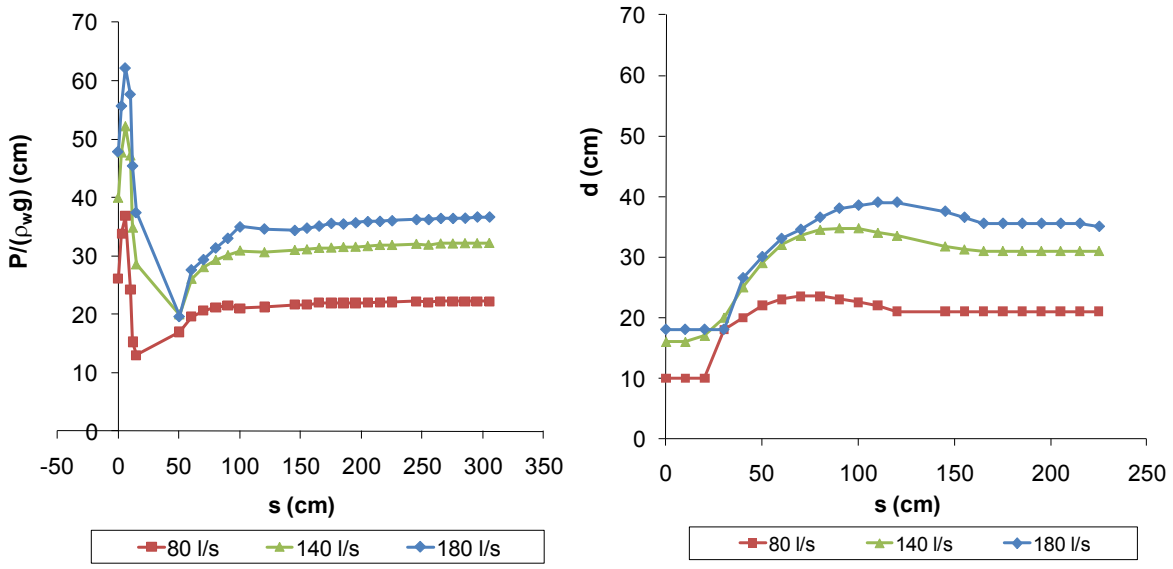

a) b)

Fig. 2 - STEPPED type III basin: (a) pressure head; (b) flow depth.

For the two extreme discharges - 80 and 180 l/s – the pressure head and flow depth profiles along the STEPPED type III basin are shown in Fig. 3. The following conclusions can be drawn: (i) the pressure head is considerably higher than the flow depth at the impact flow region due to the significant concavity of streamlines; (ii) immediately downstream, the flow depth is higher than the pressure head because of air entrainment and flow bulking, and the convexity of streamlines; (iii)

further downstream, the flow depth and pressure head become virtually equal, as expected in the gradually varied flow region next to the hydraulic jump.

The performance of different stilling basins have been compared with that of the STEPPED type III basins , with regard to mean pressure head and flow depth. Bellow, a comparison is made with the USBR type III basin, a type I basin downstream of a stepped chute and the STEPPED type III basin without chute blocks.

Comparison between USBR type III and STEPPED type III basins

Along with flow depth and pressure head data acquired at the STEPPED type III basin, the profile proposed by the USBR for type III basins for both parameters is presented in Fig. 3. The adjustment between flow depth in both basins is acceptable although for the USBR type III basin the peak is observed to be sharper and to occur upstream from the peak for the STEPPED type III basin. The pressure head profiles compare fairly well except at the entrance of the basin, where those observed for the STEPPED type III basin show considerably higher values than those suggested in Peterka (1958).

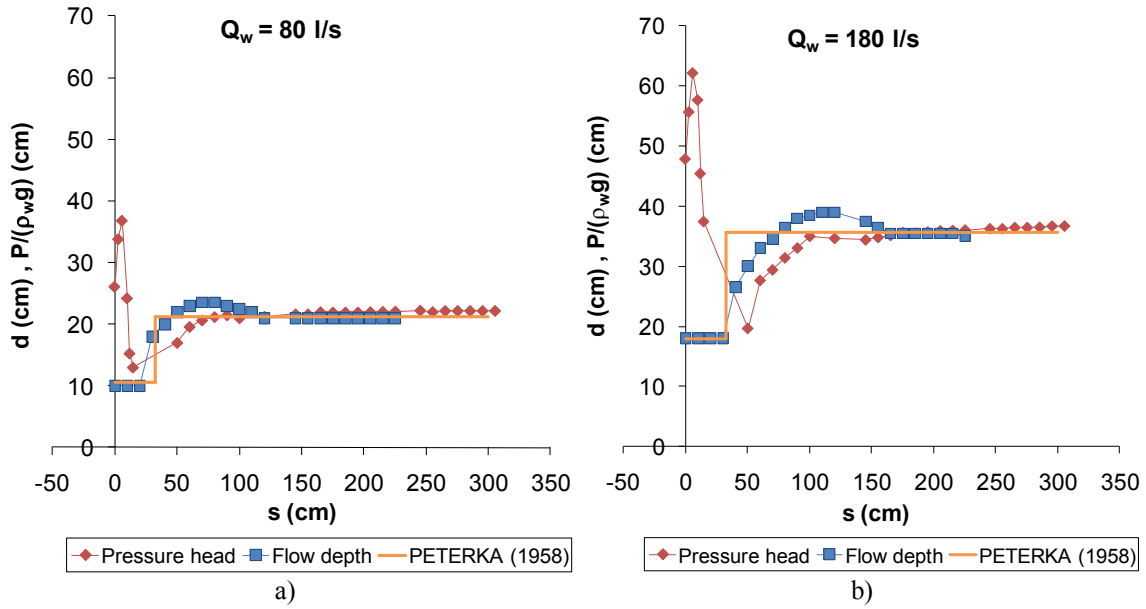

Fig. 3 - Comparison between USBR type III and STEPPED type III basins: flow depth and pressure head for (a) Q_w = 80 l/s; (b) Q_w = 180 l/s.

Comparison between STEPPED type III and STEPPED type I basins

A comparison is made between the pressure head in the studied STEPPED type III basin and in the STEPPED type I basin studied by Meireles et al. (2005) (Fig. 4).

Maximum values are observed to be similar in both basins and minimum values in the STEPPED type III basin are not as small as in the STEPPED type I basin. The main difference, however, is that in the STEPPED type III basin the hydraulic jump stabilizes much faster than in the STEPPED type I basin. This conclusion is in agreement with the differences observed between USBR type I and III basins.

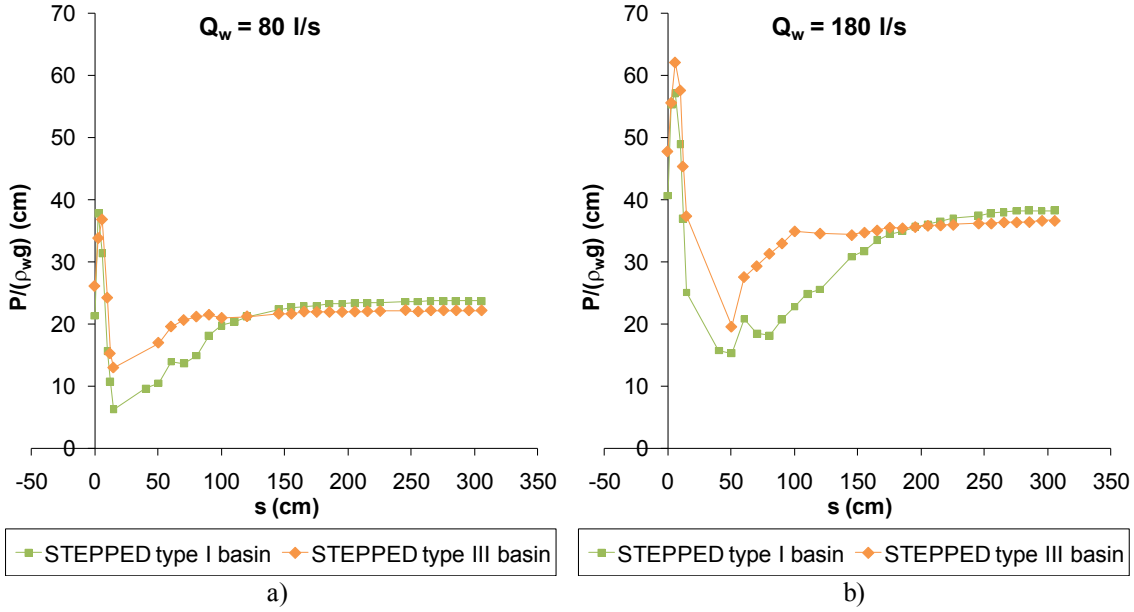

Fig. 4 - Comparison between pressure head along the STEPPED type III and the STEPPED type I basins for (a) Q_w = 80 l/s; (b) Q_w = 180 l/s.

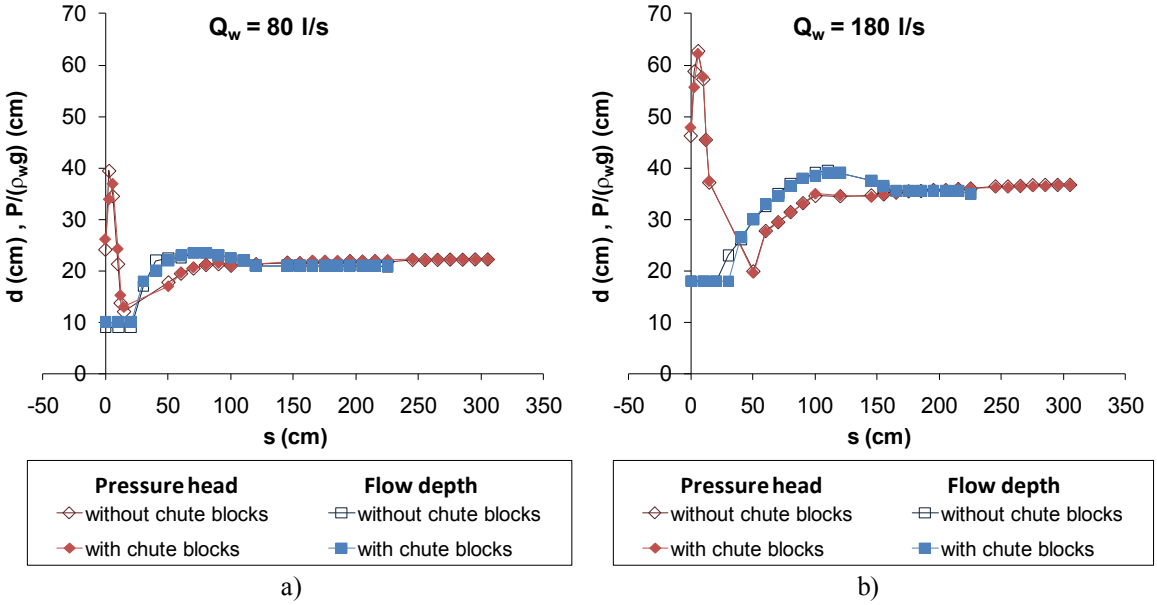

Fig. 5 - Comparison between STEPPED type III basin with chute blocks and STEPPED type III basin without chute blocks: flow depth and pressure head.

Comparison between STEPPED type III basins with and without chute blocks

Results of flow depth and pressure head for the STEPPED type III basin with and without chute blocks are virtually equal (Fig. 5). Peterka (1958) recommends the use of chute blocks at the entrance of USBR type II and III basins to allow flow mixing, promote the formation of more energy dissipating eddies and help in the stabilization of the hydraulic jump. It is believed that the configuration of the steps along the chute helps in the mixing of the flow, eventually making the existence of chute blocks irrelevant to the flow characteristics along the stilling basin.

4. CONCLUSIONS

This study presents some relevant flow characteristics along a basin designed according to the recommendations for USBR type III basins design, and located downstream of a stepped chute.

The main results are summarized as follows: (1) at the entrance of the basin, the pressure head is much higher than both the flow depth and the respective hydrostatic pressure; (2) the adjustment between flow depths along the studied basin and at a USBR type III basin is acceptable; (3) the pressure head profiles at the entrance of the STEPPED type III basin show considerably larger values than those suggested by Peterka (1958), for USBR type III basins; (4) as between USBR type I and III basins, the hydraulic jump stabilizes much faster than in the type I basin downstream of a stepped chute; (5) the differences in the characteristics of the flow for the basin with or without chute blocks are negligible.

It is acknowledged that the present study was limited to one chute step height and one type of stilling basin. Further investigations should be performed with different chute step heights and stilling basins to validate the findings for a wider range of combined stepped spillways and energy dissipators. In future work, it would also be interesting to extend the pressure field data, namely by using pressure transducers.

ACKNOWLEDGMENTS This study was supported by the Portuguese National Science Foundation (FCT), through Project PTDC/ECM/108128/2008. Currently, the first author is supported by a PhD scholarship granted by FCT (Grant No. SFRH/BD/38003/2007).

REFERENCES

Amador, A., Sánchez-Juny, M. and Dolz, J. (2009). “Developing flow region and pressure fluctuations on steeply sloping stepped spillways.” J. Hydr. Eng., ASCE, 135 (12), 1092-1100.

André, S. (2004). "High velocity aerated flows over stepped chutes with macro-roughness elements." PhD thesis, EPFL, Lausanne, Switzerland.

Boes, R. M., and Hager, W. H. (2003). "Two phase flow characteristics of stepped spillways." J. Hyd. Eng., ASCE, 129 (9), 661-670.

Chanson, H. (2002). "The hydraulics of stepped chutes and spillways." Balkema, Lisse, The Netherlands.

Cardoso, G., Meireles, I., and Matos, J. (2007). "Pressure head along baffle stilling basins downstream of steeply sloping stepped chutes" Proc. 32th IAHR Congress, Venice, Italy. (In CD.)

Diez-Cascon, J., Blanco, J.L., Revilla, J. and Garcia, R. (1991). "Studies on the hydraulic behavior of stepped spillways." Water Power & Dam Const., 43 (9), 22-26.

Felder, S., and Chanson, H. (2009). "Energy dissipation, flow resistance, and gas liquid interfacial area in skimming flows on moderate-slope stepped spillways." Env. Fluid Mech., 9 (4), 427-441.

Gomes, J. F. (2006). "Campo de pressões: condições de incipiência à cavitação em vertedouros em degraus com declividade 1V:0,75H." (Pressure field: conditions of incipient cavitation in stepped spillways with slope 1V:0.75H.) PhD thesis, UFRGS, Porto Alegre, Brazil (in Portuguese).

Hager, W. H. (1992). "Energy dissipators and hydraulic jump." Water Science and Technology Library, Vol. 8, Kluwer Academic Publishers, Dordrecht/Boston/London.

Matos, J. (2000). "Hydraulic design of stepped spillways over RCC dams" Proc. 1st Intl Workshop on Hydraulics of Stepped Spillway, Zurich, Switzerland, A. A. Balkema Publisher, Rotterdam, The Netherlands, 187-194.

Meireles, M. (2004). "Emulsionamento de ar e dissipação de energia do escoamento em descarregadores em degraus." (Hydraulics of skimming flow and residual energy on stepped spillways) MSc thesis, IST, Lisbon, Portugal (in Portuguese).

Meireles, I., Matos, J., and Melo, J. F. (2005). "Pressure head and residual energy in skimming flow on steeply sloping stepped spillways." Proc. 31th IAHR Congress, Theme D, 2654-2663, Seoul, South Korea. (In CD.)

Meireles, I., Matos, J. and Melo, J. F. (2006). "Skimming flow properties upstream of air entrainment inception on steeply sloping stepped chutes." Proc. Intl Symposium on Hydraulic Structures, IAHR, Ciudad Guayana, Venezuela. (In CD.)

Meireles, I., and Matos, J. (2009). "Skimming flow in the non-aerated region of stepped spillways over embankment dams." J. Hyd. Eng., ASCE, 135 (8), 685-689.

Pegram, G., Officer, A. and Mottram, S. (1999). "Hydraulics of skimming flow on modeled stepped spillways." J. Hyd. Eng., ASCE, 125 (4), 361-368.

Peterka, A. J. (1958). "Hydraulic design of stilling basins and energy dissipators" in Engineering Monograph Nr. 25, 8th Edition, U.S. Department of the Interior, Water and Power Resources Service, Denver, USA.

Renna, F. (2004). "Caratterizzazione fenomenologica del moto di un fluido bifasico lungo scaricatori a gradini." Ph.D. thesis, Politecnico di Bari, Cosenza, Italy (in Italian).

Sánchez-Juny, M. (2001). "Comportamiento hidráulico de los aliviaderos escalonados en presas de hormigón compactado. Análisis del campo de presiones." (Hydraulic behavior of stepped spillways in RCC dams. Analysis of the pressures field.) PhD thesis, UPC, Barcelona, Spain (in Spanish).

Tozzi, M. J. (1992). "Caracterização/Comportamento de escoamentos em vertedouros com paramento em degraus." (Characterization of the flow in stepped spillways.) PhD thesis, University of São Paulo, São Paulo, Brazil (in Portuguese).

Tozzi, M. J. (1994). "Residual energy in stepped spillways." Water Power & Dam Const., 46 (5), 32-34.

Yasuda, Y. and Othsu, I. (1999). "Flow resistance in skimming flow stepped channels.", Proc. 28th IAHR Congress, Theme B, B 14, Graz, Austria (In CD.)

Yasuda, Y. and Othsu, I (2003). "Effect of step cavity area on flow characteristics of skimming flows on stepped chutes." Proc. 30th IAHR Congress, Theme D, 703-710, Thessaloniki, Greece. (In CD.)

4.4 SKIMMING FLOW IN THE NON-AERATED REGION OF STEPPED SPILLWAYS OVER EMBANKMENT DAMS

Sub-chapter 4.4 was published in the Journal of Hydraulic Engineering, from the American Association of Civil Engineers, in August 2009, Vol. 135, nº 8, pages 685-689. The authors are I. Meireles and J. Matos.

This subchapter concerns to experimental results obtained in the 1V:2H slope stepped channel of IST and is focused on the hydraulic characteristics of the skimming flow in the non-aerated region.

ABSTRACT 4.4-1
1. INTRODUCTION 4.4-1
2. BACKGROUND 4.4-2
3. EXPERIMENTAL SET-UP 4.4-3
4. FLOW PROPERTIES AT THE INCEPTION POINT 4.4-4
5. FLOW PROPERTIES UPSTREAM OF THE INCEPTION POINT 4.4-5
   5.1. Velocity distribution 4.4-5
   5.2. Clear-water depth 4.4-6
   5.3. Energy dissipation 4.4-7
6. CONCLUSIONS 4.4-7
NOTATION 4.4-8
REFERENCES 4.4-9

SKIMMING FLOW IN THE NON-AERATED REGION OF STEPPED SPILLWAYS OVER EMBANKMENT DAMS

ABSTRACT

Traditionally, research on stepped spillway hydraulics has been focused on the air-water flow region, but, for the hydraulic design of small embankment dams experiencing relatively large overtopping flows, the non-aerated region can be very important. Empirical formulae are presented for predicting skimming flow properties upstream of the point of inception of air entrainment for 1V:2H sloping stepped spillways, and the location and flow depth at the point of inception. Particular emphasis is placed on the clear-water depth, velocity distribution, and the energy dissipation characteristics in the developing non-aerated flow region. The velocity distribution is described well by a power law. The normalized clear-water depth and the normalized specific energy varied with the relative distance along the spillway and the effect of the normalized critical depth was negligible. Finally, the rate of energy dissipation was small, which has direct implications for the design of the downstream energy dissipator.

Keywords: Embankment dams, stepped spillways, skimming flow, energy dissipation, non-aerated flow characteristics.

---

1. INTRODUCTION

Recent re-evaluation of the design flood of several embankment dams around the world showed that many have inadequate spillway capacity, which can result in dam overtopping. The overtopping of embankment dams can cause the failure of the structure as a whole, unless a protective system is considered. Safe overtopping protection methods are often an economical option when compared to providing additional conventional spillway capacity. These include grass-covered channels or embankments, geotextile and membranes, reno mattresses, riprap, gabions, concrete blocks, reinforced concrete slab, roller compacted concrete and soil cement. Use of the contemporary roller compacted concrete (RCC) construction technique on the downstream face of a dam naturally leads to a stepped surface protection system. RCC construction techniques produce reduced cost and faster construction and the steps increase energy dissipation compared to conventional smooth spillways, contributing to the reduction or elimination of the downstream energy dissipator.

Extensive research has been developed for estimating the flow properties on stepped spillways for chute slopes typical of either embankment or concrete dams, downstream of the inception point, including air entrainment, characteristic flow depths and velocity (e.g., Gaston 1995; Chamani and Rajaratnam 1999; Matos 2000; Chanson 2001; Boes and Hager 2003a,b; Ohtsu et al. 2004; André 2004; Renna 2004; Meireles 2004; Gonzalez 2005). In contrast a very limited number of studies addressed some of the non-aerated flow properties on stepped spillways over embankment dams (Meireles et al. 2006, Gonzalez and Chanson 2007), which may be important for their hydraulic design, particularly on small dams.

This paper presents an experimental study regarding the main non-aerated skimming flow properties on a 1V:2H sloping stepped chute, typical of RCC overtopping protection. These flow properties include the main flow properties upstream from, and the location and flow depth at the inception point, namely the clear-water depth, the velocity distribution, the kinetic energy correction coefficient, and the specific energy.

2. BACKGROUND

For a given stepped spillway, the flow pattern may be either nappe, transition or skimming flow for increasing discharge (e.g., Ohtsu and Yasuda 1997; Matos 2001; Chanson and Toombes 2004). In the skimming flow regime, for which RCC overtopping protection systems are usually designed, the water skims over the step edges with the step cavity filled with circulating fluid. Skimming flow regions down stepped spillways are fairly similar to those found on self-aerated flow over conventional chutes (e.g., Ruff and Frizell 1994; Matos 2000, Chanson 2001). Fig. 1 shows typical flow regions down stepped spillways over small embankment dams.

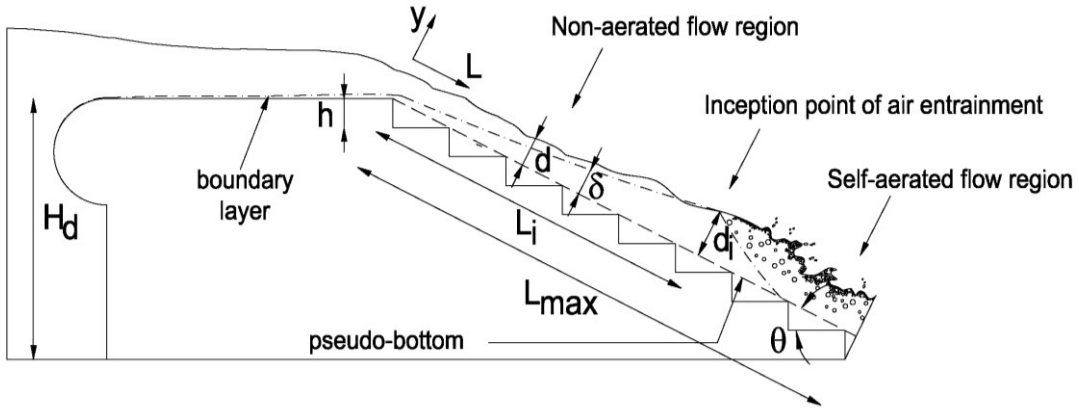

Figure 1 - Skimming flow down stepped spillways over small embankment dams – definition sketch.

On a given stepped spillway, the point of inception of air entrainment moves downstream with increasing discharge. To examine the importance of the non-aerated region, geometric characteristics and design discharges of various embankment dams with RCC overtopping protection presented by McLean and Hansen (1993) were analyzed, with the location of the point of inception, L_i, being estimated as in Chanson (2001). Non-aerated flow conditions were predicted to occur over a significant distance of the chute for several dams and air entrainment would not

occur at all for five of them. Hence, the study of the non-aerated flow properties may be important for hydraulic design purposes, particularly for small embankment dams.

3. EXPERIMENTAL SET-UP

Experimental tests were conducted on a stepped chute assembled at the Laboratory of Hydraulics and Water Resources, IST, Lisbon, 0.50 m high (from crest to toe), slope of 1V:2H (26.6º from horizontal), and width of 0.70 m. The original chute was used by Fael (2000) and further readapted in subsequent studies (André and Ramos 2003, Cabrita 2007). Two step heights (h) were tested in the latter studies, namely 2.5 and 5.0 cm.

The facility comprises an uncontrolled broad-crested weir followed by a stepped chute. The weir is 0.5 m long, 0.5 m high and incorporates a semi-circular upstream corner to reduce flow separation at the entrance. From the hydraulic point of view, the weir is long enough to be classified as broad-crested (Chow 1959; Hager and Schwalt 1994), ensuring that critical flow conditions occur at the crest for all measured flow rates.

The discharge was measured with an electromagnetic flowmeter installed in the supply pipe. Tests were carried out for unit discharges (q_w) ranging from 0.03 to 0.08 m^2/s, corresponding to the skimming flow regime.

A Prandtl-Pitot tube with 8 mm external diameter and a point gauge with a reading accuracy of ± 0.1 mm were respectively used for measuring velocity and clear-water depths at several cross sections, in the non-aerated flow region. The instrumentation was mounted in a trolley and the error in the longitudinal, transverse and vertical positions were estimated as being less than 5, 1 and 0.1 mm, respectively. The unit discharge obtained via the flowmeter was compared to that obtained experimentally from the integration of the velocity profile. In practically all tests, the relative differences were found to be lower than 8%, and the average value was lower than 5%. The experimental data were acquired in the framework of studies carried out by André and Ramos (2003) and Cabrita (2007) (Table 1).

Table 1 – Summary of experimental investigations on the IST stepped chute.

Reference	Slope (degree)	Step height (m)	Discharge (m^2/s)	Measurements
André and Ramos (2003)	26.6	0.025	0.03-0.07	Clear-water depth inception point properties
		0.050	0.04-0.08	Clear-water depth inception point properties
Cabrita (2007)	26.6	0.050	0.05-0.08	Velocity profiles

4. FLOW PROPERTIES AT THE INCEPTION POINT

Experimental data of the inception point location, L_i, and depth, d_i, obtained in the present study agree well with data acquired in other stepped chutes with uncontrolled broad-crested weirs and slopes typical of embankment dams subject to overtopping ($16 \leq \theta^o \leq 26.6$), namely those by Chanson (2001), Chanson and Toombes (2002), Yasuda and Chanson (2003), and Gonzalez (2005). Based on these data, the following formulae are obtained for L_i and d_i (Fig. 2)

$$\frac{L_i}{k} = 5.25\left(F_*\right)^{0.95} \quad (1)$$

$$\frac{d_i}{k} = 0.28\left(F_*\right)^{0.68} \quad (2)$$

for $1.9 \leq F^* \leq 10$ where F* is the roughness Froude number defined as $F_* = q_w \Big/ \sqrt{g \sin\theta\, k^3}$, with g the acceleration due to gravity, θ the spillway slope, and k the roughness height perpendicular to the pseudo-bottom formed by the external edges of the steps, defined as $k = h\cos\theta$.

Fig. 2 includes results obtained from the formulae proposed by Chanson (2001), which were tested for a wide range of θ and F*, varying from 7 to 55º and from 1 to 100, respectively. The results suggest that Chanson's formulae overestimate L_i and d_i on 16 to 26.6º sloping stepped spillways, particularly for small values of F*.

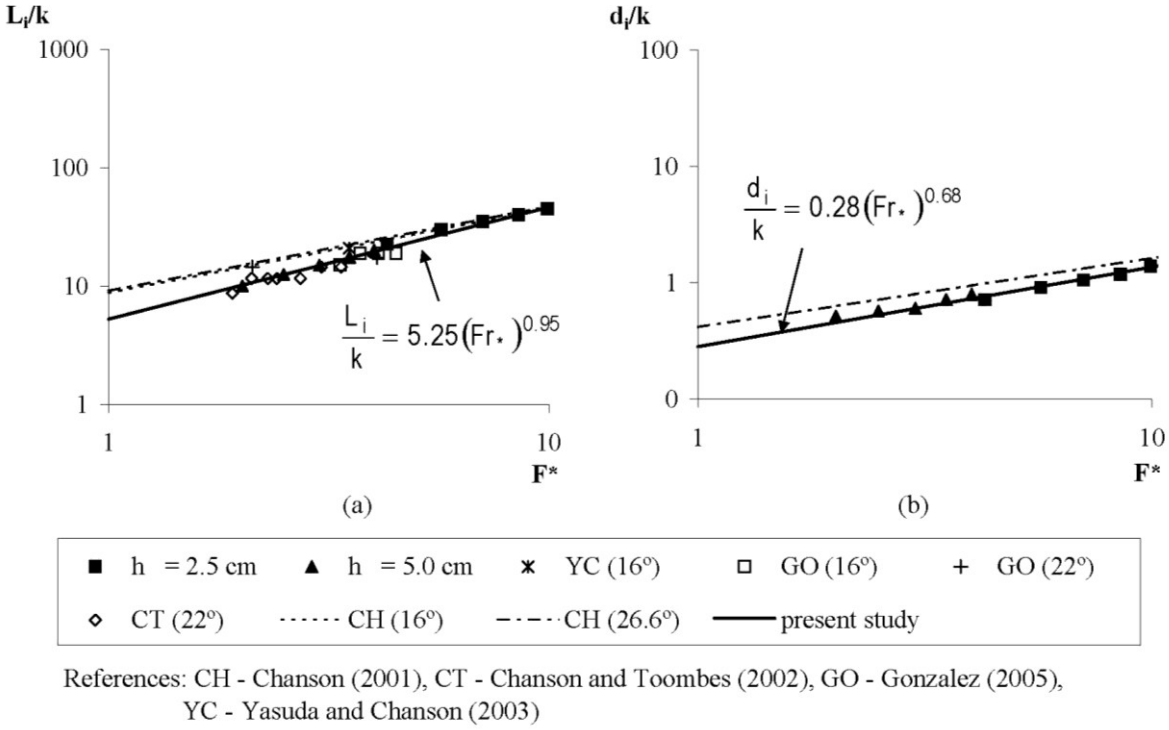

References: CH - Chanson (2001), CT - Chanson and Toombes (2002), GO - Gonzalez (2005), YC - Yasuda and Chanson (2003)

Figure 2 - Flow properties at the point of inception of air entrainment on stepped chute slopes typical of embankment dams subject to overtopping: a) location; b) clear-water depth.

5. FLOW PROPERTIES UPSTREAM OF THE INCEPTION POINT

5.1. VELOCITY DISTRIBUTION

The normalized velocity profile in non-aerated flows over stepped spillways may be expressed by a power law

$$\frac{V}{V_{max}} = \left(\frac{y}{\delta}\right)^{1/N} \qquad 0 < y/\delta < 1 \qquad (3)$$

where V is the time-averaged velocity, V_{max} the free-stream velocity, y is the normal coordinate originating at the pseudo-bottom, and δ is the boundary layer thickness defined as the perpendicular distance from the pseudo-bottom to the point where the velocity is 0.99 V_{max}.

For 5 cm high steps, velocity profiles V(y) were obtained on the chute centerline at several cross sections, coincident with the step edges, for several discharges (Fig. 3a). Good agreement of the experimental data with Equation (3) with N = 5.1 is observed although the data indicate that V/V_{max} is underestimated by Equation (3) for $y/\delta < 0.2$. In general, the relative distance along the chute with origin at its upstream end (L/L_i, where L is the streamwise coordinate originating at the upstream end of the spillway) does not significantly affect N, namely $4.4 \leq N \leq 6.3$, for $0.38 \leq L/L_i \leq 1.00$ (if the data point is less than 1.00 then it is in the non-aerated zone; equal to 1.00 at the inception point; greater than 1.00 in the aerated zone). Chanson (2001) obtained N = 5.0, for a single discharge, from the LDA measurements taken by Ohtsu and Yasuda (1997) on a 1V:2.9H stepped chute, for h = 5 cm and $q_w = 0.089$ m^2/s.

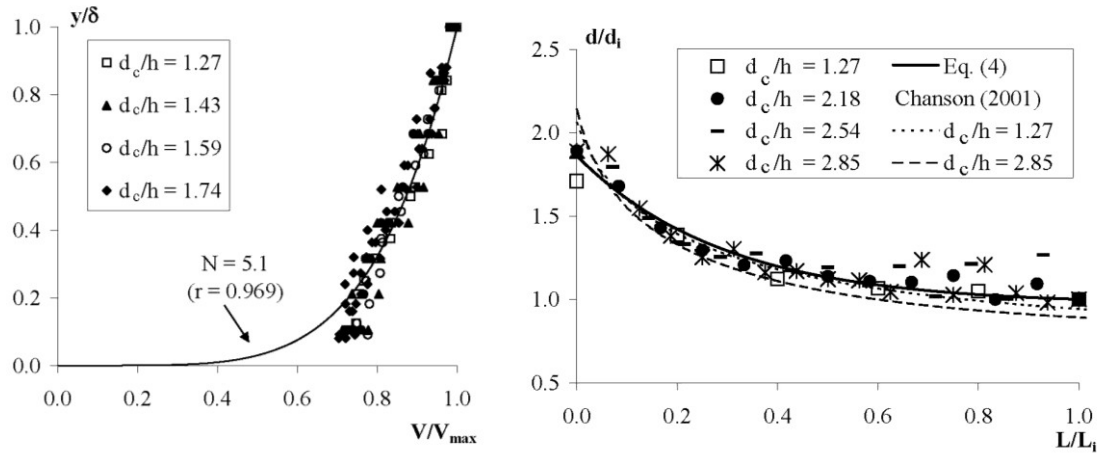

a) b)

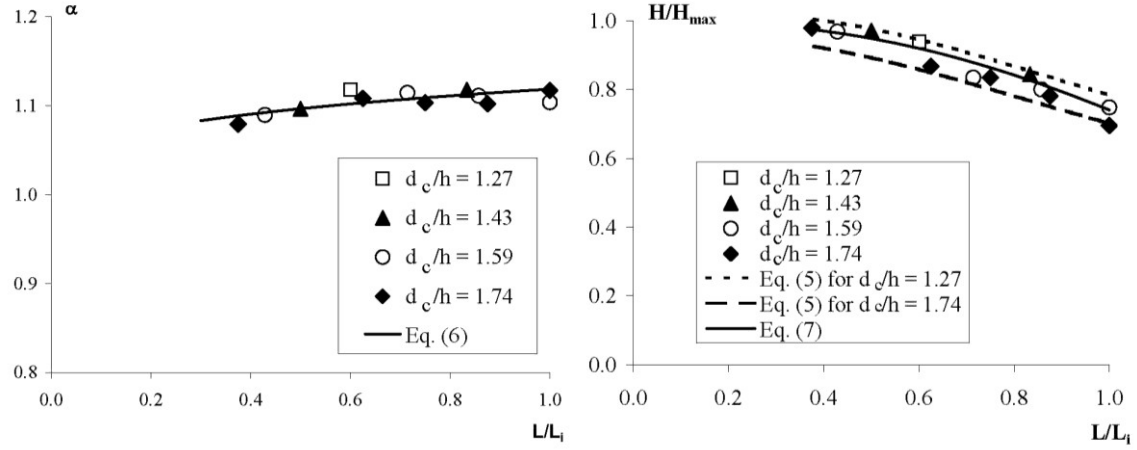

c) d)

Figure 3 - Flow properties upstream of the inception point: a) velocity distribution – experimental data in the non-aerated flow regime over 5 cm high steps versus the power law (N = 5.1); b) normalized clear-water depth – experimental data versus Equation (4) and the application of Chanson (2001) stepped chute flow calculations for the non-aerated flow region, based on the IST chute data for estimating L_i and d_i; c) kinetic energy correction coefficient – experimental data versus Equation (6); d) rate of energy dissipation – experimental data versus Equation (5) normalized by H_{max}, applied by using Equations (1), (2), (4) and (6), and Equation (7).

5.2. CLEAR-WATER DEPTH

Measurements of the clear-water depth, d, on the IST stepped chute, for step heights of 2.5 and 5 cm, were obtained by visual observation through the sidewalls and using a point gauge along the chute centerline. Only the latter data are analyzed herein. The free surface exhibits a slightly wavy pattern along the chute, particularly near the inception point, where it is more difficult to take accurate measurements. Based on theoretical and empirical formulae, Chanson (2001) and Gonzalez and Chanson (2007) presented stepped chute calculations for the non-aerated developing flow region allowing determination of d. This formulation was compared with the experimental data gathered at the IST chute (Meireles et al. 2006). Fairly good agreement was observed, although near the inception point the application of the stepped chute calculations slightly underestimates the experimental data.

Based on the IST data, the normalized clear-water depth (d/d_i) for $L/L_i < 1$ is practically independent of d_c/h between 1.27 and 2.85, but depends strongly on L/L_i (Fig. 3b). Based on experimentally measured d_i and L_i, the following relation may be suggested, for $1.27 \leq d_c/h \leq 2.85$:

$$\frac{d}{d_i} = 0.971 + 0.891\,e^{-3.41(L/L_i)} \quad (4)$$

If the formulae of Chanson (2001) for predicting L_i and d_i were used, d/d_i would be considerably underestimated, due to the overestimation of d_i for 16 to 26.6º sloping chutes and small F_*, as shown in Fig. 2b.

5.3. ENERGY DISSIPATION

The specific energy can be expressed by

$$H = d\cos\theta + \alpha \frac{q_w^{\,2}}{d^2(2g)} \tag{5}$$

where α is the kinetic energy correction coefficient.

Based on velocity profiles, α was computed as a function of L/L_i (Fig. 3c), and expressed as:

$$\alpha = 1 + 0.119 \left(\frac{L}{L_i}\right)^{0.296} \tag{6}$$

for $0.38 \leq L/L_i \leq 1.00$.

The normalized specific energy, H/H_{max}, is observed to be little influenced by d_c/h being predominantly governed by L/L_i (Fig. 3d), and may be reasonably expressed for $0.38 \leq L/L_i \leq 1.00$ as

$$\frac{H}{H_{\max}} = \exp\left[0.30\left(\frac{L}{L_i}\right)^{2.5}\right] \tag{7}$$

where H_{max} is the maximum specific energy at any section along the chute (at the chute toe, $H_{max} = H_d + 1.5\, d_c$).

The results obtained from applying Equation (5), based on Equations (1), (2), (4) and (6), are also shown in Fig. 3d, for two values of d_c/h. The agreement with the data is judged to be satisfactory. The specific energy at the downstream end of a spillway, or residual specific energy (H_{res}), is obtained as the specific energy at $L = L_{max}$ (being L_{max} the length of the spillway measured along the chute slope).

For the present study, in the developing flow region the rate of energy dissipation is small (Fig. 3d), where $H/H_{max} > 0.8$, which is much lower than that usually reported for stepped spillways. This has direct implications for the design of the downstream energy dissipator.

6. CONCLUSIONS

Herein, the results of an experimental study conducted on a 1V:2H sloping stepped chute, typical of embankment dams subject to overtopping, assembled at the Laboratory of Hydraulics and Water Resources, IST, Lisbon, were presented. Attention was initially given to the point of inception with the presentation of formulae to predict its properties for small Froude numbers. The data of several authors, including those of the present study, showed good agreement with the proposed formulae. Theoretical considerations and empirical formulae were presented to estimate flow properties in the developing flow region upstream of the inception point of air entrainment, namely the velocity distribution, the clear-water depth, the kinetic energy correction coefficient, and the residual

specific energy. The rate of energy dissipation was observed to be significantly lower than that usually reported for stepped spillways nearing uniform flow conditions.

ACKNOWLEDGMENTS The authors wish to acknowledge the comments of Prof. Hubert Chanson. The first author, formerly Visiting Scholar at UCDavis and financially supported by a Fulbright/FLAD Research Grant, wants to extend the thanks to Prof. Fabián Bombardelli for his advices. The financial support granted by INAG, Portuguese Water Institution (Project 2003/2029/INAG), is also acknowledged.

NOTATION

d - clear-water depth;

d_c - critical depth;

d_i - clear-water depth at the inception point;

F_* - roughness Froude number, defined as $F_* = q_w \Big/ \sqrt{g \sin\theta\, k^3}$;

g - acceleration due to gravity;

h - step height;

H - specific energy;

H_d - spillway height;

H_{max} - maximum specific energy at any section along the chute (at the chute toe, $H_{max} = H_d + 1.5\ d_c$);

H_{res} - residual specific energy;

k - roughness height perpendicular to pseudo-bottom, defined as $k = h\cos\theta$;

L - streamwise coordinate originating at the upstream end of the spillway;

L_i - streamwise coordinate at the inception point, originating at the upstream end of the spillway;

L_{max} - length of the spillway measured along the chute slope;

N - velocity distribution exponent;

q_w - water discharge per unit width;

V - flow velocity;

V_{max} - free-stream velocity;

y - transverse coordinate originating at the pseudo-bottom;

α - kinetic energy correction coefficient;

θ - spillway slope;

δ - boundary layer thickness.

REFERENCES

André, M. and Ramos, P. (2003). "Hidráulica de descarregadores de cheia em degraus: aplicação a descarregadores com paredes convergentes." Graduate Research Report, IST, Lisbon, Portugal (in Portuguese).

André, S. (2004). "High velocity aerated flows over stepped chutes with macro-roughness elements." PhD thesis, EPFL, Lausanne, Switzerland.

Boes, R. M. and Hager, W. H. (2003a). "Two-phase flow characteristics of stepped spillways." J. Hydr. Eng., ASCE, 129(9), 661-670.

Boes, R. M. and Hager, W. H. (2003b). "Hydraulic design of stepped spillways." J. Hydr. Eng., ASCE, 129(9), 671-679.

Cabrita, J. (2007). "Caracterização do escoamento deslizante sobre turbilhões em descarregadores de cheias em degraus com paredes convergentes." MSc thesis, IST, Lisbon, Portugal (in Portuguese).

Chamani, M. R., and Rajaratnam, N. (1999). "Characteristics of skimming flow over stepped spillways." J. Hydr. Eng., ASCE, 125(4), 361-368.

Chanson, H. (2001). "The hydraulics of stepped chutes and spillways." Balkema, Lisse, The Netherlands.

Chanson, H. and Toombes, L. (2002). "Experimental investigations of air entrainment in transition and skimming flows down a stepped chute." Can. J. Civil Eng., 29(1), 145-156.

Chanson, H. and Toombes, L. (2004). "Hydraulics of stepped chutes: the transition flow." J. Hydr. Res., IAHR, 42(1), 43-54.

Chow, V. T. (1959). "Open-channel hydraulics." McGraw-Hill, New York, USA.

Fael, C. (2000). "Escoamento em quedas sucessivas: ocorrência e dissipação de energia." MSc thesis, IST, Lisbon, Portugal (in Portuguese).

Gaston, M. (1995). "Air entrainment and energy dissipation on a stepped block spillway.", MSc thesis, Colorado State University, Fort Collins, Colorado, USA.

Gonzalez, C. (2005). "An experimental study of free-surface aeration on embankment stepped chutes." PhD thesis, University of Queensland, Brisbane, Australia.

Gonzalez, C. and Chanson, H. (2007). "Hydraulic design of stepped spillways and downstream energy dissipators for embankment dams." Dam Engineering, 17(4), 223-244.

Hager, W. and Schwalt, M. (1994). "Broad crested weirs." J. Irrigation and Drainage Eng., ASCE, 120(1), 13-26.

Matos, J. (2000). "Hydraulic design of stepped spillways over rcc dams." Proc. 1st Int. Workshop on Hydraulics of Stepped Spillway, Zurich, Switzerland, H.-E. Minor and W.H. Hager, eds., A.A. Balkema Publisher, Rotterdam, The Netherlands, 187-194.

Matos, J. (2001). “Discussion on 'Onset of skimming flow on stepped spillways.' by Chamani and Rajaratnam”, J. Hydr. Eng., ASCE, 118(7), 519-521.

McLean, F. G. and Hansen, K. D. (1993). “Roller compacted concrete for embankment overtopping protection.” Geotechnical Practice for Dam Rehabilitation, ASCE, New York, USA.

Meireles, M. (2004). “Emulsionamento de ar e dissipação de energia do escoamento em descarregadores em degraus.” MSc thesis, IST, Lisbon, Portugal (in Portuguese).

Meireles, I.; Cabrita, J. and Matos, J. (2006). “Non-aerated skimming flow properties on stepped chutes over embankment dams.” Proc. Int. Junior Researcher and Engineer Workshop on Hydraulic Structures, Montemor-o-Novo, Portugal, J. Matos and H. Chanson, eds., Report CH61/06, Div. of Civil Engineering, The University of Queensland, Brisbane, Australia, Dec., 91-99.

Ohtsu, I. and Yasuda, Y. (1997). “Characteristics of flow conditions on stepped channels.” Proc. 27th IAHR Int. Congress, San Francisco, USA, F. M. Holly and A. Alsaffar, eds., 583-588. (In CD.)

Ohtsu, I.; Yasuda, Y. and Takahashi, M. (2004). “Flow characteristics of skimming flows in stepped channels.” J. Hydr. Eng., ASCE, 130(9), 860-869.

Renna, F. (2004). “Caratterizzazione fenomenologica del moto di un fluido bifasico lungo scaricatori a gradini.” PhD thesis, Politecnico di Bari, Cosenza, Italy (in Italian).

Ruff, J. F. and Frizell, K. H. (1994). “Air concentration measurement in highly turbulent flow on a steeply-sloping chute.” Proc. Hydraulic Engineering Conference, ASCE, Buffalo, USA.

Yasuda, Y. and Chanson, H. (2003). “Micro- and macro-scopic study of two-phase flow on a stepped chute.” Proc. 30th IAHR Congress, Thessaloniki, Greece, J. Ganoulis and P. Prinos, eds., 695-702. (In CD.)

Chapter 5

Numerical study

5.1 LABORATORY MEASUREMENTS AND MULTI-BLOCK NUMERICAL SIMULATIONS OF THE MEAN FLOW AND TURBULENCE IN THE NON-AERATED SKIMMING FLOW REGION OF STEEP STEPPED SPILLWAYS

Sub-chapter 5.1 was published online in the journal Environmental Fluid Mechanics in August 2010. The authors are F. A. Bombardelli, I. Meireles and J. Matos.

This subchapter concerns to numerical results obtained with *Flow-3D*® simulating the 1V:0.75H slope stepped channel of LNEC and is focused on the hydraulic characteristics of the skimming flow in the non-aerated region, mainly presenting a comparison between experimental and numerical data for steps 0.04 m high and unit discharge of 0.18 m^2/s in terms of boundary-layer development, self-similar velocity profiles and inception point. Turbulence analysis are also performed.

ABSTRACT 5.1-1
1. INTRODUCTION.....5.1-1
2. EXPERIMENTAL SET-UP 5.1-5
3. MATHEMATICAL MODEL.....5.1-7
3.1. General flow and transport model 5.1-7
3.2. Location of the free surface.....5.1-9
3.3. Additional boundary conditions 5.1-11
3.4. Sub-model/boundary condition for the air entrainment through the free surface.....5.1-12
4. NUMERICAL MODEL: FEATURES AND IMPLEMENTATION OF RUNS.....5.1-12
4.1. Main features of the code.....5.1-12
4.2. Numerical model implementation: Geometry, grid, and mesh-convergence tests 5.1-13
5. COMPARISON OF EXPERIMENTAL AND NUMERICAL RESULTS.....5.1-15
5.1. Verification of the volumetric flow rate (discharge), water depth and velocity distribution 5.1-15
5.2. Boundary layer development 5.1-20
5.3. Turbulence statistics 5.1-22
6. SENSITIVITY ANALYSES OF THE NUMERICAL SIMULATIONS 5.1-24
6.1. Turbulence models and turbulence mixing length.....5.1-24
6.2. Sub-model for air entrainment 5.1-26
6.3. Evaluation of the computational results and theoretical models 5.1-26
7. CONCLUSIONS.....5.1-26
REFERENCES 5.1-27

LABORATORY MEASUREMENTS AND MULTI-BLOCK NUMERICAL SIMULATIONS OF THE MEAN FLOW AND TURBULENCE IN THE NON-AERATED SKIMMING FLOW REGION OF STEEP STEPPED SPILLWAYS

ABSTRACT

We present and discuss the results of a comprehensive study addressing the non-aerated region of the skimming flow in steep stepped spillways. Although flows in stepped spillways are usually characterized by high air concentrations concomitant with high rates of energy dissipation, the non-aerated region becomes important in small dams and/or spillways with high specific discharges. A relatively large physical model of such spillway was used to acquire data on flow velocities and water levels and, then, well-resolved numerical simulations were performed with a commercial code to reproduce those experimental conditions. The numerical runs benefited from the ability of using multi-block grids in a Cartesian coordinate system, from capturing the free surface with the TruVOF method embedded in the code, and from the use of two turbulence models: the k-ε and the RNG k-ε models. Numerical results are in good agreement with the experimental data corresponding to three volumetric flow rates in terms of the time-averaged velocities measured at diverse steps in the spillway, and they are in very satisfactory agreement for water levels along the spillway. In addition, the numerical results provide information on the turbulence statistics of the flow. This work also discusses important aspects of the flow, such as the values of the exponents of the power-law velocity profiles, and the characteristics of the development of the boundary layer in the spillway.

Keywords: stepped spillway, non-aerated flow, multi-phase flows, two-phase flows, experimental data, back-flushing Pitot tube, conductivity probe, numerical simulations, computational fluid dynamics (CFD), turbulence modeling, k-ε model, RNG k-ε model.

---

1. INTRODUCTION

The main hydraulic advantage of stepped spillways is the ability to dissipate more energy than smooth, conventional spillways. Although this is a strong reason to use stepped spillways, it was not until the improvement of roller compacted concrete (RCC) technology by the end of the 20th century that the interest in stepped spillways was definitively renewed (Amador et al. 2006;

Chanson 2009). Currently, there is a considerable interest in evaluating the performance of stepped spillways over RCC dams for high specific discharges, in either the design of new spillways, or the re-analysis of existing spillways due to an update in the probable maximum flood.

In general terms, for moderate unit discharges, large quantities of air entrain upstream of the spillway toe after the boundary layer reaches the water depth. For higher specific discharges, the boundary layer can not reach the free surface at relatively short distances, and the non-aerated region dominates large portions of the flow in the spillway.

In the last two decades, extensive experimental research has been developed to characterize the flow on conventional stepped spillways for chute slopes typical of either embankment or concrete dams downstream of the inception point of air entrainment, including the assessment of variables such as air concentration and velocity distribution (e.g., Chamani and Rajaratnam 1999; Matos 2000; Chanson 2002; Boes and Hager 2003a; Ohtsu et al. 2004; André 2004; Meireles 2004; Renna 2004; Gonzalez 2005; Felder and Chanson 2009) or the pressure field on the steps (e.g., Sánchez-Juny 2001; Yasuda and Ohtsu 2003; André 2004; Amador 2005; Gomes 2006). Empirical models have been developed for predicting the main air-water flow properties along the chute by Hager and Boes (2000), Matos (2000), Chanson (2001), Boes and Hager (2003a, b), Meireles (2004), Renna (2004) and Ohtsu et al. (2004). In spite of this considerable number of studies, and to the best of our knowledge, only Amador (2005), Amador et al. (2006), Meireles et al. (2006), Gonzalez and Chanson (2007), Carvalho and Amador (2008) and Meireles and Matos (2009) have focused on the flow properties of the non-aerated flow region of stepped spillways.

In addition to studies in physical models, recent advances in computational codes and hardware technology allow for new opportunities to employ numerical solutions as a supplement to the available experimental tools for the analysis of flow in stepped spillways, and for helping in the design of such structures. In fact, numerical flow models can be used to optimize the layout of hydraulic structures to a certain degree, and then physical models can be used to study the three-dimensional (3-D) details of the flow, as shown for instance by Bombardelli et al. (2000) and Caisley et al. (1999). Further improvement of theoretical and numerical models will contribute strongly to the design of hydraulic structures, especially when combined with detailed turbulence models such as Large Eddy Simulations (LES), and with more reliable models for two-phase flows (see Bombardelli 2003, as an example).

The number of studies on computational fluid dynamics (CFD) focusing on hydraulic structures has increased notably in the last ten years (e.g., Unami et al. 1999; Song and Zhou 1999; Bombardelli et al. 2000; Savage and Johnson 2001; Chatila and Tabbara 2004; Savage et al. 2004; Higgs and Frizell 2004; Dargahi 2006; Ho et al. 2006; Ye et al. 2006; Paxson and Savage 2006; Johnson and Savage 2006; Bhuiyan and Hey 2007). A small number of simulations of the skimming flow over stepped spillways have been communicated very recently (Chen et al. 2002; Cheng et al. 2004a, b; Tabbara et al. 2005; Arantes 2007; Carvalho and Amador 2008), describing both the aerated and non-aerated flow regions. A detailed analysis of the above contributions for stepped spillways is presented in Table 1, revealing the following features/issues:

i) The comparisons between numerical and experimental results in those papers have been mostly of qualitative nature;

ii) whereas Chen et al. (2002) (see also Yasuda et al. 2004), Cheng et al. (2004a, b) and Arantes (2007) solved the flows of water and air altogether (which was defined as Partial Volume-of-Fluid (VoF) method in Bombardelli et al. 2001), Tabbara et al. (2005) employed a numerical strategy based on re-meshing each time step. In turn, Carvalho and Amador (2008) used a purported VoF method, but they did not report comparisons of numerical results with data of the location of free surface;

iii) some of the simulations have been developed using unstructured grids with good resolution near the walls but with a lower resolution near the free surface;

iv) only the papers by Cheng et al. (2004a, b) and Carvalho and Amador (2008) include discussions on the distribution of turbulence statistics in the steps through contours of the turbulent kinetic energy (TKE) obtained numerically;

v) experimental data obtained in some papers to validate the numerical simulations corresponded to relatively small facilities with potential significant scale effects;

vi) to the best of our knowledge, very few numerical analyses of the non-aerated flow region which present and discuss comprehensive comparisons of computational results with data have been published in reputed peer-reviewed literature. Thus, more work is needed to understand completely the flow.

This paper therefore addresses the mean flow and turbulence statistics in the non-aerated flow region of steep stepped spillways. We have undertaken extensive experimental tests in a relatively large scale model at the National Laboratory of Civil Engineering (LNEC), in Lisbon, Portugal, and performed well-resolved simulations with the commercial, CFD code FLOW-3D® at the University of California, Davis, and Portugal. In addition to test the prediction capability of the commercial code through comparisons with our own experiments (an important task in its own right), we focus on investigating the following scientific issues with both experimental and numerical techniques:

a) What is the evolution of the flow depth in the stepped spillway?

b) What is the evolution of the boundary layer in the stepped spillway?

c) What are the exponents of the power law representing the velocity profiles?

The paper is organized as follows. In Section 2, we present the experimental set-up. Sections 3 and 4 discuss the theoretical and numerical models employed. Section 5 presents comparisons of experimental and numerical results, focusing on the scientific questions stated above. Section 6 discusses the sensitivity analysis of the numerical solutions, followed by the conclusions.

Table 1 - Summary of features of previous numerical investigations on stepped spillways.

Author (year)	Commercial software	Computational method	Treatment of free-surface	Resolution	Turbulence model	Non-aerated / aerated flow	Slope	Solution scheme	Comparison with data
Chen et al. (2002)	NA	Finite volumes	Partial VoF	Decreasing resolution with the distance from the wall	k-ε	Non-aerated and aerated flow	1V:0.75H	Solves the flow of water and air	Issues with the measurements in the aerated region (Yasuda et al. 2004)
Cheng et al. (2004a, b)	NA	Finite volumes	Partial VoF	12 points in the vertical; low resolution in the reservoir	k-ε (contours of k shown)	Aerated flow	1V:2.5H	Solves the flow of water and air	
Tabbara et al. (2005)	ADINA-F	Finite elements	Remeshing	Decreasing resolution with the distance from the wall	k-ε	Non-aerated flow	1V:0.58H	Re-meshing in each time step	Only measured and modeled water depths
Arantes (2007)	Ansys CFX 10.0	Finite elements/finite volumes	Partial VoF	Decreasing resolution with the distance from the wall	Reynolds stress	Non-aerated & aerated flow	1V:0.75H	Solves the flow of water and air	
Carvalho & Amador (2008)	NA	Finite volumes/finite differences	VoF	Fine grid; nearly the same resolution in the entire domain	Not specified	Non-aerated flow	1V:0.8H	Solves only the water flow	
Present study	*FLOW-3D*®	Finite volume/finite differences	TruVOF	Fine grid; same resolution in the entire domain	k-ε and RNG (contours of k and ε shown)	Non-aerated flow	1V:0.75H	Solves only the water flow; mesh-independent solution	Comp. water vel., water levels, growth of the boundary layer and inception-point

2. EXPERIMENTAL SET-UP

The relatively large scale experimental model comprises a stepped chute, a stilling basin, and a recirculation system. The crest shape of the chute fits the U.S. Army Corps of Engineers, Waterways Experimental Station (WES) standard spillway profile, having a few steps with variable height to follow the profile (Fig. 1). The height of the spillway chute is 2.9 m (from crest to toe); the width is 1 m; and the slope is 1V:0.75H (53 degrees from horizontal; Fig. 2). The stilling basin has a length of 5 m and the same width of the spillway. The basin finishes with a sluice gate which promotes the formation of a hydraulic jump.

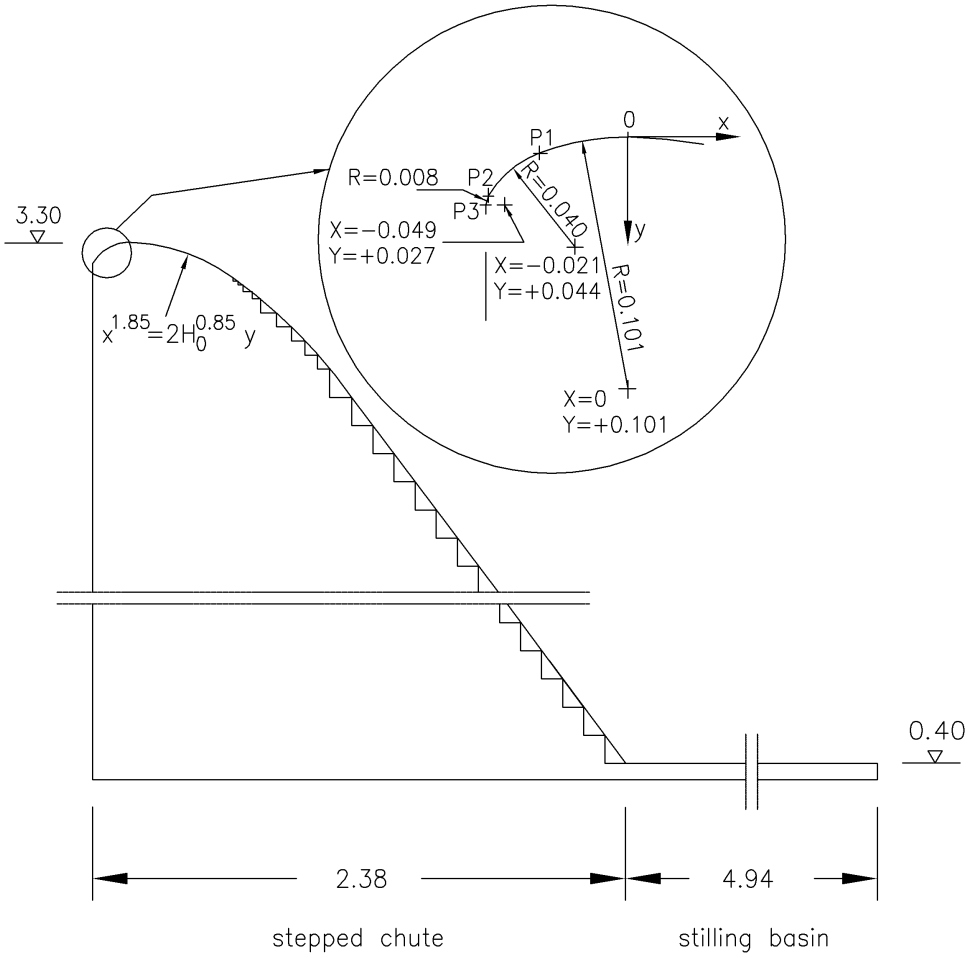

Figure 1 - Schematic diagram of the spillway (dimensions in meters).

Although this paper discusses only the non-aerated region of the flow, air concentrations and water velocities were measured in several step edges of the spillway with a conductivity probe and a back-flushing Pitot tube developed and calibrated by the U.S. Bureau of Reclamation (Matos and Frizell 1997; 2000; see Fig. 2). The air concentration data were used to estimate the equivalent clear water depth, as well as to correct the differential pressure head data in the wavy region, so as to obtain the local time averaged velocity. The conductivity probe has two platinum wires with a diameter of 0.2 mm. With the back-flushing Pitot tube, the total and static-pressure heads were measured through 1-mm and 0.5-mm diameter holes, respectively. Continuous back-flushing of the

Pitot tube was provided to avoid the entrance of air in the Pitot tube. Water was supplied from a reservoir with constant head which fed both the static-pressure and the total head ports of the Pitot tube. The back-flushing flow rate to each port was controlled by needle valves. A practically zero back-flushing flow rate was adopted in all tests. The output signal of the instrument was scanned at 30 kHz for 90 s with a posteriori filtering to 30 Hz to save memory and storage. Further details can be found in Matos and Frizell (2000).

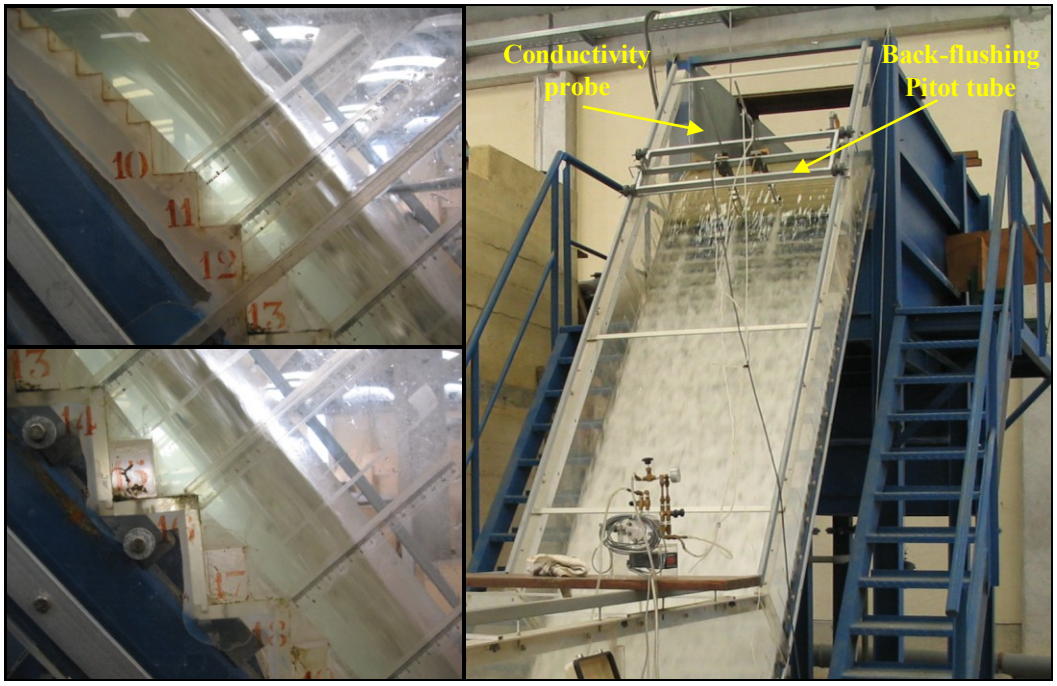

Figure 2 - Experimental flume and instrumentation (conductivity probe and back-flushing Pitot tube) at LNEC.

The instruments were mounted on a trolley equipped with Vernier scales, and the accuracy for vertical distance measurements was of ±0.1 mm. The error for longitudinal distance measurements was estimated to be less than 5 mm. In the transverse direction, the error was estimated to be less than 1 mm.

We measured water depths with the help of point gauges at the chute centerline; we also undertook visual observations of the water depth at the sidewalls assisted by rulers installed in the flume. The volume flow rate (discharge) was measured with a Bazin weir located at the downstream end of the stilling basin, with value differences smaller than 8.8% (average of 5.5%) when compared with velocity checks. Experimental tests were carried out for a step height (h) of 4 cm and unit discharges (q_w) ranging from 0.08 to 0.18 m^2/s, corresponding to the skimming flow regime (Chanson 2002).

Time-averaged velocities (V) were obtained through:

$$V = \sqrt{\frac{2\,\Delta P}{\rho_w\,(1 - C)}} \qquad (1)$$

where ΔP is the difference between the total pressure head and the static pressure head, measured with the back-flushing Pitot tube; ρw is the density of water; and C is the local air concentration. In the non-aerated region, C refers to the air entrapped in the contorted free surface. (Near the inception point, C can also denote the presence of air bubbles inside the flow, due to the difference between instantaneous and averaged inception point locations.) In fact, because of the waviness and turbulent nature of the flow, measurement points close to the free surface suffered from instances in which the instrumentation remained uncovered by water. The values of velocity close to the free surface correspond, therefore, to an average of moments of complete submergence and moments of uncovered condition of the back-flushing Pitot tube and the conductivity probe. Even though Eq. (1) takes into account this phenomenon, these values of velocity should be taken with caution due to the high frequency of the free-surface waves as opposed to the time response of the Pitot tube (Matos et al. 2002). For this reason, local velocity data where air concentration is different from zero have been indicated with unfilled symbols whereas filled symbols refer to data where air concentration is equal to zero (see Figs 4, 5, 7, 9, 14 and 15).

Observations undertaken with tracers, along with the conductivity probe and the back-flushing Pitot tube located in different verticals for each cross section, revealed an essentially two-dimensional (2-D) flow above the step cavities, as expected. This is consistent with the relatively large width of the channel (Chow 1959). However, visualization of the flow within the step cavities showed that it was markedly 3-D (e.g., Matos et al. 1999; Chanson 2002; Gonzalez and Chanson 2007; Gonzalez and Chanson 2008). Notwithstanding this clear fact, we decided to undertake a 2-D simulation of the entire flow, in agreement with most previous numerical works (see Table 1).

3. MATHEMATICAL MODEL

3.1. GENERAL FLOW AND TRANSPORT MODEL

Our theoretical models are based upon the mixture equations for an air-water flow. We follow Buscaglia et al. (2002), Bombardelli (2003, 2004), Bombardelli et al. (2007), and Bombardelli and Jha (2009) in employing equations for a dilute mixture. The equations can be obtained via two consecutive averaging procedures (Crowe et al. 1998; Prosperetti and Tryggvason 2007): 1) an ensemble averaging, which basically addresses the bubble-to-bubble distance, and b) a turbulence averaging, which addresses turbulence scales larger than the inter-bubble distance (Bombardelli 2004). Length scales of turbulence range from the Kolmogorov length scale to the largest scales of the flow (dictated by the flow depth or width; see Gioia and Bombardelli 2002). We believe that the length and time scales associated with the ensemble average are smaller than the intermediate to large scales pertaining to turbulence (Buscaglia et al. 2002; Bombardelli 2004; Bombardelli et al. 2007; Bombardelli and Jha 2009). Consequently, we believe that the ensemble average represents only scales of the order of the bubble-to-bubble distance. Other authors have interpreted the ensemble average assuming that it considers all length scales (Drew and Passman 1999). Based on our hypothesis, we understand that an additional turbulence (time) average of the equations is necessary, to account for the intermediate and large scales of turbulence (see also Hrenya and

Sinclair 1997; and discussion in Chapter 8 of Prosperetti and Tryggvason 2007 on the nature of the averaging procedures). The models have naturally the single-phase flow as a special case.

Although our main interest is the flow in the non-aerated region of the spillway, we needed to solve the two-phase flow equations to represent as accurately as possible the flow in the aerated region and in the stilling basin (see below). The mixture equations for a 3-D dilute flow are as follows:

$$\nabla \cdot \overline{\underline{u}_m} = 0 \tag{2}$$

$$\frac{\partial\left(\rho_0 \ \overline{\underline{u}_m}\right)}{\partial t} + \nabla \cdot \left(\rho_0 \ \overline{\underline{u}_m} \otimes \overline{\underline{u}_m}\right) = \underline{B} - \nabla \overline{p} + \mu \ \nabla \cdot \left(\nabla \overline{\underline{u}_m} + \nabla \overline{\underline{u}_m}^T\right) - \nabla \cdot \left(\rho_0 \ \overline{\underline{u}'_m \otimes \underline{u}'_m}\right) \tag{3}$$

where $\overline{\underline{u}_m}$ refers to the time–averaged mixture velocity vector; ρ_0 indicates the reference density; $\underline{B}$ is the vector of body forces; $\overline{p}$ denotes the time–averaged, modified pressure (Buscaglia et al. 2002; Rodi 1984); μ refers to the dynamic viscosity; t is the time coordinate; and $\underline{u}'_m$ indicates the fluctuating mixture velocity vector. In turn, $\otimes$ refers to the tensor product; T denotes the transpose of a tensor; and the underline indicates vectors. For this problem, the only acting body forces are those from the gravitational field. In order to account for turbulence, the Boussinesq model considers the Reynolds stresses to be proportional to the gradient of mean velocity, as follows (Rodi 1984):

$$-\ \rho_0 \ \overline{\underline{u}'_m \otimes \underline{u}'_m} \ = \ \mu_T \ \left(\nabla \overline{\underline{u}}_m + \nabla \overline{\underline{u}}_m{}^T\right) - \frac{2}{3} \ \rho_0 \ k \ \underline{\underline{I}} \tag{4}$$

$$\mu_T = \rho_0 \ C_\mu \ \frac{k^2}{\varepsilon} \tag{5}$$

where μ_T is the eddy dynamic viscosity; and C_μ is a coefficient of the order of 0.09. k denotes in turn the turbulent kinetic energy (TKE), defined in this context as: $k = \frac{1}{2} \overline{\underline{u}'_m \cdot \underline{u}'_m}$; ε is the dissipation rate of TKE; and $\underline{\underline{I}}$ denotes the identity tensor. The standard k-ε turbulence model (Launder and Spalding 1972), and the RNG k-ε model (Yakhot and Orszag 1986; Yakhot and Smith 1992) were used in this work. The RNG k-ε model is usually considered to provide more accurate results than the k-ε model in flows with low turbulence intensity and, very importantly, in flows with important shear regions, such as the flow under study in this paper (Flow Science 2008).

The theoretical model also incorporates a transport equation for the air which is entrained at the free surface as follows:

$$\frac{\partial C}{\partial t} + \nabla \cdot \left[\left(\overline{\underline{u}_m} + \underline{W}_s\right) C\right] = \nabla \cdot \left(\underline{\underline{D}} \cdot \nabla C\right) \tag{6}$$

where C is the volumetric concentration of air; $\underline{W}_s$ is the slip-velocity vector (which points in the positive vertical direction); and $\underline{\underline{D}}$ denotes the air-diffusivity tensor.

This equation is solved in the water volumes, as detailed in next section and Fig. 3(b). According to the hierarchical framework of possible two-phase models developed by Bombardelli (2004), Bombardelli et al. (2007), and Bombardelli and Jha (2009), this corresponds to a pseudo-single-phase flow model. FLOW-3D® offers different alternatives for the implementation of equations such as this last one, treating the problem as a two-fluid problem or as a pseudo-single-phase one. Since our focus is on the non-aerated flow region, we selected the last alternative in our computations. More research will be developed regarding this issue in the near future according to our research plans.

We adopted 2-D versions of the equations presented above, which agrees with the simulations developed by Savage and Johnson (2001) and Johnson and Savage (2006), albeit for smooth, conventional spillways.

3.2. LOCATION OF THE FREE SURFACE

The above equations are valid within a domain Ω which includes the flow in the stepped spillway and the stilling basin, and it is limited by the incoming flow in the tank, the outgoing flow downstream of the stilling basin, the solid boundary in the spillway, and the free surface (Fig. 3(a)). The location of the free surface is a priori unknown, involving the need to calculate that location each time step, starting from an initial condition.

The *TruVOF* (embedded in FLOW-3D®; see Hirt and Nichols 1981) is used in this work to capture the free surface. *TruVOF* is a donor-acceptor algorithm and employs three key elements (Bombardelli et al. 2001). The first element is constituted by the definition and use of the F function, which depicts the fractional volume of fluid occupying each cell; its value ranges from zero (no fluid in the volume) to one (cell completely filled with fluid). The free surface is defined to be located at a position pertaining to intermediate values of the fractional volume in the cells. A value of F =0.5 is usually employed for that purpose (Flow Science 2008). The second element is the use of an appropriate advection numerical method for the equation governing the transport of the VoF function (Eq. (7)) that is designed to ensure a small numerical diffusion of the free surface. At each time step, the function F is obtained by solving the following equation:

$$\frac{\partial F}{\partial t} + \nabla \cdot \left(\underline{\bar{u}}_m \, F \right) = 0 \tag{7}$$

in the entire domain (Ferziger and Peric 2002). Finally, an important third element is the application of boundary conditions at the free surface (Fig. 3(b)).

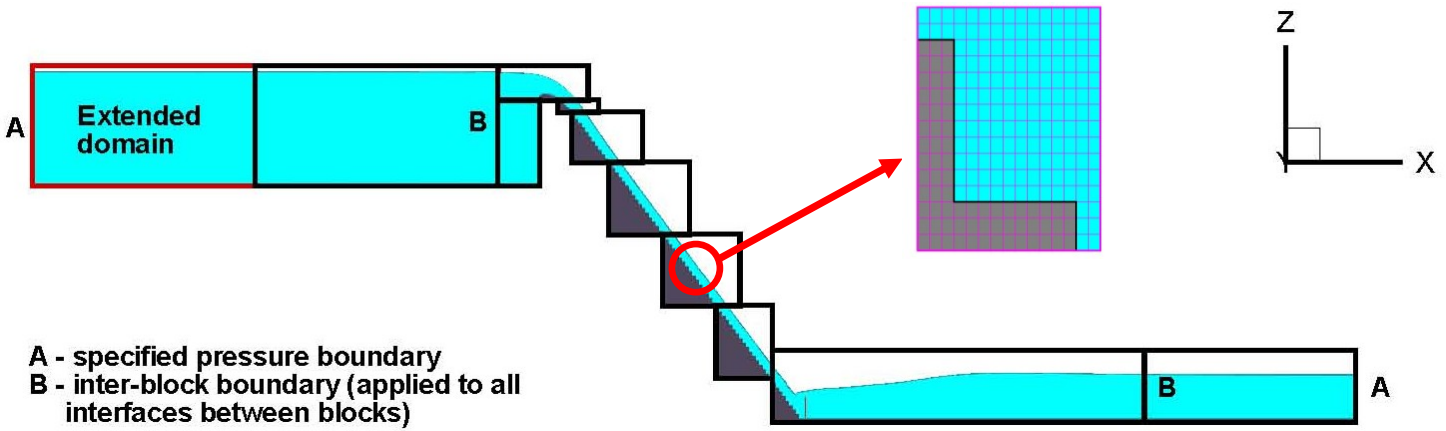

a)

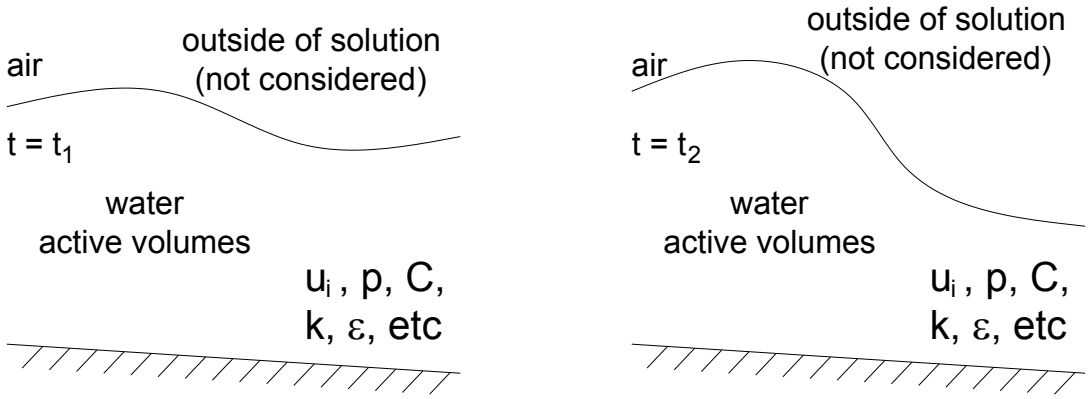

b)

Figure 3 - a) Model geometry and distribution of blocks in the multi-block grid. The figure includes the "short" and "extended" computational domains. Rectangles denote the blocks of the multi-block gridding operation. Notice the savings in computational effort produced by the location of the blocks. b) Schematic showing that transport equations are solved in the liquid only in FLOW-3D® (Ferziger and Peric 2002, page 384).

Unlike in other methods published recently (see Matthews et al. 1999; 2001, for example), the flow and transport equations are solved only in cells with liquid, because the gas is assumed to possess negligible inertia. The gas is considered only able of applying a normal pressure on a liquid surface (Fig. 3(b)). Once the free surface location is defined each time step, the model given by Eqs (2)-(6) is numerically solved within the water domain limited by the free surface (Fig. 3(b)) while the air outside the free surface does not participate of the "active volumes" of the computation. The *TruVOF* method enjoys the following advantages: a) minimum storage of information, since only one variable, F , has to be stored; b) adequate (small) computational cost; and c) good accuracy for fine meshes.

3.3. ADDITIONAL BOUNDARY CONDITIONS

We specified pressure boundary conditions in both upstream and downstream boundaries, based on the water depths observed experimentally (Figs 3). Although we did not have experimental information within the stilling basin, we included it in the computational domain to enforce the physical boundaries where we had pressure data. We checked that the selected boundary conditions did not produce spurious waves in the computational domain (see Storti et al. 2008 for a discussion on boundary conditions for flows with a change in flow condition within the domain).

We imposed null velocities normal to the step walls (Pope 2000; Bombardelli 2010), and employed the usual "wall functions" for the turbulence statistics (Ferziger and Peric 2002). These functions are (Pope 2000; Ferziger and Peric 2002; Chung 2006)

$$k\big|_w = \frac{u_*^{\,2}}{\sqrt{c_\mu}};\ \varepsilon\big|_w = \frac{u_*^{\,3}}{(\kappa\ y_1)} \tag{8}$$

where u_* is the wall-friction (shear) velocity, obtained iteratively by the use of the semi-logarithmic velocity law, κ is the von-Kármán constant, and y_1 is the normal distance perpendicular to the wall (Flow Science 2008). The steps developed to compute u_* and the turbulence statistics at the wall are: a) determination of the direction normal to the wall in the wall volume; b) the cell-centered flow velocity at the wall volume is decomposed into parallel (uparallel) and perpendicular (uperpendicular) components; c) the average distance to the wall, y_1 , is calculated as half of the volume width in the direction normal to the wall; d) u_* is computed using uparallel and y_1 in an iterative way. Given the numerous simulations in which these wall functions have been used in the last decades (e.g., Rodi 1984; Wilcox 1993; Pope 2000; Ferziger and Peric 2002; Chung 2003, page 688), we believe that they provide a tested description of the boundary conditions for turbulence statistics for this case (see discussion in Pope 2000).

Boundary conditions imposed at, and a sub-model for the air entrainment through the free surface are detailed below.

3.4. SUB-MODEL/BOUNDARY CONDITION FOR THE AIR ENTRAINMENT THROUGH THE FREE SURFACE

A sub-model included in the commercial code is able to simulate the natural entrainment of air due to turbulence at the free surface. When any disturbance of size L_T at the free surface is associated with a larger energy per unit volume, P_T, than the energy of the stabilizing forces (related to gravity and the surface tension), P_d, the sub-model allows a volume of air to enter the mixture flow (Hirt 2003). The equations of the sub-model are as follows:

$$L_T = c_\mu \left(\frac{3}{2}\right)^{1/2} \frac{k^{3/2}}{\varepsilon};\ P_d = \rho_m\ g_n\ L_T + \frac{\sigma}{L_T};\ P_T = \rho_m\ k \tag{9}$$

If $P_T > P_d$:

$$\delta V = C_{air}\ A_s \left[\frac{2\ (P_T - P_d)}{\rho_m}\right]^{1/2} \tag{10}$$

where g_n is the component of the vector of the acceleration of gravity in the direction normal to the free surface; σ is the surface tension; C_{air} is a coefficient of proportionality; A_s is the surface area; and δV is the volume of air allowed to enter the flow through the free surface per unit time. According to Hirt (2003), a good first guess is C_{air}= 0.5, which assumes on average that air is trapped over about half the surface area of the raised disturbance.

4. NUMERICAL MODEL: FEATURES AND IMPLEMENTATION OF RUNS

4.1. MAIN FEATURES OF THE CODE

In this research we used the commercial code FLOW-3D®, which constitutes a general purpose CFD program (Flow Science 2008). The equations of the mathematical model presented above are solved by the method of finite volumes/finite differences in a Cartesian, staggered grid. The code has been employed to simulate flows through hydraulic structures (see, for instance, Bombardelli et al. 2000; Bombardelli et al. 2001; Savage and Johnson 2001; Johnson and Savage 2006) and flows through river reaches and bends (see, for example, Wade et al. 2002; Rodríguez et al. 2004; Abad et al. 2008). In FLOW-3D®, the tasks of building the grid and defining the geometry are completely independent. This property allows for modifications on the obstacles without making changes on the grid (e.g., for different configurations of the objects in the problem), or for modifications on the grid keeping the original geometry intact (e.g., for refinement of the solution).

The domain can be constituted by single- or multi-block grids. This last feature permits the optimization of the mesh in areas with complicated obstacle geometries, and reduces the memory requirements and the computational cost. Pressures, velocities and concentrations are computed separately in each grid block, and information from blocks is transferred among them. This exchange of data among blocks is done differently for pressures, velocities and other solution

variables. While the pressures and velocities are interpolated linearly, the scalars and turbulence statistics are "overlaid" (Barkhudarov 2004). In these simulations we used multiple blocks.

The full geometry can be incorporated into FLOW-3D® through different methodologies: a) a "solid modeler," which is based on the exploitation of general quadratic functions; b) Computer-Aided-Design (CAD) files, usually through stereolithography (STL) files; or c) topographic data (i.e., ASCII files with x, y, z data). After both the geometry and the grid are defined, the FAVOR™ technique allows the obstacles to be embedded in the grid (Hirt and Sicilian 1985). FAVOR™ stands for Fractional Area/Volume Obstacle Representation and consists of the computations of areas and volumes obstructed to flow due to the solid boundaries: those area or volume fractions are incorporated in the model equations. More information can be found in Flow Science (2008).

4.2. NUMERICAL MODEL IMPLEMENTATION: GEOMETRY, GRID, AND MESH-CONVERGENCE TESTS

The geometry was generated using AutoCAD, based on the dimensions of the physical model; it was then imported into the code as an STL file. The domain was discretized using ten blocks to optimize the mesh in accordance to the given geometry, as shown in Fig. 3(a). The domain included a distance upstream of the face of the spillway to allow for a "buffer" zone for the boundary condition imposed at the upstream boundary (i.e., whereas the pressure was imposed, the velocities were not; see, for instance, Rodríguez et al. 2004). In order to assess the influence of such distance on the numerical results, we tested two domains with different "buffer" zone lengths: 2.5 m (short) and 4.5 m (extended). The runs were developed in a personal computer with a Pentium 2.66 Ghz processor and 8 Gb of RAM; the evolution in time was used as a relaxation to the final steady state. The steady state is checked through monitoring the flow kinetic energy displayed by the code in its GUI (Graphical User Interface). Steady state was typically reached after several stages of stop-re-start of runs of a few tens of seconds of simulation time each.

Fig. 4 displays velocity profiles at distances of 0.64, 1.14, and 1.34 m from the crest of the spillway, in order to compare the numerical results obtained with three meshes of 2.0 (Run 12), 2.2 (Run 43) and 2.4 (Run 44) million volumes, respectively, detailed in Table 2, for a q_w of 0.18 m^2/s. Whereas the mesh with 2.0 million volumes was composed by cells of 3 mm in the x direction and 4 mm in the vertical direction, the meshes with 2.2 and 2.4 million volumes were composed by cells of 2.85 mm in the x direction and 3.8 mm in the vertical direction, and 2.7 mm in the x direction and 3.6 mm in the vertical direction, respectively. Results show the condition pertaining to a final steady state. The three meshes yielded virtually the same results for the velocity profiles and the water depths, as seen in Figs 4, meaning that a mesh-converged solution was attained (we were not interested in obtaining the mesh convergence rate). The mesh with 2.0 million volumes was then used throughout the simulations.

Table 2 – Data on meshes for simulations with FLOW-3D® for assessment of mesh convergence (qw = 0.18 m2/s).

Name	N° of blocks	N° of cells	Min. size of cells (m)	Max. size of cells (m)
Run 12	10	2.0E+06	3.00E-03	4.00E-03
Run 43	10	2.2E+06	2.85E-03	3.80E-03
Run 44	10	2.4E+06	2.70E-03	3.60E-03

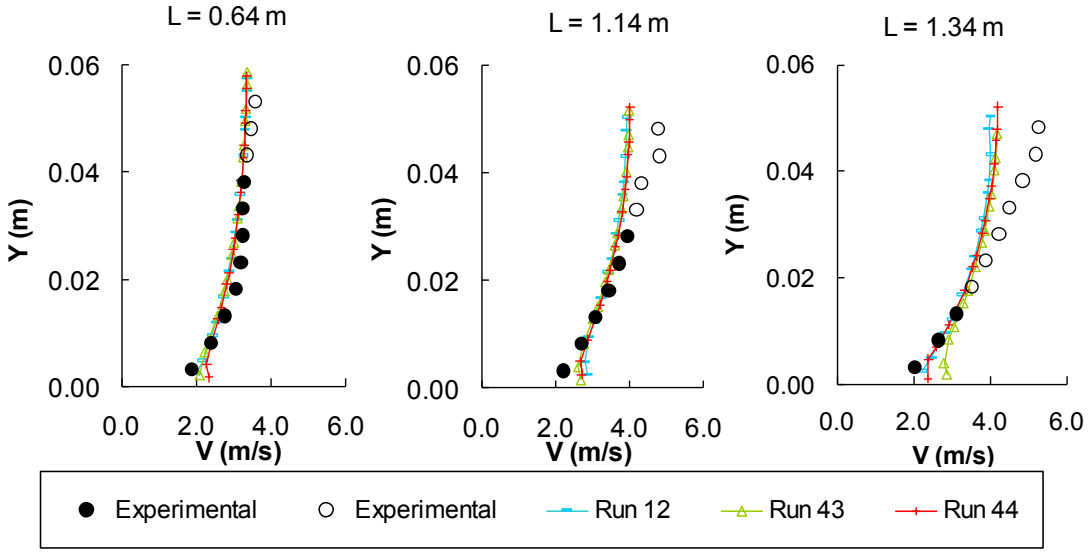

a)

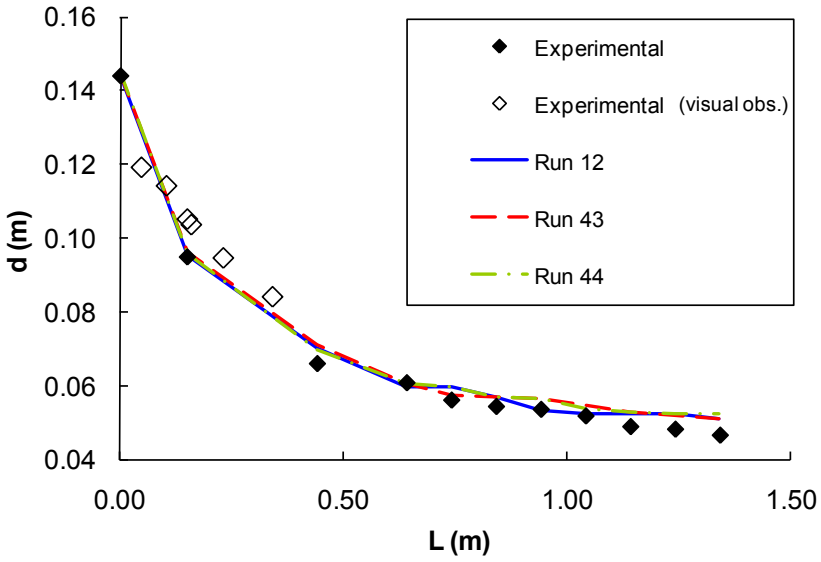

b)

Figure 4 - Results of the mesh convergence analysis: comparison of results for three meshes of 2.0, 2.2 and 2.4 million volumes: a) water velocities at different distances from the crest of the spillway (unfilled symbols refer to points with measurements affected by either the unsteady motion of the free surface or the unsteadiness of the location of the inception point; filled symbols indicate points in good standing); b) water levels at different distances from the crest of the spillway. q_w = 0.18 m^2/s

Fig. 5 presents a comparison of modeled velocities at the same distances from the crest of the spillway specified in Fig. 4, showing that the "short" and "extended" domains offer virtually the same results, with the natural savings in computational time associated with the former. Differences among results with both runs were smaller than 2% in the local velocities and 0.5% in the water depths and volumetric flow rate (or discharge; see below), which we considered negligible.

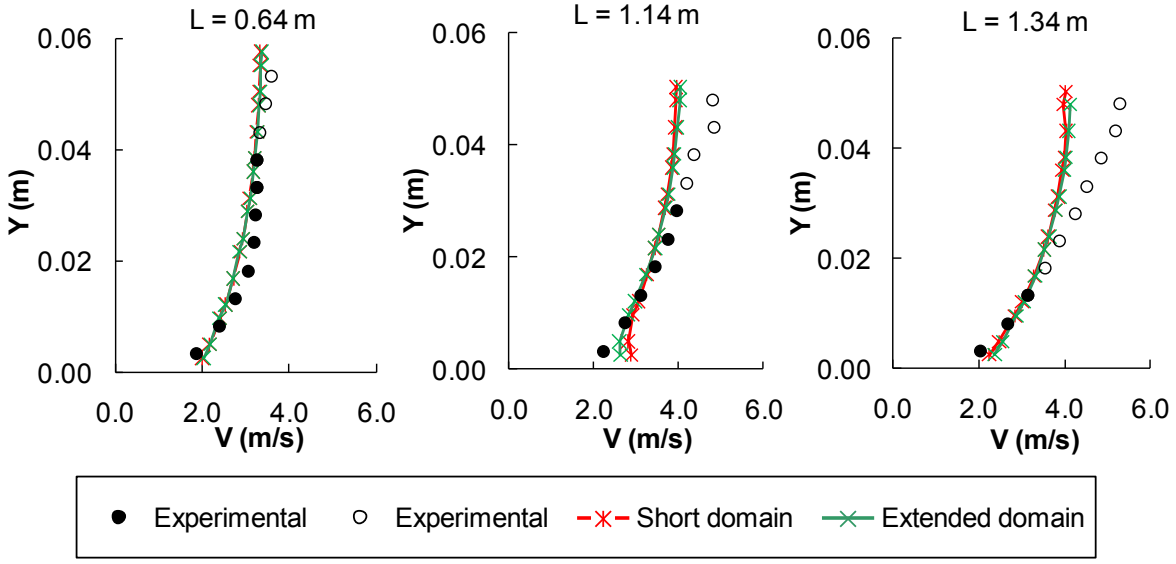

Figure 5 - Comparison among experimental and numerical results obtained for the "short" and "extended" domains, regarding water velocities. Unfilled symbols refer to points with measurements affected by either the unsteady motion of the free surface or the unsteadiness of the location of the inception point; filled symbols indicate points in good standing. q_w = 0.18 m^2/s

5. COMPARISON OF EXPERIMENTAL AND NUMERICAL RESULTS

5.1. VERIFICATION OF THE VOLUMETRIC FLOW RATE (DISCHARGE), WATER DEPTH AND VELOCITY DISTRIBUTION

To verify that the model provided the right discharge, we integrated numerically the results of velocity in several flow cross sections, using the trapezoidal rule (Burden and Faires 2004). Relative differences among experimental and numerical values of discharge for the non-aerated flow region of the spillway were less than 5% (average difference of 2.4%) for q_w = 0.18 m^2/s, which constitutes an excellent agreement, especially considering that this difference is within the experimental error in observing flow discharge. The same level of agreement was obtained for q_w = 0.08 m^2/s and 0.14 m^2/s.

Comparisons of measured and modeled water depths (d) are presented in Fig. 6 for q_w = 0.18 m^2/s, where L is measured from the crest of the spillway (Fig. 1). Visual observations of the flow in the physical model indicated that the time-averaged position of the free surface exhibited a slightly wavy pattern along the chute, particularly near the inception point. This is in agreement with

observations from previous authors (Chanson 2002). This feature was also noticed during the acquisition of data with the conductivity probe, the back-flushing Pitot tube, and the point gauges. Similar to the experimental data, a wavy pattern was obtained in the numerical result (Fig. 6). A very satisfactory agreement can be observed between both results. Differences between experimental and numerical results in Fig. 6 are less than 9%. An assessment of the error in the location of the free surface from the numerical result can be made from the definition that FLOW-3D® uses for that purpose (i.e., the value of F =0.5), and from considerations of mesh size. We estimated this error to be smaller than 1 mm, which is much smaller than the measured depths in the physical model.

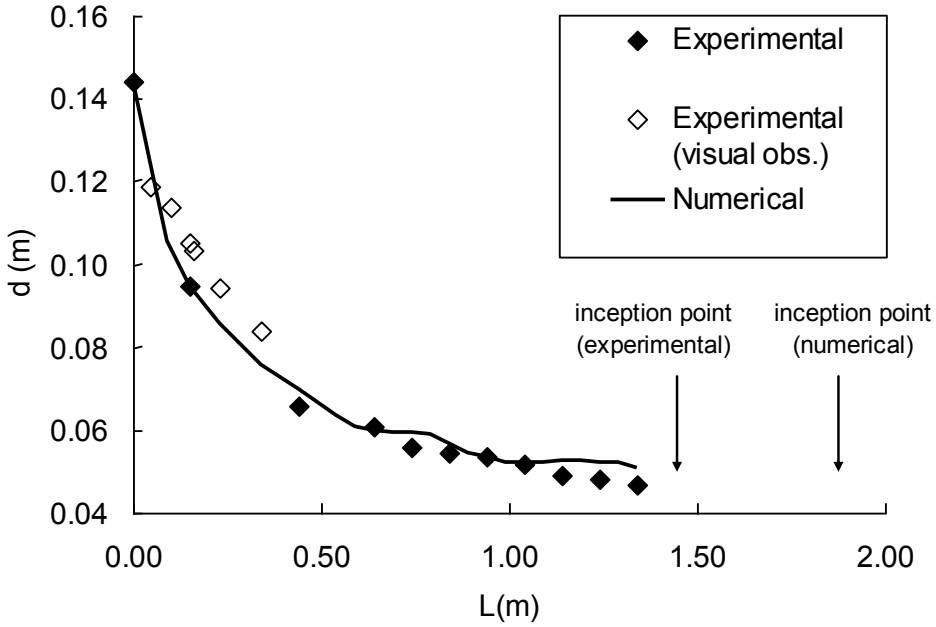

Figure 6 - Comparison among simulated and measured water flow depths. q_w = 0.18 m^2/s

The shape of the velocity profiles obtained with FLOW-3D® (solid lines), presented in Fig. 7 for q_w = 0.18 m^2/s, follows relatively closely the experimental one. In general, it can be observed that good agreement has been obtained, especially for the filled symbols where the differences are mainly smaller than 10% (7% on average). Notwithstanding this good agreement, the numerical solution seems to produce slightly more uniform velocity profiles than observed, which could in principle be associated with the pseudo-bottom normal diffusion generated by the turbulence closure. (The pseudo-bottom is defined as the surface tangent to the corners of the consecutive steps.) Differences may also stem from three-dimensional flow structures and effects that are not captured in a 2-D simulation, such as vortex stretching and self-induced velocity which contribute to "dissipate" eddies in 3-D (see Bombardelli et al. 2009). Similar agreement was obtained for other discharges, as shown below.

It is interesting also to notice that some of the simulated velocity profiles show a zone of almost constant velocity close to the pseudo-bottom. While such behavior has been observed in some experimental works in the past (see Gonzalez 2005; and Boes and Hager 2003a), not all works

report it. Certainly, we did not find it in our experiments. More research is needed to clarify this issue.

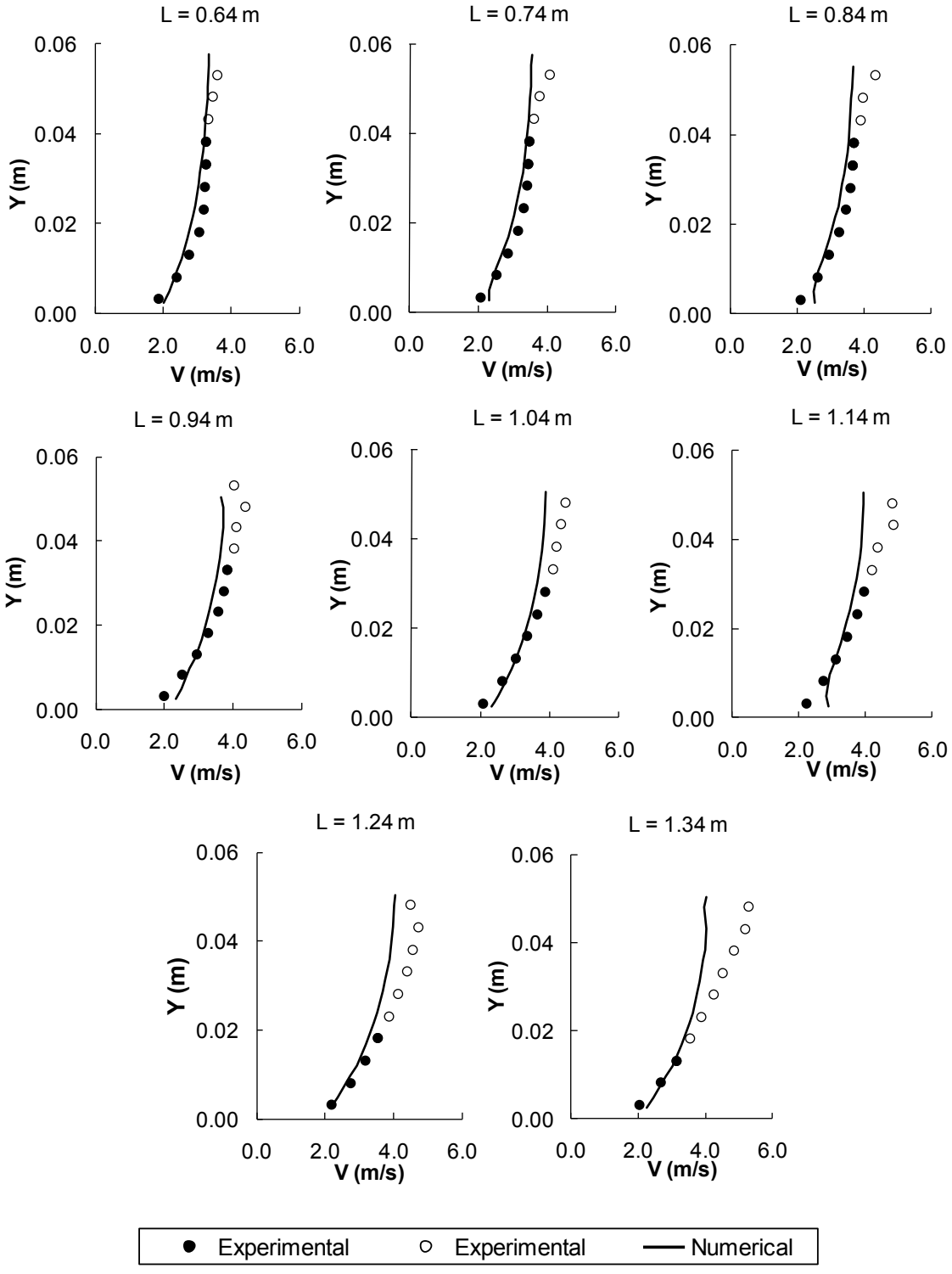

Figure 7 - Velocity distribution upstream of the point of inception: comparison among simulated and measured results. Unfilled symbols refer to points with measurements affected by either the unsteady motion of the free surface or the unsteadiness of the location of the inception point; filled symbols indicate points in good standing. q_w = 0.18 m^2/s

Because upstream of the inception point the velocity outside of the boundary layer is given by V_{max}, it is customary to consider a power-law velocity profile expressed by (Chanson 2002):

$$\frac{V}{V_{max}} = \left(\frac{y}{\delta}\right)^{1/N} \qquad 0 \leq y/\delta \leq 1 \qquad (11)$$

where V_{max} is the free-stream velocity; y is the transverse coordinate originating at the pseudo-bottom; δ is the boundary layer thickness defined as the perpendicular distance from the pseudo-bottom to the point where the velocity is 0.99 V_{max}; and N is an exponent, to be determined from experiments and numerical simulations. This assumes a self-similar behavior for the velocity profiles (Barenblatt 1996; Gioia and Bombardelli 2002).

Fig. 8 presents the velocity profiles normalized by V_{max} for q_w = 0.18 m^2/s. Numerical results of this paper show significantly better agreement with experimental data than those presented by Cheng et al. (2004b) for the air-water flow region, as expected. The agreement is of the same nature throughout the spillway. Velocity profiles present similar distributions to those observed by Amador et al. (2006) for the non-aerated flow region. In the step cavities, recirculating zones become well defined (not shown herein).

Fig. 9 presents comparisons between observed and modeled velocity profiles for specific discharges of 0.08, 0.14 and 0.18 m^2/s, at 0.64 and 0.74 m from the crest of the spillway. It is possible to see that the agreement obtained is of the same satisfactory quality as explained above. For q_w = 0.08 m^2/s, a smaller number of points was observed experimentally because of the shallower water depth. Similar level of agreement was obtained for a stepped spillway with steps of 8 cm, and a specific discharge of 0.18 m^2/s (not shown herein).

From both the experimental and numerical results, we obtained values of the exponent N of Eq. (11) equal to 3.4 and 5.4, respectively. Whereas the experimental value of the exponent is close to the exponents reported for the non-aerated or aerated regions in steep stepped chutes (Matos 2000; Chanson 2002, page 158; Meireles 2004; Renna 2004; Amador 2005), the numerical counterpart is closer to the exponent obtained for less steep slopes, either on the non-aerated (Ohtsu and Yasuda 1997; Meireles and Matos 2009) or on the gradually varied or quasi uniform aerated flow regions (Boes and Hager 2003a; André 2004). In turn, Felder and Chanson (2009) found a value of N =10 for the velocity profile in the aerated region.

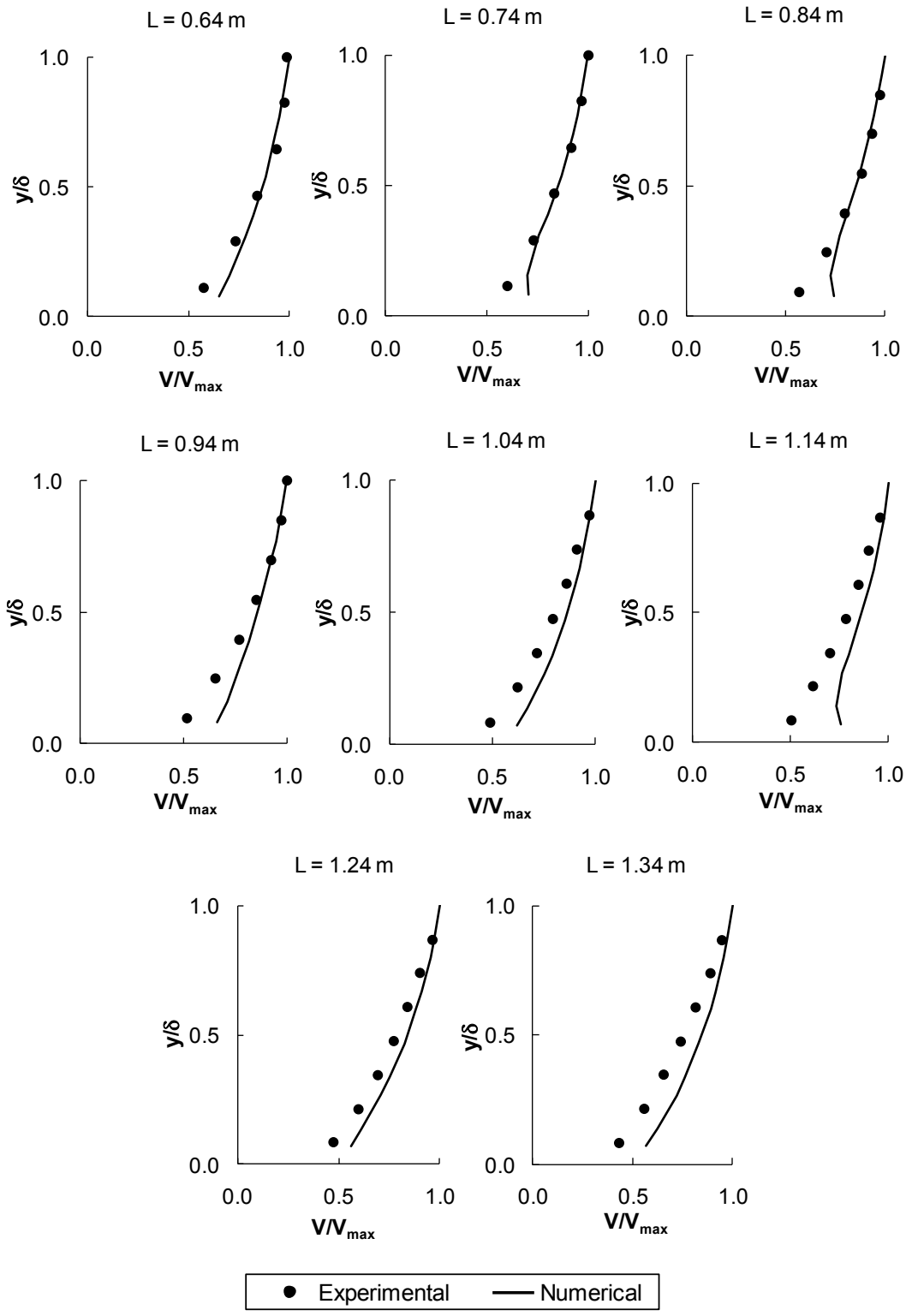

Figure 8 - Comparison among simulated and measured water flow depths. $q_w = 0.18\ m^2/s$

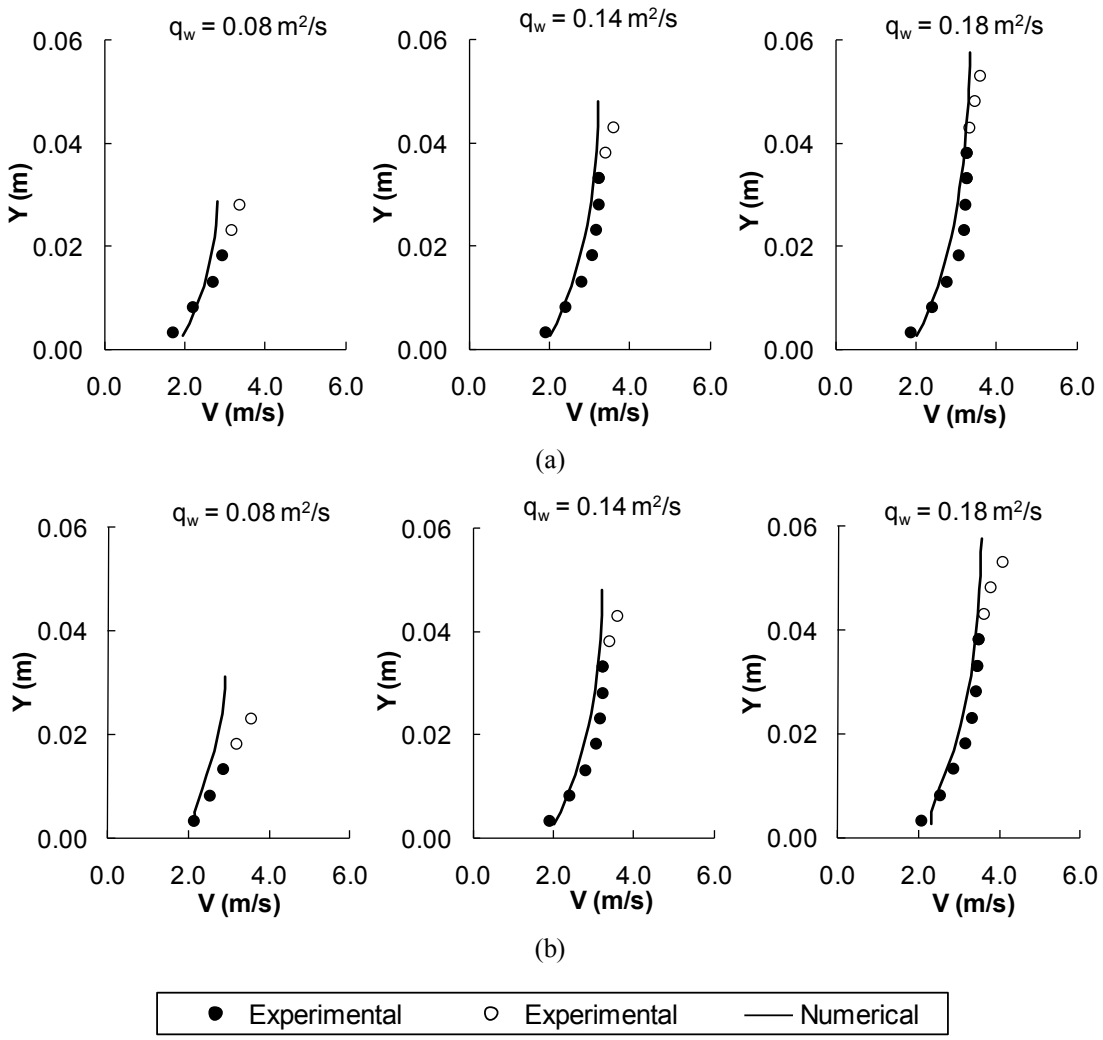

Figure 9 - Comparison among experimental and numerical velocities for unit discharges of 0.08, 0.14 and 0.18 m^2/s for: a) L= 0.64 m and b) L = 0.74 m. Unfilled symbols refer to points with measurements affected by either the unsteady motion of the free surface or the unsteadiness of the location of the inception point; filled symbols indicate points in good standing.

5.2. BOUNDARY LAYER DEVELOPMENT

Fig. 10 presents a fairly good agreement between the normalized boundary layer thickness (δ/L) obtained by definition from the experiments (open symbols), and from the simulations with FLOW-3D® (filled symbols), for several values of the normalized distance along the spillway (L/k_s). k_s is the roughness height perpendicular to the pseudo-bottom, $k_s = h\cos\theta$, with h denoting the step height; θ is the angle of the spillway; and L is measured from the crest of the spillway. Similarly to smooth spillways (e.g., Cain and Wood 1981), the growth of the boundary layer can be estimated by an equation of the type

$$\frac{\delta}{L} = a\left(\frac{L}{k_s}\right)^{-b} \tag{12}$$

where a and b are real numbers. For q_w = 0.18 m^2/s, we obtained a=0.223 and b=0.497 from experiments (for $26.7 < L/k_s < 55.8$) and a=0.27 and b=0.55 from numerical data (for $18.5 < L/k_s < 72.5$). The expressions proposed by Chanson (2002) and Amador (2005) for δ/L are also presented in Fig. 10. The formula proposed by Chanson (2002) is based on model and prototype data tested for a wide range of angles and conditions. Amador's equation was developed from experiments undertaken in a 1V:0.8H stepped spillway, with a=0.112 and b=0.309. The agreement between the data of the current paper with Amador's expression or Chanson's equation is fairly good for L/k_s values larger than approximately 40. For lower L/k_s values, the agreement with Amador's expression was better than the agreement with Chanson's equation. To show the different behaviors, all formulations are presented in Fig. 10 for the range $15 < L/k_s < 75$. (Outside of their domain of application, the expressions are presented with thinner lines.). The discrete nature of the velocity profiles (both experimental and numerical) increases the difficulty in estimating the boundary layer thickness for each cross section along the spillway, contributing to the differences observed. In addition, it is worth highlighting that the values of b obtained in our work and elsewhere are larger than the value of 0.13 found for smooth chutes (Chow 1959), denoting the well-known faster development of the boundary layer in stepped spillways.

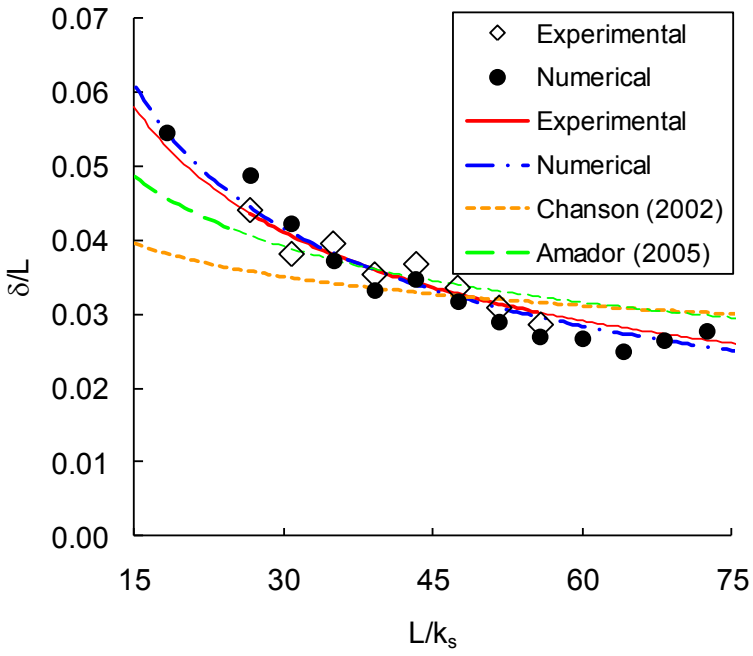

Figure 10 - Development of the boundary layer: comparison among simulated and measured results, regressions to the data, and formulations of Chanson (2002) and Amador (2005). q_w = 0.18 m^2/s

The inception point of air entrainment corresponds to the section where the growing boundary layer reaches the free surface. The location of the inception point was obtained from the numerical results comparing the spatial variation of the water flow depth and the boundary layer thickness (Fig. 11).

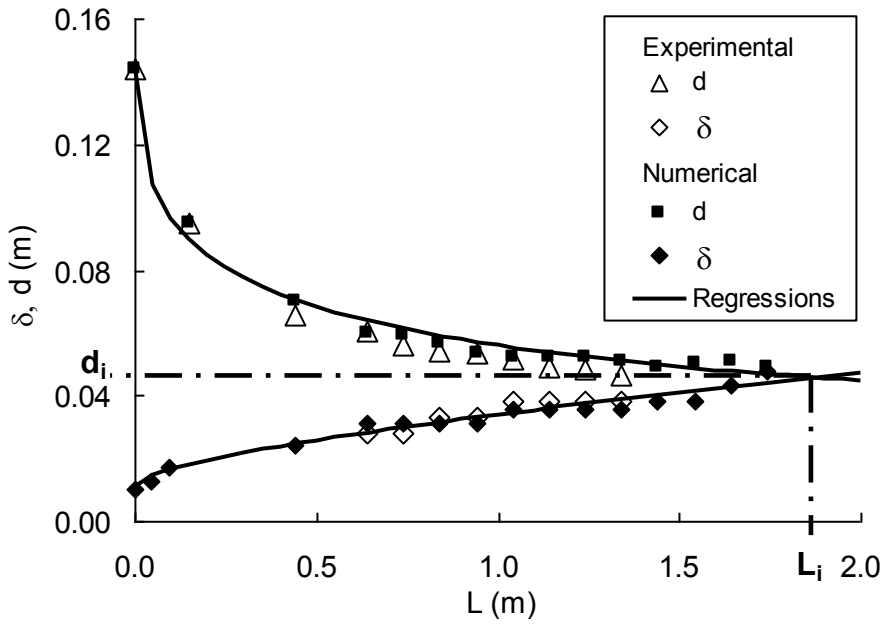

Figure 11 - Development of the boundary layer and variation of the water depth. Estimation of the inception point depth and location. q_w = 0.18 m²/s

In Table 3, it is possible to see that the numerical result of L_i, the location of the inception point, compares fairly well with the experimental relations presented by Chanson (2002, page 148). Although numerical and experimental water depth and boundary layer thickness results are close, the spatial variations of the numerical predictions of water depth and δ are slightly smaller than the experimental counterparts, contributing to the observed difference in L_i. In addition, a slightly greater depth at the inception point, d_i, was obtained from Chanson's regressions.

Table 3 - Comparison of measured and modeled results regarding the depth and location of the inception point.

Source	L_i (m)	d_i (m)
Regression (Chanson 2002)*	1.75	0.053
Experimental result	1.44	0.046
Numerical result	1.87	0.046

$L_i = (h \cos\theta)\, 9.719\, (\sin\theta)^{0.0796}\, F_*^{0.713}$ (location of the inception point)

$d_i = (h \cos\theta)\, 0.4034\, (\sin\theta)^{-0.04}\, F_*^{0.592}$ (depth of the inception point)

$F_* = q_w / \sqrt{g \sin\theta\, (h \cos\theta)^3}$ (Froude number)

h: step height; θ: angle of the spillway; q_w: discharge per unit width; g: acceleration of gravity.

(*) See also Felder and Chanson (2009)

5.3. TURBULENCE STATISTICS

TKE is generated in the steps and in other parts of the flow through the velocity gradients (Rodi 1984; Pope 2000). Numerical predictions show an increase in TKE along the spillway, for any

given distance from the pseudo-bottom (Fig. 12(a)), which is the result of the development of the boundary layer. Figs 12(b) and (c) show details of Fig. 12(a), depicting higher values of TKE at the center of the step cavities. These results are qualitatively similar to those presented by Cheng et al. (2004a, b), obtained from a numerical study of the air-water flow region. In addition, these results agree in shape with the experimental evidence presented by Amador et al. (2006) acquired with the use of a PIV system.

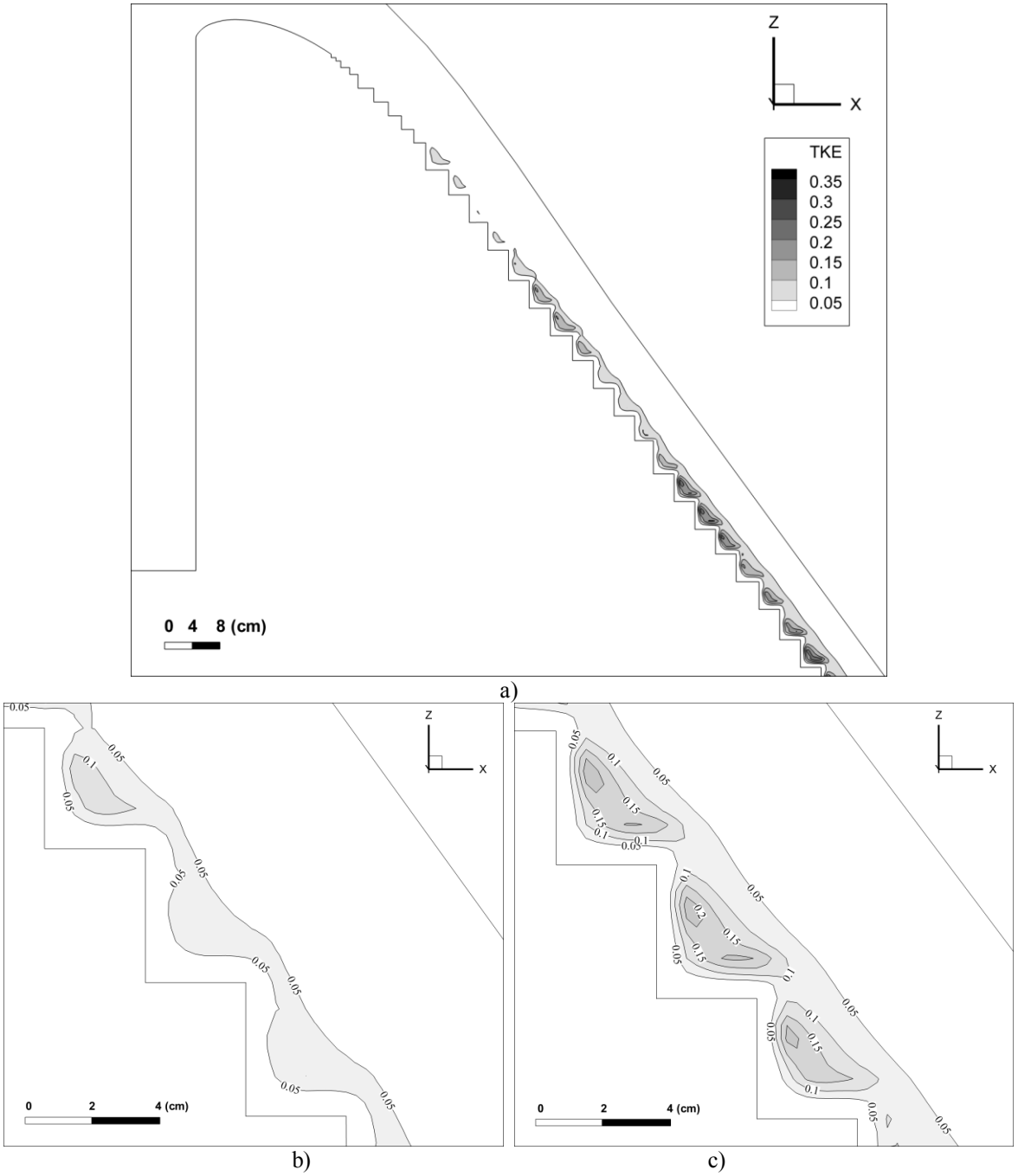

Figure 12 - Field of turbulent kinetic energy (TKE) obtained via numerical simulations (in m^2s^2): a) Evolution of the TKE in the non-aerated region of the spillway; b) detail of TKE at steps 17, 18 and 19; c) detail of TKE at steps 22, 23 and 24. Contours show asymmetry in the steps, as observed experimentally (Chanson 2002). q_w = 0.18 m^2/s

Fig. 13 presents contours of the computed dissipation rate of TKE. The patterns are similar to those presented for the TKE, possibly indicating that the steps are mostly regions of both creation and dissipation of TKE, in spite of the fact that some transfer of TKE between steps occurs. Figs 12 and 13 also help identifying the development of the so-called "roughness layer," akin to wall flows with large roughness elements (see Jiménez 2004 for a detailed discussion on the influence of roughness on the flow).

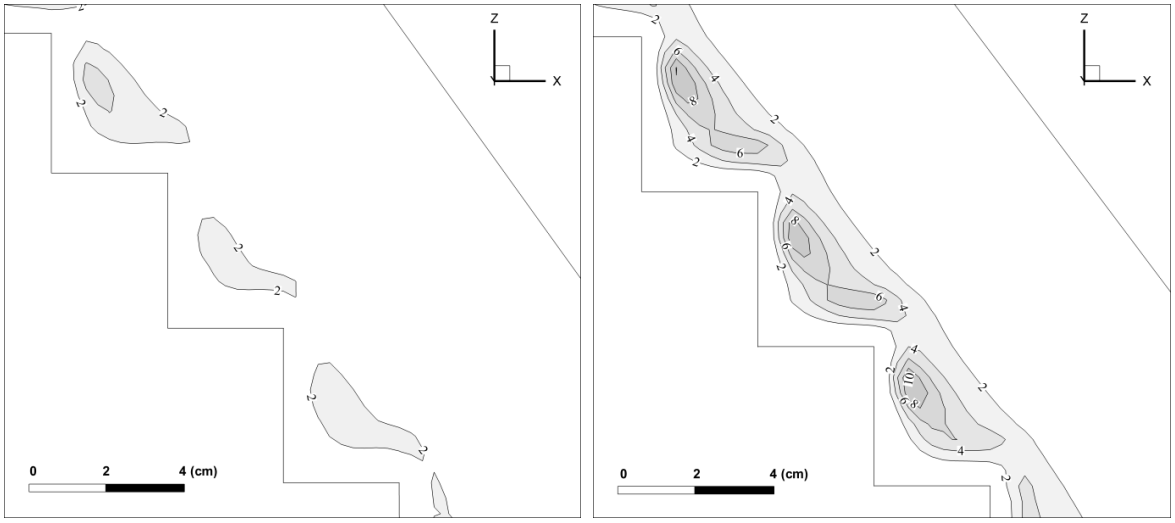

a) b)

Figure 13 - Field of dissipation rate of TKE obtained via numerical simulations (in m^2s^3): a) detail of dissipation rate of TKE at steps 17, 18 and 19; b) detail of dissipation rate of TKE at steps 22, 23 and 24.

6. SENSITIVITY ANALYSES OF THE NUMERICAL SIMULATIONS

In order to explore the influence of diverse modeling parameters and sub-models on the results, several additional runs were developed.

6.1. TURBULENCE MODELS AND TURBULENCE MIXING LENGTH

Simulations performed with the k-ε model and the RNG k-ε model (Yakhot and Orszag 1986; Yakhot and Smith 1992) provided very similar results (Fig. 14). Very small differences of about 1% in the local velocities and water flow depths, and of less than 0.5% in the discharges, were observed. For this reason, even if the RNG k-ε model is in general regarded as having wider applicability than the k-ε model, the present study shows that the k-ε model offers as accurate results of velocities, water flow depth and discharge as the RNG k-ε model for the stepped spillway problem. Furthermore, it can be noticed that the turbulent diffusion in the pseudo-bottom normal direction is similar for both closures.

FLOW-3D® includes a turbulent mixing length (TLEN) for the k-ε and RNG k-ε turbulence models to regulate the dissipation rate of TKE and the eddy dynamic viscosity (see also Johnson and Savage 2006). If TLEN is too high (low), the dissipation rate can be under- (over-) predicted and the eddy dynamic viscosity can be unrealistically high (low) (recall Eq. (5)). Two different simulations were performed, one with the default value used by FLOW-3D® (which is 7% of the

smallest domain dimension) and another with TLEN equal to 7% of the flow depth in the non-aerated flow region of the spillway. This last value is about 50 times smaller than the default value. No noticeable differences were observed among the results of the two simulations. The relative differences in the velocities were usually of about 0.3%, and the relative differences in the discharges and water depths were smaller than 1%.

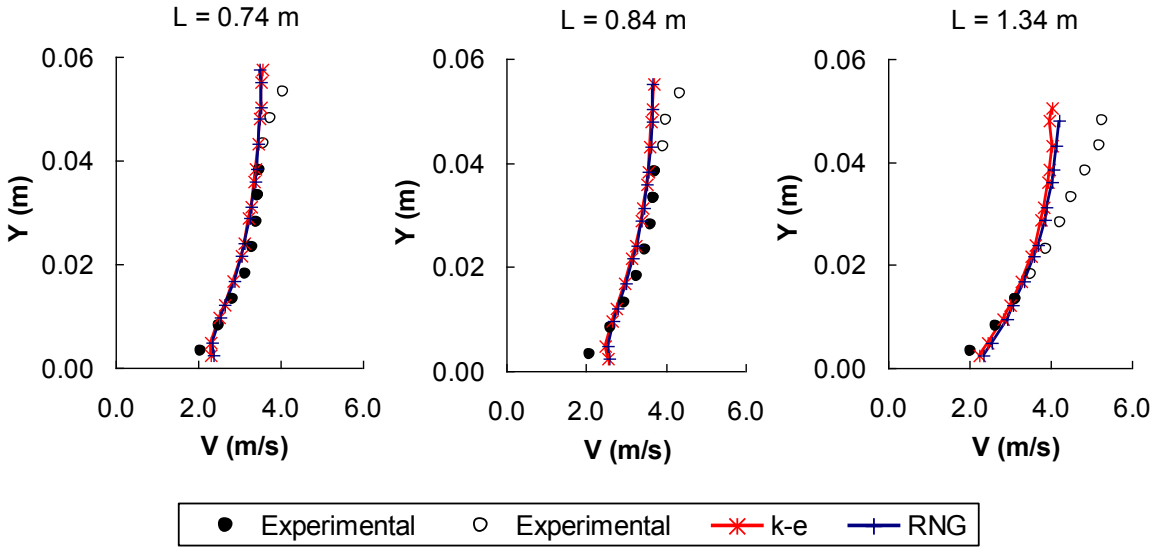

Figure 14 - Sensitivity analysis corresponding to the turbulence model: Comparison among experimental and numerical results obtained using the *k-ε* and RNG *k-ε* turbulence models regarding water velocities. *Unfilled symbols* refer to points with measurements affected by either the unsteady motion of the free surface or the unsteadiness of the location of the inception point; filled symbols indicate points in good standing. q_w = 0.18 m²/s

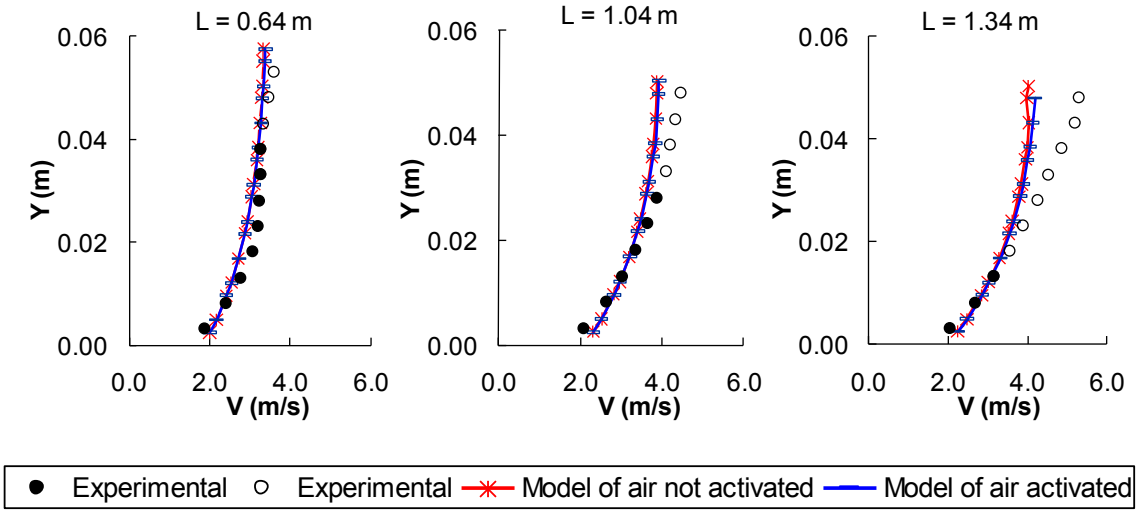

Figure 15 - Sensitivity analysis corresponding to the sub-model of air incorporation: Comparison among experimental and numerical results obtained with and without the sub-model of air incorporation regarding water velocities. *Unfilled symbols* refer to points with measurements affected by either the unsteady motion of the free surface or the unsteadiness of the location of the inception point; filled symbols indicate points in good standing. q_w = 0.18 m²/s

6.2. SUB-MODEL FOR AIR ENTRAINMENT

Almost no difference was observed among the results with and without the activation of the sub-model for air-entrainment in the non-aerated region of the spillway, as expected (Fig. 15). In the runs shown herein, the gas was assumed to move at the velocity of the mixture in all directions. Discharges, water flow depths, and TKE values also gave similar results. This constitutes a much needed check to test the correctness of the computations.

6.3. EVALUATION OF THE COMPUTATIONAL RESULTS AND THEORETICAL MODELS

This paper provided an assessment of the non-aerated region of the skimming flow over steep stepped spillways, and completely characterized the flow features. Numerical simulations offer assistance to the design of this type of structures at the time they provide information on the flow details. Although some authors have decided to address the aerated flow from the start, focusing on the non-aerated region seems to be a natural first step in building more complex models. The ultimate interest is to have a set of complete models for the characterization of velocities, water levels, air concentrations and turbulence statistics in the entire spillway.

Throughout the non-aerated portion of the spillway, model predictions offered an accurate description of velocity profiles, of boundary layer development and of water depths. The model also predicted fairly well the location of the inception point and its depth for three discharges, taking into account the complex nature of the phenomenon. This suggests that the selected theoretical model is adequate for the non-aerated region, and that the numerical integration has been adequate.

Having said that, it becomes clear that this theoretical model needs improvement for the aerated region in order to be able to capture the increase of flow depth due to air entrainment, the non-dilute nature of the two-phase flow, the combination of the water/bubble and air/drop flows, and the interaction of phases (Chanson 2002). The current theoretical model can provide only a slight increase in the flow depth in the aerated region and can offer air concentrations only accurate close to the pseudo-bottom. We are currently at the development stage of those more sophisticated models which, naturally, fall outside of the scope of this paper. Jha and Bombardelli (2010) have very recently addressed the non-dilute sediment-laden flow in open channels with success and, thus, such work is a good starting point for our developments. We believe that the incorporation of more formal two-phase flow theories to the current model may yield the desired answers.

7. CONCLUSIONS

This paper has addressed the flow in steep stepped spillways. Our work focused on the non-aerated portion of skimming flows. Although flows in stepped spillways are usually characterized by high air concentrations concomitant with high rates of energy dissipation, the non-aerated region becomes important in small dams and/or spillways with high specific discharges.

Experiments combined with numerical simulations confirmed the wavy pattern of the free surface, especially close to the inception point. The two results showed a very satisfactory agreement.

Results on the development of the boundary layer in this paper were not significantly different from results reported by other authors for moderate to large normalized distances along the chute; however, in the upstream reach of the spillway, near the crest, differences increased. Our results put forward values of the exponents a and b, of the equation for the boundary-layer development, equal to a=0.223 and b=0.497 (experiments) and a=0.27 and b=0.55 (numerical result). In turn, the exponents of the self-similar velocity profiles were found to be in agreement with published results for similar geometric and flow conditions, varying in our case between 3.4 (experiments) and 5.4 (numerical).

The runs developed in this paper show that the use of a k-ε model combined with the *TruVOF* method allow for an accurate representation of the flow features in the non-aerated region of the structure. No significant differences were observed in the simulations with this closure and the k-ε RNG model. The use of the *TruVOF*, in particular, allows for an accurate yet economic technique which proves to be superior to re-meshing or to other versions of the method which solve for both the water and air flows. Further, the multi-block gridding feature embedded in FLOW-3D®, which helps in optimizing the mesh, was crucial for saving computational time, and showed a clear advantage with respect to other techniques in other software packages.

ACKNOWLEDGMENTS Fabián Bombardelli gratefully acknowledges the support of the California Department of Water Resources (DWR), through Award 4600007984 TO BD01, and the California Water Resources Control Board (CAWRCB), through Award 06-447-300 TO 5. Inês Meireles was a Visiting Scholar at the University of California, Davis, during the months of September 2007 to March 2008, and was financially supported by a Fulbright/FLAD Research Grant. This support is gratefully acknowledged. The financial support granted by INAG, Portuguese Water Institution (Project 2003/2029/INAG), and by the Portuguese Foundation for Science and Technology (FCT), through Project PTDC/ECM/108128/2008, is also gratefully acknowledged. Currently, Inês Meireles is supported by FCT, Grant No. SFRH/BD/38003/2007.

REFERENCES

Abad, J. D., Rhoads, B. L., Guneralp, I., and García, M. H. (2008). "Flow structure at different stages in a meander bend with bendway weirs." J. Hydr. Eng., ASCE, 134(8), 1052-1063.

Amador, A. (2005). "Comportamiento hidráulico de los aliviaderos escalonados en presas de hormigón compactado." Ph.D. thesis, UPC, Barcelona, Spain (in Spanish).

Amador, A., Sanchez-Juni, M., Dolz, J. (2006). "Characterization of the non-aerated flow region in a stepped spillway by PIV." J. Fluid Engineering, ASME, 138(6), 1266-1273.

André, S. (2004). "High velocity aerated flows over stepped chutes with macro-roughness elements." Ph.D. thesis, EPFL, Lausanne, Switzerland.

Arantes, E. J. (2007). "Caracterização do escoamento sobre vertedouros em degraus via CFD." Ph.D. thesis, EESC/USP, São Carlos, Brazil (in Portuguese).

Barenblatt, G. I. (1996). “Scaling, self-similarity, and intermediate asymptotics.” Cambridge University Press, UK.

Barkhudarov, M. R. (2004). “Multi-block gridding technique for Flow-3D.” Flow Science Technical Notes, Flow Science, Inc., TN59, available online.

Bhuiyan, A. B. M., and Hey, R. (2007). “Computation of three-dimensional flow field created by weir-type structures.” Engineering Applications of Computational Fluid Mechanics, 1(4), 350-360.

Boes, R. M., and Hager, W. H. (2003a). “Two phase flow characteristics of stepped spillways.” J. Hydr. Eng., ASCE, 129(9), 661-670.

Boes, R. M., and Hager, W. H. (2003b). “Hydraulic design of stepped spillways.” J. Hydr. Eng., ASCE, 129(9), 671-679.

Bombardelli, F. A., García, M. H., and Caisley, M. E. (2000). “2-D and 3-D numerical simulation of abrupt transitions in open-channel flows. Application to the design of canoe chutes.” Proc. 4th. Int. Conf. on Hydroinformatics, IAHR, Iowa City, IA, USA. (In CD.)

Bombardelli, F. A., Hirt, C. W., and García, M. H. (2001). “Discussion on ‘Computations of Curved Free Surface Water Flow on Spiral Concentrators’, by Matthews et al.” J. Hydr. Eng., ASCE, 127(7), 629-631.

Bombardelli, F. A. (2003). “Characterization of coherent structures from parallel, LES computations of wandering effects in bubble plumes.” Proc. 2003 World Water and Environmental Resources Congress, Environmental & Water Resources Institute (EWRI), ASCE, Philadelphia, PA, USA, P. Bizier and P. DeBarry (Ed.). (In CD.)

Bombardelli, F. A. (2004). “Turbulence in multiphase models for aeration bubble plumes.” Ph.D. thesis. University of Illinois at Urbana-Champaign.

Bombardelli, F. A. (2010). "Water distribution systems." Chapter 41 in Environmental Fluid Mechanics, H. J. Fernando (Ed.) (in press).

Bombardelli, F. A., Buscaglia, G. C., Rehmann, C. R., Rincón, L. E., and García, M. H. (2007). “Modeling and scaling of aeration bubble plumes: a two-phase flow analysis.” J. Hyd. Res., IAHR, 45(5), 617-630.

Bombardelli, F. A., and Jha, S. K. (2009). “Hierarchical modeling of dilute, suspended-sediment transport in open channels.” Environ. Fluid Mech., 9(2), 207-230.

Bombardelli, F. A., Cantero, M. I., García, M. H., and Buscaglia, G. C. (2009). “Numerical aspects of the simulation of discontinuous saline underflows: the lock-exchange problem.” J. Hyd. Res., IAHR, 47(6), 777-789.

Burden, R. L., and Faires, J. D. (2004). “Numerical analysis.” Eighth Edition, Brooks-Cole Publishing.

Buscaglia, G. C., Bombardelli, F. A., and García, M. H. (2002). “Numerical modeling of large scale bubble plumes accounting for mass transfer effects.” Int. J. Multiphase Flow, 28, 1763-1785.

Cain, P., and Wood, I. R. (1981). “Measurements of self-aerated flow on a spillway.” J. Hydr. Eng., ASCE, 107(HY11), 1407-1424.

Caisley, M. E., Bombardelli, F. A., and García, M. H. (1999). “Hydraulic model study of a canoe chute for low-head dams in Illinois.” Civil Engineering Studies, Hydraulic Engineering Series No-63, University of Illinois at Urbana-Champaign.

Carvalho, R., and Amador, A. (2008). “Physical and numerical investigation of the skimming flow over a stepped spillway.” Proc. 3rd. IAHR Int. Symposium on Hydraulic Structures, Nanjing, China, 1767-1772. (In CD.)

Chamani, M. R., and Rajaratnam, N. (1999). “Characteristics of skimming flow over stepped spillways.” J. Hydr. Eng., ASCE, 125(4), 361-368.

Chanson, H. (2001). “Hydraulic design of stepped spillways and downstream energy dissipators.” Dam Engineering, 11(4), 205-242.

Chanson, H. (2002). “The hydraulics of stepped chutes and spillways.” Balkema, Lisse, The Netherlands.

Chanson, H. (2009). “Turbulent air-water flows in hydraulic structures: dynamic similarity and scale effects.” Environ. Fluid Mech., 9(2), 125-142.

Chatila, J., and Tabbara, M. (2004). “Computational modeling of flow over an ogee spillway.” Comp. & Struct., Elsevier, 82, 1805-1812.

Chen, Q., Dai, G., and Liu, H. (2002). “Volume of fluid model for turbulence numerical simulation of stepped spillway overflow.” J. Hydr. Eng., ASCE, 128(7), 683-688.

Cheng, X., Luo, L., and Zhao, W. (2004a). “Study of aeration in the water flow over stepped spillway.” Proc. World Water Congress 2004, ASCE, Salt Lake City, Utah, USA.

Cheng, X., Luo, L., Zhao, W., and Li, R. (2004b). “Two-phase flow simulation of aeration on stepped spillway.” Progress in Natural Science, 14(7), 626-630.

Chow, V. T. (1959). “Open-channel hydraulics.” McGraw-Hill, USA.

Chung, T. J. (2006). “Computational fluid dynamics” Cambrigde University Press, USA.

Crowe, C., Sommerfeld, M., and Tsuji, Y. (1998). “Multiphase flows with droplets and particles.” CRC Press, USA.

Dargahi, B. (2006). “Experimental study and 3D numerical simulations for a free-overflow spillway.” J. Hydr. Eng., ASCE, 132(9), 899-907.

Drew, D. A., and Passman, S. L. (1999). “Theory of multicomponent fluids.” Springer, Vol. 135 of Applied Mathematical Sciences.

Felder, S., and Chanson, H. (2009). “Energy dissipation, flow resistance, and gas liquid interfacial area in skimming flows on moderate-slope stepped spillways.” Environmental Fluid Mechanics, 9(4), 427-441.

Ferziger, J. H., and Peric, M. (2002). "Computational methods for fluid dynamics." Springer.

Flow Science, Inc. (2008). FLOW-3D User's Manual, Version 9.3, Los Alamos, New Mexico, USA.

Gioia, G., and Bombardelli, F. A. (2002). "Scaling and similarity in rough channel flows." Phys. Rev. Lett., 88(1), 014501.

Gomes, J. F. (2006). "Campo de pressões: Condições de incipiência à cavitação em vertedouros em degraus com declividade 1V:0,75H." Ph.D. thesis, UFRGS, Porto Alegre, Brazil (in Portuguese).

Gonzalez, C. (2005). "An experimental study of free-surface aeration on embankment stepped chutes." Ph.D. thesis, University of Queensland, Brisbane, Australia.

Gonzalez, C., and Chanson, H. (2007). "Hydraulic design of stepped spillways and downstream energy dissipators for embankment dams." Dam Engineering, XVII(4), 223-244.

Gonzalez, C., and Chanson, H. (2008). "Turbulence and cavity recirculation in air-water skimming flows on a stepped spillway." J. Hydr. Res., IAHR, 46(1), 65-72.

Hager, W., and Boes, R. M. (2000). "Backwater and drawdown curves in stepped spillway flow." Proc. 1st Int. Workshop on Hydraulics of Stepped Spillway, Zurich, Switzerland, A. A. Balkema Publisher, Rotterdam, The Netherlands, 129-136.

Hrenya, C. M., and Sinclair, J. L. (1997). "Effects of particle-phase turbulence in gas-solid flows." AIChE J., 43(4), 853-869.

Higgs, J., and Frizell, K. W. (2004). "Investigation of the Lake Plant Pump Station - Lower Colorado River Authority." Hydraulic Laboratory Report HL-2004-02, Denver Technical Center, Bureau of Reclamation, United States Department of the Interior, Denver, Colorado, December, 2004.

Hirt, C. W., and Nichols, B. D. (1981). "Volume of Fluid (VOF) method for the dynamics of free boundaries." J. Comp. Physics, 39, 201-225.

Hirt, C. W., and Sicilian, J. M. (1985). "A porosity technique for the definition of obstacles in rectangular cell meshes." Proc. 4th Int. Conf. Ship Hydro., National Academy of Science, Washington, DC, USA.

Hirt, C. W. (2003). "Modeling turbulent entrainment of air at a free surface." Technical Note 61, Flow Science, Inc. (FSi-03-TN61).

Ho, D. K. H., Cooper, B. W., Riddette, K. M., and Donohoo, S. M. (2006). "Application of numerical modelling to spillways in Australia." Dams and Reservoirs, Societies and Environment in the 21st Century, Berga et al. (Ed.), Taylor & Francis Group, London, UK.

Jha, S. K. and Bombardelli, F. A. (2010). "Toward two-phase flow modeling of nondilute sediment transport in open channels. " J. Geophysical Research, 115, F03015.

Jiménez, J. (2004). "Turbulent flows over rough walls." Annual Review of Fluid Mechanics, 36, 173-196.

Johnson, M. C., and Savage, B. M. (2006). "Physical and numerical comparison of flow over ogee spillway in the presence of tailwater." J. Hydr. Eng., ASCE, 132(12), 1353-1357.

Launder, B. E., and Spalding, D. B. (1972). "Lectures in mathematical models of turbulence." Academic Press.

Matos, J., and Frizell, K. W. (1997). "Air concentration measurements in highly turbulent aerated flow". Proc. 27th IAHR Congress, Theme D, Vol. 1, San Francisco, USA, S. S. Y. Wang and T. Carstens (Ed.), 149-154. (In CD.)

Matos, J. (2000). "Hydraulic design of stepped spillways over RCC dams." Proc. 1st Int. Workshop on Hydraulics of Stepped Spillway, Zurich, Switzerland, A. A. Balkema Publisher, Rotterdam, The Netherlands, 187-194.

Matos, J., and Frizell, K. W. (2000). "Air concentration and velocity measurements on self-aerated flow down stepped chutes." Proc. ASCE 2000 Conference, Minneapolis, USA.

Matos, J., Frizell, K. H., André, S., and Frizell, K. W. (2002). "On the performance of velocity measurement techniques in air-water flows." Proc. EWRI/IAHR Joint Conference on Hydraulic Measurements & Experimental Methods, ASCE, Estes Park, USA.

Matos J., Sanchez-Juny M., Quintela A., Dolz J. (1999). "Characteristic depth and pressure profiles in skimming flow over stepped spillways." Proc. 29th IAHR congress, Graz, Austria.

Matthews, B. W., Fletcher, C. A. J., Partridge, A. C., and Vasquez, S. (1999). "Computations of curved free surface water flow on spiral concentrators." J. Hydr. Eng., ASCE, 125(11), 1126-1139.

Matthews, B. W., Fletcher, C. A. J., Partridge, A. C., and Vasquez, S. (2001). "Computations of curved free surface water flow on spiral concentrators. Closure" J. Hydr. Eng., ASCE, 127(7), 631-631.

Meireles, M. (2004). "Emulsionamento de ar e dissipação de energia do escoamento em descarregadores em degraus." M.Sc. thesis, IST, Lisbon, Portugal (in Portuguese).

Meireles, I., and Matos, J. (2009). "Skimming flow in the non-aerated region of stepped spillways over embankment dams." J. Hydr. Eng., ASCE, 135(8), 685-689.

Meireles, I., Matos, J., and Melo, J. F. (2006). "Skimming flow properties upstream of air entrainment inception on steeply sloping stepped chutes." Proc. Int. Symposium on Hydraulic Structures, IAHR, Ciudad Guayana, Venezuela. (In CD.)

Ohtsu, I., and Yasuda, Y. (1997). "Characteristics of flow conditions on stepped channels." Proc. 27th. IAHR Congress, San Francisco, Theme D, 583-588. (In CD.)

Ohtsu, I., Yasuda, Y., and Takahashi, M. (2004). "Flow characteristics of skimming flows in stepped channels." J. Hydr. Eng., ASCE, 130(9), 860-869.

Paxson, G., and Savage, B. (2006). "Labyrinth spillways: comparison of two popular U.S.A. design methods and consideration of non-standard approach conditions and geometries." Proc. Int. Junior Researcher and Engineer Workshop on Hydraulic Structures, J. Matos and H. Chanson (Ed.),

Report CH61/06, Div. of Civil Eng., The University of Queensland, Brisbane, Australia (ISBN 1864998687).

Pope, S. B. (2000). “Turbulent flows.” Cambridge University Press, UK.

Prosperetti, A., and Tryggvason, G. (2007). “Computational methods for multiphase flow.” Cambridge Press, UK.

Renna, F. (2004). “Caratterizzazione fenomenologica del moto di un fluido bifasico lungo scaricatori a gradini.” Ph.D. thesis, Politecnico di Bari, Cosenza, Italy (in Italian).

Rodi, W. (1984). “Turbulence models and their application in hydraulics.” State-of-the-Art Paper, IAHR.

Rodríguez, J. F., Bombardelli, F. A., García, M. H., Frothingham, K., Rhoads, B. L., and Abad, J. D. (2004). “High-resolution numerical simulation of flow through a highly sinuous river reach.” Water Resources Management, Kluwer Academic Publishers, 18, 177-199.

Sánchez-Juny, M. (2001). “Comportamiento Hidráulico de los Aliviaderos Escalonados en Presas de Hormigón Compactado. Análisis del Campo de Presiones.” Ph.D. thesis, UPC, Barcelona, Spain (in Spanish).

Savage, B. M., and Johnson, M. C. (2001). “Flow over ogee spillway: physical and numerical model case study.” J. Hydr. Eng., ASCE, 127(8), 640-649.

Savage, B., Frizell, K., and Crowder, J. (2004). “Brains versus brawn: the changing world of hydraulic model studies.” Proc. 2004 Annual Conference, Association of State Dam Safety Officials (ASDSO), Phoenix, USA.

Song, C. C. S., and Zhou, F. (1999). “Simulations of free surface flow over spillway.” J. Hydr. Eng., ASCE, 125(9), 959-967.

Storti, M. A., Nigro, N. M., Paz, R. R., and Dalcín, L. (2008) “Dynamic boundary condition in computational fluid dynamics.” Computer Methods in Applied Mechanics and Engineering, 197(13-16), 1219-1232.

Tabbara, M., Chatila, J., and Awwad, R. (2005). “Computational simulation of flow over stepped spillways.” Computers & Structures, Elsevier, 83, 2215-2224.

Unami, K., Kawachi, T., Babar, M. M., and Itagaki, H. (1999). “Two-dimensional numerical model of spillway flow.” J. Hydr. Eng., ASCE, 125(4), 369-375.

Wade R. J., Rhoads B. L., Rodriguez J., Daniels M., Wilson D., Herricks E.E., Bombardelli F., Garcia M., Schwartz J. (2002). “Integrating science and technology to support stream naturalization near chicago, Illinois. ” J. American Water Resources Association, AWRA, 38(4), 931-944.

Wilcox, D.C. (1993). “ Turbulence modeling for CFD.” DCW Industries, USA.

Yakhot, V., and Orszag, S. A. (1986). “Renormalization group analysis of turbulence. I. Basic theory.” J. Scientific Computing, 1(1), 3-51.

Yakhot, V., and Smith, L. M. (1992) "The renormalization group, the e-expansion, and the derivation of turbulence model." J. Scientific Computing. 3, 35.

Yasuda, Y., and Ohtsu, I. (2003). "Effect of step cavity area on flow characteristics of skimming flows on stepped chutes." Proc. 30th IAHR Int. Congress, Thessaloniki, Greece, 703-710. (In CD.)

Yasuda, Y., Takahashi, M., and Ohtsu, I. (2004). "Discussion on 'Volume of fluid model for turbulence numerical simulation of stepped spillway overflow,' by Chen et al." J. Hydr. Eng., ASCE, 130(2), 170.

Ye, M., Wu, C., Chen, Y., and Zhou, Q. (2006). "Case study of an s-shaped spillway using physical and numerical models." J. Hydr. Eng., ASCE, 132(9), 892-898.

5.2 BOUNDARY-LAYER DEVELOPMENT, SELF-SIMILAR VELOCITY PROFILES, AND TURBULENCE STATISTICS IN THE NON-AERATED SKIMMING FLOW REGION OF STEEP STEPPED SPILLWAYS

This subchapter concerns to numerical results obtained with *Flow-3D*® simulating the 1V:0.75H slope stepped channel of LNEC and is focused on the hydraulic characteristics of the skimming flow in the non-aerated region, extending previous subchapter analysis to more step heights and discharges. New insights on the self-similarity of k and ε in the boundary layer development region for macro-rough flows are also presented.

ABSTRACT 5.2-1

1. INTRODUCTION 5.2-1

2. DESCRIPTION OF DATA COLLECTION 5.2-3

3. THEORETICAL AND NUMERICAL MODEL DESCRIPTION 5.2-6

4. COMPARISON OF NUMERICAL RESULTS TO DATA 5.2-7
   - 4.1. Verification of the volumetric flow rate (discharge) 5.2-7
   - 4.2. Time-averaged velocity profiles 5.2-8
   - 4.3. Boundary layer thickness 5.2-11
   - 4.4. Flow depth 5.2-12

5. ANALYSIS OF THE VELOCITY PROFILES EXPONENT, BOUNDARY LAYER DEVELOPMENT AND FLOW RESISTANCE 5.2-12
   - 5.1. Exponent of velocity profiles 5.2-12
   - 5.2. Boundary-layer development 5.2-14
   - 5.3. Flow resistance 5.2-16

6. ANALYSIS OF SELF-SIMILARITY OF k AND ε IN THE BOUNDARY LAYER DEVELOPMENT REGION 5.2-19

7. CONCLUSIONS 5.2-21

APPENDIX 1: THEORETICAL MODEL 5.2-22

APPENDIX 2: DETAIL MESH CONVERGENCE 5.2-24

APPENDIX 3: BOUNDARY LAYER DEVELOPMENT 5.2-25

REFERENCES 5.2-26

BOUNDARY-LAYER DEVELOPMENT, SELF-SIMILAR VELOCITY PROFILES, AND TURBULENCE STATISTICS IN THE NON-AERATED SKIMMING FLOW REGION OF STEEP STEPPED SPILLWAYS

ABSTRACT

We focus on the details of the skimming flow in the developing, non-aerated region of steep stepped spillways. We present results of a study combining experimental measurements and numerical simulations. The flow in a large model, featuring a stepped 2.9-m high chute, was tested for two different step heights, 4 and 8 cm. In addition, a commercial code was used to replicate the experimental conditions. Seven different combinations of step height and discharge were measured and simulated. We corroborated that the numerical simulations accurately reproduce this type of flow in terms of discharge, velocity, boundary layer thickness and flow depth, as anticipated in a recent paper by the authors (Bombardelli et al. 2010). However, we verified this for a wider range of discharges and step heights. In addition, the experimental and numerical data allowed us to obtain new coefficients for formulae describing the boundary layer development, velocity profiles and flow resistance. At last, information on the turbulence statistics obtained from the numerical results is presented, observing the existence of self-similarity of k and ε for roughness Reynolds numbers ($k_s^+ = (k_s)_{mean} V_{\max} / \nu$) up to 6.8×10^4.

Keywords: stepped spillway, non-aerated flow, multi-phase flows, experimental data, back-flushing Pitot tube, conductivity probe, numerical simulations, computational fluid dynamics (CFD), turbulence modeling, k-ε model, RNG k-ε model, boundary-layer development, flow resistance, velocity distribution, air entrainment, turbulent kinetic energy, turbulent energy dissipation.

---

1. INTRODUCTION

In the last decades of the 20th century, there has been a renewed interest in the use of stepped spillways in dams due to the improvement of the roller compacted concrete technology (RCC) in dam engineering (Amador et al. 2006; Chanson 2009). The RCC technique consists in disposing "dry" concrete (drier than conventional concrete) in layers of about 0.3 m, spreading the blend with asphalt-paving equipment, and then compacting it with rollers. Figure 1 shows the Pedrógão dam, finished in 2005, which is the first RCC dam built in Portugal.

a) b)

Figure 1 - Pedrógão Dam, Portugal (dam height: 29 m; slope: 51º; steps height: 0.6 m; design unit discharge: 39.9 m^2s^{-1}): a) view of the downstream face of the dam; b) detail of the crest.

The flow past these structures usually presents high concentrations of air downstream of the inception point (the section where air begins to be entrained in the water body), which occurs relatively close to the crest of the spillway. However, for large specific discharges the aerated region in the spillway starts farther downstream of the crest of the structure, giving rise to a large non-aerated region. The flow in the non-aerated region is characterized by the development of the turbulent boundary layer, featuring a self-similar power law for velocities (Barenblatt 1996), and a boundary-layer thickness which increases at a larger rate than the laminar counterpart. Contrary to the relatively large number of experimental papers devoted to the aerated region of spillways (e.g., Chamani and Rajaratnam 1999; Matos 2000; Boes and Hager 2003a,b; Chanson 2004; Ohtsu et al. 2004; Gomes et al. 2006; Gonzalez and Chanson 2007; Meireles et al. 2007; Sánchez-Juny et al. 2008; Relvas and Pinheiro 2008; Felder and Chanson 2009; Amador et al. 2009), the non-aerated region of stepped spillways has been the subject of only a few experimental papers (Amador et al. 2006, 2009; Meireles et al. 2006; Gonzalez and Chanson 2007; and Meireles and Matos 2009). Further, the number of studies addressing this region using numerical techniques is in comparison very small (Chen et al. 2002; Tabbara et al. 2005; Arantes 2007; Carvalho and Amador 2008; and Bombardelli et al. 2010).

Regarding the solution schemes considered in previous numerical works, several approaches have been employed: Chen et al. (2002) and Arantes (2007) solved for the combined flows of water and air (which Bombardelli et al. 2001 defined as Partial Volume-of-Fluid, VoF, method); and Tabbara et al. (2005), using ADINA-F, employed re-meshing each time step. Both approaches involve large computational efforts in terms of simulation time. Carvalho and Amador (2008) used a purported VoF method, but did not validate the results regarding the free-surface location. In Chen et al. (2002), Tabbara et al. (2005) and Arantes (2007), the simulations were developed using unstructured grids with good resolution near the walls but with not so much detail close to the free-surface. In turn, Bombardelli et al. (2010) used the *TruVOF*™ method of *FLOW-3D*®. In our

previous paper, we validated the numerical results via comparisons with our own data, in terms of discharges, water depths, and flow velocities. We also provided numerically- and experimentally-obtained values for the exponents of the self-similar velocity profiles, and for the parameters for the formulas describing the development of the boundary layer.

Flows in stepped spillways have been usually analized in light of the need for design guidelines. However, from a purely fluid-mechanics point of view, the non-aerated region of stepped spillways can be described as a boundary-layer flow in which the presence of large roughness elements (the steps) and, therefore, the step-generated turbulence determine the nature of the boundary-layer development. Therefore, it affords a singular opportunity to assess flow interacting with "macro-roughness" elements. To the best of our knowledge, no paper has analyzed *in detail* the influence of step height and/or discharge on the properties of the boundary-layer development in steep stepped spillways, such as the exponent of the power law representing the velocity profile, the parameters of the growth of the boundary-layer thickness, the friction factor and Manning's n distribution along the spillway, or the self-similarities of turbulence statistics. Consequently, in this paper we endeavor to discuss those issues, basing our analysis on experimental observations and numerical simulations. Section 2 describes the experiments developed and Section 3 summarizes the employed theoretical and numerical models. Section 4 presents comparisons of experimental and numerical results, in terms of volumetric flow rate, time-averaged velocity profiles, boundary layer thickness and flow depth. Section 5 presents an analysis of the velocity profiles exponent, boundary layer development and flow resistance from experimental and numerical and Section 6 proposes self-similar laws for the turbulent kinetic energy and its dissipation based in the numerical data, followed by the conclusions.

2. DESCRIPTION OF DATA COLLECTION

Experimental data was collected at the National Laboratory of Civil Engineering (LNEC), in Lisbon, Portugal, by Matos (1999) and Meireles (2004). Both sets of experiments were carried out in a 1-m wide, 0.50-m deep and 3.35-m long (in the zone of constant slope) stepped channel, with slope of 1V:0.75H (≈ 53 degrees from horizontal). However, the steps heights were 4 and 8 cm, respectively. The upstream end of the ogee crest is smooth, followed by variable size steps (two 0.5-cm, two 1-cm, five 2-cm and one 4-cm high steps) to adopt a profile identical to that proposed by the Waterways Experiment Station (WES), U. S. Army Corps of Engineers (Fig. 2). The design head is H_0 = 0.2 m and corresponds to a unit discharge, q_0, of 0.2 m^2/s for a discharge coefficient, C_0, equal to 0.5. (The stage discharge curve in a WES ogee crests is given by $Q_0 = C_0 b\sqrt{2g}H_0^{3/2}$, where b is the channel width and g is the acceleration of gravity. This last value was obtained according to the results presented by Abecasis (1977) (in Quintela 1998) for WES ogee crests.)

Water is supplied to a reservoir with a length of 4 m, which discharges to the stepped channel. The supply is performed by a 350-mm internal diameter pipe and adjusted by a gate valve. At the downstream end of the stepped channel a stilling basin is located, followed by a channel 10 m long. At the end of this channel, a Bazin weir allows to measure the volume flow rate (discharge).

Experimental tests were carried out for unit discharges (q_w) ranging from 0.08 to 0.20 m^2/s, corresponding to the skimming flow regime (e.g., Chanson 2002). Table 1 presents a summary of the seven different tested conditions along with the three conditions tested and reported in Bombardelli et al. (2010); this last study was mainly focused on the discharge of 0.18 m^2/s, though.

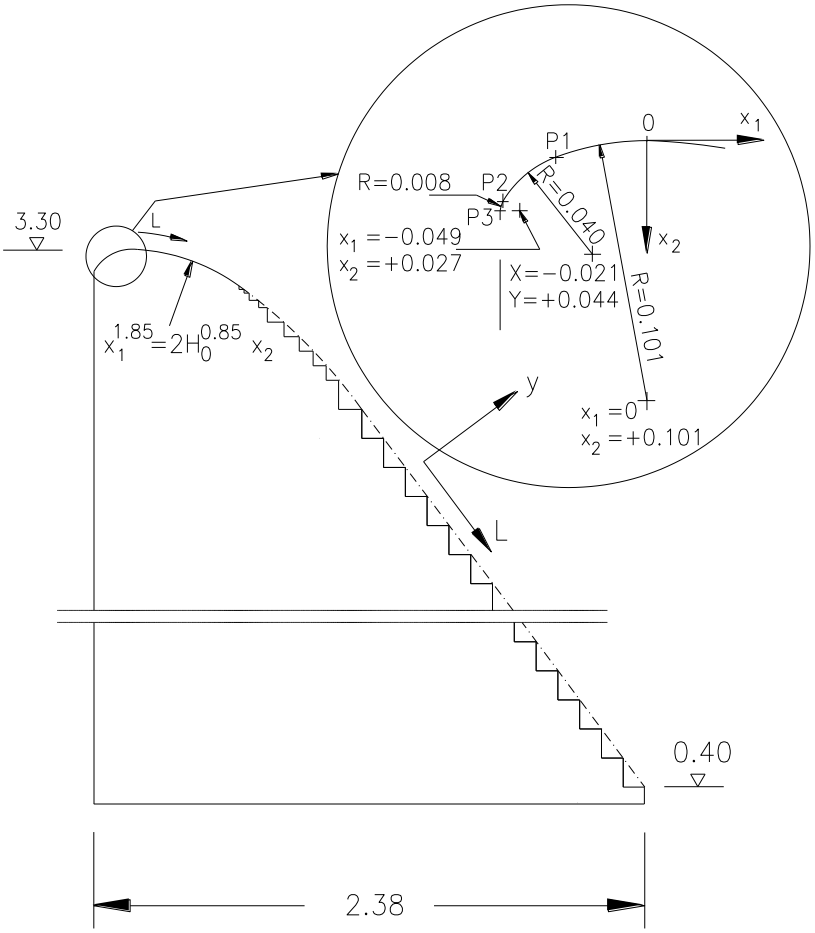

Figure 2 - Dimensional schematic of the stepped channel with detail of crest (dimensions in meters).

Data acquisition was performed with the help of point gauges, devices for measuring air concentrations and water velocities, and a Bazin weir. At the upstream end of the channel, where the water profile is smooth, we acquired water depths with the use of point gauges. Downstream of the crest of the weir, air concentrations, equivalent clear-water depths and time averaged water velocities were measured. The device for measuring air concentrations is composed by a conductivity probe. Air data are captured when one of the two 0.2-mm diameter platinum wires detects a bubble or is uncovered. The device for measuring water velocities is composed by a standard Pitot tube, attached to a differential pressure transducer, and supplied by a reservoir with constant head. This reservoir feeds continuously both the static-pressure and the total head ports of the Pitot tube to avoid the entrance of air. The flow rate to each port is controlled by needle valves and the total and static-pressure heads are measured through the 1-mm and 0.5-mm diameter holes of the Pitot tube. Both devices were developed and calibrated by the U.S. Bureau of Reclamation

(Matos and Frizell 1997; 2000). Although this study focused on the non-aerated flow, air concentrations were detected. These concentrations corresponded to: a) intermittent entrapped air captured by the probe between water waves (partially uncovered condition of the probe); b) entrained air bubbles upstream of the time-averaged point of inception location due to the unsteadiness of the instantaneous inception point; or c) air entrained and entrapped due to a combination of both (see Wilhelms and Gulliver 2005 for definition of entrapped and entrained air, and Matos and Frizell 2000 for air concentration detection details). The equivalent clear-water depth was calculated from:

$$\mathrm{d} = \int_0^{\mathrm{Y}_\varphi} (1 - \mathrm{C})\,\mathrm{dy} \qquad (1)$$

where Y_φ is the depth where the air concentration is φ%, assumed equal to 90% in the present study, C is the local air concentration, and y is the transverse coordinate originating at the pseudo-bottom, defined as the surface tangent to consecutive step edges. In the non-aerated region, equivalent clear-water depth represents a fictitious flow depth which would occur in absence of free-surface waviness. In turn, the time-averaged velocity (u) was obtained via

$$u = \sqrt{\frac{2\,\Delta P}{\rho_w\,(1 - C)}} \qquad (2)$$

where ΔP is the difference between the total and the static pressure heads (measured with the back-flushing Pitot tube); and ρ_w is the density of water,. Further details can be found in Matos and Frizell (1997, 2000).

Table 1 – Summary of the performed experimental and numerical simulations.

References	q_w (m^2/s)	h (m)
Bombardelli et al. (2010)	0.08	4
	0.14	4
	0.18	4
Present study	0.08	4
	0.14	4
	0.18	4
	0.08	8
	0.14	8
	0.18	8
	0.20	8

The Pitot tube and the conductivity probe were fixed to a movable trolley in association with Vernier scales. The accuracy in measuring vertical distances was of ±0.1 mm. The error in the position of the instruments was estimated to be less than 5 mm in the longitudinal direction, and less than 1 mm in the transverse direction.

Experimental measurements and numerical simulations of this study were conducted assuming a quasi-two-dimensional (*2-D*) flow, as performed by other authors for smooth and stepped spillways (Savage and Johnson 2001; Johnson and Savage 2006 and Bombardelli et al. 2010), although visual observation of the flow revealed a distinctly *3-D* flow structure inside the step cavities (e.g., Matos 2000; Chanson 2002; Gonzalez and Chanson 2007).

3. THEORETICAL AND NUMERICAL MODEL DESCRIPTION

We applied the theory described in Bombardelli et al. (2010), where the theoretical models are based upon the mixture equations for an air-water flow (Buscaglia et al. 2002; Bombardelli 2003, 2004; Bombardelli et al. 2007; and Bombardelli and Jha 2009). The equations, presented in Appendix 1, are obtained through two consecutive averaging procedures (Crowe et al. 1998; Prosperetti and Tryggvason 2007): a) an ensemble averaging, to address scales of the order of the distance between bubbles, and b) a turbulence averaging, to represent turbulence scales larger than the bubble-to-bubble distance (Bombardelli 2004). (The reader can see Hrenya and Sinclair (1997), Buscaglia et al. (2002), Bombardelli (2004) and Bombardelli and Jha (2009) for further details.) The models have single-phase flow models as a special case. With the purpose of accounting for turbulence, the eddy-viscosity concept (Rodi 1984) was considered and the standard k-ε turbulence model (Harlow and Nakayama 1967; Launder and Spalding 1972; see Appendix 1) was used. In flows with low turbulence intensity and with important shear layers, like the one under study in this paper, the *RNG* k-ε model is usually considered to be more accurate (Flow Science 2008). However, results of water depth, velocity and discharge did not benefit from considering the *RNG* k-ε model instead of the k-ε model in previous simulations (Bombardelli et al. 2010). Thus, we kept using the k-ε model in these simulations.

The mixture equations described above are valid within a domain Ω composed by the flow in the tank, the stepped spillway and the stilling basin, limited by the incoming flow in the tank, the outgoing flow downstream of the stilling basin, and the solid boundary (Fig. 3). Contrarily to other boundary conditions, free-surface location varies with time and, thus, has to be obtained each time step. The free-surface was captured using the *TruVOF*^{TM} method (Hirt and Nichols 1981; see Bombardelli et al. 2001; Bombardelli et al. 2010; and Appendix 1 for a description of the method). As opposed to other methods, cells totally filled with gas are disregarded in the simulations, because gas is assumed to have negligible inertia and to be only able of applying a normal pressure on a liquid surface.

Upstream and downstream boundaries were specified as pressure boundary conditions. In the solid boundaries were imposed null velocities normal to the walls and the usual "wall functions" for the turbulence statistics (Ferziger and Peric 2002; Bombardelli et al. 2010; see Appendix 1) were taken into account. All the other boundaries were assumed to be symmetry planes, by default.

We performed numerical simulations with *FLOW-3D*®, where the mixture equations are solved using a finite volumes/finite differences method in a structured Cartesian grid (Flow Science 2008). In this commercial CFD code, grid and geometry are defined separately. In the present study, a *CAD* file with the geometry of the physical model was imported into the code as a stereolithography (STL) file. After both the geometry and the grid are defined, the geometry is embedded in the grid by the *FAVOR*™ technique (Hirt and Sicilian 1985), which computes the fractional areas and volumes obstructed to flow (see Flow Science 2008 for details). The domain was tested with two distances upstream of the face of the spillway to allow for a "buffer" zone for the boundary condition imposed at the upstream boundary. More information and a comparison between different "buffer" zone sizes can be found in Bombardelli et al. (2010). In these simulations we used multiple blocks, in a total of ten, to optimize the grid in accordance to the given geometry, as shown in Fig. 3. The upstream tank and the stilling basin were included in the computational domain to impose physical boundaries where we had information on pressures. Several simulations were performed to ensure grid convergence (see Appendix 2) finishing with a domain of uniform cells of 3 mm in the x direction and 4 mm in the vertical direction, corresponding to a total of 2 million volumes.

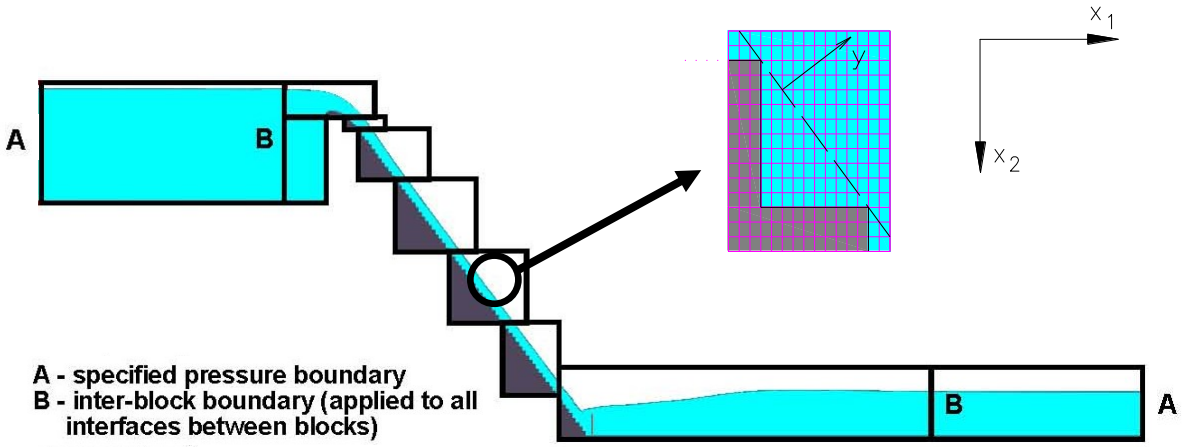

Figure 3 - Model geometry and multi-block grid: geometry composed by the upstream reservoir, stepped channel and stilling basin; grid composed by 10 blocks.

4. COMPARISON OF NUMERICAL RESULTS TO DATA

4.1. VERIFICATION OF THE VOLUMETRIC FLOW RATE (DISCHARGE)

Because discharge was not imposed in the numerical simulations, we calculated this parameter for each tested case by integrating numerically the results of the velocity profile. We used the trapezoidal rule (Burden and Faires 2004). Excellent results were obtained, with relative differences among experimental and numerical values smaller than 6% (average difference of 2.9%). (Keep in mind that these differences are within the range of expected experimental error.)

Some recent studies on smooth, conventional ogee spillways successfully validated numerical results calculating the coefficient of discharge or the discharge (e.g., Olsen and Kjellesvig 1998 and Savage and Johnson 2001). Fig. 4 presents a successful comparison between normalized discharges obtained experimentally and numerically for a *stepped* spillway (present study) and for a conventional spillway (Savage and Johnson 2001). Results obtained from the U.S. Bureau of Reclamation and U.S. Army Corps of Engineers design monographs are also included. Excellent agreement is observed.

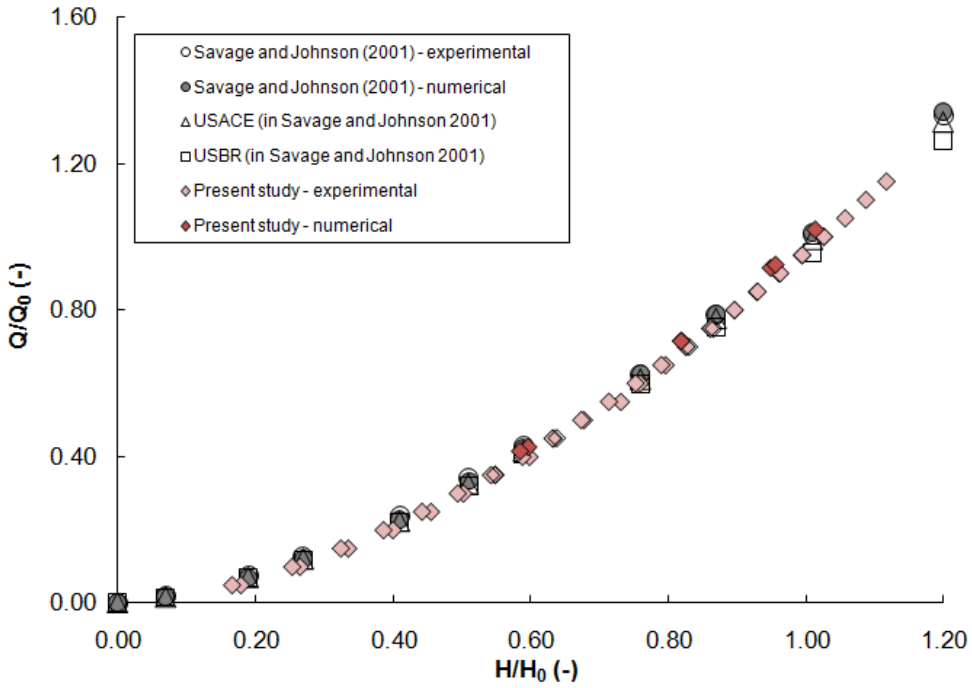

Figure 4 - Normalized stage-discharge curve: comparison among simulated and measured results from the present study, simulated an measured results from Savage and Johnson (2001), and results from USACE and USBR.

4.2. TIME-AVERAGED VELOCITY PROFILES

Flow in the non-aerated region of stepped spillways is characterized by a strong unsteadiness of the boundary layer and of the water depth; this results in a very intricate flow, even if only the "averaged" flow is to be studied (Bombardelli et al. 2010; Meireles et al. 2011). For this reason, and similarly to Bombardelli et al. (2010), we indicated with unfilled symbols those points where the conductivity probe detected the presence of air in Figs 5 to 9; in turn, filled symbols refer to points where only water flow was detected. Even though Eq. (1) takes into account the presence of air in the flow, the free-surface waves have high frequency, not compatible with the time response of the Pitot tube (Matos et al. 2002). In this sense, unfilled symbols data close to the free-surface should be taken with caution.

Figures 5 a) to e) compare computed velocities with measurements, for a wide range of discharges, step heights, and distances from the crest.

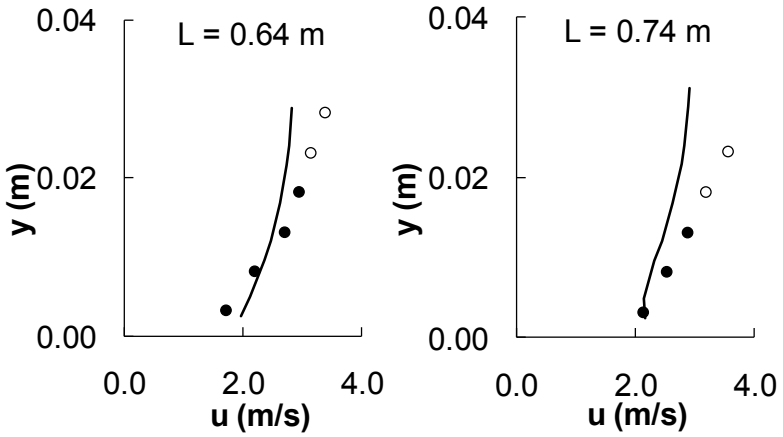
L = 0.64 m
L = 0.74 m
y (m)
u (m/s)
0.00
0.02
0.04
0.0
2.0
4.0

a)

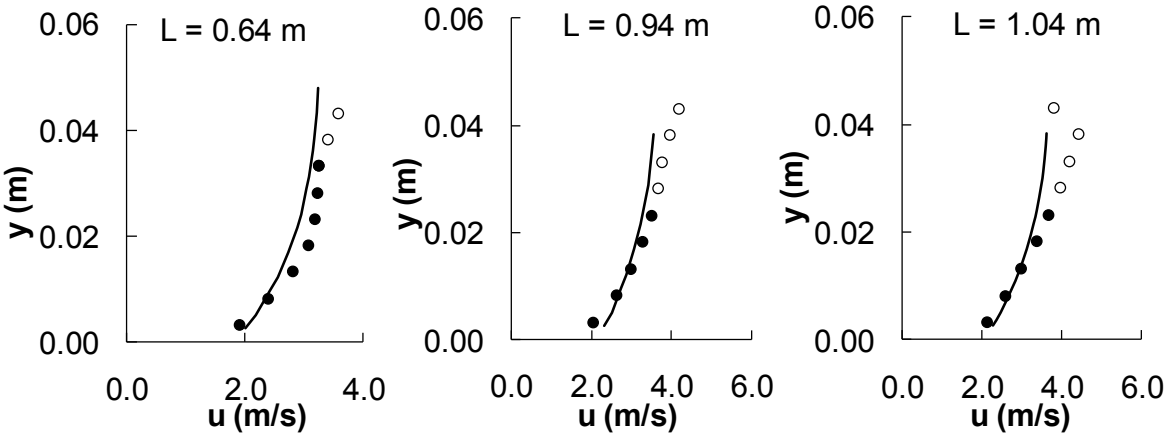
L = 0.64 m
L = 0.94 m
L = 1.04 m
y (m)
u (m/s)
0.00
0.02
0.04
0.06
0.0
2.0
4.0
6.0

b)

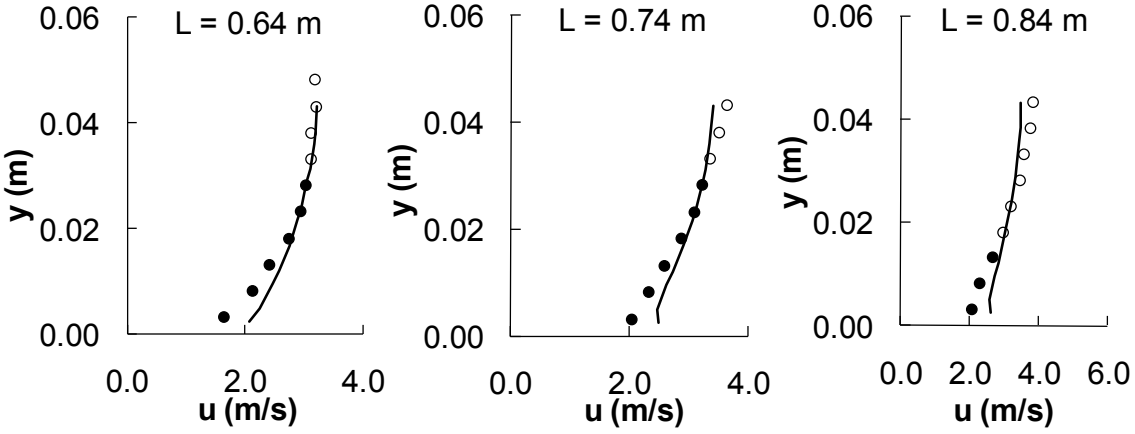
L = 0.64 m
L = 0.74 m
L = 0.84 m
y (m)
u (m/s)
0.00
0.02
0.04
0.06
0.0
2.0
4.0
6.0

c)

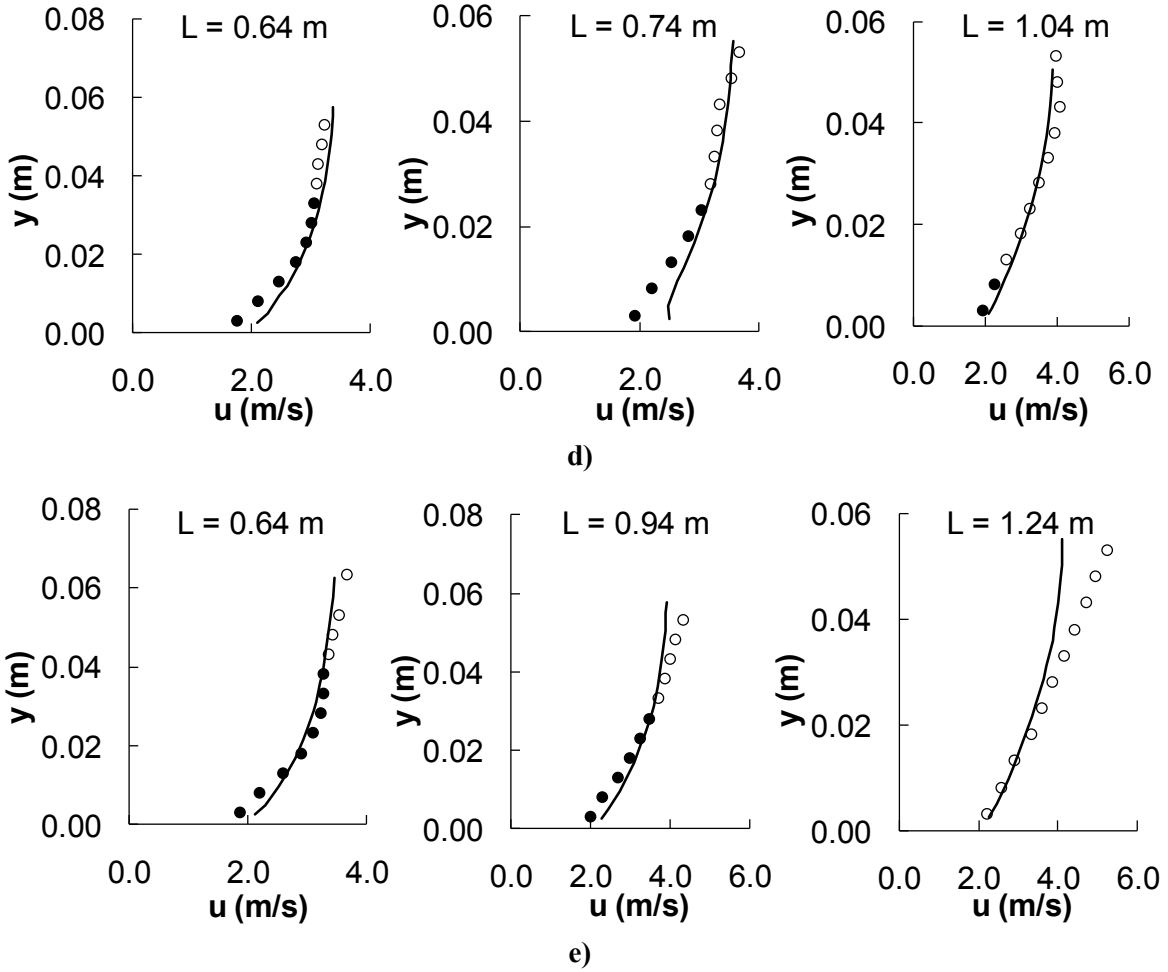

Figure 5 - Comparison among simulated and measured results of the velocity distribution upstream of the point of inception for: a) h = 4 cm and q_w = 0.08 m^2/s; b) h = 4 cm and q_w = 0.14 m^2/s; c) h = 8 cm and q_w = 0.14 m^2/s; d) h = 8 cm and q_w = 0.18 m^2/s; e) h = 8 cm and q_w = 0.20 m^2/s. Unfilled symbols refer to points with measurements affected by the unsteady motion of the free-surface and inception point; filled symbols refer to points where air concentration is equal to zero. The profiles correspond to the corners of the steps.

In accord with Bombardelli et al. (2010), the velocity values obtained with *FLOW-3D*® (solid lines) are in good agreement with the experimental ones throughout the spillway, irrespective of discharge or step height. Relative differences are mainly smaller than 10% (8% in average) for the filled symbols.

The velocity field is in close qualitative agreement with data presented by Amador et al. (2006), obtained using the PIV technique. In the step cavities, the flow recirculation is well defined (not shown herein) and the main flow skims over the step edges. Inside the cavities, in opposition to the main flow, larger values of the turbulent kinetic energy and dissipation of turbulent kinetic are observed, and those values are asymmetric within the cavities (see Bombardelli et al. 2010). This asymmetry was already reported by Chanson (2002) and can be observed in the experimental velocity and turbulent kinetic energy fields obtained by Amador et al. (2006).

4.3. BOUNDARY LAYER THICKNESS

In analogy with smooth chute flows, in stepped chute flows the boundary layer thickness, δ, is customarily defined as the perpendicular distance from the pseudo-bottom to the point where the velocity is 99% of the free-stream velocity, u_{max}.

Fig. 6 presents examples of good agreement between the normalized boundary layer thickness (δ/L) obtained, by definition from the experiments (open symbols), and from the simulations with *FLOW-3D*® (filled symbols), for several values of the normalized distance along the spillway (L/k_s). k_s is the roughness height perpendicular to the pseudo-bottom, $k_s = h\cos\theta$, with h denoting the step height; θ is the angle of the spillway; and L is measured from the crest of the spillway. (With exception to the turbulence analysis in the last section of the paper, k_s is assumed constant and calculated using the step height at the zone of the chute of constant slope, as usually considered.) The same level of agreement was observed for the other simulations. The method for determining numerical boundary layer thickness values is described in Appendix 3.

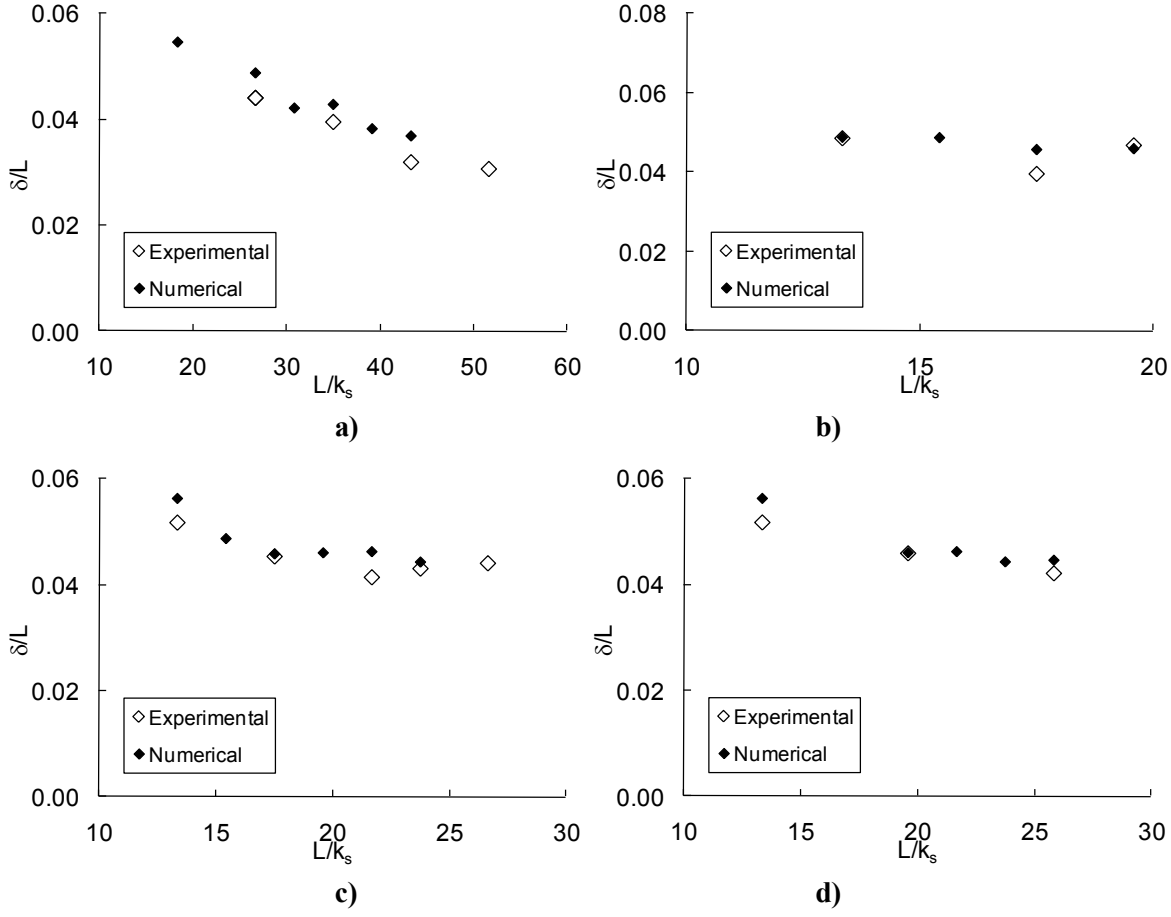

Figure 6 - Development of the boundary layer: comparison among simulated and measured results for a) h = 4 cm and q_w = 0.14 m²/s; b) h = 8 cm and q_w = 0.14 m²/s; c) h = 8 cm and q_w = 0.18 m²/s; d) h = 8 cm and q_w = 0.20 m²/s.

4.4. FLOW DEPTH

Modeled and measured water depths, d, showed an excellent agreement. The regression proposed by Meireles et al. (2011) based on experimental data obtained in several facilities, describes adequately both experimental and numerical results, with exception to the zone closer to the crest, where the channel is curved and the steps have variable size. Fig. 7 presents a comparison of all experimental and numerical data. To that end, we normalized water depths and the distances from the crest of the spillway, with d_i and L_i, respectively, both obtained from the equations proposed by Meireles et al. (2011). d_i stands for equivalent clear-water depth at the inception point whereas L_i stands for its location. Relative differences between experimental and numerical results are mainly smaller than 8% (4% in average). We estimated the error in the numerical values of the free-surface location to be smaller than 1 mm, from observation of the dimensions of the grid cells, flow orientation in relation to the cells, and from values of the function F used by *FLOW-3D*® to detect this location (Bombardelli et al. 2010).

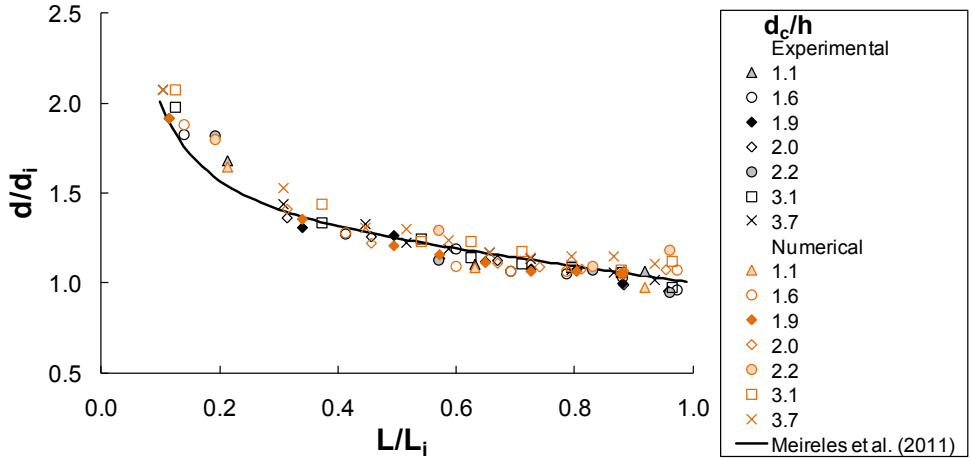

Figure 7 - Normalized water flow depths: comparison among simulated and measured results. Presentation of a regression obtained by Meireles et al. (2011) for experimental data of several authors. d_c indicates the critical depth computed by definition.

In accord with the observations of Chanson (2002), Bombardelli et al. (2010) and Meireles et al. (2011), both experimental and numerical data captured the wavy pattern of the time-averaged flow depth close to the inception point (not shown herein).

5. ANALYSIS OF THE VELOCITY PROFILES EXPONENT, BOUNDARY LAYER DEVELOPMENT AND FLOW RESISTANCE

5.1. EXPONENT OF VELOCITY PROFILES

Assuming self-similarity (Barenblatt 1996; Gioia and Bombardelli 2002; Carosi and Chanson 2007), it is customary to approximate the velocity distribution in steep chutes by a power law expressed by (Cain and Wood 1981; Wood 1991; Chanson 2002):

$$\frac{u}{u_{max}} = \left(\frac{y}{\delta}\right)^{1/N} \qquad 0 \le y/\delta \le 1 \qquad (10)$$

where u_{max} is the free-stream velocity; y is the transverse coordinate originating at the pseudo-bottom and $1/N$ is an exponent to be determined from experiments and the numerical simulations. In Bombardelli et al. (2010), we found N to be equal to 3.4 and 5.4 from the experimental and numerical velocity profiles, respectively. To obtain these values, we followed the results pertaining to $q_w = 0.18$ m^2/s and $h = 4$ cm. In this paper, we obtained an overall value of the coefficient N equal to 4.7 from the numerically obtained velocity profiles (Fig. 8) which is of the order of magnitude of the value 3.4 obtained experimentally (see Meireles et al. 2011). The experimental result is consistent with the range of values reported for the non-aerated and aerated regions in steep stepped chutes (Table 2) and although the corresponding numerical value is higher than values reported in any of the experimental studies, it is still smaller than N values reported in the literature for both the non-aerated and the aerated regions of similar smooth spillways (N = 6.3: Cain and Wood 1981; N = 6: Chanson 1993).

Table 2 – Results of *N* for different studies on steep stepped channels.

References	*h* (cm)	*slope* (V/H)	$N_{non\text{-}aerated}$ (-)	$N_{aerated}$ (-)
Matos (1999)	8	1/0.75	3.3	3.9
Meireles (2004)	4	1/0.75	3.5	4.4
Renna (2004)	2 & 4	1/0.75	3.4	3.8
Amador et al. (2009)	5	1/0.8	3.0	-
Meireles et al. (2011)	2, 4 & 8	1/0.75	3.4	-
This study (numerical)	4 & 8	1/0.75	4.7	-

It is interesting to compare this velocity distribution in stepped spillways with profiles used in open-channel flows with macro-roughness. For instance, Smart et al. (2002) focused on flow resistance of relatively rough flows (i.e., flows for which the bed roughness is large relative to flow depth). These authors discussed a power velocity law, $u/u_* = C(R_v/Z_0)^{1/N}$, where u_* is the shear velocity; and generically R_v is the volume of water per unit area of bed and Z_0 is an hydraulic roughness parameter. The power law exponent was observed to increase from 1/6 (as presented by Manning's equation) to 1/2, for flows with high bed roughness. Smart et al. (2002) suggested $N = 2$ and $C \approx 1$ for $2.5 < R_v/Z_0 < 45$, based on experimental evidence. Following Smart et al. (2002), R_v can be considered in the present study equal to the averaged flow depth (measuring from the inner step edge; i.e., $R_v = d + h\cos\theta$) and Z_0 can be the step size dimension in the direction perpendicular to the flow (i.e., $Z_0 = h\cos\theta$). Our flow conditions correspond to $1.7 < R_v/Z_0 < 3.7$, which can be clearly interpreted as flows with high relative roughness. Overall, flows in conventional open channels and stepped spillways show a decrease in N with increasing relative roughness. Chen (1991) summarized several studies focused on alluvial and gravel bed

flows where $N = 4$. Physically, lower N corresponds to higher flow resistance, which was already discussed by Chen (1991) for uniform pipe and channel flows ($N = \kappa\sqrt{8/f_u}$, where κ is the von Kármán coefficient, equal to 0.4, and f_u is the friction factor for uniform flow).

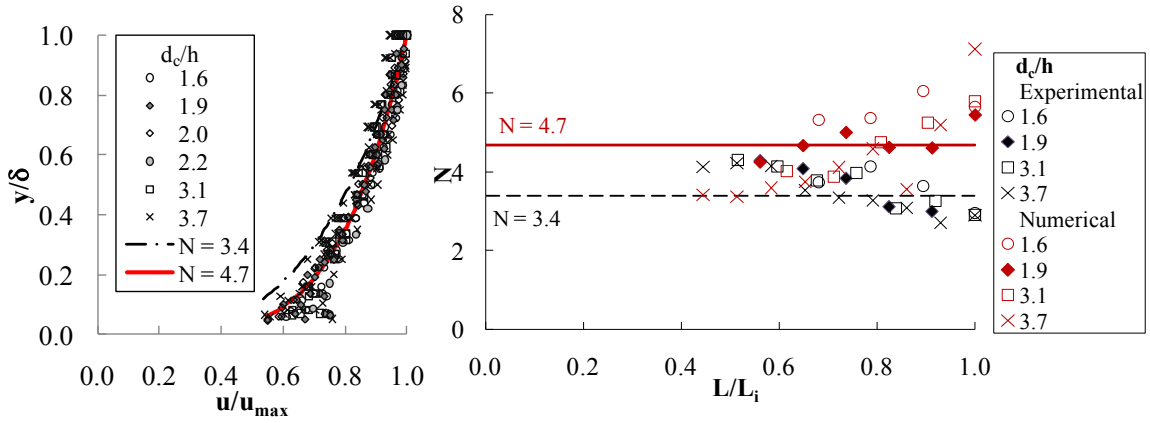

a) b)

Figure 8 - Analysis of velocity profiles for 0.04 < *h* (m) < 0.08 and 0.08 < q_w (m^2/s) < 0.20: a) comparison among the regressions for simulated (*N* = 4.7) and measured (*N* = 3.4) results, and numerical data; b) comparison among simulated and measured results of *N*, and the respective averages.

In Fig. 8a), a portion of the numerical data does not follow the power law near the pseudo-bottom (y/δ < 0.2), where a slightly smaller velocity gradient is observed. We already observed this pattern in numerical simulations (Bombardelli et al. 2010), but not in our experiments (Meireles et al. 2011). In Fig. 8b) we present the variation of N with the distance from the crest of the spillway. We observed a larger range of variability of N for the numerical data ($3.4 \leq N \leq 7.1$) than for the experimental counterpart ($2.7 \leq N \leq 4.3$). One of the sources of these differences might be due to the definition of $u_{\max}$, as discussed in Appendix 3. Another source of differences could be as follows. According to Nikora and Smart (1997) in flows with small relative submergence (relation between the characteristic dimensions of flow and bed roughness) the velocity field is mainly three-dimensional. Differences among diverse values of N could then be due to the impossibility to capture *3-D* turbulence features in a *2-D* simulation, in addition to a small numerical diffusion (Bombardelli et al. 2010).

5.2. BOUNDARY-LAYER DEVELOPMENT

Fig. 9 presents data on boundary-layer thickness obtained experimentally and numerically for all the studied cases, showing an excellent agreement. We extend herein previous results reported in Bombardelli et al. (2010). Similarly to smooth spillways (e.g., Cain and Wood 1981), it is observed that all the results tend to collapse in an equation of the type

$$\frac{\delta}{L} = a\left(\frac{L}{k_s}\right)^{-b} \qquad (11)$$

where a and b are real numbers. For the experimental data, the best fit is obtained with a=0.114 and b=0.311 (for $10 < L/k_s < 140$), as presented by Meireles et al. (2011); for the numerical simulations that fit is obtained with a=0.132 and b=0.343 (for $10 < L/k_s < 60$). The expressions proposed by Tozzi (1992), Chanson (2002) and Amador et al. (2009) for δ/L are also presented in Fig. 9. As observed by Bauer (1954) for a smooth spillway, the discharge has no significant effect on the thickness of the boundary layer. Bauer (1954) also observed a small effect of the slope on the boundary layer thickness. Results of Meireles and Matos (2009), obtained for a stepped chute of slope 1V:2H, present close agreement with those presented herein, although they pertain to a small range of flows with very small Froude numbers. Tozzi (1992) proposed a = 0.08 and b = 0.233, as recommended by the U.S. Army Corps of Engineers for smooth chutes (ACE 1990), since his experimental data, obtained in a stepped chute of slope 1V:0.75H, was in close agreement with these coefficients. The agreement between data of the present study and Amador's expression is good. The regression for experimental data is almost coincident to Amador's expression, but values of the normalized boundary layer thickness obtained from numerical simulations are slightly higher. In turn, Tozzi's and Chanson's equations give rather smaller values, specially for small L/k_s ($L/k_s < 40$). The discrete nature of the experimental and numerical profiles complicates the estimation of the boundary layer thickness, specially for the smaller discharges, contributing to the observed scatter. (Experimental data was obtained every 5 mm in the respective verticals, and numerical data is available in intervals up to 5 mm, due to grid constrains.)

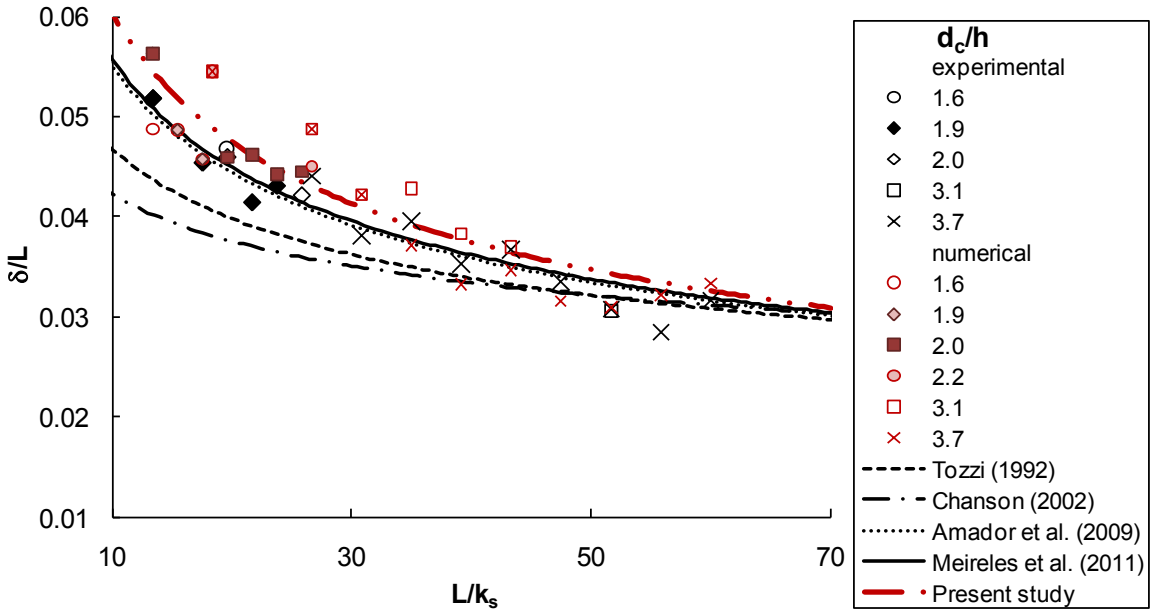

Figure 9 - Development of the boundary layer: comparison among simulated and measured results for 0.04 < *h* (m) < 0.08 and 0.08 < q_w (m^2/s) < 0.20 and formulations of Tozzi (1992), Chanson (2002), Amador et al. (2009) an Meireles et al. (2011). We introduce our own formulation obtained from the simulated results.

5.3. FLOW RESISTANCE

Flow resistance on skimming flows in stepped spillways is primarily due to form losses (Chanson 2002). In agreement with other studies focused on these flows, the Darcy-Weisbach formula is presently used to characterize the flow resistance. Values of Manning's *n* are also calculated and Manning's formula is suggested to be used, alternatively.

We derived the von Kármán momentum equation within the boundary layer in stepped channels from the continuity and momentum equations, following closely the derivation presented by Rouse (1959). We consider the component of the mean velocity normal to the channel, at the pseudo-bottom, $\bar{v}_0$, negligible and the streamwise component, $\bar{u}_0$, different from zero, from observation of the experimental velocity field acquired by Amador (2005). Although experimental evidence shows that the difference $\left(\overline{u'^2} - \overline{v'^2}\right)$ within the boundary layer is distinct from zero, we assumed that difference to be approximately constant in the streamwise direction, as considered by different authors (e.g., Pope 2000). The von Kármán momentum equation for stepped channels is then:

$$c_f = 2\frac{d\delta_2}{dL} + \frac{4\delta_2 + 2\delta_1}{u_{max}}\frac{du_{max}}{dL} \tag{12}$$

where c_f is the skin-friction coefficient, defined as $c_f = \tau_w / \left(1/2\,\rho U^2\right)$ (Rouse 1946; Pope 2000; Kundu and Cohen 2004); τ_w is the shear stress; and δ_1 and δ_2 are the displacement and momentum thicknesses (defined in Appendix 3), respectively. Adopting the power law for the velocity profile presented as Equation (10), δ_1 and δ_2 can be obtained as follows:

$$\delta_1 = \frac{\delta}{1+N} \tag{13}$$

$$\delta_2 = \delta\left[\left(1+\frac{1}{N}\right)^{-1} - \left(1+\frac{2}{N}\right)^{-1}\right] \tag{14}$$

$d\,u_{max}/dL$ was determined via a linear variation of u_{max}, as expressed by the experimental and numerical data. We assume δ_2 to increase linearly with L in analogy with the experimental results of Djenidi et al. (1999) in the turbulent boundary layer over transverse square cavities.

From the von Kármán momentum equation, it is then possible to calculate the skin-friction coefficient, c_f. The results are presented in Fig. 10, where we also plotted the results of the friction factor, *f*, computed as four times the skin friction coefficient (Pope 2000). Experimental and numerical data are close, although numerical data is about 10% smaller than the experimental counterpart. For the computations, *N* was considered to be equal to 3.4 and 4.7 for the experimental and numerical data, respectively. Considering N = 3.4, the expression proposed by Chen (1991) for uniform flow ($N = \kappa\sqrt{8/f_u}$) gives f = 0.111, which is in the range of the experimental and numerical results of the present study, in the developing flow region.

In this paper, we also explore for the first time the use of Manning's coefficient to characterize the resistance to the flow in stepped spillways. Manning's empirical formula, derived theoretically from the phenomenological theory of turbulence by Gioia and Bombardelli (2002), is expressed by

$$U = \frac{1}{n} R_h^{2/3} S^{1/2} \tag{15}$$

where U is the mean velocity of the flow; n is the resistance coefficient; R_h is the hydraulic radius; and S is the slope of the channel. All parameters are in the International System (SI). Manning's n can be related to the friction factor as follows (Bombardelli and Garcia 2003):

$$f = \frac{8 g n^2}{R_h^{1/3}} \tag{16}$$

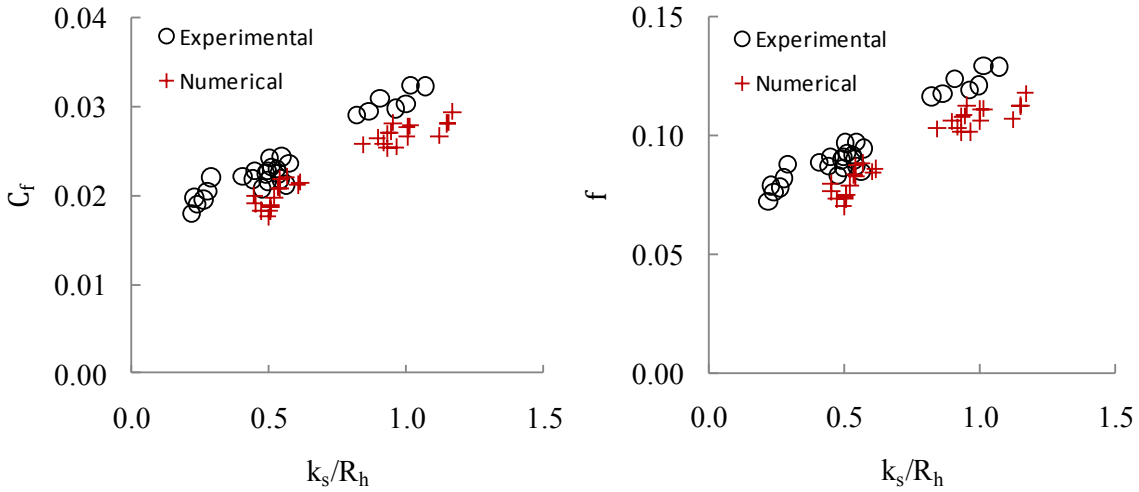

Figure 10 - Skin-friction coefficient and friction factor: comparison among simulated and measured results for 0.04 < *h* (m) < 0.08 and 0.08 < q_w (m^2/s) < 0.20.

A Strickler-type relation has been provided by different authors to relate n and k_s (Strickler 1923; Ackers 1961; Chow 1959; Yen 1992):

$$n = const. k_s^{1/6} \tag{17}$$

This relation is valid, in principle, for small roughness elements. In general, it would be possible to state:

$$n = C_n k_s^{p} \tag{18}$$

where C_n and p are constants. Using (16) and (18) yields

$$f = \frac{8 g C_n^{2}}{R_h^{1/3}} k_s^{2p} \tag{19}$$

or $f = 8\,g\,C_n^{\,2}\left(\frac{k_s^{\,p}}{R_h^{\,1/6}}\right)^2 = a\left(\frac{k_s^{\,p}}{R_h^{\,1/6}}\right)^2$, where $a = 8\,g\,C_n^{\,2}$. From experimental and numerical data, we obtained $a = 0.163$ and $p = 0.234$, and $a = 0.135$ and $p = 0.185$ respectively. Fig. 11 shows both the data and the regressions, which offer a new relationship between Manning's n and k_s. Surprisingly, the results can be expressed in the form $f \sim \frac{k_s^{\,1/2.7}}{R_h^{\,1/3}}$ and $f \sim \frac{k_s^{\,1/2.1}}{R_h^{\,1/3}}$ respectively for experimental and numerical data, being in close agreement with the scaling $f \sim (k_s/R_h)^{1/3}$ obtained from the empirical Strickler-type relation (17). Although Bombardelli and Garcia (2003) observed that Strickler-type formulas give large errors for $n > 0.02$, this analysis reveals that even if this limit was exceeded for the tested experimental and numerical data, the corresponding error is not large.

Amador et al. (2006) calculated the skin-friction coefficient for several step cavities and obtained a global constant mean value of 0.031 for all the data, corresponding to $f = 0.124$, and pertaining to a range of k_s/R_h from 0.85 to 0.93, in opposition to the broader range of data presented herein ($0.22 < k_s/R_h < 1.17$). Even though the experimental data of Amador et al. (2006) do not allow to observe the crescent tendency of the skin-friction coefficient with k_s/R_h, they are close to the values obtained experimentally in the present study for the same range of k_s/R_h. At last, Chanson (2002) presents friction factor results obtained by a large number of authors for the aerated region, but they show an extremely high scatter.

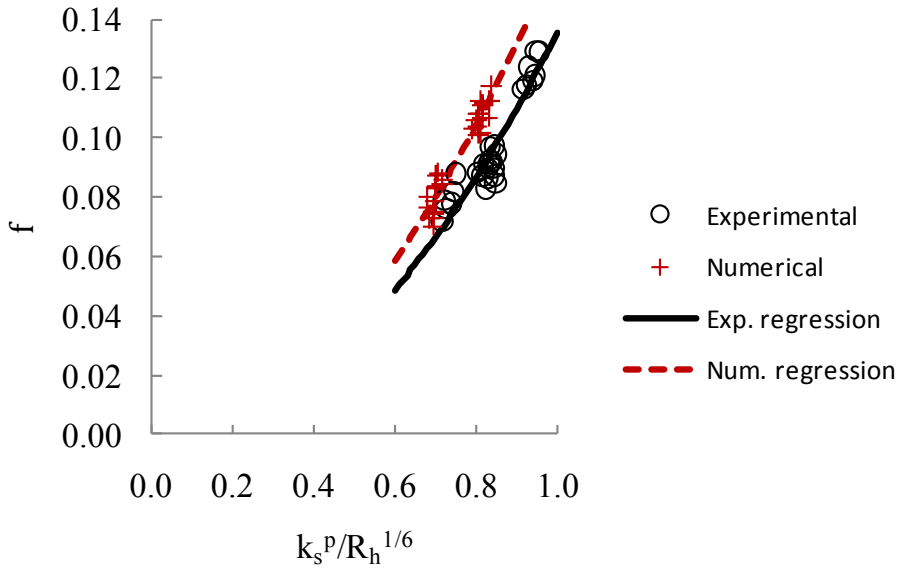

Figure 11 - Friction factor in the developing flow of steep stepped spillways: comparison among simulated and measured results as a function of $k_s^P/R_h^{1/6}$.

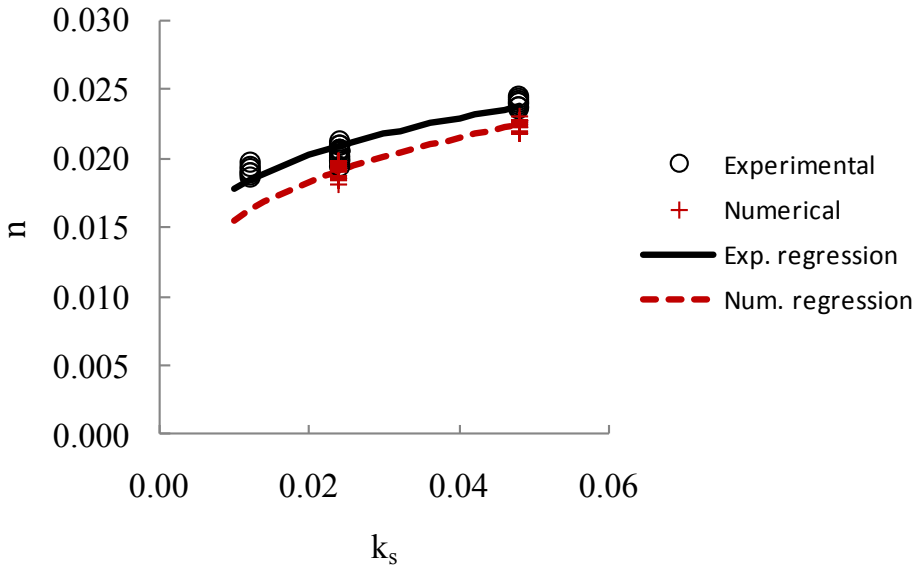

Figure 12 - Manning's *n* in the developing flow of steep stepped spillways: comparison among results obtained from the experiments and simulations.

6. ANALYSIS OF SELF-SIMILARITY OF k AND ε IN THE BOUNDARY LAYER DEVELOPMENT REGION

Nezu and Nakagawa (1993) summarized evidence on the existence of self-similarity of the normalized turbulent kinetic energy, k/u_*^2, and its dissipation rate, $\varepsilon\, d/u_*^3$, for fully developed open-channel flows, irrespective of Reynolds numbers, Froude numbers, and wall roughness, where k is the turbulent kinetic energy (TKE); ε is the dissipation of turbulent kinetic energy; and u_* is the friction velocity. Data used to prove this self-similarity varied in the range $0.46 < F < 3.12$ and $0 < k_s^+ < 136$, where F is the Froude number and k_s^+ is the roughness Reynolds number, defined as $k_s^+ = ku_*/\nu$; ν is the viscosity; and k is the wall roughness. Nezu and Nakagawa (1993) reported in those plots data of boundary layer and pipe flows showing agreement with the self-similar equations. Nikora and Smart (1997), in turn, observed self-similarity of the vertical distribution of the dissipation rate of turbulent kinetic energy for gravel-bed river flows. Similarly to previous results valid for mountain rivers (Aberle and Smart 2003), in the present study water depths are of the same order of magnitude as the bottom roughness. However, we are not aware of any study focused on this kind of analysis in developing boundary layers and steep slopes.

The vertical distribution of k and ε are explored. In river flows k and ε are normalized considering u_* and d as characteristic velocity and length scales (e.g., Nezu and Nakagawa 1993, Nikora and Smart 1997). In this case, we selected the velocity outside of the boundary layer, u_{max}, and the boundary layer thickness, δ, as scales. The normalized relations are, then, of the type $k/u_{max}^2 = f(y/\delta)$ and $\varepsilon\,\delta/u_{max}^3 = f(y/\delta)$, respectively and the numerical results can be seen in Figures 13 and 14. Results are presented for different roughness Reynolds numbers, k_s^+ (e.g., Poggi et al. 2003, Jimenez 2004), with k_s^+ defined herein as

$$k_s^+ = \frac{(k_s)_{mean} u_{\max}}{\nu} \tag{24}$$

where $(k_s)_{mean}$ is the averaged macro-roughness, to take into account the smooth crest and the variable size steps. ($(k_s)_{mean} = 1/L \int_0^L k_s dL$, where k_s is assumed null in the smooth crest and variable in the zone of variable size steps.) The figures suggest the existence of self-similarity of the TKE and ε for roughness Reynolds numbers up to 6.8×10^4.

For $k_s^+ \leq 6.4 \times 10^4$ we found the following similarity laws:

$$\frac{k}{u_{\max}^2} = 8.01 \cdot 10^{-3} e^{-3y/\delta} \tag{25}$$

$$\frac{\varepsilon \delta}{u_{\max}^3} = 6.79 \cdot 10^{-4} \frac{e^{-1.87y/\delta}}{\sqrt{y/\delta}} \tag{26}$$

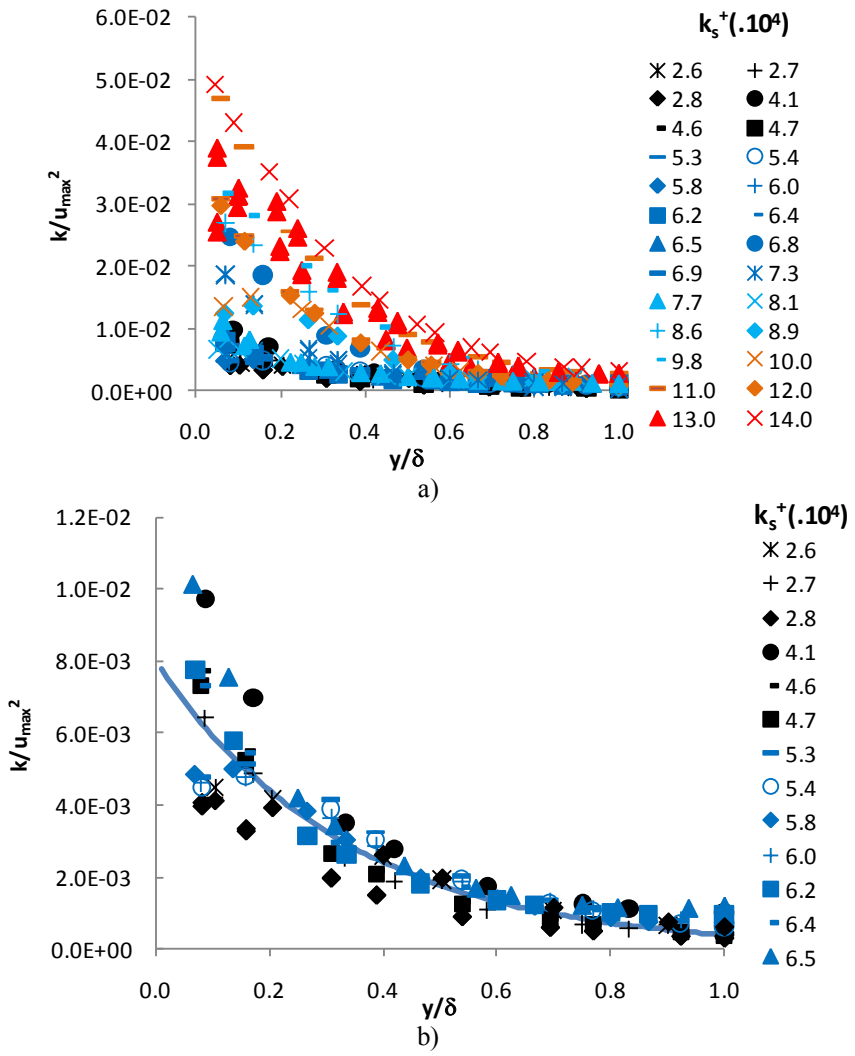

Figure 13 - Self-similarity law for *k*: a) all data; b) for $k_s^+ \leq 6.4 \times 10^4$.

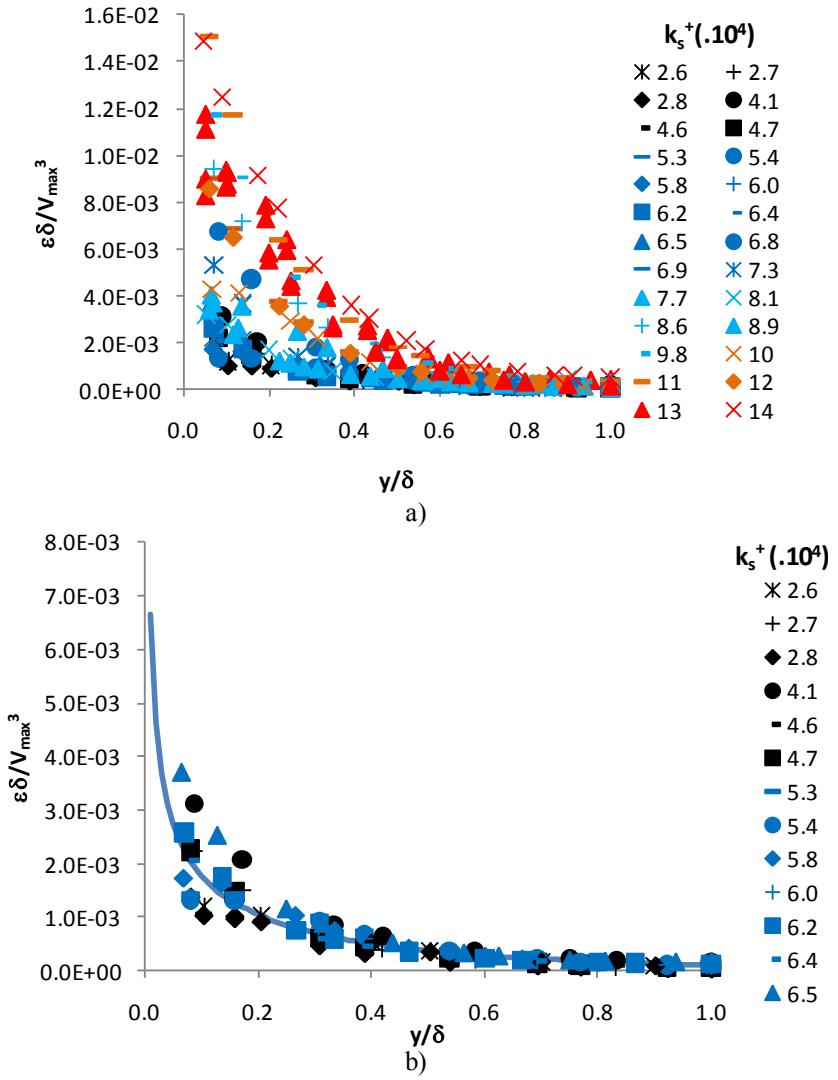

Figure 14 - Self-similarity law for ε : a) all data; b) for $k_s^+ \leq 6.4\times10^4$.

These results indicate that self-similarity in flows with macro-roughness elements is reserved to those flows in which the roughness elements are moderate. Under those circumstances, the transfer of momentum at the pseudo-bottom follows the mechanism described by Gioia and Bombardelli (2002), in which the eddies of size of the roughness elements scale with the size of the eddies in the water column.

7. CONCLUSIONS

The comparison between simulated and measured results presented in this paper confirmed and extended the domain of validity of the results obtained in our previous paper (Bombardelli et al. 2010), regarding the prediction capability of a commercial code for the flow in the developing region of steep stepped spillways. *FLOW-3D®* was observed to simulate accurately discharge, velocity profiles, boundary layer thickness and water depth along the non-aerated region of those spillways.

Experimental and numerical results of the boundary layer thickness presented in this paper were very close to the expression developed by Amador et al. (2009) for a similar stepped chute. Our results suggest values of the exponents a and b of the equation of boundary layer development equal to $a = 0.114$ and $b = 0.311$ (experiments) and $a = 0.132$ and $b = 0.343$ (numerical results). Conversely, although the exponents of the self-similar velocity profiles obtained from the experiments are in close agreement with other experimental studies ($N = 3.4$, on average) the numerical data returned slightly higher results ($N = 4.7$, on average).

Expressions for the friction factor of the type $f = a\left(k_s{}^p / R_h{}^{1/6}\right)^2$ were proposed based on experimental ($a = 0.163$; $p = 0.234$) and numerical ($a = 0.135$; $p = 0.185$) data, along with expressions for Manning's n, function of the form roughness. A surprising proximity of the development of the friction factor to the behavior described by Manning's formula is also observed.

At last, numerical turbulence statistics information brings in evidence the self-similarity of normalized k and ε in the boundary layer development region for roughness Reynolds numbers up to 6.8×10^4.

ACKNOWLEDGMENTS The authors acknowledge the support of the Portuguese National Science Foundation (FCT), though Project PTDC/ECM/108128/2008. Currently, Inês Meireles is supported by FCT, Grant No. SFRH/BD/38003/2007. Fabián Bombardelli gratefully acknowledges the support of the California Department of Water Resources (DWR) and the California Water Resources Control Board (CAWRCB).

APPENDIX 1: THEORETICAL MODEL

The mixture equations for a *3-D* air-water flow are as follows:

$$\frac{\partial \overline{u_{m_i}}}{\partial x_i} = 0 \tag{A1.1}$$

$$\rho_0 \left[\frac{\partial \overline{u_{m_i}}}{\partial t} + \frac{\overline{u_{m_j}} \partial \left(\overline{u_{m_i}} \right)}{\partial x_j} \right] = \rho_0 B_i + \mu \frac{\partial^2 \overline{u_{m_i}}}{\partial x_j{}^2} - \frac{\partial \overline{p}}{\partial x_i} - \frac{\partial \overline{u_{m_i}' u_{m_j}'}}{\partial x_j} \tag{A1.2}$$

where $\overline{u_{m_i}}$ is the i-th component of the time–averaged mixture velocity; ρ_0 is the reference density; B_i is the component of the body forces in the direction x_i; $\overline{p}$ is the time–averaged, modified pressure (Buscaglia et al. 2002; Rodi 1984); μ is the dynamic viscosity; t is the time coordinate; and u_{m_i}' is the component of the fluctuating mixture velocity in the direction x_i. In the present problem, the body forces account only for gravity. Turbulence is modeled using the Boussinesq approach, which considers the Reynolds stresses to be proportional to the gradient of mean velocity, as follows (Rodi 1984):

$$-\rho_0 \overline{u_{m_i}' u_{m_j}'} = \mu_T \left(\frac{\partial \overline{u_{m_i}}}{\partial x_j} + \frac{\partial \overline{u_{m_j}}}{\partial x_i} \right) - \frac{2}{3} \rho_0 k \delta_{ij} \tag{A1.3}$$

$$\mu_T = \rho_0 \, C_\mu \, \frac{k^2}{\varepsilon} \tag{A1.4}$$

where μ_T is the eddy dynamic viscosity; and C_μ is a coefficient equal to 0.09. k denotes the turbulent kinetic energy (TKE), defined in this context as: $k = 1/2 \left(\overline{u_{m_i}' u_{m_i}'} \right)$; and ε is the dissipation rate of TKE. In turn, δ_{ij} is the Kronecker delta ($\delta_{ij} = 1$ for $i = j$ and $\delta_{ij} = 0$ for $i \neq j$). Transport equations for k and ε are considered to obtain μ_T; herein we employed the standard *k-ε* turbulence model (Harlow and Nakayama 1967; Launder and Spalding 1972). Although the Renormalization Group (RNG) *k-ε* turbulence model (Yakhot and Orszag 1986, Yakhot and Smith 1992) is usually regarded as having a wider applicability due to the explicit derivation of the equation constants as opposed to the standard *k-ε* model, where the constants are found empirically, we did not observe noticeable differences in the results by considering the two models (see Bombardelli et al. 2010). For this reason, only the standard *k-ε* turbulence model was used, where the transport equations for k and ε are as follows

$$\rho_0 \left[\frac{\partial k}{\partial t} + \overline{u_{m_j}} \frac{\partial k}{\partial x_j} \right] = \frac{\partial}{\partial x_j} \left(\frac{\mu_T}{\sigma_k} \frac{\partial k}{\partial x_j} \right) + \mu_T \left(\frac{\partial \overline{u_{m_i}}}{\partial x_j} + \frac{\partial \overline{u_{m_j}}}{\partial x_i} \right) \frac{\partial \overline{u_{m_i}}}{\partial x_j} + G - \rho_0 \varepsilon \tag{A1.5}$$

$$\begin{aligned} \rho_0 \left[\frac{\partial \varepsilon}{\partial t} + \overline{u_{m_j}} \frac{\partial \varepsilon}{\partial x_j} \right] = & \frac{\partial}{\partial x_j} \left(\frac{\mu_T}{\sigma_\varepsilon} \frac{\partial \varepsilon}{\partial x_j} \right) + \\ & C_{1\varepsilon} \frac{\varepsilon}{k} \left[\mu_T \left(\frac{\partial \overline{u_{m_i}}}{\partial x_j} + \frac{\partial \overline{u_{m_j}}}{\partial x_i} \right) \frac{\partial \overline{u_{m_i}}}{\partial x_j} + C_{3\varepsilon} G \right] - \rho_0 C_{2\varepsilon} \frac{\varepsilon^2}{k} \end{aligned} \tag{A1.6}$$

where G is the buoyancy term, and σ_k, σ_ε, $C_{1\varepsilon}$, $C_{2\varepsilon}$ and $C_{3\varepsilon}$ are constants, with default of 1.0, 1.3, 1.44, 1.92 and 0.2.

These equations are valid within a domain Ω, limited by the incoming flow in the tank; the outgoing flow downstream of the stilling basin; the solid boundary in the tank, spillway and stilling basin; and the free-surface. *TruVOF* (embedded in *FLOW-3D*®; see Hirt and Nichols 1981) is used in this work to track the free-surface. The *TruVOF* method exploits three key components (see Bombardelli et al. 2001; Bombardelli et al. 2010). The volume fraction function, F, is obtained by solving the following equation:

$$\frac{\partial F}{\partial t} + \frac{\partial \left(F \overline{u_{m_i}} \right)}{\partial x_i} = 0 \tag{A1.7}$$

At last, the third component consists in defining properly the boundary conditions at the free-surface to capture precisely the free-surface dynamics.

APPENDIX 2: DETAIL MESH CONVERGENCE

We presented in Bombardelli et al. (2010) an analysis of mesh convergence. To that end, we compared numerical results obtained with three grids of 2.0, 2.2 and 2.4 million volumes, as detailed in Fig. A2.1 and Table A2.1.

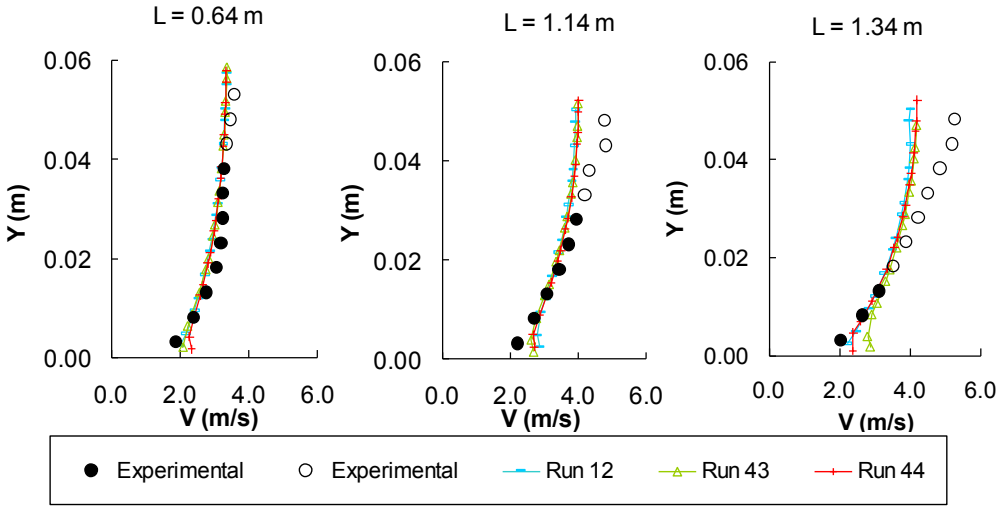

a)

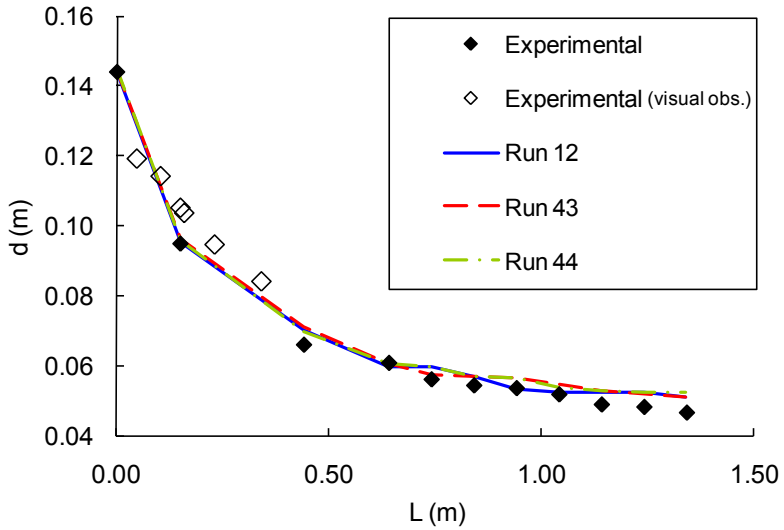

b)

Figure A2.1 - Results of the mesh convergence analysis for q_w = 0.18 m^2/s and h = 4 cm: comparison of results for three meshes of 2.0, 2.2 and 2.4 million volumes: a) water velocities at different distances from the crest of the spillway (unfilled symbols refer to points with measurements affected by either the unsteady motion of the free-surface or the unsteadiness of the location of the inception point; filled symbols indicate points where air concentration is equal to zero.); b) water levels at different distances from the crest of the spillway (in Bombardelli et al. 2010).

All the results pertain to a final steady state condition. Computations with these three grids yielded virtually the same results for the velocity profiles and the water depths (Fig. A2.1). Therefore, we selected the grid of 2.0 million volumes as the grid for the analysis. This grid corresponds to a uniform cell size of 3 mm in the x direction and 4 mm in the vertical direction.

Based on the large number of volumes employed in the numerical solution, we immediately realized that we were in the region of mesh convergence, as depicted by the horizontal line in Fig. 8.3.1 (a) of Chung (2002). For comparison, previous authors have used smaller numbers of volumes/elements than we did: Tabbara et al. (2005), up to 8,644 elements; Carvalho and Amador (2008), up to 76,800 volumes. In addition, it is possible to show that our resolution well represents a large range of the turbulence scales. In fact, we computed the Kolmogorov length scale from the numerical results for the steps. Adopting numerical values of the dissipation rate of turbulent kinetic energy, we computed values of the Kolmogorov length scale $\left(\eta_k = \left(\nu^3/\varepsilon\right)^{1/4}\right)$ up to 0.1 mm. Taking into account that the upper limit for the dissipation range is about 50-60 times the Kolmogorov length scale (Pope 2000; Davidson 2005), we can observe that our simulations with a mesh size of 4 mm are solving all scales of the energy-containing range, and likely most scales of the inertial sub-range, which is more than convenient for a numerical solution based on the Reynolds-Averaged Navier-Stokes equations.

Table A2.1 – Data on meshes for simulations with *FLOW-3D*® for assessment of mesh convergence for q_w = 0.18 m²/s and h = 4 cm (in Bombardelli et al. 2010).

Name	Nº of blocks	Nº of cells	Min. size of cells (m)	Max. size of cells (m)
Run 12	10	2.0E+06	3.00E-03	4.00E-03
Run 43	10	2.2E+06	2.85E-03	3.80E-03
Run 44	10	2.4E+06	2.70E-03	3.60E-03

APPENDIX 3: BOUNDARY LAYER DEVELOPMENT

In the developing flow region of stepped spillways the velocity profile can be divided in two regions: i) the lower region, inside the boundary layer, where the velocity gradient is relatively important, and ii) the upper region, above the boundary layer, where the velocity is virtually constant. Figure 5 shows that, from the numerical simulations, even if the velocity gradient decreases away from the pseudo-bottom, gradients different from zero are observed in the expected constant velocity region. For this reason, the determination of the boundary layer thickness and velocity outside of the boundary layer is not easy. The boundary layer thickness located, by definition, at the point where the velocity is 99% of the maximum time-averaged velocity, was obtained by observation of the point where the velocity gradient becomes nearly negligible. To determine the velocity outside of the boundary layer two different procedures were considered: i) average of the velocities above the boundary layer; ii) velocity at the boundary layer divided by 0.99. These methodologies were consistently applied to all data. Although these two methodologies returned velocities with differences up to 2%, the corresponding exponents of the self-similar

power law (*1/N*) had differences up to 20% (Fig. A3.1), revealing a strong sensitivity of *N* to slight differences in u_{max}. Contrarily, no apparent difference was noticed in the boundary layer thickness, and normalized profiles of the turbulent kinetic energy and its dissipation.

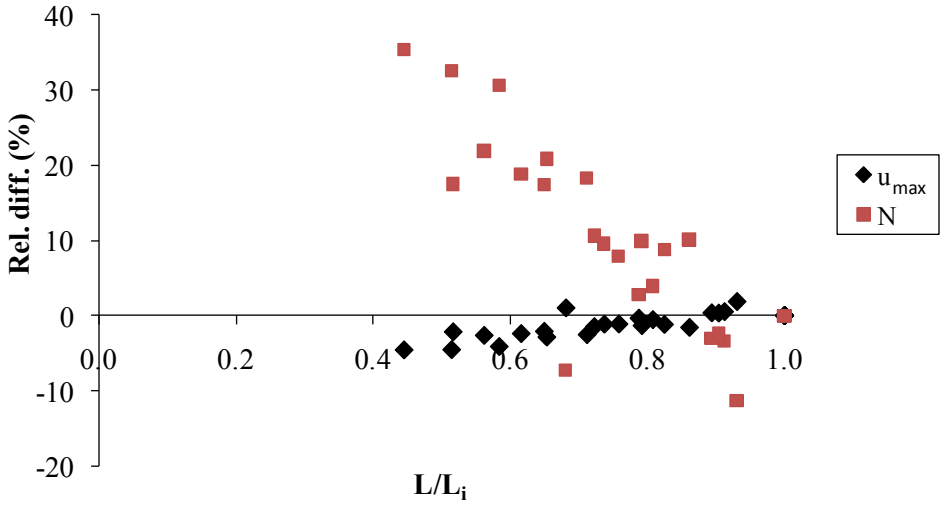

Figure A3.1 - Influence in *N* of different methodologies to calculate u_{max}.

The displacement and momentum thicknesses were calculated following three different methodologies: a) use of Eqs (13) and (14), considering an averaged *N* pertaining to all numerical data; b) employ of Eqs (13) and (14), but considering a different *N* for each velocity distribution; and c) use their definition and develop a numerical integration of the velocity profiles:

$$\delta_1 = \int_0^{\delta} \left(1 - \frac{u}{u_{max}}\right) dy \qquad \text{(A3.1)}$$

$$\delta_2 = \int_0^{\delta} \frac{u}{u_{max}} \left(1 - \frac{u}{u_{max}}\right) dy \qquad \text{(A3.2)}$$

For the former two methodologies, a high scatter was observed in the results of δ_1 and δ_2 (and consequently of f) due to the nature of the velocity profiles. In this regard, we consider more accurate to determine δ_1 and δ_2 from the first methodology, which uses the averaged velocity profile.

REFERENCES

Abecasis, F. (1977). "The behaviour of spillway crests under flows higher than the design flow." J. Hydr. Res., IAHR, 41(3), 259-269. Proc. 19th IAHR Congress, Vol. 4, Baden-Baden, 559-566.

Aberle, J., and Smart, G. M. (2003). "The influence of roughness structure on flow resistance on steep slopes." J. Hydr. Res., IAHR, 41(3), 259-269.

ACE (1990). "Hydraulic design of spillways." Engineer Manual 1110-2-1603, U.S. Army Corps of Engineers, Washington DC, USA.

Ackers, P. (1961). “The hydraulic resistance of drainage conduits.” Proc. Inst. Civ. Eng. London, 19, 307-336.

Amador, A. (2005). “Comportamiento hidráulico de los aliviaderos escalonados en presas de hormigón compactado. ” Ph.D. thesis, UPC, Barcelona, Spain (in Spanish).

Amador, A., Sanchez-Juny, M., Dolz, J. (2006). “Characterization of the non-aerated flow region in a stepped spillway by PIV.” J. Fluid Eng., ASME, 138(6), 1266-1273.

Amador, A., Sanchez-Juny, M., and Dolz, J. (2009). “Developing flow region and pressure fluctuations on steeply sloping stepped spillways.” J. Hyd. Eng., ASCE, 135(12), 1092-1100.

Arantes, E. J. (2007). “Caracterização do escoamento sobre vertedouros em degraus via CFD.” Ph.D. thesis, EESC/USP, São Carlos, Brazil (in Portuguese).

Barenblatt, G. I. (1996). “Scaling, self-similarity, and intermediate asymptotics.” Cambridge University Press, UK.

Barkhudarov, M. R. (2004). “Multi-block gridding technique for flow-3D.” Flow Science Technical Notes, Flow Science, Inc., TN59, available online.

Bauer, W. J. (1954). “Turbulent boundary layer on steep slopes.” Transactions, ASCE, 119, 1212-1233.

Boes, R. M., and Hager, W. H. (2003a). “Two phase flow characteristics of stepped spillways.” J. Hydr. Eng., ASCE, 129(9), 661-670.

Boes, R. M., and Hager, W. H. (2003b). “Hydraulic design of stepped spillways.” J. Hydr. Eng., ASCE, 129(9), 671-679.

Bombardelli, F. A. (2003). “Characterization of coherent structures from parallel, LES computations of wandering effects in bubble plumes.” Proc. 2003 World Water and Environmental Resources Congress, Environmental & Water Resources Institute (EWRI), ASCE, Philadelphia, PA, USA, P. Bizier and P. DeBarry (eds.). (In CD.)

Bombardelli, F. A. (2004). “Turbulence in multiphase models for aeration bubble plumes.” Ph.D. thesis. University of Illinois at Urbana-Champaign.

Bombardelli, F. A. and García, M. H. (2003). “Hydraulic design of large-diameter pipes.” J. Hydr. Eng., ASCE, 129(11), 839-846.

Bombardelli, F. A., and Jha, S. K. (2009). “Hierarchical modeling of dilute, suspended-sediment transport in open channels.” Environ. Fluid Mech., 9(2), 207-230.

Bombardelli, F. A., Buscaglia, G. C., Rehmann, C. R., Rincón, L. E., and García, M. H. (2007). “Modeling and scaling of aeration bubble plumes: a two-phase flow analysis.” J. Hyd. Res., IAHR, 45(5), 617-630.

Bombardelli, F. A., Hirt, C. W., and García, M. H. (2001). “Discussion on ‘Computations of curved free surface water flow on spiral concentrators’, by Matthews et al.” J. Hydr. Eng., ASCE, 127(7), 629-631.

Bombardelli, F. A., Meireles, I. and Matos, J. (2010). “Laboratory measurements and multi-block numerical simulations of the mean flow and turbulence in the non-aerated skimming flow region of steep stepped spillways.” Env. Fluid Mechanics, Springer (published online).

Burden, R. L., and Faires, J. D. (2004). “Numerical analysis.” Eighth Edition, Brooks-Cole Publishing.

Buscaglia, G. C., Bombardelli, F. A., and García, M. H. (2002). “Numerical modeling of large scale bubble plumes accounting for mass transfer effects.” Int. J. Multiphase Flow, 28, 1763-1785.

Cain, P., and Wood, I. R. (1981). “Measurements of self-aerated flow on a spillway.” J. Hydr. Eng., ASCE, 107(HY11), 1407-1424.

Carosi, G., and Chanson, H. (2007). “Self-similarity of air-water flows in skimming flow on stepped spillway.” Proc. 32nd IAHR Congress, Venice, Italy, C2.b. (In CD.)

Carvalho, R., and Amador, A. (2008). “Physical and numerical investigation of the skimming flow over a stepped spillway.” Proc. 3rd IAHR Int. Symposium on Hydraulic Structures, Nanjing, China, 1767-1772. (In CD.)

Chamani, M. R., and Rajaratnam, N. (1999). “Characteristics of skimming flow over stepped spillways.” J. Hydr. Eng., ASCE, 125(4), 361-368.

Chanson, H. (1993). “Self-aerated flows on chutes and spillways.” J. Hydr. Eng., ASCE, 119(2), 220-243.

Chanson, H. (2002). “The hydraulics of stepped chutes and spillways.” Balkema, Lisse, The Netherlands.

Chanson, H. (2004). "Environmental hydraulics of open channel flows." Elsevier-Butterworth-Heinemann, Oxford, UK.

Chanson, H. (2009). “Turbulent air-water flows in hydraulic structures: dynamic similarity and scale effects.” Environ. Fluid Mech., 9(2), 125-142.

Chen, C. (1991). “Unified theory on power laws for flow resistance.” J. Hydr. Eng., ASCE, Vol. 117(3), 371-389.

Chen, Q., Dai, G., and Liu, H. (2002). “Volume of fluid model for turbulence numerical simulation of stepped spillway overflow.” J. Hydr. Eng., ASCE, 128(7), 683-688.

Chow, V. T. (1959). “Open-channel hydraulics.” McGraw-Hill, USA.

Chung, T. J. (2002). “Computational fluid dynamics.” Cambridge University Press, USA.

Crowe, C., Sommerfeld, M., and Tsuji, Y. (1998). “Multiphase flows with droplets and particles.” CRC Press, USA.

Davidson, P. A. (2004). “Turbulence: an introduction for scientists and engineers.” Oxford University Press, USA.

Djenidi, L., Elavarasan, R., and Antonia, R.A. (1999). “The turbulent boundary layer over transverse square cavities.” J. Fluid Mech., 395, 271-294.

Felder, S., and Chanson, H. (2009). “Energy dissipation, flow resistance, and gas liquid interfacial area in skimming flows on moderate-slope stepped spillways.” Environmental Fluid Mechanics, 9(4), 427-441.

Ferziger, J. H., and Peric, M. (2002). “Computational methods for fluid dynamics.” Springer.

Flow Science, Inc. (2008). FLOW-3D User’s Manual, Version 9.3, Los Alamos, New Mexico, USA.

Gioia, G., and Bombardelli, F. A. (2002). “Scaling and similarity in rough channel flows.” Phys. Rev. Lett., 88(1), 014501.

Gomes, J., Amador, A., Marques, M., Matos, J., and Sánchez-Juny, M. (2006). “Hydrodynamic pressure field on steeply sloping stepped spillways.” Proc. of the Int. Junior Researcher and Eng. Workshop on Hyd. Structures. J. Matos and H. Chanson, eds., Report CH61/06, Div. of Civil Eng., The University of Queensland, Brisbane, Australia.

Gonzalez, C., and Chanson, H. (2007). “Hydraulic design of stepped spillways and downstream energy dissipators for embankment dams.” Dam Engineering, Vol. XVII(4), 223-244.

Harlow, F.H., and Nakayama, P.I. (1967). “Turbulence transport equations.” Phys. of Fluids, 10, 2323.

Hirt, C. W., and Nichols, B. D. (1981). “Volume of Fluid (VOF) method for the dynamics of free boundaries.” J. Comp. Physics, 39, 201-225.

Hirt, C. W., and Sicilian, J. M. (1985). “A porosity technique for the definition of obstacles in rectangular cell meshes.” Proc. 4th Int. Conf. Ship Hydro., National Academy of Science, Washington, DC, USA.

Hrenya, C. M., and Sinclair, J. L. (1997). “Effects of particle-phase turbulence in gas-solid flows.” AIChE J., 43(4), 853-869.

Jiménez, J. (2004). “Turbulent flows over rough walls.” Annual Review of Fluid Mechanics, 36, 173-196.

Johnson, M. C., and Savage, B. M. (2006). “Physical and numerical comparison of flow over ogee spillway in the presence of tailwater.” J. Hydr. Eng., ASCE, 132(12), 1353-1357.

Kundu, P.K., and Cohen, I.M. (2004). “Fluid mechanics”, Elsevier Academic Press, USA.

Launder, B. E., and Spalding, D. B. (1972). “Lectures in mathematical models of turbulence.” Academic Press.

Matos (1999). "Emulsionamento de ar e dissipação de energia do escoamento em descarregadores em degraus." Ph.D. thesis, IST, Lisbon, Portugal (in Portuguese).

Matos, J. (2000). “Hydraulic design of stepped spillways over RCC dams.” Proc. 1st Int. Workshop on Hydraulics of Stepped Spillway, Zurich, Switzerland, A. A. Balkema Publisher, Rotterdam, The Netherlands, 187-194.

Matos, J., and Frizell, K. W. (1997). “Air concentration measurements in highly turbulent aerated flow”. Proc. 27th IAHR Congress, Theme D, Vol. 1, San Francisco, USA, S. S. Y. Wang and T. Carstens (eds.), 149-154. (In CD.)

Matos, J., and Frizell, K. W. (2000). “Air concentration and velocity measurements on self-aerated flow down stepped chutes.” Proc. ASCE 2000 Conference, Minneapolis, USA.

Matos, J., Frizell, K. H., André, S., and Frizell, K. W. (2002). “On the performance of velocity measurement techniques in air-water flows”. Proc. EWRI/IAHR Joint Conference on Hydraulic Measurements & Experimental Methods, ASCE, Estes Park, USA.

Meireles, M. (2004). “Emulsionamento de ar e dissipação de energia do escoamento em descarregadores em degraus.” MSc thesis, IST, Lisbon, Portugal (in Portuguese).

Meireles, I., and Matos, J. (2009). “Skimming flow in the non-aerated region of stepped spillways over embankment dams.” J. Hydr. Eng., ASCE, 135(8), 685-689.

Meireles, I., Matos, J., and Melo, J. F. (2006). “Skimming flow properties upstream of air entrainment inception on steeply sloping stepped chutes.” Proc. Int. Symposium on Hydraulic Structures, IAHR, Ciudad Guayana, Venezuela. (In CD.)

Meireles, I., Matos, J., and Frizell, K. (2007). “Measuring air entrainment and flow bulking in skimming flow over steeply sloping stepped chutes.” Proc. HMEM'07, Lake Placid, USA, EWRI/IAHR.

Meireles, I., Matos, J., Bombardelli, F.A. and Renna, F. (2011). “On the prediction of the characteristic hydraulic parameters of the non-aerated skimming flow down steep stepped spillways.” (to be submitted for publication).

Nezu, I., and Nakagawa, H., (1993). “Turbulence in open-channel flows.”, AA Balkema, Rotterdam, The Netherlands.

Nikora V. and Smart G. M. (1997). "Turbulence characteristics of new zealand gravel-bed rivers.", J. Hydr. Eng., 123(9), 764-773.

Ohtsu, I., Yasuda, Y., and Takahashi, M. (2004). “Flow characteristics of skimming flows in stepped channels.” J. Hydr. Eng., ASCE, 130(9), 860-869.

Olsen, N.R.B., and Kjellesvig, H.M. (1998). “Three-dimensional numerical flow modelling for estimation of spillway capacity.” J. Hyd. Res., IAHR, 36(5), 775-784.

Poggi, D. Porporato, A. and Ridolfi L. (2003). “Analysis of the small-scale structure of turbulence on smooth and rough walls.” Phys. of Fluids, 15(1), 35-46.

Pope, S. B. (2000). “Turbulent flows.” Cambridge University Press, UK.

Prosperetti, A., and Tryggvason, G. (2007). "Computational methods for multiphase flow." Cambridge Press, UK.

Quintela, A. (1998). "Hidráulica. ", Fundação Calouste Gulbenkian, Portugal (in Portuguese).

Relvas, A. T. and Pinheiro, A. N. (2008). "Inception point and air concentration in flows on stepped chutes lined with wedge-shaped concrete blocks" J. Hydr. Eng., ASCE, 134(8), 1042-1051.

Renna, F. (2004). "Caratterizzazione fenomenologica del moto di un fluido bifasico lungo scaricatori a gradini." PhD thesis, Politecnico di Bari, Cosenza, Italy (in Italian).

Rodi, W. (1984). "Turbulence models and their application in hydraulics." State-of-the-Art Paper, IAHR.

Rouse, H. (1946). "Elementary mechanics of fluids.", John Wiley & Sons, Inc., New York, USA.

Rouse, H. (1959). "Advanced mechanics of fluids.", John Wiley & Sons, Inc., New York, USA.

Sánchez-Juny, M., Bladé, E., and Dolz, J. (2008). "Analysis of pressures on a stepped spillway." J. Hydr. Res., IAHR, 46(3), 410-414.

Savage, B. M., and Johnson, M. C. (2001). "Flow over ogee spillway: physical and numerical model case study." J. Hydr. Eng., ASCE, 127(8), 640-649.

Smart, G.M., Duncan M.J., and Walsh J.M. (2002). "Relatively rough flow resistance equations." J. Hyd. Eng., ASCE, 128(6), 568-78.

Strickler, A. (1923). "Contributions to the questionof a velocity formula and roughness data for streams, channels and close pipelines." Translation by T. Roesgen and W.R. Brownlie, W. M. Keck Laboratory of Hydraulics and Applied Science, California Institute of Technology, 1981.

Tabbara, M., Chatila, J., and Awwad, R. (2005). "Computational simulation of flow over stepped spillways." Computers & Structures, Elsevier, 83, 2215-2224.

Tozzi, M. J. (1992). "Caracterização/comportamento de escoamentos em vertedouros com paramento em degraus." Ph.D. thesis, Escola Politécnica da Universidade de S. Paulo, Brazil (in Portuguese).

Wilhelms, S. C., and Gulliver, J. S. (2005). "Bubbles and waves description of self-aerated spillway flow." J. Hydr. Res., IAHR, 43(5), 522-531.

Wood, I. R. (1991). "Free-surface air entrainment on spillways". Air entrainment in free-surface flows, Ed. Ian R. Wood, IAHR, Hydraulic Structures Design Manual nº 4, Hydraulic Design Considerations, Balkema, pp. 55-84.

Yakhot, V., and Orszag, S. A. (1986). "Renormalization group analysis of turbulence. I. Basic theory." J. Scientific Computing, 1(1), 3-51.

Yakhot, V., and Smith, L. M. (1992) "The renormalization group, the E-Expansion, and the derivation of turbulence model." J. Scientific Computing, 3, 35.

Yen, B. C. (1992) “Hydraulic resistance in open channels.” Channel flow resistance: Centennial of Manning's formula, B.C. Yen, ed., Water Resources Publications, Littleton, Colo., 1-135.

5.3 PREDICTORS FOR THE INCEPTION OF AIR ENTRAINMENT IN FLOWS ON STEEP STEPPED SPILLWAYS: AN ANALYSIS

This subchapter concerns to the analysis of the different existent criteria to predict the location of the inception point of air entrainment inflows on steep stepped spillways. For that purpose, experimental data, acquired in the 1V:0.75H slope stepped channel of LNEC, and numerical data, obtained with *Flow-3D*® simulating the previous facility, are used.

ABSTRACT 5.3-1

1. INTRODUCTION 5.3-1

2. EXPERIMENTAL MEASUREMENTS 5.3-3

3. NUMERICAL SIMULATIONS 5.3-5

4. ANALYSIS OF THE CRITERION FOR AIR ENTRAINMENT 5.3-5

5. CONCLUSION AND FINAL REMARKS 5.3-11

NOTATION 5.3-11

REFERENCES 5.3-12

PREDICTORS FOR THE INCEPTION OF AIR ENTRAINMENT IN FLOWS ON STEEP STEPPED SPILLWAYS: AN ANALYSIS

ABSTRACT

We discuss, apply and validate a physics-based criterion for air entrainment in flows on steep stepped spillways. The criterion is embedded in the computational fluid dynamics (CFD) code *FLOW-3D*®, and it is intended for general water/air interfaces. To the best of our knowledge, this is the first time such validation is undertaken for any flow in general, and for the flow in steep stepped spillways in particular. To undertake the validation, we employed experimental data and numerical results. We observed an overall good performance of the criterion, especially considering the intrinsic difficulties in defining the time-averaged location and depth of the inception point due to the unsteadiness of the flow.

Keywords: computational fluid dynamics (CFD), reynolds-averaged Navier-Stokes equations, multi-phase flows, two-phase flows, inception point, air entrainment, stepped spillways, turbulence, k-ε model.

---

1. INTRODUCTION

The flow on steep stepped spillways presents two clearly distinct zones: a) A non-aerated region, characterized by a smooth profile close to the spillway crest (Lane 1939, Bauer 1954, Chanson 2002, Meireles et al. 2011a), and by subsequent free-surface disturbances of increasing wave amplitude, which end with the inception point of air entrainment; and b) an aerated zone, in which high amounts of air entrain into the water body, quickly reaching the spillway bottom, and where bulking and splashing "white waters" are visually observed. The flow in these two regions of single- and two-phase flow is obviously markedly different. As examples of those differences, experimental observations developed in the last decades show that the aerated flow is characterized by a drag reduction opposed to the equivalent non-aerated flow and by the bulking of the flow. It is then of vital importance to determine as accurately as possible the location where air entrainment begins. Unfortunately, this is not an easy task, given the unsteadiness of the flow at the inception point (see Meireles et al. 2011a for a complete discussion regarding this issue).

Most previous attempts at determining the location of the inception point in stepped spillways experimentally were based on visual observations (e.g. Sorensen 1985, Tozzi 1992, Bindo et al. 1993, Sanchez-Juny 2001, Chanson and Toombes 2002, Yasuda and Chanson 2003, Sanagiotto 2003, Dai Prá 2004, Gonzalez 2005, Relvas and Pinheiro 2008, Bung 2009). The clear disadvantage of this methodology is that different researchers likely obtain different values of the location and depth of the inception point. On the other hand, some authors started to determine this location based on more "objective" experimental techniques. Boes and Hager (2003) decided to analyze the values of the air concentration at the pseudo-bottom formed by the step edges; Amador et al. (2009) studied the development of the boundary layer and the shape of the time-averaged velocity profiles; Matos et al. (2000) and Meireles et al. (2011a) used boundary layer, equivalent clear-water depth, and air concentration data to address the location of the inception point; and Meireles and Matos (2009), in a flatter stepped chute, where the waviness of the flow is less significant, considered the development of both the boundary layer and its intersection with the water depth; and. Matos et al. (2000) observed that the cross-section of inception determined by the development of the boundary layer and the equivalent clear-water depth is always located upstream of the position obtained by visual observations, and Meireles et al. (2011a) quantified this difference to be as large as 30%.

Regarding theoretical predictors for the onset of air entrainment, two main types of criteria have been proposed for channels in general. These criteria are based on: a) the balance between destabilizing and stabilizing physical mechanisms (e.g. Volkart 1980, Falvey and Ervine 1988, Ferrando and Rico 2002, Hirt 2003), and b) the relation between values of the turbulent shear stress close to the free surface and the stabilizing streesses (Chanson 2004, 2009). Two of these predictors are detailed below.

Early studies focusing on self-aerated flows past spillways associated air entrainment with turbulence intensity close to the free surface (e.g. Lane 1939, Hickox 1945), leading to the idea that the entrainment of air in the flow starts at the cross section where the turbulent boundary layer reaches the free surface (e.g. Halbronn 1952, 1954, Bauer 1954). However, it has been observed more recently that in addition to the boundary layer being fully developed (Keller et al. 1974, Volkart 1980, Falvey and Ervine 1988) it is necessary that the surface eddies possess sufficient energy to raise small liquid elements above the free surface in order to entrain air. A portion of these elements will thus trap air and carry it into the body of water. This physical concept is expressed mathematically as a balance between destabilizing forces associated with turbulence, and the stabilizing forces of surface tension and gravity (Volkart 1980, Falvey and Ervine 1988, Ferrando and Rico 2002, Hirt 2003). A criterion developed by Hirt (2003) for general gas-water flows is embedded in the commercial computational fluid dynamics (CFD) code *FLOW-3D®*. When a disturbance *energy* per unit volume, P_T, related to a disturbance of size L_T at the free surface, overcomes the *energy* of the stabilizing forces, P_D, a volume of air δV is allowed to enter the flow (Hirt 2003). The equations are as follows (Hirt 2003, Bombardelli et al. 2011):

$$L_T = C_\mu \left(\frac{3}{2}\right)^{1/2} \frac{k^{3/2}}{\varepsilon} \tag{1}$$

$$P_T = \rho_0 \, k \, ; \;\; P_D = \rho_0 \, g_n \, L_T + \frac{\sigma}{L_T} \tag{2}$$

$$\delta V = \begin{cases} C_{air} \, A_s \left[\dfrac{2\left(P_T - P_d\right)}{\rho_0}\right]^{1/2} & if \;\; P_T \geq P_D \\ 0 & if \;\; P_T < P_D \end{cases} \tag{3}$$

where C_μ is a coefficient equal to 0.09; k denotes the turbulent kinetic energy (TKE), defined in the context of mixture variables (Bombardelli et al. 2011) as $k = 1/2 \left(\overline{u_{m_i}' u_{m_i}'}\right)$, where $\left(\overline{u_{m_i}' u_{m_j}'}\right)$ are the Reynolds stresses and the primes indicate the fluctuations of velocity component i (and summation is implied in repeated indices); ε refers to the dissipation rate of TKE (DTKE); ρ_0 is the reference density; g_n is the component of the vector of the acceleration of gravity in the direction normal to the free surface; σ is the coefficient of surface tension; and A_s is the surface area. C_{air} in turns, accounts the fraction of that area occupied by the perturbation.

An alternative approach considers that the incorporation of air into the flow occurs when the turbulent shear stress close to the free surface is larger than the stabilizing force coming from surface tension per unit area, expressed for a spherical bubble as (adapted from Chanson 2004, 2009)

$$\left|\rho_0 \overline{u_{m_i}' u_{m_j}'}\right| > \sigma \frac{\pi\left(r_1 + r_2\right)}{A} \tag{4}$$

where r_1 and r_2 denote the two principal radii of curvature of the deformation (disturbance) of the free surface and A refers to the area of that surface disturbance. Although physically easy to grasp, the observation and quantification of the shear stress close to the free surface is not an easy task.

In this technical note, we test the criterion embedded in *FLOW-3D®* for the case of the flow through steep stepped spillways, using experimental measurements and numerical computations. To the best of our knowledge, this is the first time this criterion is rigorously tested, either in stepped spillways or for any other flow.

2. EXPERIMENTAL MEASUREMENTS

We performed an experimental investigation of the flow through stepped spillways in a facility constituted by a stepped channel (Figure 1), a stilling basin and a recirculation

system. The stepped channel is 1-m wide, 0.50-m deep and 3.35-m long (in the zone of constant slope), with a slope of 1V:0.75H (≈ 53 degrees from the horizontal). Experimental tests were carried out for step heights of 4 and 8 cm (h), and unit discharges (q_w) ranging from 0.08 to 0.20 m^2/s, corresponding to the skimming flow regime (Chanson 2002). The instrumentation was composed by point gauges, a conductivity probe, a back-flushing Pitot tube, and a Bazin weir. The volume flow rate (discharge) was measured with a Bazin weir located at the downstream end of the stilling basin, with value differences smaller than 10% when compared with velocity checks. More details on the equipment and data acquisition are given in Matos and Frizell (1997, 2000), Matos (1999) and Meireles (2011).

Figure 1 - Stepped channel at LNEC with steps 8 cm high.

Two methods were employed to determine the location of the inception point experimentally: 1) where the boundary layer intersects the free-surface; and 2) where the white waters appear. Because of instrumentation limitations (uncovered conditions for the Pitot tube; response time of the Pitot tube; see Bombardelli et al. 2010), the observed flow variables near the free-surface can present unreliable values and thus limit the computation of the boundary layer thickness. For this reason, when applying the first method, profiles of air concentration were measured in addition to velocities and equivalent clear-water depths (Matos et al. 2000, Meireles et al. 2011a). Although according to Volkart (1980) the destabilizing forces only overcome the stabilizing forces downstream of the section where the boundary layer reaches the free surface, the distance among those sections is usually negligible for design purposes. In this regard, recent studies on spillway flows still determine the inception point as the location where the boundary layer reaches the free-surface (e.g. Wood 1991, Chanson 1996, Ferrando and Rico 2002, Wilhelms and Gulliver 2005,

Meireles and Matos 2009, Meireles et al. 2011a), for which no information on the turbulence statistics is needed. Using the second method, the section where the white waters appear was determined by selecting the cross section where air bubbles are observed to be permanently present in the entire depth. (This is the most widely-used method; e.g. Matos 1999, André and Ramos 2003, Meireles 2004, Renna 2004, Relvas and Pinheiro 2008.)

3. NUMERICAL SIMULATIONS

We employed a theoretical model based on the concept of the flow of a mixture, as described in Bombardelli et al. (2010) and in Meireles et al. (2011b). The two-dimensional (2-D) version of the mixture equations was applied to a domain composed by the flow in the upstream tank, the stepped channel and the stilling basin. The specified boundary conditions were set as: 1) pressure boundary conditions in the incoming flow in the tank and the outgoing flow downstream of the stilling basin; 2) null velocities normal to the walls in the solid boundaries; 3) usual "wall functions" for the turbulence statistics (Ferziger and Peric 2002; Bombardelli et al. 2010).

We performed numerical simulations of the test cases observed experimentally with the code *FLOW-3D*®, where the mixture equations are solved by using a finite volumes/finite differences method (Flow Science 2008). A structured Cartesian grid is defined independently of the geometry and subsequently the geometry is embedded in the grid by the *FAVOR*™ technique (Hirt and Sicilian 1985), which computes the fractional areas and corresponding fractional volumes open to flow (see Flow Science 2008 for details). The *TruVOF*™ (Volume-of-Fluid) method (Hirt and Nichols 1981, Bombardelli et al. 2001) was used for capturing the free surface. In our simulations a *CAD* file representing the geometry of the experimental facility was imported into the code as a stereolithography (STL) file and subsequently embedded in a multi-block grid. The grid was composed by ten blocks, with uniform cells of 3 mm (horizontal direction) per 4 mm (vertical direction), corresponding to a total of 2 million volumes (Bombardelli et al. 2010, Meireles et al. 2011b). Mesh convergence was tested through comparison of results with other meshes (Bombardelli et al. 2010). We obtained good agreement of numerical predictions with observations for velocities, equivalent clear-water depths, boundary-layer thickness and inception-point location and depth. Other outputs of the model are the turbulence statistics (k and ε).

From the numerical data, the inception point was located at the section where: 1) the boundary layer intersects the free-surface; and 2) the destabilizing energy due to turbulence overcomes the stabilizing energy due to gravity and surface tension.

4. ANALYSIS OF THE CRITERION FOR AIR ENTRAINMENT

Figures 2 to 8 present the determination of the location and depth of the inception point for the conditions of unit discharge and step height indicated in the figure captions, where d is the equivalent clear-water depth (defined, in the non-aerated region as a fictitious flow

depth which would occur in absence of free-surface waviness), δ is the boundary layer thickness, L is the streamwise coordinate originating at the upstream end of the spillway, and L_i and d_i are the location of, and the equivalent clear-water depth at the inception point, respectively. In Figures a), experimental and numerical data were employed to obtain the inception point location and depth, whereas the destabilizing and stabilizing energies were computed from the numerical results and used in Figures b). In order to utilize the expressions for P_D and P_T, the values of k and ε where obtained from the numerical simulations for the volume closest to the free surface. In turn, a value of $\sigma = 7.3 \cdot 10^{-2}\ N/m$ was employed. In Figures a), numerical and experimental data are close (see Bombardelli et al. 2010, Meireles et al. 2011b) and Meireles 2011) and, although the values of the boundary layer thickness in $L = 0$ are observed not to affect the results of L_i and d_i, it is interesting to notice that, contrarily to what has been usually considered for spillways flows, *FLOW-3D®* returns non-negligible boundary layer values at the spillway crest for the several simulated conditions. Regressions to numerical data were developed. As can be gathered from the figures, the methodologies do not yield exactly the same values of the location of the inception point (as expected). Nonetheless, the predictions of the location of the inception point provided by the energetic method embedded in *FLOW-3D®* are within satisfactory proximity to those obtained via other methods. Disregarding visual observation, it is possible to note that the location and the depth of the inception point may mainly vary according to the type of data and methodology, in about ±10%.

Figure 9 summarizes the experimental and numerical results regarding the location of the inception point and the corresponding equivalent clear-water depth, obtained using the described methods. In the figure, k_s is the roughness height perpendicular to the pseudo-bottom ($k_s = h\cos\theta$, where θ is the spillway slope) and F_* is the roughness Froude number ($F_* = q_w \Big/ \sqrt{g \sin\theta\, k_s^3}$). The scatter in the experimental results, regardless the methodology employed, reflects the difficulty in defining the time-averaged inception point location due to the unsteadiness of the flow depth and boundary layer thickness (Meireles et al. 2011a). In spite of the complexity of the phenomenon of air entrainment in steep stepped spillways, the averaged experimental and numerical results are relatively close, independently of the method used. Further, Figure 9 shows that the points are adequately represented by the empirical expressions of Chanson (2002), Amador et al. (2009) and Meireles et al. (2011a). Our results confirm Volkart's findings regarding the location of the inception point. Given the relatively mild slopes of the free surface, the results regarding the equivalent clear-water depths at the inception point also present a smaller scatter (see Figure 9b).

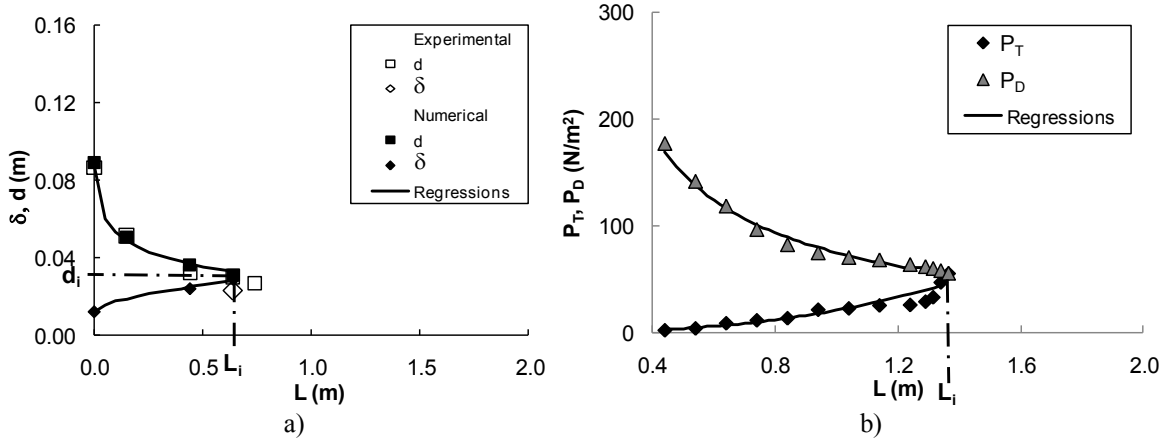

a) b)

Figure 2 - Determination of the equivalent clear-water depth and location of the inception point from experimental and numerical data. Results pertain to conditions for h = 4 cm and q_w = 0.08 m^2/s, and were obtained: a) by using the criterion based on the intersection of the boundary layer and the equivalent clear-water depth; b) by using the concepts of stabilizing and destabilizing energies.

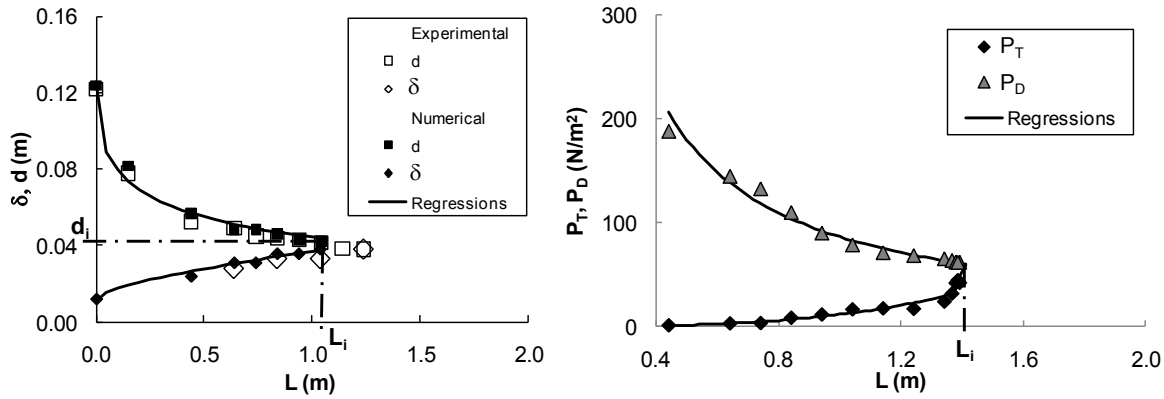

a) b)

Figure 3 - Determination of the equivalent clear-water depth and location of the inception point from experimental and numerical data. Results pertain to conditions for h = 4 cm and q_w = 0.14 m^2/s, and were obtained: a) by using the criterion based on the intersection of the boundary layer and the equivalent clear-water depth; b) by using the concepts of stabilizing and destabilizing energies.

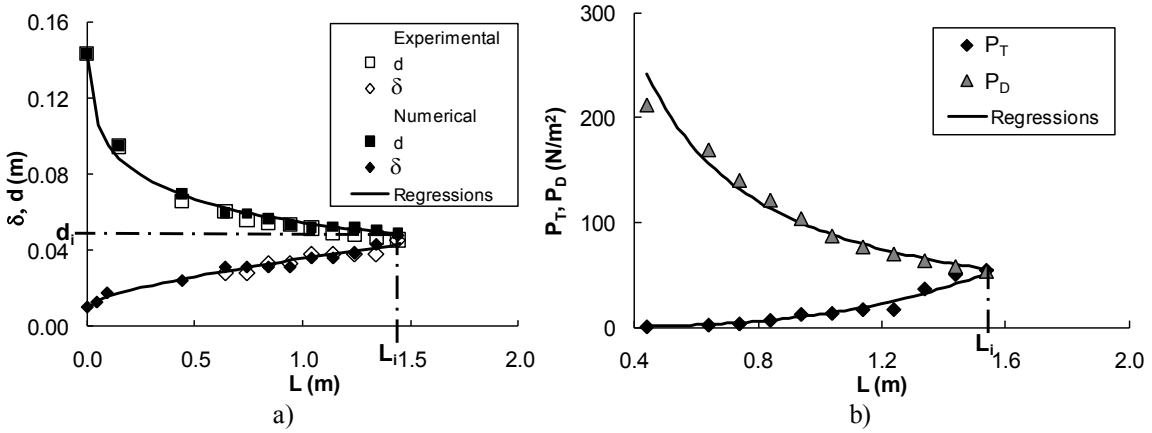

Figure 4 - Determination of the equivalent clear-water depth and location of the inception point from experimental and numerical data. Results pertain to conditions for h = 4 cm and q_w = 0.18 m^2/s, and were obtained: a) by using the criterion based on the intersection of the boundary layer and the equivalent clear-water depth; b) by using the concepts of stabilizing and destabilizing energies.

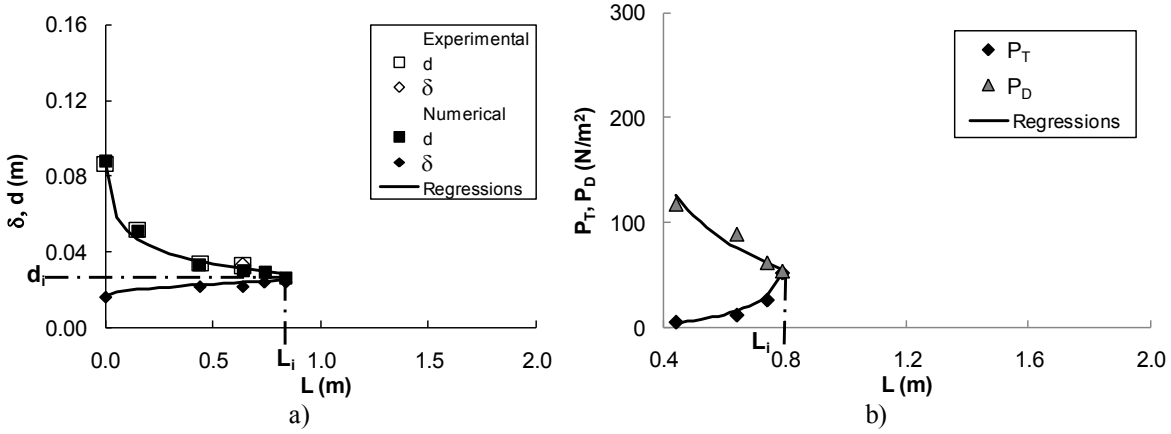

Figure 5 - Determination of the equivalent clear-water depth and location of the inception point from experimental and numerical data. Results pertain to conditions for h = 8 cm and q_w = 0.08 m^2/s, and were obtained: a) by using the criterion based on the intersection of the boundary layer and the equivalent clear-water depth; b) by using the concepts of stabilizing and destabilizing energies.

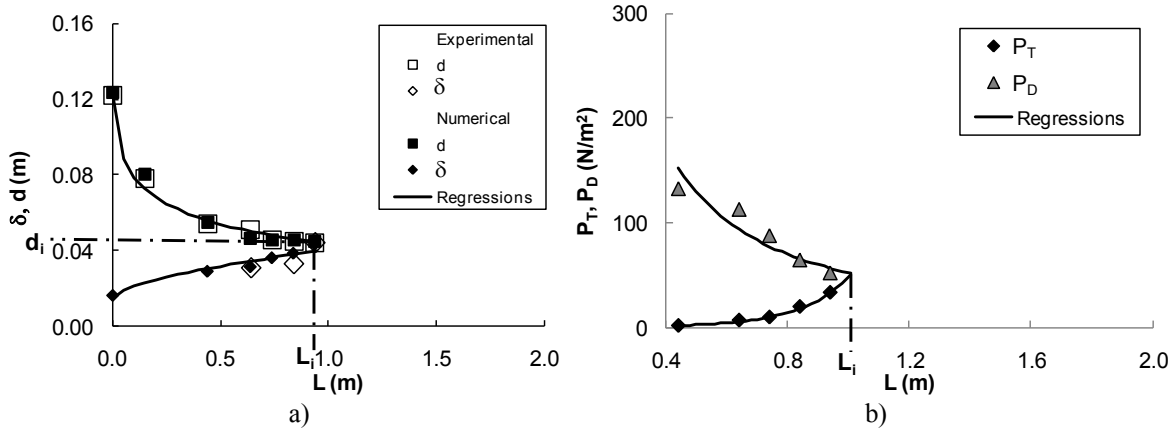

Figure 6 - Determination of the equivalent clear-water depth and location of the inception point from experimental and numerical data. Results pertain to conditions for h = 8 cm and q_w = 0.14 m^2/s, and were obtained: a) by using the criterion based on the intersection of the boundary layer and the equivalent clear-water depth; b) by using the concepts of stabilizing and destabilizing energies.

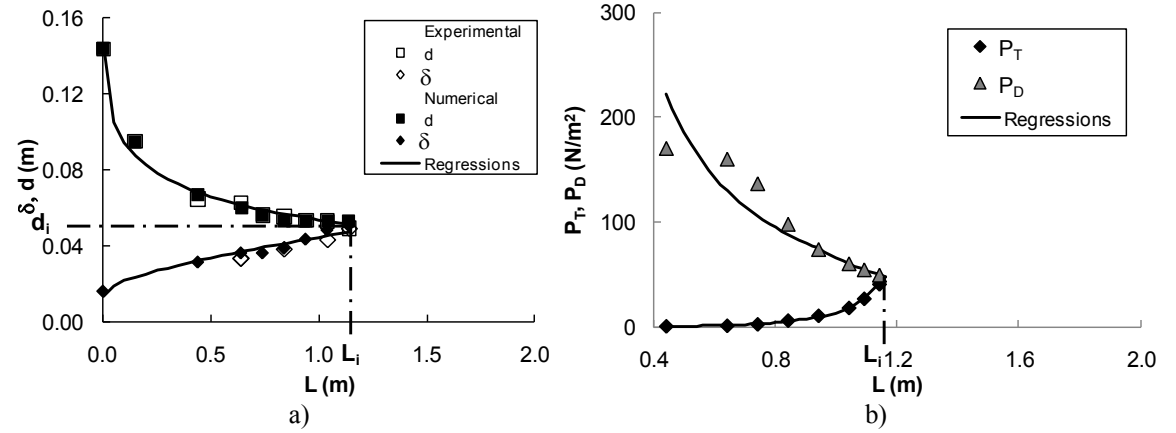

Figure 7 - Determination of the equivalent clear-water depth and location of the inception point from experimental and numerical data. Results pertain to conditions for h = 8 cm and q_w = 0.18 m^2/s, and were obtained: a) by using the criterion based on the intersection of the boundary layer and the equivalent clear-water depth; b) by using the concepts of stabilizing and destabilizing energies.

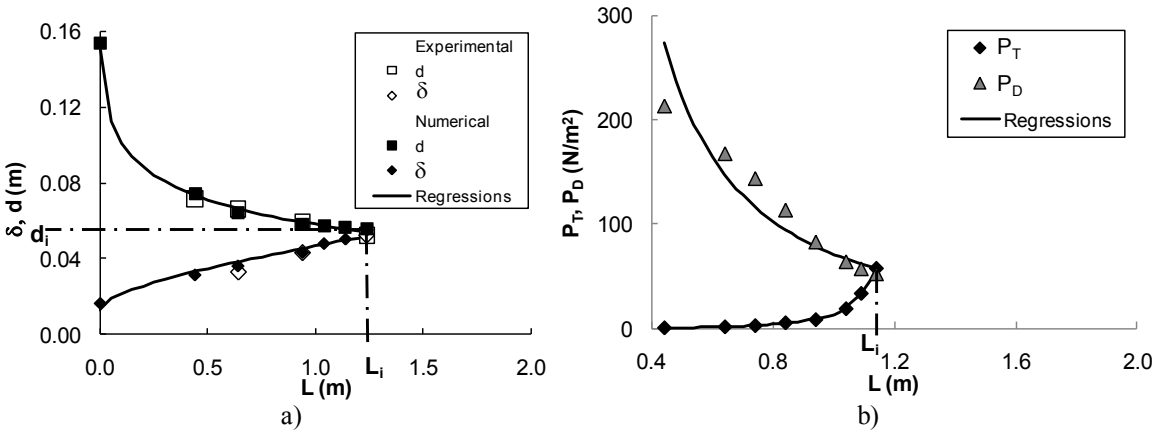

Figure 8 - Determination of the equivalent clear-water depth and location of the inception point from experimental and numerical data. Results pertain to conditions for h = 8 cm and q_w = 0.20 m^2/s, and were obtained: a) by using the criterion based on the intersection of the boundary layer and the equivalent clear-water depth; b) by using the concepts of stabilizing and destabilizing energies.

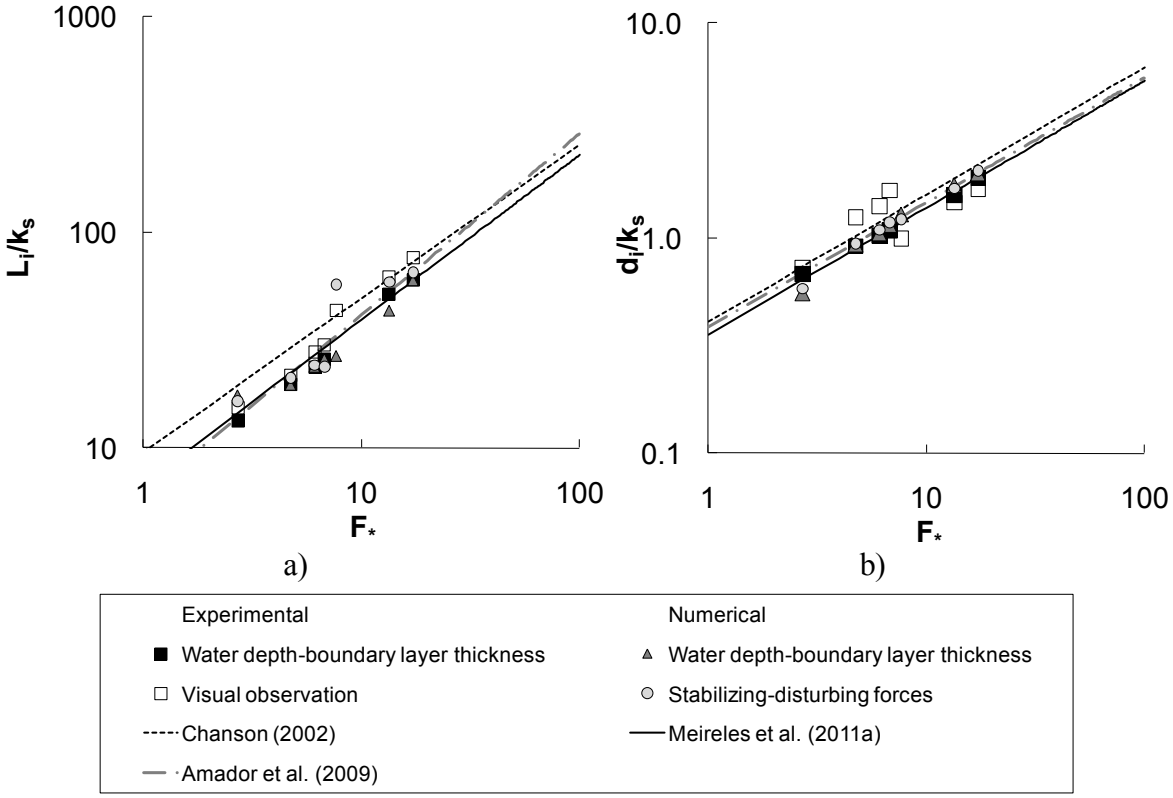

Chanson (2002): $L_i = (h\cos\theta)\,9.719\,(\sin\theta)^{0.0796}\,F_*^{0.713}$; Amador et al. (2009): $L_i = k_s \cdot 5.982\,(F_*)^{0.840}$; and Meireles et al. (2011a): $L_i = k_s \cdot 6.753\,(F_*)^{0.765}$

Figure 9 - Features of the inception point for 0.04 < h (m) < 0.08 and 0.08 < q_w (m^2/s) < 0.20. Comparison among simulated and measured results obtained from several methodologies for: a) location; b) equivalent clear-water depth.

5. CONCLUSION AND FINAL REMARKS

We used experimental and numerical data to determine the section of inception of air entrainment in stepped spillways. Different experimental methods to locate the inception point provide close predictions. We can also conclude that the energetic method embedded in *FLOW-3D*® predicts satisfactorily the location (and indirectly the depth through the *TruVOF*™ method) for the inception point. Since one of the purposes of the current research is to develop theoretical/numerical models for the two-phase flow in stepped spillways, this result offers a very encouraging outcome. Further, since it is relatively easy to implement, we believe it could be included as well in other software packages.

ACKNOWLEDGMENTS The authors acknowledge the support of the Portuguese National Science Foundation (FCT), through Project PTDC/ECM/108128/2008. Currently, IM is supported by FCT, Grant No. SFRH/BD/38003/2007.

NOTATION

L - streamwise coordinate originating at the upstream end of the spillway;
k_s - roughness height perpendicular to the pseudo-bottom;
θ - spillway slope;
F_* - roughness Froude number ($F_* = q_w \Big/ \sqrt{g \sin\theta \, k_s^3}$);
d - equivalent clear-water depth;
δ - boundary layer thickness;
L_i - location of the inception point;
d_i - equivalent clear-water depth at the inception point;
ε - dissipation rate of TKE (DTKE);
ρ_0 - reference density;
g_n - component of the vector of the acceleration of gravity in the direction normal to the free surface;
σ - coefficient of surface tension;
A_s - surface area;
C_{air} - fraction of the surface area that is occupied by the perturbation;
C_μ - coefficient equal to 0.09;
k - turbulent kinetic energy (TKE);
$\left(\overline{u_{m_i}' u_{m_j}'}\right)$ - Reynolds stresses;
P_T - disturbance *energy* per unit volume;
L_T - size of the disturbance at the free surface;
P_D - *energy* of the stabilizing forces;
δV - volume of air;
r_1 and r_2 - two principal radii of curvature of the deformation of the free surface;
A - area of the surface disturbance;
h - step heights;
q_w - unit discharge.

REFERENCES

Amador, A., Sanchez-Juny, M., Dolz, J. (2006). "Characterization of the non-aerated flow region in a stepped spillway by PIV." J. Fluid Eng., ASME, 138(6), 1266-1273.

Amador, A., Sanchez-Juny, M., and Dolz, J. (2009). "Developing flow region and pressure fluctuations on steeply sloping stepped spillways." J. Hyd. Eng., ASCE, 135(12), 1092-1100.

André, M. and Ramos, P. (2003). "Hidráulica de descarregadores de cheia em degraus: aplicação a descarregadores com paredes convergentes. " Graduate Research Report. IST, Lisbon, Portugal (in Portuguese).

Bauer, W. J. (1954). "Turbulent boundary layer on steep slopes." Transactions, ASCE, 119, 1212-1233.

Boes, R. M., and Hager, W. H. (2003a). "Two phase flow characteristics of stepped spillways." J. Hydr. Eng., ASCE, 129(9), 661-670.

Boes, R. M., and Hager, W. H. (2003b). "Hydraulic design of stepped spillways." J. Hydr. Eng., ASCE, 129(9), 671-679.

Bombardelli, F. A. (2003). "Characterization of coherent structures from parallel, les computations of wandering effects in bubble plumes." Proc. 2003 World Water and Environmental Resources Congress, Environmental & Water Resources Institute (EWRI), ASCE, Philadelphia, PA, USA, P. Bizier and P. DeBarry (eds.). (In CD.)

Bombardelli, F. A. (2004). "Turbulence in multiphase models for aeration bubble plumes." Ph.D. thesis. University of Illinois at Urbana-Champaign.

Bombardelli, F. A. and García, M. H. (2003). "Hydraulic design of large-diameter pipes." J. Hydr. Eng., ASCE, 129(11), 839-846.

Bombardelli, F. A., and Jha, S. K. (2009). "Hierarchical modeling of dilute, suspended-sediment transport in open channels." Environ. Fluid Mech., 9(2), 207-230.

Bombardelli, F. A., Buscaglia, G. C., Rehmann, C. R., Rincón, L. E., and García, M. H. (2007). "Modeling and scaling of aeration bubble plumes: a two-phase flow analysis." J. Hyd. Res., IAHR, 45(5), 617-630.

Bombardelli, F. A., Hirt, C. W., and García, M. H. (2001). "Discussion on 'Computations of curved free surface water flow on spiral concentrators', by Matthews et al." J. Hydr. Eng., ASCE, 127(7), 629-631.

Bombardelli, F. A., Meireles, I. and Matos, J. (2010). "Laboratory measurements and multi-block numerical simulations of the mean flow and turbulence in the non-aerated skimming flow region of steep stepped spillways." Env. Fluid Mechanics, Springer (published online).

Buscaglia, G. C., Bombardelli, F. A., and García, M. H. (2002). “Numerical modeling of large scale bubble plumes accounting for mass transfer effects.” Int. J. Multiphase Flow, 28, 1763-1785.

Cain, P., and Wood, I. R. (1981). “Measurements of self-aerated flow on a spillway.” J. Hydr. Eng., ASCE, 107(HY11), 1407-1424.

Chanson, H. (1996). “Air bubble entrainment in free-surface turbulent shear flows. ” Academic Press, London, UK

Chanson, H. (2002). “The hydraulics of stepped chutes and spillways.” Balkema, Lisse, The Netherlands.

Chanson, H. (2004). "Environmental hydraulics of open channel flows." Elsevier-Butterworth-Heinemann, Oxford, UK.

Chanson, H. (2009). “Turbulent air-water flows in hydraulic structures: dynamic similarity and scale effects.” Environ. Fluid Mech., 9(2), 125-142.

Chow, V. T. (1959). “Open-channel hydraulics.” McGraw-Hill, USA.

Djenidi, L., Elavarasan, R., and Antonia, R.A. (1999). “The turbulent boundary layer over transverse square cavities.” J. Fluid Mech., 395, 271-294.

Falvey, H.T. and Ervine, D.A. (1988). "Aeration in jets and high velocity flows." Intl Symp. on Model-Prototype Correlation in Hydraulic Structures, ASCE-IAHR, Colorado, USA, 25-55.

Felder, S., and Chanson, H. (2009). “Energy dissipation, flow resistance, and gas liquid interfacial area in skimming flows on moderate-slope stepped spillways.” Environmental Fluid Mechanics, 9(4), 427-441.

Ferrando, A.M., and Rico, J.R. (2002). “On the incipient aerated flow in chutes and spillways.” J. Hyd. Res., IAHR, 40(1), 95-97.

Ferziger, J. H., and Peric, M. (2002). “Computational methods for fluid dynamics.” Springer.

Flow Science, Inc. (2008). FLOW-3D User’s Manual, Version 9.3, Los Alamos, New Mexico, USA.

Gioia, G., and Bombardelli, F. A. (2002). “Scaling and similarity in rough channel flows.” Phys. Rev. Lett., 88(1), 014501.

Gomes, J., Amador, A., Marques, M., Matos, J., and Sánchez-Juny, M. (2006). “Hydrodynamic pressure field on steeply sloping stepped spillways.” Proc., of the Int. Junior Researcher and Eng. Workshop on Hyd. Structures. J. Matos and H. Chanson, eds., Report CH61/06, Div. of Civil Eng., The University of Queensland, Brisbane, Australia.

Gonzalez, C., and Chanson, H. (2007). “Hydraulic design of stepped spillways and downstream energy dissipators for embankment dams.” Dam Engineering, Vol. XVII(4), 223-244.

Halbronn, G. (1952). “Etude de la mise en régime des écoulements sur les ouvrages à forte pente: application au problème de l'entrainement d'air.” La Houille Blanche, 7(5/6), 347-371 (in French).

Halbronn, G., (1954). “Discussion on 'Turbulent boundary layer on steep slopes.' by Bauer”, Transactions ASCE, 119,1234–1242.

Harlow, F.H., and Nakayama, P.I. (1967). “Turbulence transport equations.” Phys. of Fluids, 10, 2323.

Hickox, H. (1945). “Air entrainment on spillway faces.” Civil Eng., 15(12), 562-563.

Hirt, C. W., and Nichols, B. D. (1981). “Volume of Fluid (VOF) Method for the dynamics of free boundaries.” J. Comp. Physics, 39, 201-225.

Hirt, C. W., and Sicilian, J. M. (1985). “A porosity technique for the definition of obstacles in rectangular cell meshes.” Proc. 4th Int. Conf. Ship Hydro., National Academy of Science, Washington, DC, USA.

Hirt, C. W. (2003). “Modeling turbulent entrainment of air at a free surface.” Technical Note 61, Flow Science, Inc. (FSi-03-TN61).

Hrenya, C. M., and Sinclair, J. L. (1997). “Effects of particle-phase turbulence in gas-solid flows.” AIChE J., 43(4), 853-869.

Jiménez, J. (2004). “Turbulent flows over rough walls.” Annual Review of Fluid Mechanics, 36, 173-196.

Johnson, M. C., and Savage, B. M. (2006). “Physical and numerical comparison of flow over ogee spillway in the presence of tailwater.” J. Hydr. Eng., ASCE, 132(12), 1353-1357.

Keller, R.J., Lai, K.K. and Wood, I.R. (1974). “Developing region in self-aerated flows.” J. Hydraul. Div. (ASCE) 100(HY4), 553–568.

Lane, E.W. (1939). “Entrainment of air in swiftly flowing water. “ Civil Eng., 9(2), 89-91.

Matos (1999). "Emulsionamento de ar e dissipação de energia do escoamento em descarregadores em degraus." Ph.D. thesis, IST, Lisbon, Portugal (in Portuguese).

Matos, J. (2000). “Hydraulic design of stepped spillways over RCC dams.” Proc. 1st Int. Workshop on Hydraulics of Stepped Spillway, Zurich, Switzerland, A. A. Balkema Publisher, Rotterdam, The Netherlands, 187-194.

Matos, J., and Frizell, K. W. (1997). “Air concentration measurements in highly turbulent aerated flow”. Proc. 27th IAHR Congress, Theme D, Vol. 1, San Francisco, USA, S. S. Y. Wang and T. Carstens (eds.), 149-154.

Matos, J., and Frizell, K. W. (2000). “Air concentration and velocity measurements on self-aerated flow down stepped chutes.” Proc. ASCE 2000 Conference, Minneapolis, USA.

Matos, J., Frizell, K. H., André, S., and Frizell, K. W. (2002). “On the performance of velocity measurement techniques in air-water flows”. Proc. EWRI/IAHR Joint Conference on Hydraulic Measurements & Experimental Methods, ASCE, Estes Park, USA.

Matos, J., Sanchéz, M., Quintela, A., and Dolz, J. (2000). "Air entrainment and safety against cavitation damage in stepped spillways over RCC dams". Proc. 1st International Workshop on Hydraulics of Stepped Spillway, Zurich, Switzerland.

Meireles, I., and Matos, J. (2009). "Skimming flow in the non-aerated region of stepped spillways over embankment dams." J. Hydr. Eng., ASCE, 135(8), 685-689.

Meireles, I., Matos, J., and Melo, J. F. (2006). "Skimming flow properties upstream of air entrainment inception on steeply sloping stepped chutes." Proc. Int. Symposium on Hydraulic Structures, IAHR, Ciudad Guayana, Venezuela. (In CD.)

Meireles, I. (2011). "Hydraulics of stepped chutes: experimental-numerical-theoretical study." Ph.D. thesis. University of Aveiro, Aveiro, Portugal.

Meireles, I., Matos, J., Bombardelli, F.A. and Renna, F. (2011a). "On the prediction of the characteristic hydraulic parameters of the non-aerated skimming flow down steep stepped spillways." (in preparation).

Meireles, I., Bombardelli, F.A., and Matos, J. (2011b). "Boundary-layer development, self-similar velocity profiles, inception point location and turbulence in the non-aerated skimming flow region of steep stepped spillways." (in preparation).

Ohtsu, I., Yasuda, Y., and Takahashi, M. (2004). "Flow characteristics of skimming flows in stepped channels." J. Hydr. Eng., ASCE, 130(9), 860-869.

Relvas, A. T. and Pinheiro, A. N. (2008). "Inception point and air concentration in flows on stepped chutes lined with wedge-shaped concrete blocks" J. Hydr. Eng., ASCE, 134(8), 1042-1051.

Renna, F. (2004). "Caratterizzazione fenomenologica del moto di un fluido bifasico lungo scaricatori a gradini." PhD thesis, Politecnico di Bari, Cosenza, Italy (in Italian).

Sánchez-Juny, M., Bladé, E., and Dolz, J. (2008). "Analysis of pressures on a stepped spillway." J. Hydr. Res., IAHR, 46(3), 410-414.

Savage, B. M., and Johnson, M. C. (2001). "Flow over ogee spillway: physical and numerical model case study." J. Hydr. Eng., ASCE, 127(8), 640-649.

Smart, G.M., Duncan M.J., and Walsh J.M. (2002). "Relatively rough flow resistance equations." J. Hyd. Eng., ASCE, 128(6), 568-78.

Tozzi, M. J. (1992). "Caracterização/comportamento de escoamentos em vertedouros com paramento em degraus." Ph.D. thesis, Escola Politécnica da Universidade de S. Paulo, Brazil (in Portuguese).

Volkart, P. (1980). "The mechanism of air bubble entrainment in self-aerated flow." Int. J. of Multiphase Flow, Pergamon/Elsevier, 6, 411-423.

Wilhelms, S. C., and Gulliver, J. S. (2005). "Bubbles and waves description of self-aerated spillway flow." J. Hydr. Res., IAHR, 43(5), 522-531.

Wood, I. R. (1991). “Free-surface air entrainment on spillways”. Air entrainment in free-surface flows, Ed. Ian R. Wood, IAHR, Hydraulic Structures Design Manual nº 4, Hydraulic Design Considerations, Balkema, 55-84.

5.4 EXPERIMENTAL AND NUMERICAL INVESTIGATION OF THE NON-AERATED SKIMMING FLOW ON STEPPED SPILLWAYS OVER EMBANKMENT DAMS

Sub-chapter 5.4 was published in the proceedings of the 1st European IAHR congress in May 2010. The authors are I. Meireles, F. A. Bombardelli and J. Matos.

This subchapter concerns to numerical results obtained with *Flow-3D*® simulating the 1V:2H slope stepped channel of IST and is focused on the hydraulic characteristics of the skimming flow in the non-aerated region, presenting a comparison between experimental and numerical data.

ABSTRACT 5.4-1

1. INTRODUCTION 5.4-1

2. PHYSICAL MODEL 5.4-2

3. NUMERICAL MODEL 5.4-3

   3.1. Governing equations 5.4-3

   3.2. Boundary conditions 5.4-4

   3.3. Numerical model implementation 5.4-4

4. RESULTS 5.4-5

   4.1. Discharge 5.4-5

   4.2. Water depth 5.4-5

   4.3. Velocity distribution 5.4-6

5. FINAL REMARKS 5.4-7

REFERENCES 5.4-8

EXPERIMENTAL AND NUMERICAL INVESTIGATION OF THE NON-AERATED SKIMMING FLOW ON STEPPED SPILLWAYS OVER EMBANKMENT DAMS

ABSTRACT

The majority of studies on the hydraulics of stepped spillways has been centered in the air-water flow region and undertaken with the use of physical models. However, for certain geometry, higher discharges can lead to a non-aerated flow along the spillway, of special interest in small embankment dams designed for relatively large overtopping flows. Moreover, the increasing capabilities of computers, both in terms of software and hardware, provide new opportunities to make use of computational fluid dynamics (CFD) to analyze the flow in the non-aerated and aerated regions of stepped spillways.

A study was completed to compare water depth, velocity and discharge data on the non-aerated flow region of a stepped spillway using both physical and numerical models. Experimental data was acquired in a physical model assembled at the IST, Technical University of Lisbon, Portugal. The model is 0.50 m high (from crest to toe), has a slope of 1V:2H, and a width of 0.70 m. A step height of 5.0 cm was tested, for unit discharges corresponding to the skimming flow regime. Additionally, a commercially available code was used to reproduce the experimental conditions.

A good agreement between numerical and experimental results is shown, indicating that numerical models can be used as a complementary tool in the design and analysis of the flow in stepped spillways.

---

1. INTRODUCTION

The high standards of current lifestyle and awareness of the impacts of a dam failure (e.g., loss of life, cost of rebuilding the dam, cost of damage downstream and loss of a source of water supply) lead to the need of increasing the degree of safety provided by the design flood. In addition, the new concepts and methods of estimating extreme floods frequently lead to the need of increasing spillway capacity. In embankment dams, an increase in spillway capacity can be obtained by allowing the dam overtopping with the use of roller compacted concrete (RCC) as a protective system, which drives naturally to a downstream stepped face.

In general, the growth of the boundary layer is faster than in conventional spillways and the entrainment of air in the flow occurs close to the crest. A number of papers has been published to

address the air-water flow in stepped spillways with slope typical of that found on embankment dams (e.g., Boes and Hager 2003a, b, Ohtsu et al. 2004, André 2004, Gonzalez and Chanson 2008, Felder and Chanson 2009). For certain geometry, higher discharges can lead to a significant non-aerated flow region along the spillway, of special interest in small embankment dams designed for experiencing relatively large overtopping flows. Nevertheless, only a small number of studies has focused the non-aerated flow on stepped spillways over embankment dams (Meireles et al. 2006, Gonzalez and Chanson 2007, Meireles and Matos 2009).

Traditionally, investigation on stepped spillways has been conducted with physical models. The increasing capabilities of computers, both in terms of software and hardware, led to the raise of new studies centered in the numerical simulation of the hydraulics of stepped spillways (Chen et al. 2002, Cheng et al. 2004a, b, Tabbara et al. 2005, Arantes 2007, Carvalho and Amador 2008). However, a systematic study which permits to validate numerical models for flows down stepped spillways is still unavailable. This paper presents preliminary results of an ongoing research on numerical modeling of stepped spillways.

2. PHYSICAL MODEL

The experimental facility comprises a broad-crested weir followed by a stepped chute, a stilling basin and a recirculation system assembled at the Laboratory of Hydraulics and Water Resources, IST, Lisbon, Portugal (Fig. 1). The stepped chute is 0.5 m high (from crest to toe), 0.7 m wide, and has a slope of 1V:2H (26.6 degrees from horizontal). The stilling basin is 3.7 m long and 0.7 m wide, and the overshot gate located in its downstream end allows the formation of a hydraulic jump. For more information see Meireles and Matos (1999). Presented tests were undertaken in the framework of the Graduate Research Report of André and Ramos (2003) and the Master of Science Thesis of Cabrita (2007) for a step height of 0.05 m and unit water discharges (q_w) ranging from 0.05 to 0.07 m^2/s, corresponding to the skimming flow regime.

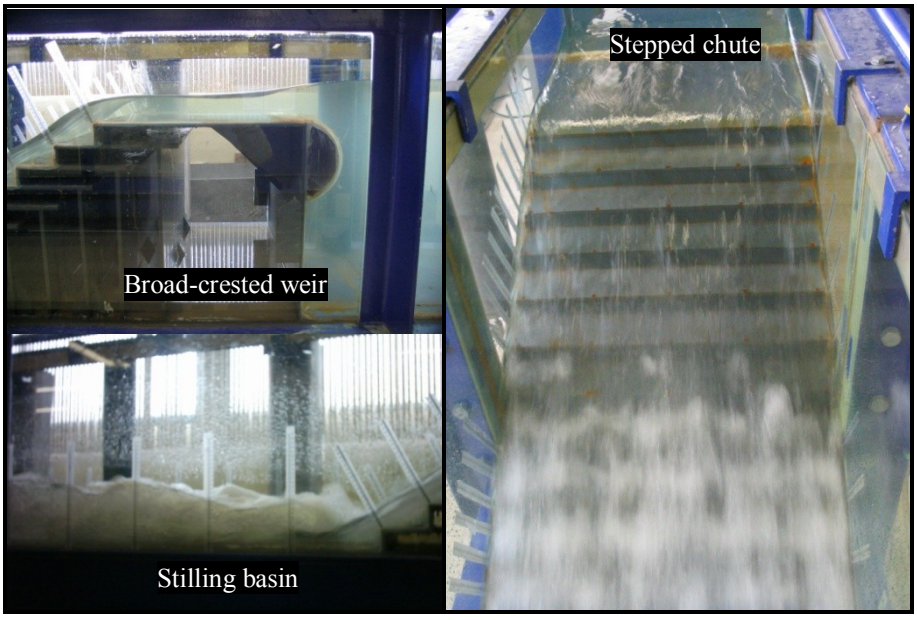

Fig. 1 - Experimental facility.

Along the non-aerated region, clear-water depth (d) and velocity (V) were measured in the chute centerline with a point gauge with a reading accuracy of ± 0.1 mm and a Prandtl-Pitot tube with 8 mm external diameter. The discharge was measured with an electromagnetic flowmeter installed in the supply pipe.

3. NUMERICAL MODEL

FLOW-3D® is a general purpose computational fluid dynamics (CFD) program for modeling a wide variety of fluid flow and heat transfer phenomena (Flow Science 2008). It uses the finite volume/finite differences method to solve the full three-dimensional equations of motion in a Cartesian, staggered grid. The full geometry is included in FLOW-3D® by the use of a "solid modeler", Computer-Aided-Design (CAD) files, or topographic data. After both the geometry and the grid are defined, the geometry is embedded in the computational grid using the Fractional Area-Volume Obstacle Representation (FAVOR™) technique (Hirt and Sicilian 1985). FAVOR™ is a porosity technique which catalogues cells between 0 and 1 expressing the fraction occupied by an object (resulting in 1 when completely filled with the object). This makes grid generation and geometry definition completely independent.

In FLOW-3D® free surface tracking is performed by the Volume-of-Fluid (VoF) method (Hirt and Nichols 1981), which requires three key elements to be implemented: locating the surface, maintaining sharp definition of free surface, and applying free-surface boundary conditions. The definition of cells in empty, full, or partially filled with fluid is similar to the FAVOR™ method.

3.1. GOVERNING EQUATIONS

The governing equations for a 3-D flow are as follows:

$$\nabla \cdot \underline{\bar{u}} = 0 \tag{1}$$

$$\frac{\partial\left(\rho_0\, \underline{\bar{u}}\right)}{\partial t} + \nabla \cdot \left(\rho_0\, \underline{\bar{u}} \otimes \underline{\bar{u}}\right) = \underline{B} - \nabla \bar{p} + \mu\, \nabla \cdot \left(\nabla \underline{\bar{u}} + \nabla \underline{\bar{u}}^{T}\right) - \nabla \cdot \left(\rho_0\, \overline{\underline{u}' \otimes \underline{u}'}\right) \tag{2}$$

where $\underline{\bar{u}}$ = time–averaged velocity vector; ρ_0 = reference density; $\underline{B}$ = vector of body forces (for this specific problem composed only of gravity); $\bar{p}$ = time–averaged pressure; μ = dynamic viscosity; t = time coordinate; and $\underline{u}'$ = fluctuating velocity vector. Additionally, $\otimes$ = tensor product; T = transpose of a tensor; and the underline indicates vectors. The Reynolds stresses, i.e., last term of eq. (2) is an additional unknown term to the original Navier-Stokes equations. To close the problem the standard RNG k-ε model was used.

Based on the observed 2-D nature of the flow, 2-D versions of the above equations were adopted herein, which is consistent with the procedure of Savage and Johnson (2001).

3.2. BOUNDARY CONDITIONS

The already described VoF model is used by FLOW-3D® to calculate the position of the free water surface. In this problem, pressure boundary conditions were specified in both upstream and downstream boundaries, in correspondence with values observed experimentally, and null velocities normal to the steps were imposed. The usual wall functions for the turbulence statistics were employed.

3.3. NUMERICAL MODEL IMPLEMENTATION

The geometry was generated by importing an Autocad file, based on the dimensions of the physical model. The entire set of steps in the spillway was considered, including the broad-crested weir, the upstream tank and the stilling basin downstream of the spillway toe. The domain is presented in Fig. 2. Cells are aligned with the flow down the spillway to obtain a faster convergence. Two domain removing components have been considered to deactivate two large open areas in the mesh that are likely to stay void of fluid and other solution quantities throughout the simulation. The reduction of active cells contributes to the minimization of memory and computational time. In fact, due to the shape and size of the obstacle geometry, adequate simulations with a single-block without any domain removing component would be too computer demanding. The small size of the steps and flow depth along the spillway requires a fine grid to correctly capture geometry and flow, but to reproduce the inflow and outflow conditions realistically, a large domain that includes the entire experimental set-up is necessary. It was observed that the single-block grid with domain removing components allowed for a fine grid that at the same time adapted to the obstacles geometry. Without the use of several blocks instead of only one, the so called multi-block gridding option, simulations avoided small errors usually associated with the transfer of information among inter-blocks. Nevertheless, a detailed study on the capabilities of the code with single- and multi-blocks should be carried out in the future.

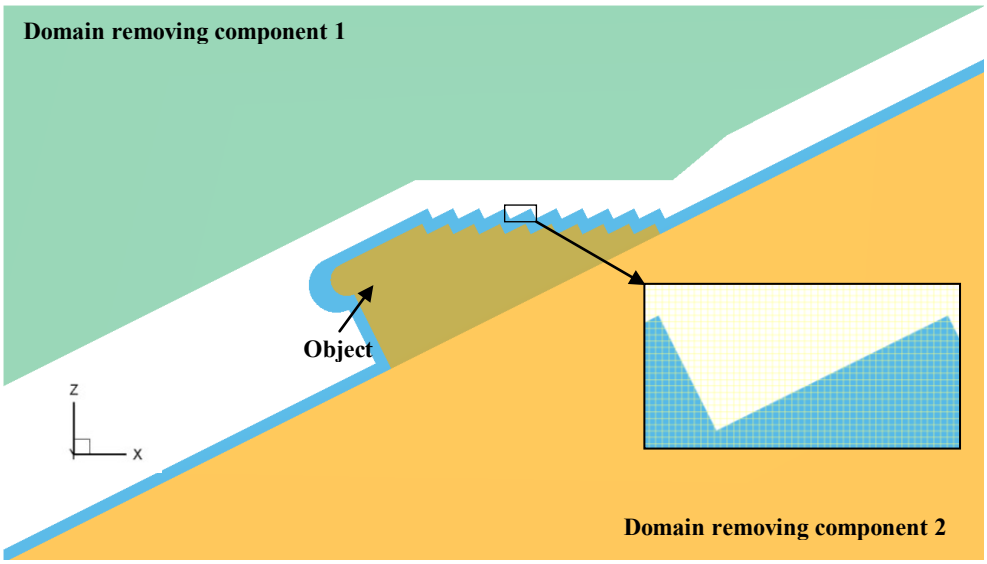

Fig. 2 - Computational domain.

Attention was given to mesh convergence, which can be defined as the reduction of the error when small meshes are used. This study shows results for a mesh of 1.6E+06 cells, which corresponds to cells of 2.5 (H) mm x 2.5 (V) mm in the entire domain.

4. RESULTS

The main objective of this study is to make a comparison between results obtained in a physical model and with a numerical model for skimming flow over a stepped spillway with slope typical of that found on embankment dams. Detailed comments on the results are presented bellow.

4.1. DISCHARGE

Because in the simulations water discharge was not imposed as boundary condition, the results of velocity in several sections along the chute have been integrated numerically to verify that the numerical model provided an accurate value of the discharge. The relative difference among experimental and numerical values was in average less than 4% for the three simulated discharges, which constitutes a satisfactory agreement. Relative difference is defined as $|\varphi_n-\varphi_e|/|\varphi_e| \times 100$, where φ_n is the value of an hydraulic parameter (e.g., discharge, water depth) obtained in the numerical model and φ_e is the correspondent value in the experimental model.

4.2. WATER DEPTH

As experimentally observed, the free surface exhibits a slightly wavy pattern along the non-aerated region with increasing amplitude downstream, having its maximum at the inception point. Comparison of measured and modeled water depths along the non-aerated region, for the discharge of 0.05 m^2/s, are presented in Fig. 3, where L is the streamwise coordinate originating at the upstream end of the spillway. Good agreement can be observed between both results with relative differences smaller than 6%. The main differences occurred at the inception point, where the wavy flow makes difficult to take accurate measurements.

Although for the discharges of 0.06 and 0.07 m^2/s there are no experimental data for comparison with the numerical solution, the writers employed the empirical formulae of Meireles and Matos (2009) to determine the water surface profile along the non-aerated region. The authors presented an expression for the normalized water depth ($d/d_i = f(L/L_i)$) along with expressions to determine the location of the inception point (L_i) and the correspondent clear-water depth (d_i) to be applied to spillways with slopes between 16 and 26.6º with horizontal and $F_* < 10$, where F_* is the roughness Froude number defined as $F_* = q_w \Big/ \sqrt{g \sin\theta\, k^3}$ (where g is the gravity acceleration and $k = h\cos\theta$, being h the step height). The differences between results are expressed in Fig. 4 for discharges of 0.06 and 0.07 m^2/s, along with the differences between experimental and numerical results for 0.05 m^2/s. Water depths compared quite favourably and relative differences between numerical and modeled or experimental results are in the same range.

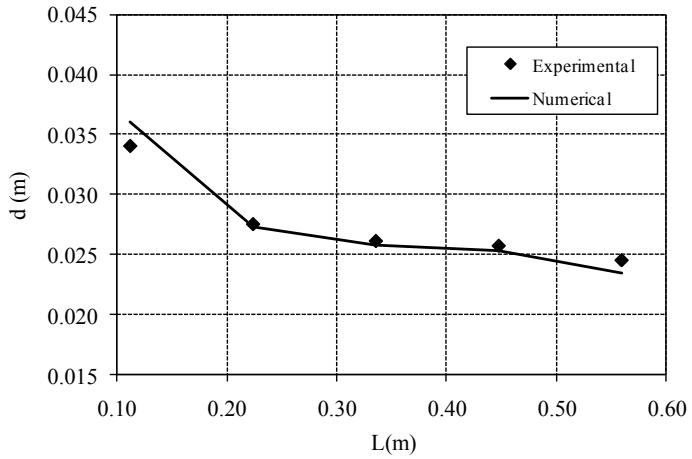

Fig. 3 – Clear-water depth: comparison between experimental and numerical results for q_w = 0.05 m^2/s.

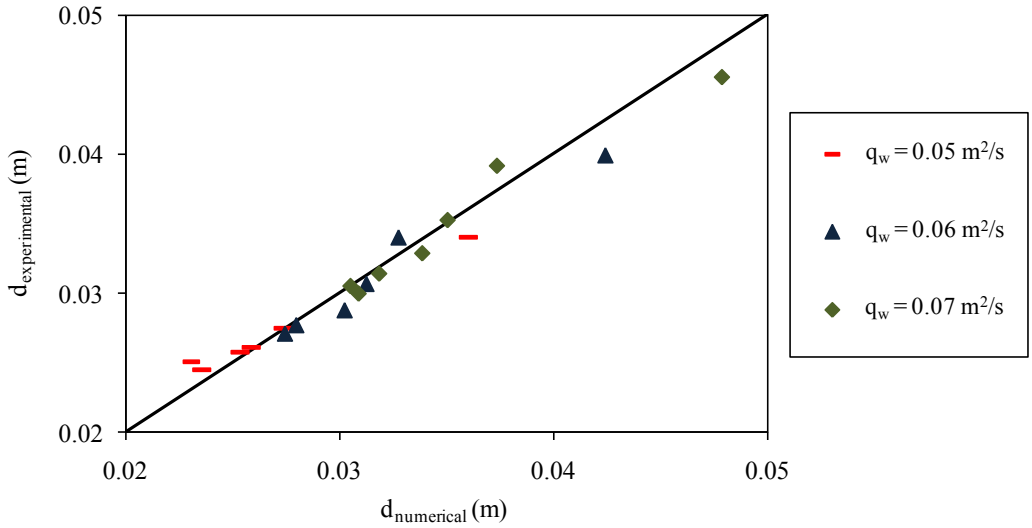

Fig. 4 – Clear-water depth: differences between experimental results (q_w = 0.05 m^2/s), results obtained with the empirical formulae of Meireles and Matos (2009) (q_w = 0.06-0.07 m^2/s) and numerical results.

4.3. VELOCITY DISTRIBUTION

In the non-aerated flow region close to the spillway crest, the boundary layer grows. At the point where the boundary layer reaches the free surface, entrainment of air starts taking place. This feature leads to differences in the velocity profiles along the non-aerated region. Near the crest, velocity profiles are almost constant with a fast increase in velocity near the pseudo-bottom (the surface tangent to the corner of the steps), revealing that the thickness of the boundary layer is still small (Fig. 5). The region of constant, or potential, velocity is decreasing downstream with the growth of the boundary layer and at the inception point has completely disappeared (Fig. 6). Simultaneously, the mean velocity increases downstream being at the inception point about 80% higher than in the beginning of the spillway. Both experimental and numerical results show this behaviour.

The shape of the velocity profiles obtained with FLOW-3D® follows relatively closely that of the experimental velocity profiles. Relative differences between experimental and numerical results were smaller than 10% in the steps belonging to the non-aerated region. At the inception point differences are larger (up to 20%) due to the difficulties of locating precisely the point experimentally. Examples of velocity profiles in the non-aerated flow and at the inception point are given in Figs 5 and 6, respectively, for the three studied discharges.

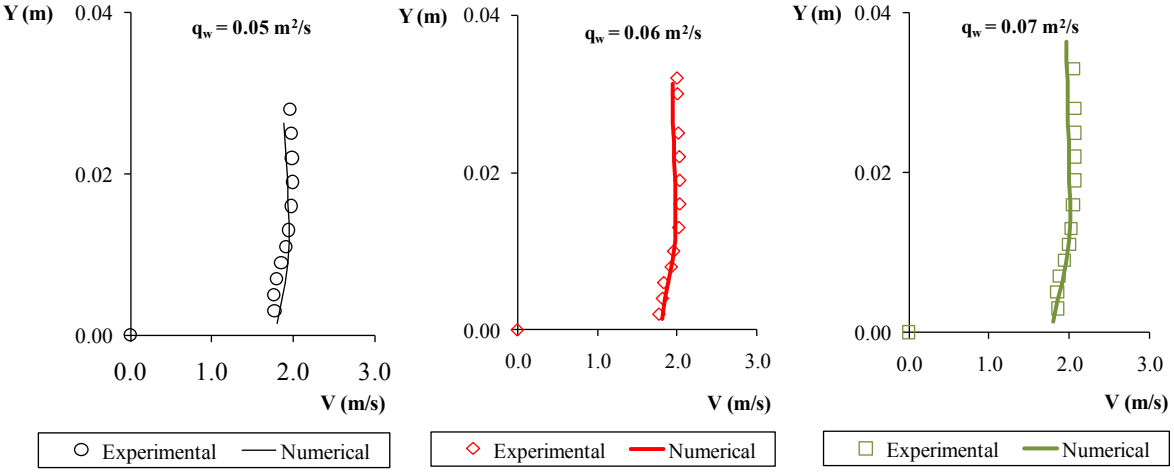

Fig. 5 – Velocity distribution: comparison between experimental and numerical results at L = 0.22 m.

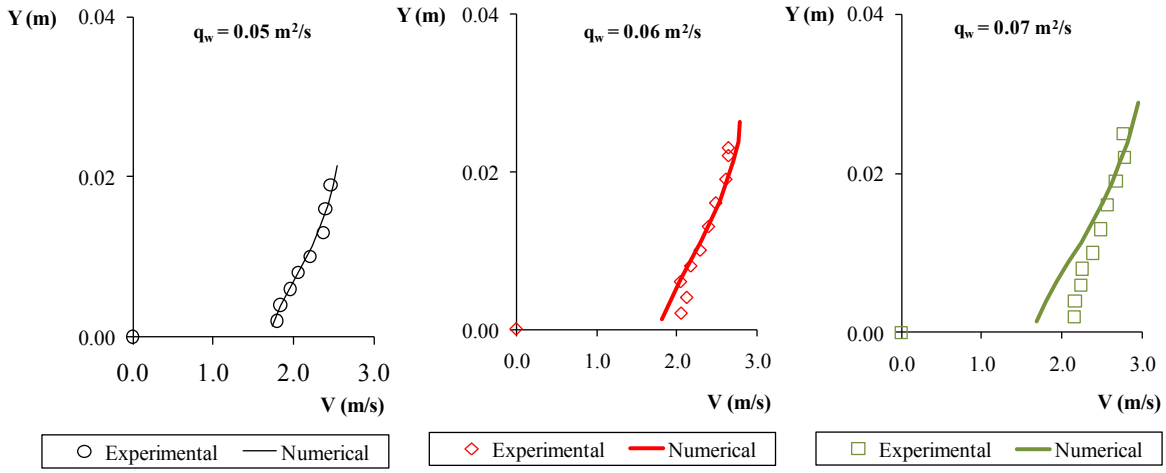

Fig. 6 – Velocity distribution: comparison between experimental and numerical results at the inception point.

5. FINAL REMARKS

This paper provides a first step in the validation of numerical codes to accurately reproduce the behaviour of the flow on stepped spillways. Present study is only focused in the non-aerated region of the flow along stepped spillways over embankment dams and makes use of a commercial code, FLOW-3D®.

The main flow characteristics predicted by the numerical model agreed well with the experiments. However, a more detailed study would be valuable. There is a need to further address issues like

the dependence of the results on the chosen turbulence model or the effect of using multi-block or single-block with domain removing components in the accuracy of the results and in the total computational time. The analysis of variables like the turbulent kinetic energy or the velocity field is also of interest.

The results presented in the paper show that numerical tools are sufficiently advanced to allow for an adequate representation of the main flow characteristics along the non-aerated region of stepped spillways. Water depth, velocity distribution and flow rate have been accurately predicted, with relative differences up to 9.8%.

Lastly, the results of this study are an indication that numerical models can be used in order to improve the understanding of the flow in stepped spillways, in general, or to help in practical specific cases. In fact, numerical methods start to provide practicing engineers with a complementary tool which can be used to help in the design, re-analysis and rehabilitation of stepped spillways, before performing physical model studies. This tool may be very useful in the re-evaluation of a dam spillway capacity for higher flows.

ACKNOWLEDGMENTS This study was supported by the Portuguese National Science Foundation (FCT), through Project PTDC/ECM/108128/2008. Currently, the first author is supported by a PhD scholarship granted by FCT (Grant No. SFRH/BD/38003/2007).

REFERENCES

André, M. and Ramos, P. (2003). "Hidráulica de descarregadores de cheia em degraus: aplicação a descarregadores com paredes convergentes." Graduate Research Report, IST, Lisbon, Portugal (in Portuguese).

André, S. (2004). "High velocity aerated flows over stepped chutes with macro-roughness elements." PhD thesis, EPFL, Lausanne, Switzerland.

Arantes, E. J. (2007). "Caracterização do escoamento sobre vertedouros em degraus via CFD." PhD thesis, EESC/USP, São Carlos, Brazil (in Portuguese).

Boes, R. M. and Hager, W. H. (2003a). "Two phase flow characteristics of stepped spillways." J. of Hydr. Eng., ASCE, 129(9), 661-670.

Boes, R. M. and Hager, W. H. (2003b). "Hydraulic design of stepped spillways." J. Hydr. Eng., ASCE, Vol. 129, No. 9, pp. 671-679.

Cabrita, J. (2007). "Caracterização do escoamento deslizante sobre turbilhões em descarregadores de cheias em degraus com paredes convergentes" MSc thesis, IST, Lisbon, Portugal (in Portuguese).

Carvalho, R. and Amador, A. (2008). "Physical and numerical investigation of the skimming flow over a stepped spillway." Proc. 3rd. IAHR Int. Symposium on Hydraulic Structures, Nanjing, China, 1767-1772. (In CD.)

Chen, Q., Dai, G. and Liu, H. (2002). “Volume of fluid model for turbulence numerical simulation of stepped spillway overflow.” J. Hydr. Eng., ASCE, 128(7), 683-688.

Cheng, X., Luo, L. and Zhao, W. (2004a). “Study of aeration in the water flow over stepped spillway.” Proc. World Water Congress 2004, ASCE, Salt Lake City, Utah, USA.

Cheng, X., Luo, L., Zhao, W. and Li, R. (2004b). “Two-phase flow simulation of aeration on stepped spillway.” Progress in Natural Science, 14(7), 626-630.

Felder, S. and Chanson, H. (2009). “Energy dissipation, flow resistance, and gas liquid interfacial area in skimming flows on moderate-slope stepped spillways.” Environmental Fluid Mechanics, 9(4), 427-441.

Flow Science (2008). FLOW-3D User’s Manuals Version 9.2.1. Flow Science, Inc., Los Alamos, New Mexico, USA.

Hirt, C. and Nichols, B. (1981). "Volume of Fluid (VOF) method for the dynamics of free boundaries." J. Comp. Physics, 39, 201-225

Gonzalez, C. and Chanson, H. (2007). “Hydraulic design of stepped spillways and downstream energy dissipators for embankment dams.” Dam Engineering, 17(4), 223-244.

Gonzalez, C. and Chanson H. (2008). “Turbulence and cavity recirculation in air-water skimming flows on a stepped spillway.” J. Hydr. Res., IAHR, 46(1), 65-72.

Hirt, C. and Sicilian, J. (1985). "A porosity technique for the definition of obstacles in rectangular cell meshes." Proc. Fourth Int. Conf. Ship Hydro., National Academy of Science, Washington, DC, USA.

Meireles, I., Cabrita, J. and Matos, J. (2006). “Non-aerated skimming flow properties on stepped chutes over embankment dams.” Proc. Intl Junior Researcher and Engineer Workshop on Hydraulic Structures, Montemor-o-Novo, Portugal, J. Matos and H. Chanson, eds., Report CH61/06, Div. of Civil Engineering, The University of Queensland, Brisbane, Australia, Dec., 91-99.

Meireles, I. and Matos, J. (2009). “Skimming flow in the non-aerated region of stepped spillways over embankment dams.” J. Hydr. Eng., ASCE, 135(8), 685-689.

Ohtsu, I., Yasuda, Y. and Takahashi, M. (2004). “Flow characteristics of skimming flows in stepped channels.” J. Hydr. Eng., ASCE, 130(9), 860-869.

Savage, B. M. and Johnson, M. C. (2001). “Flow over ogee spillway: physical and numerical model case study.” J. Hydr. Eng., ASCE, 127(8), 640-649.

Tabbara, M., Chatila, J., and Awwad, R. (2005). “Computational simulation of flow over stepped spillways.” Computers & Structures, Elsevier, 83, 2215-2224.

Chapter 6

Theoretical study

6.1 THEORETICAL MODEL OF THE MEAN FLOW IN THE NON-AERATED SKIMMING FLOW REGION OF STEEP STEPPED SPILLWAYS

This subchapter concerns to theoretical results obtained with a theoretical model developed based in the integration of the Navier-Stokes equations in the depth for the skimming flow in the non-aerated region. A comparison between experimental data of the 1V:0.75H slope stepped channel of LNEC and results of the theoretical model is also performed.

ABSTRACT 6.1.1

1. INTRODUCTION 6.1.1

2. EXPERIMENTAL SET-UP 6.1.2

3. THEORETICAL MODEL 6.1.4

3.1. Governing equations 6.1.4

3.2. Boundary-layer approximations 6.1.6

3.3. Vertically integrated balance equations 6.1.6

3.4. Theoretical model implementation 6.1.9

4. CONCLUSIONS 6.1.14

NOTATION 6.1.14

REFERENCES 6.1.15

THEORETICAL MODEL OF THE MEAN FLOW IN THE NON-AERATED SKIMMING FLOW REGION DOWN STEEP STEPPED SPILLWAYS

ABSTRACT

The majority of the research on stepped spillway hydraulics has been done experimentally. More recently, some authors have also attempted to approach this topic numerically. However, to the authors best knowledge, there is no evidence of a study centered in a theoretical model. This paper presents a theoretical model of the skimming water flow on steep stepped spillways. A simplified 1D theoretical model based on the integration of the Navier-Stokes equations in the depth was developed to predict the averaged characteristics of the flow. The results are in good agreement with the experiments acquired in a physical model constructed in the National Laboratory of Civil Engineering in Lisbon, Portugal.

Keywords: theoretical model, experimental measurements, turbulence, stepped spillway, skimming flow, RANS, non-aerated flow.

---

1. INTRODUCTION

The scientific interest on stepped spillways is noticed by the extensive research that has been developed over the past decades. The studies developed have been aimed at estimating the flow properties on stepped spillways for chute slopes typical of either embankment or concrete dams. There are experimental studies focused on flow properties upstream of the inception point (Amador et al. 2006, Meireles et al. 2006, Gonzalez and Chanson 2007, Hunt and Kadavy 2010) and downstream of the inception point, including the air concentration and velocity distribution (e.g., Gaston 1995, Chamani and Rajaratnam 1999, Matos 2000, Chanson 2001, Boes and Hager 2003a, Ohtsu et al. 2004, André 2004, Meireles 2004, Renna 2004, Gonzalez 2005) or the pressure field on the steps (e.g., Sánchez-Juny 2001, Yasuda and Ohtsu 2003, André 2004, Amador 2005, Gomes 2006). Empirical models have also been developed for predicting the main air-water flow properties along the chute, namely by Hager and Boes (2000), Matos (2000), Boes and Hager (2003a,b), Meireles (2004), Renna (2004) and Ohtsu et al. (2004). With the recent advances in computer software and hardware technology, new studies focused on numerical simulation of stepped spillway flows have also been presented (Chen et al. 2002, Cheng et al. 2004, Tabbara et al. 2005 and Arantes 2007).

One important aspect within the hydraulic performance of the skimming flow over stepped spillways is the location of the inception point. This marks the initiation of free-surface aeration and is a result of the interception the turbulent boundary with the overlaying region of irrotational flow (Falvey 1980), provided the turbulent energy at the free-surface is strong enough (Wood 1991).

Recently, there have been significant revisions of the peak discharge rates to be considered in the operation of existing dams, resulting in a growing interest in evaluating the hydraulic performance of existent stepped spillways. In addition, climatic changes studies point out for more extreme rain events in the future (e.g., Gordon et al. 1992; Trenberth 1998, 1999; Easterling et al. 2000). For high discharge scenarios, non-aerated flow conditions can occur on a significant part or even the total extent of the spillway. Contrarily to the need in characterizing and estimating the characteristics of the non-aerated flow region, at the moment only a reduced number of studies focused on this subject.

This research is aimed at developing a theoretical model of the water flow on the non-aerated flow region of steep stepped spillways. The Navier-Stokes equations are used has a starting base to predict the main characteristics of the non-aerated flow and a simplified 1D model is developed to determine the free-surface profile development. The results are in good agreement with the experiments acquired in a physical model constructed in the National Laboratory of Civil Engineering in Lisbon, Portugal and the experiments by Amador et al. (2009). To the best of our knowledge there has been no previous study aimed at developing a theoretical model of the flow over stepped spillways. However, some approaches have been recently presented for smooth spillways (e.g., Castro-Orgaz 2009).

The paper is organized as follows. In Section 2, the experimental facility and instrumentation are described. In Section 3 the theoretical model for the non-aerated flow region of steep stepped spillways is presented. Its implementation and comparison with experimental data are also presented in this section.

2. EXPERIMENTAL SET-UP

Experimental data was acquired in a large model assembled at the National Laboratory of Civil Engineering, LNEC (Fig. 1). The facility comprises an upstream reservoir, an uncontrolled WES crest (with variable size steps to follow the standard profile), a stepped chute 2.90 m high (from crest to toe) and 1.00 m wide with a slope of 1V:0.75H (53 degrees from horizontal), a stilling basin, and a recirculation system.

Studies of Matos (1999), Meireles (2004) and Renna (2004) were carried out for three different step heights (h) of 0.08, 0.04 and 0.02 m, respectively. Unit discharges (q_w) ranging from 0.05 to 0.20 m^2/s, corresponding to the skimming flow regime, were tested. In the present study only data from Matos 1999 and Meireles 2004 are analyzed.

In the zone of constant slope the local air concentration, C, and water velocity, V, were measured with a conductivity probe and a backflushing Pitot tube developed and calibrated by the U.S. Bureau of Reclamation. Velocity was thus obtained from:

$$V = \sqrt{\frac{2\,\Delta P}{\rho_w\ (1 - C)}} \tag{1}$$

where ΔP is the difference between the total pressure head and the static pressure head, measured with the back-flushing Pitot tube and ρ_w is the water density.

The clear-water depth was obtained from

$$\mathrm{H} = \int_0^{Y_\varphi} (1 - \mathrm{C})\,\mathrm{dy} \tag{2}$$

where $Y\varphi$ is the depth where the air concentration is φ%, assumed herein equal to 90%, as usually considered (e.g., Matos 2000; Chanson 2002; Boes and Hager 2003), and y is the transverse coordinate originating at the pseudo-bottom, defined herein as the surface tangent to consecutive step edges. The equivalent clear-water depth is a fictitious depth representing the flow depth when assuming the inexistence of free-surface undulation and of air bubbles in the flow (Meireles et al. 2011).

Figure 1 - Experimental facility and instrumentation (conductivity probe and back-flushing Pitot tube) at LNEC.

3. THEORETICAL MODEL

3.1. GOVERNING EQUATIONS

The geometry of the stepped spillway was assumed to be simply represented as presented in Figure 2. The cross-section is taken to be rectangular, although variation in the lateral direction is neglected (see Chow 1959), for what the flow is well described by two dimensions only. The x-coordinate is defined to be directed down the stepped spillway, tangentially to the pseudo-bottom (formed by the step edges), and the z-coordinate is directed upward, normal to the pseudo-bottom.

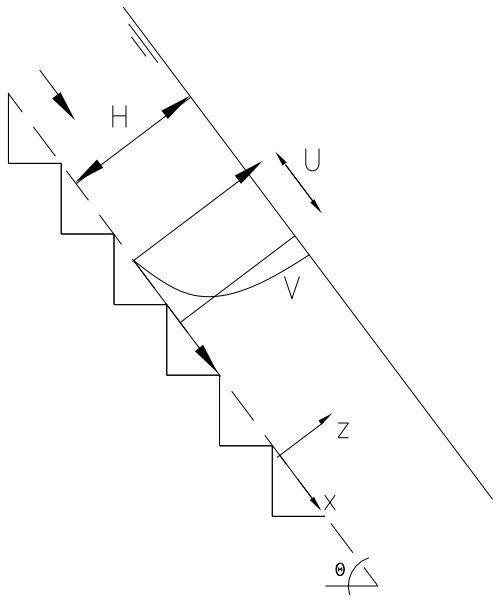

Figure 2 - Scheme of a stepped chute with constant slope.

In this case, the differential equations that govern the flow are:

Fluid mass conservation

$$\frac{\partial u}{\partial x}+\frac{\partial w}{\partial z}=0 \tag{2}$$

Momentum conservation

$$\text{x: } \rho\left[\frac{\partial u}{\partial t}+u\frac{\partial u}{\partial x}+w\frac{\partial u}{\partial z}\right]=-\frac{\partial p}{\partial x}+\mu\left(\frac{\partial^2 u}{\partial x^2}+\frac{\partial^2 u}{\partial z^2}\right)+\rho g_x \tag{3}$$

$$\text{z: } \rho\left[\frac{\partial w}{\partial t}+u\frac{\partial w}{\partial x}+w\frac{\partial w}{\partial z}\right]=-\frac{\partial p}{\partial z}+\mu\left(\frac{\partial^2 w}{\partial x^2}+\frac{\partial^2 w}{\partial z^2}\right)-\rho g_z \tag{4}$$

where ρ is the fluid density, u and w are the velocity components in x and z, respectively, t is the time, p is the pressure, μ is the dynamic viscosity, and $\vec{g}$ is the gravitational acceleration.

Due to the spillway angle with the horizontal, θ, the vector of gravitational acceleration can be decomposed into two components, $\vec{g} = (g_x; g_z) = (g\sin\theta; -g\cos\theta)$, and considering that

$$u\frac{\partial u}{\partial x} = \frac{1}{2}\frac{\partial(u^2)}{\partial x} \tag{4}$$

$$w\frac{\partial u}{\partial z} = \frac{\partial(uw)}{\partial z} + \frac{1}{2}\frac{\partial(u^2)}{\partial x} \tag{5}$$

replacing in (2) and (3), we obtain

$$\rho\left[\frac{\partial u}{\partial t} + \frac{\partial(u^2)}{\partial x} + \frac{\partial(uw)}{\partial z}\right] = -\frac{\partial p}{\partial x} + \mu\left(\frac{\partial^2 u}{\partial x^2} + \frac{\partial^2 u}{\partial z^2}\right) + \rho g\sin\theta \tag{6}$$

$$\rho\left[\frac{\partial w}{\partial t} + \frac{\partial(uw)}{\partial x} + \frac{\partial(w^2)}{\partial z}\right] = -\frac{\partial p}{\partial z} + \mu\left(\frac{\partial^2 w}{\partial x^2} + \frac{\partial^2 w}{\partial z^2}\right) - \rho g\cos\theta \tag{7}$$

Using the Reynolds decomposition, u, w and p are splitted into mean and a fluctuating parts (represented respectively by an over bar and a prime): $u = \bar{u} + u'$; $w = \bar{w} + w'$; $p = \bar{p} + p'$. Applying standard techniques to average (1), (6) and (7) over turbulence yields

Mean fluid mass conservation

$$\frac{\partial \bar{u}}{\partial x} + \frac{\partial \bar{w}}{\partial z} = 0 \tag{8}$$

Mean momentum conservation

$$\text{x: } \rho\left[\frac{\partial \bar{u}}{\partial t} + \frac{\partial(\bar{u}^2)}{\partial x} + \frac{\partial(\overline{u'^2})}{\partial x} + \frac{\partial(\bar{u}\bar{w})}{\partial z} + \frac{\partial(\overline{u'w'})}{\partial z}\right] = -\frac{\partial \bar{p}}{\partial x} + \mu\left(\frac{\partial^2 \bar{u}}{\partial x^2} + \frac{\partial^2 \bar{u}}{\partial z^2}\right) + \rho g\sin\theta \tag{9}$$

$$\text{z: } \rho\left[\frac{\partial \bar{w}}{\partial t} + \frac{\partial(\bar{u}\bar{w})}{\partial x} + \frac{\partial(\overline{u'w'})}{\partial x} + \frac{\partial(\bar{w}^2)}{\partial z} + \frac{\partial(\overline{w'^2})}{\partial z}\right] = -\frac{\partial \bar{p}}{\partial z} + \mu\left(\frac{\partial^2 \bar{w}}{\partial x^2} + \frac{\partial^2 \bar{w}}{\partial z^2}\right) - \rho g\cos\theta$$

(10)

Considering that $\nu = \mu/\rho$ and assuming the new terms as being additional stresses, (9) and (10) can be rewritten as follows:

$$\frac{\partial \bar{u}}{\partial t} + \frac{\partial(\bar{u}^2)}{\partial x} + \frac{\partial(\bar{u}\bar{w})}{\partial z} = -\frac{1}{\rho}\frac{\partial \bar{p}}{\partial x} + \nu\left(\frac{\partial^2 \bar{u}}{\partial x^2} + \frac{\partial^2 \bar{u}}{\partial z^2}\right) + g\sin\theta - \frac{\partial(\overline{u'^2})}{\partial x} - \frac{\partial(\overline{u'w'})}{\partial z} \tag{11}$$

$$\frac{\partial \overline{w}}{\partial t}+\frac{\partial\left(\overline{u}\,\overline{w}\right)}{\partial x}+\frac{\partial\left(\overline{w}^{2}\right)}{\partial z}=-\frac{1}{\rho}\frac{\partial \overline{p}}{\partial z}+\nu\left(\frac{\partial^{2}\overline{w}}{\partial x^{2}}+\frac{\partial^{2}\overline{w}}{\partial z^{2}}\right)-g\cos\theta-\frac{\partial\left(\overline{u'w'}\right)}{\partial x}-\frac{\partial\left(\overline{w'}^{2}\right)}{\partial z} \quad (12)$$

The last two terms of (11) and (12) denote the kinematic Reynolds stresses.

3.2. BOUNDARY-LAYER APPROXIMATIONS

The boundary-layer approximations for a two-dimensional flow down a stepped spillway are considered. As before, variation in the lateral (y) direction is neglected. Based on experimental observations, it is assumed that within this flow the scalings $u >> w$, $\frac{\partial}{\partial z} >> \frac{\partial}{\partial x}$, and $\frac{\partial^2}{\partial z^2} >> \frac{\partial^2}{\partial x^2}$ hold and that the distances in the x-direction are of order L and in the z-direction of order δ, where L is streamwise distance and δ is the boundary layer thickness. The flow regime is steady state and corresponds to large Reynolds numbers, implying that the pressure forces are of the order of the inertia forces (Pope 2000). Considering the continuity equation, we can say that $\frac{U}{L}\sim\frac{W}{\delta}$ or $W\sim\delta\frac{U}{L}$ (where $\sim$ is to be interpreted as "of order").

Under these constraints, the equations of mean momentum balance (11) and (12) become

$$\frac{\partial\left(\overline{u}^{2}\right)}{\partial x}+\frac{\partial\left(\overline{u}\,\overline{w}\right)}{\partial z}=-\frac{1}{\rho}\frac{\partial \overline{p}}{\partial x}+\nu\frac{\partial^{2}\overline{u}}{\partial z^{2}}+g\sin\theta-\frac{\partial\left(\overline{u'w'}\right)}{\partial z} \quad (13)$$

$$\frac{1}{\rho}\frac{\partial \overline{p}}{\partial z}+g\cos\theta=0 \quad (14)$$

3.3. VERTICALLY INTEGRATED BALANCE EQUATIONS

In order to reduce our model to 1-D, the integration in z has to be done. Integrating in the z-direction the equation of mean momentum balance in z, (14), yields the following relation

$$\int_0^{z^*}\frac{1}{\rho}\frac{\partial \overline{p}}{\partial z}dz=-g\cos\theta\int_0^{z^*}dz \quad (15)$$

where z* is the distance from the pseudo-bottom.

Considering that the wall is the pseudo-bottom, pressure at the wall is given by

$$\overline{p}_{wall}=\overline{p}_{|0}=\int_0^{H}\rho g\cos\theta dz \quad (16)$$

where H is the water depth.

Then, from (15) and (16) results that the pressure distribution in z is given by

$$-\frac{1}{\rho}\bar{p}_{|z^*} = -g\cos\theta\left(H - z^*\right) \tag{17}$$

which derived over x to obtain the variation along the spillway yields

$$-\frac{1}{\rho}\frac{\partial \bar{p}}{\partial x} = -g\cos\theta\frac{\partial}{\partial x}\left(H - z^*\right) = -g\cos\theta\frac{dH}{dx} \tag{18}$$

Now, the momentum balance in x, (13), integrates to yield

$$\begin{aligned}&\int_0^H \frac{\partial\left(\bar{u}^2\right)}{\partial x}dz + \int_0^H \frac{\partial\left(\bar{u}\bar{w}\right)}{\partial z}dz = -\int_0^H g\cos\theta\frac{dH}{dx}dz + \int_0^H \nu\frac{\partial^2\bar{u}}{\partial z^2}dz \\ &+\int_0^H g\sin\theta dz - \int_0^H \frac{\partial\left(\overline{u'w'}\right)}{\partial z}dz\end{aligned} \tag{19}$$

which is equal to

$$\begin{aligned}&\int_0^H \frac{\partial\left(\bar{u}^2\right)}{\partial x}dz + \bar{u}\bar{w}_{|H} - \bar{u}\bar{w}_{|0} = -g\cos\theta\int_0^H \frac{dH}{dx}dz \\ &+\nu\frac{\partial\bar{u}}{\partial z}\bigg|_H - \nu\frac{\partial\bar{u}}{\partial z}\bigg|_0 + g\sin\theta\int_0^H dz - \overline{u'w'}_{|H} + \overline{u'w'}_{|0}\end{aligned} \tag{20}$$

From this point on, it is necessary to make several assumptions in order to allow for a tractable model. The terms $\bar{u}\bar{w}_{|H}$ and $-\overline{u'w'}_{|H}$ can be disregarded because the flow velocity does not have average or fluctuating components in z at the free-surface ($z = H$). From the experiments of Amador (2005) and from results of CFD simulation (Bombardelli et al. 2010, Meireles et al. 2011) the velocity at the pseudo-bottom is also observed to be mainly one-dimensional. In this regard, $-\bar{u}\bar{w}_{|0}$ can disappear from (20). Since, by definition, the velocity in x is constant outside of the boundary layer, $\nu\partial\bar{u}/\partial z\big|_H$ is also null. Regarding the terms $-\nu\partial\bar{u}/\partial z\big|_0 + \overline{u'w'}_{|0}$ the shear stress (τ_w) can be obtained, by definition, as:

$$\frac{\tau_w}{\rho} = \nu\frac{\partial\bar{u}}{\partial z}\bigg|_0 - \overline{u'w'}\big|_0 \tag{21}$$

which includes shear stress due to water viscosity and shear stress induced by turbulence. At the pseudo-bottom $w' \neq 0$, thus,

$$-\nu\frac{\partial\bar{u}}{\partial z}\bigg|_0 + \overline{u'w'}_{|0} = -\frac{\tau_w}{\rho} \tag{22}$$

At this point, a new term can be introduced, the non-dimensional skin friction coefficient C_f, which corresponds to the normalization of the shear stress by a reference velocity (Pope 2000; Kundu and Cohen 2004)

$$C_f = \frac{\tau_w}{(1/2)\rho U^2} \tag{23}$$

which rearranged is equivalent to

$$-\frac{\tau_w}{\rho} = -\frac{1}{2} C_f U^2 \tag{24}$$

Putting all together, the momentum balance in x, (20), is reduced to

$$\int_0^H \frac{\partial \bar{u}^{-2}}{\partial x} dz = -g\cos\theta \int_0^H \frac{dH}{dx} dz + g\sin\theta \int_0^H dz - \frac{1}{2} C_f U^2 \tag{25}$$

and, applying the Leibniz rule to the left side term of the equation, it becomes

$$\frac{\partial}{\partial x}\int_0^H \bar{u}^{-2} dz - \frac{dH}{dx}\bar{u}^{-2}_{|H} = -g\cos\theta \int_0^H \frac{dH}{dx} dz + g\sin\theta \int_0^H dz - \frac{1}{2} C_f U^2 \tag{26}$$

For the first term of the right side, the derivative can go outside of the integral because H only depends on x (not on z)

$$\frac{\partial}{\partial x}\int_0^H \bar{u}^{-2} dz - \frac{dH}{dx}\bar{u}^{-2}_{|H} = -g\cos\theta \frac{dH}{dx}\int_0^H dz + g\sin\theta \int_0^H dz - \frac{1}{2} C_f U^2 \tag{27}$$

At this point we only have derivatives in x, therefore the PDE can be replaced by an ODE, resulting in

$$\frac{d}{dx}\int_0^H \bar{u}^{-2} dz - \frac{dH}{dx}\bar{u}^{-2}_{|H} = -g\cos\theta \frac{dH}{dx}\int_0^H dz + g\sin\theta \int_0^H dz - \frac{1}{2} C_f U^2 \tag{28}$$

Considering now the Kinematic Boundary Condition, we can say that

$$\frac{dH}{dt} + \bar{u}_{|H} \frac{dH}{dx} = \bar{w}_{|H} \tag{29}$$

Because we are in steady state and the velocity has only component in x at the free-surface, it reduces to

$$\bar{u}_{|H} \frac{dH}{dx} = 0 \tag{30}$$

and allows (28) to be rewritten into

$$\frac{d}{dx}\int_0^{H-2} u^2\,dz = -g\cos\theta\frac{dH}{dx}H + g\sin\theta H - \frac{1}{2}C_f U^2 \tag{31}$$

Adopting an experimental self-similar law for the longitudinal velocity of the type

$$\frac{\bar{u}(x,z)}{U(x)} = f\left(\frac{z}{H}\right) \tag{32}$$

and making mathematical manipulations, (31) becomes

$$\frac{d}{dx}U^2(x)H\beta = -g\cos\theta\frac{dH}{dx}H + g\sin\theta H - \frac{1}{2}C_f U^2 \tag{33}$$

where, by definition, the Boussinesq coefficient, β, is

$$\beta = \int_0^1 f^2\left(\frac{z}{H}\right)d\frac{z}{H} \tag{34}$$

Looking at the continuity equation, (8), its integration yields

$$\int_0^H \frac{\partial\bar{u}}{\partial x}dz + \int_0^H \frac{\partial\bar{w}}{\partial z}dz = 0 \tag{35}$$

Applying the Leibniz rule and resolving the second term, results

$$\frac{\partial}{\partial x}\int_0^H \bar{u}dz - \frac{dH}{dx}\bar{u}_{|H} + 0 + \bar{w}_{|H} - \bar{w}_{|0} = 0 \tag{36}$$

But $\bar{u}_{|H}(dH/dx) = 0$ due to the Kinematic Boundary Condition. As explained above in the paper, the terms $\bar{w}_{|H}$ and $\bar{w}_{|0}$ can be disregarded and the continuity equation reduces to its simpler form

$$\frac{d}{dx}UH = 0 \tag{37}$$

3.4. THEORETICAL MODEL IMPLEMENTATION

Substituting the skin friction coefficient by one fourth of the Darcy friction factor f (defined as $f = 8\tau_w/(\rho U^2)$ and applying the continuity equation, $q_w = UH$, (33) becomes

$$\frac{d}{dx}\left[\frac{q_w^{\,2}}{H}\beta\right] + g\cos\theta H\frac{dH}{dx} - g\sin\theta H + \frac{1}{8}f\frac{q_w^{\,2}}{H^2} = 0 \tag{40}$$

which is equal to

$$\frac{d}{dx}\left[\underbrace{\frac{q_w^{\,2}}{H}\beta+\frac{g\cos\theta}{2}H^2}_{E}\right]=\underbrace{g\sin\theta H-\frac{1}{8}f\frac{q_w^{\,2}}{H^2}}_{S} \tag{41}$$

Considering the quantity inside the integral a variable E and the terms on the right side S, (41) can be discretized into

$$\frac{E_{j+1}-E_j}{\Delta x}=-\frac{1}{2}\left[S(j)+S(j+1)\right] \tag{42}$$

Equation (42) can be solved numerically using the Newton-Raphson method

$$H_2^{\,i+1}=H_2^{\,i}-\frac{f\left(H_2^{\,i}\right)}{f'\left(H_2^{\,i}\right)} \tag{43}$$

where

$$\begin{aligned}f(H_2)=&\frac{1}{\Delta x}\left[\frac{q_w^{\,2}}{H_2}\beta_2+\frac{g\cos\theta}{2}H_2^{\,2}-\frac{q_w^{\,2}}{H_1}\beta_1-\frac{g\cos\theta}{2}H_1^{\,2}\right]+\\&+\frac{1}{2}\left[\frac{1}{8}f_1\frac{q_w^{\,2}}{H_1^{\,2}}-g\sin\theta H_1+\frac{1}{8}f_2\frac{q_w^{\,2}}{H_2^{\,2}}-g\sin\theta H_2\right]\end{aligned} \tag{44}$$

$$f'(H_2)=\frac{1}{\Delta x}\left[-\frac{q_w^{\,2}}{H_2^{\,2}}\beta_2+g\cos\theta H_2\right]+\frac{1}{2}\left[-\frac{1}{4}f_2\frac{q_w^{\,2}}{H_2^{\,3}}-g\sin\theta\right] \tag{45}$$

where β_i and f_i have to be known. For that intent, empirical expressions have to be developed, based in experimental measurements taken by the authors, for the equations to be resolved.

Considering the velocity power law, the Boussinesq coefficient can be given by

$$\beta=\left(\frac{u_{\max}}{(q_w/H)}\right)^2\frac{1}{H}\left[\left(\frac{N}{N+2}\right)\delta+(H-\delta)\right] \tag{46}$$

where $u_{\max}$ is the free-stream velocity, and $1/N$ is the velocity power law exponent.

From experimental data, the Boussinesq coefficient was computed from (46) and presented in Fig. 3 as a function of the dimensionless distance from the crest x/xi. For $0.36 \le x/x_i \le 1.00$ the Boussinesq coefficient can be predicted by:

$$\beta=1+6.109\cdot10^{-2}\left(\frac{x}{x_i}\right)^{1.318} \tag{47}$$

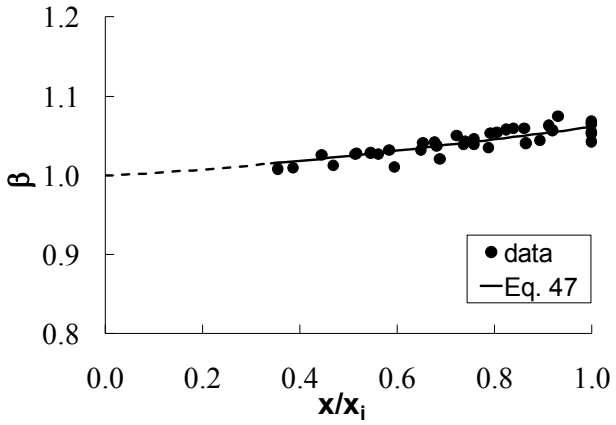

Figure 3 - Boussinesq coefficient: experimental data and empirical expression.

The friction factor is obtained from the expression proposed by Meireles et al. (2011):

$$f = \frac{8\,g\,C_n^{\,2}}{R_h^{\,1/3}}\,k_s^{\,2p} \tag{48}$$

where, from experimental data, and considering $a = 8\,g\,C_n^{\,2}$, a = 0.163 and p = 0.234.

Results for the equivalent clear-water depth and mean water velocity evolution are presented in Fig. 4 and 5, respectively. An excellent agreement is observed between model and experimental data, with observed relative differences mainly smaller than 5%. Fig. 6 presents a comparison with data obtained by Amador et al. (2009) with a PIV in a stepped model with slope 1V:0.8H, steps 0.05 m high and a unit discharge of 0.11 m^2/s. Relative differences between experimental and numerical data up to 6% are observed. It is also seen that although the experimental results are extremely well predicted by the theoretical model, the steady waves observed experimentally are not captured by the model, as a consequence of the assumptions considered to allow for a tractable model.

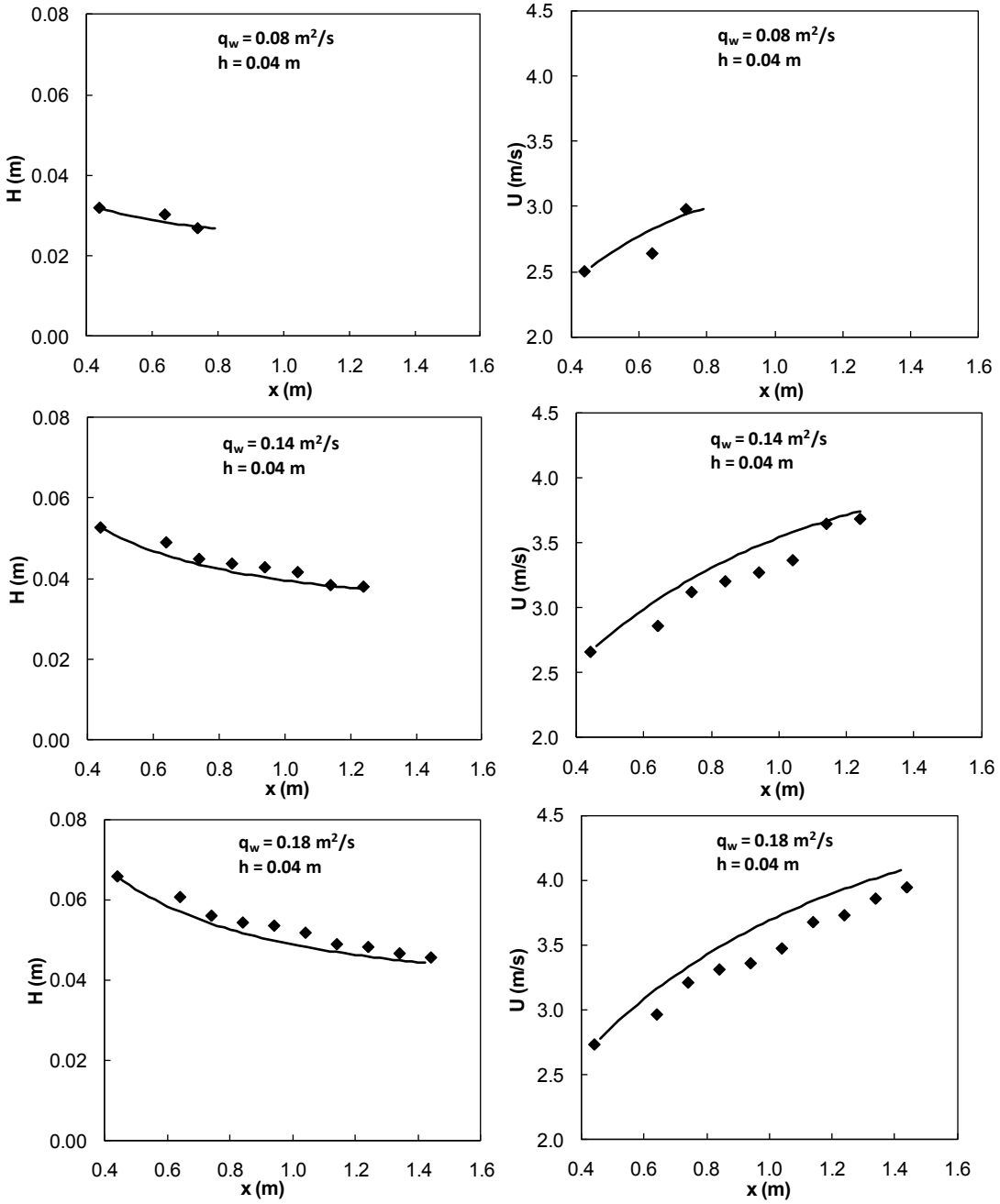

Figure 4 - Clear water depth and mean water velocity development: comparison between theoretical model and experimental results: h = 0.04 m.

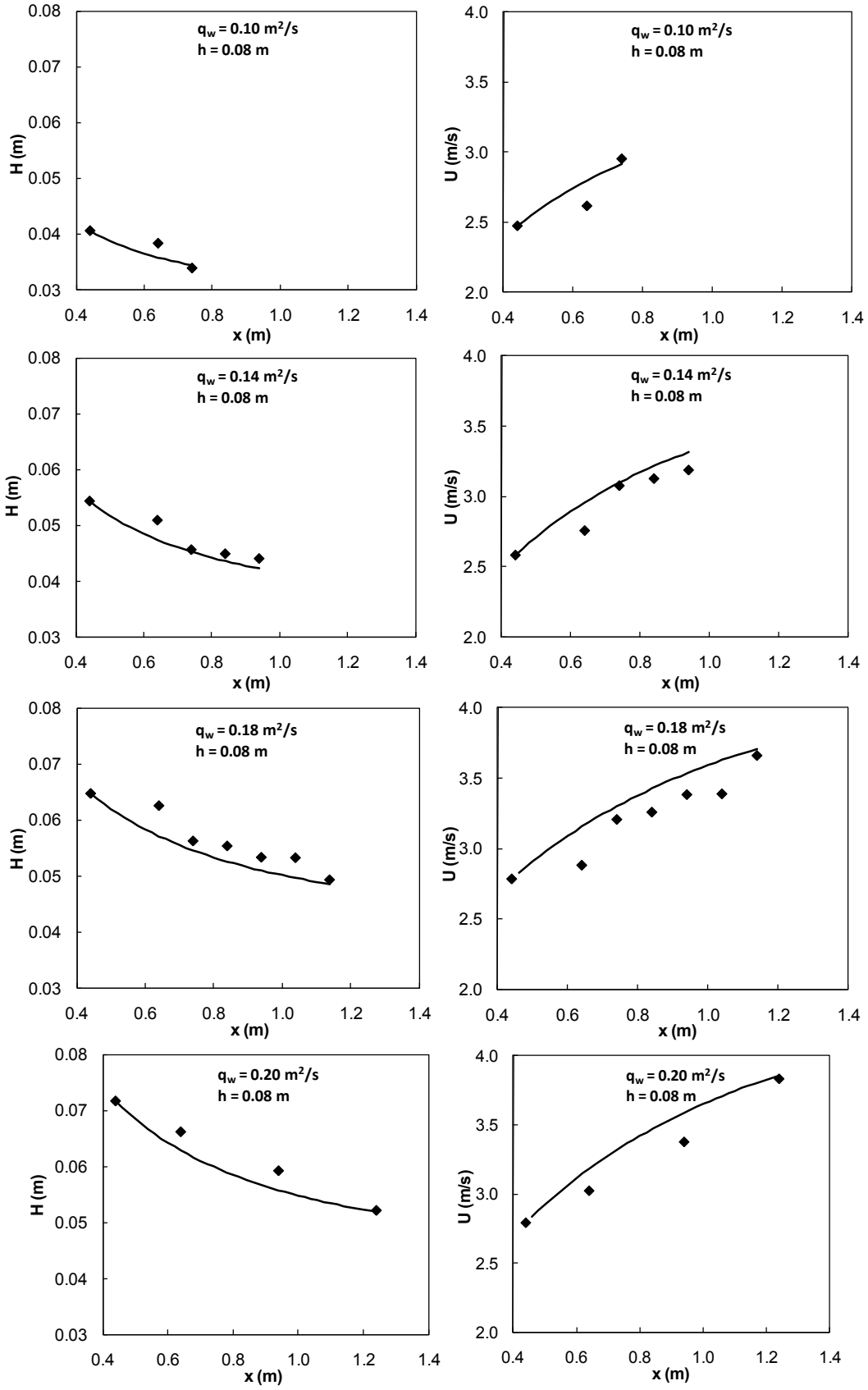

Figure 5 - Clear water depth and mean water velocity development: comparison between theoretical model and experimental results: h = 0.08 m.

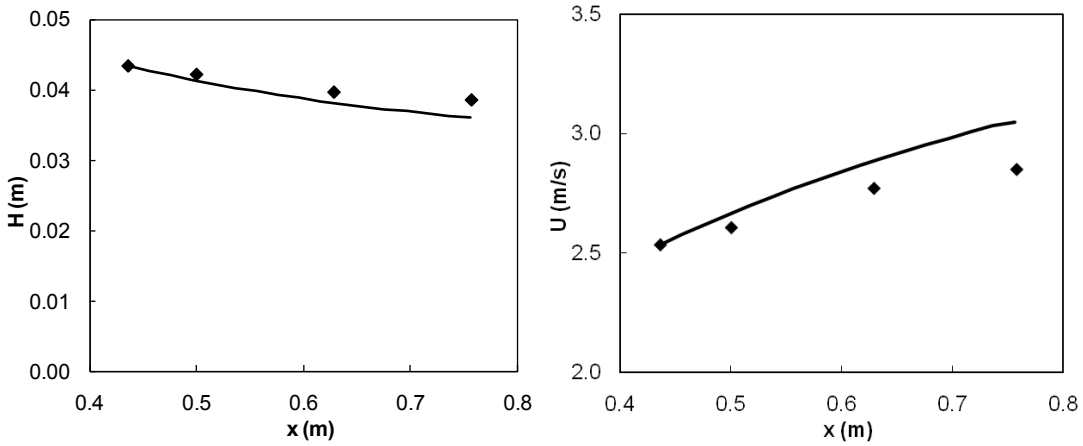

Figure 6 - Clear water depth and mean water velocity development: comparison between theoretical model and experimental results: h = 0.05 m and slope of 1V:0.8H (data from Amador et al. 2009, obtained from digitalization).

4. CONCLUSIONS

This study presents a simplified 1D theoretical model of the main flow in steep stepped chutes, derived directly from the Navier-Stokes equations. A comparison of the equivalent clear-water depth and mean water velocity results with experimental data shows extremely good agreement, indicating that the assumptions and simplifications considered in the model are adequate. However, the observed steady waves are not captured by the model.

ACKNOWLEDGMENTS The authors acknowledge the support of the Portuguese National Science Foundation (FCT), though Project PTDC/ECM/108128/2008. Currently, Inês Meireles is supported by FCT, Grant No. SFRH/BD/38003/2007.

NOTATION

C_f - non-dimensional skin friction coefficient;
E - total head;
f - Darcy friction factor;
g - gravitational acceleration;
H - clear-water depth;
p - pressure;
S_f - friction slope;
t - time;
U - mean averaged velocity;
u - velocity component in x;
u' - fluctuating term;
$\bar{u}$ - averaged term;
v - distance, in the vertical, from the reference;
w - velocity component in z;

x - coordinate directed down the stepped spillway tangential to the pseudo-bottom (formed by the step edges);

y - coordinate directed in the lateral direction;

z - coordinate directed upward, normal to the pseudo-bottom;

z^* - thickness of the boundary layer;

α - Coriolis coefficient;

β - Boussinesq coefficient;

μ - dynamic viscosity;

ρ - fluid density;

θ - spillway slope;

τ_w - shear stress.

REFERENCES

Amador, A. (2005). "Comportamiento hidráulico de los aliviaderos escalonados en presas de hormigón compactado. " Ph.D. thesis, UPC, Barcelona, Spain (in Spanish).

Amador, A., Sanchez-Juny, M., and Dolz, J. (2009). "Developing flow region and pressure fluctuations on steeply sloping stepped spillways." J. Hyd. Eng., ASCE, 135(12), 1092-1100.

Bombardelli, F. A., Meireles, I. and Matos, J. (2010). "Laboratory measurements and multi-block numerical simulations of the mean flow and turbulence in the non-aerated skimming flow region of steep stepped spillways." Env. Fluid Mechanics, Springer (published online).

Castro-Orgaz, O. (2009). "Hydraulics of developing chute flow." J. Hyd. Res., IAHR, 47(2), 185–194.

Chow, V.T. (1959). "Open-channel hydraulics." McGraw-Hill, USA.

Easterling D.R., Evans, J.L., Groisman, P.Y., Karl, T.R., Kunkel, K.E. and Ambenje, P. (2000). "Observed variability and trends in extreme climate events: a brief review." Bulletin of the American Meteorological Society, AMS, 81, 417-425.

Garcia (1996). "Hidrodinamica ambiental." Imprenta Lux, Santa Fé, Argentina (in Spanish).

Gordon, H.B.; Whetton, P.H.; Pittock, A.B.; Fowler, A.M. and Haylock, M.R. (1992). "Simulated changes in daily rainfall intensity due to the enhanced greenhouse effect: implications for extreme rainfall events." Climate Dynamics, 8, 83–102.

Hunt, S. L., and Kadavy, K. C. (2010). "Energy dissipation on flat-sloped stepped spillways: part 1. upstream of the inception point." Transactions, ASABE, 53(1), 103-109.

Kundu, P.K. and Cohen I.M. (2004). "Fluid Mechanics" Elsevier, USA.

Meireles I., Renna, F., Matos, J. and Bombardelli, F.A. (2011)."On the prediction of the hydraulic parameters of the non-aerated skimming flow down steep stepped spillway" (to be submitted for publication).

Meireles, M. (2004). “Emulsionamento de ar e dissipação de energia do escoamento em descarregadores em degraus.” MS thesis, IST, Lisbon, Portugal (in Portuguese).

Pope, S. B. (2000). “Turbulent flows.” Cambridge University Press, UK.

Trenberth, K.E. (1998). “Atmospheric moisture residence times and cycling implications for rainfall rates and climate change.” Climate Change, 39, 667–694.

Trenberth, K.E. (1999). “Conceptual framework for changes of extremes of the hydrological cucle with climate change.” Climate Change, 42, 327–339.

Chapter 7

Final considerations

7.1 SUMMARY OF THE MAIN CONCLUSIONS AND CONTRIBUTIONS

The analysis of the available literature showed a large number of studies focusing on the air-water skimming flow in stepped spillways, a limited number of studies focused on the non-aerated skimming flow in stepped spillways, and an almost complete lack of knowledge on the hydraulics of energy dissipators downstream of stepped spillways. These studies were performed, essentially, following an experimental approach, although some novel studies start to make use of Computational Fluid Dynamics (CFD) codes.

Skimming flows in stepped spillways are characterized as: 1. flows with possible coexistence of single- and two-phase flow regions; 2. flows in channels with large roughness; and 3. flows in channels with large slope. These features lead to complex mechanisms not completely known yet. In this context, the goal of this dissertation was to contribute to the knowledge of the mechanics of fluids of the skimming flow in stepped spillways. In that regard, the main contributions are the:

- Mechanistic characterization of the non-aerated flow and inception point (e.g., boundary layer development, friction factor, turbulence statistics).

- Characterization of the flow by a design approach, contributing with several easy to use empirical equations to help in the design of stepped spillways (e.g., clear-water depth, velocity, energy dissipation) and presenting conclusions on downstream energy dissipators flows.

- Implementation and validation of a CFD code, *FLOW-3D*®, for the non-aerated flow and inception point.

- Development of a theoretical model for the non-aerated flow.

One key element of this dissertation pertains to the validation of the commercial code *FLOW-3D*® to accurately reproduce the behavior of the skimming flow on stepped spillways. In this regard, the main conclusions are:

- The excellent match between experimental and numerical results in the non-aerated flow region of stepped channels allows to conclude that in the numerical simulations with *FLOW-3D*® the selected theoretical model and numerical integration were adequate for this flow region. In detail, *FLOW-3D*® was observed to simulate accurately discharge, velocity profiles, boundary layer thickness and water depth along the non-aerated flow region of steep stepped channels, and discharge, velocity profiles and water depth along the non-aerated flow region of moderate slope stepped channels. Reliable turbulent kinetic energy and turbulent kinetic energy dissipation fields were also observed, when comparing qualitatively with the experimental turbulent kinetic energy field presented by Amador et al. (2006) for a similar situation.

- The developed runs showed that the use of a k-ε model allows for an accurate representation of the flow features in the non-aerated flow region of stepped channels, since no significant differences were observed in the simulations with this closure and the *RNG* k-ε model.

- The multi-block gridding feature embedded in *FLOW-3D*®, which helps in optimizing the mesh, was crucial for saving computational time, and showed a clear advantage with respect to other techniques in other software packages.

- The air entrainment model used in *FLOW-3D*® was observed to predict accurately the location of the inception point of air entrainment. This is an extremely important conclusion, especially when the purpose is to model the two-phase flow located downstream.

Pertaining to the non-aerated region of stepped spillways, experimental and numerical data presented in this dissertation allowed to state the following conclusions:

- For steep slopes, the friction factor was observed to depend on the steps macro-roughness (characterized by the roughness height perpendicular to the pseudo-bottom) and on the geometry of the cross-section (characterized by the hydraulic radius), in agreement with the studies of Gioia and Bombardelli (2002), who derived the Manning's empirical formula based on the phenomenological theory of turbulence, and of Bombardelli and Garcia (2003), focused on the flow resistance of large-diameter pipes. Contrarily, Amador et al. (2006) suggested a constant friction factor, according to their experiments acquired in more limited conditions.

- For steep slopes, Manning's *n* or *roughness coefficient* was observed to increase with roughness, as observed in other wall flows. The use of Manning's *n* to characterize the flow resistance of stepped spillway flows is made after Gioia and Bombardelli's derivation of the Manning's empirical formula, which allows the use of Manning's formula for wider situations than the one presented by Manning in his original study.

- The normalized turbulent kinetic energy ($k/u_{max}^{\ 2}$, where k is the turbulent kinetic energy and u_{max} is the free stream velocity) and its dissipation ($\varepsilon\,\delta/u_{max}^{\ 3}$, where ε is the turbulent kinetic energy dissipation and δ is the boundary layer thickness) were observed to be self-similar for roughness Reynolds numbers up to 6.8×10^4, in steep slopes. This self-similarity is in accordance with the findings of Nezu and Nakagawa (1993) and Nikora and Smart (1997) for fully developed open channel flows and gravel bed river flows, respectively.

- The rate of energy dissipation, for both steep and moderate slope stepped channels, was observed to be small, which is in agreement with the values obtained by Hunt and Kadavy (2010) for the rate of energy dissipation in moderate slope stepped spillways.

- Time-averaged local air concentration values between 0 and 1 are observed to pertain to entrapped air captured between water waves in the contorted free-surface, as already observed by Matos (2000). However, near the time-averaged inception point, or simply inception point, *C* also denotes the presence of air bubbles inside the flow (entrained air), due to the difference between instantaneous and time-averaged inception point location.

- From the observation of the characteristics of several stepped spillways, it was observed that in small dams and/or spillways with high specific discharges the non-aerated region can occupy a large extension or the entire spillway. Although this is not *per si* a conclusion from the developed

investigation, it explains the motivation and main incidence of the study on the non-aerated region of stepped spillways.

The experimental and numerical results presented in this dissertation pertaining to the non-aerated region of stepped spillways permitted also to present the following novel contributions:

- For steep slopes, expressions are proposed to estimate the equivalent clear-water depth; boundary layer thickness; mean air concentration; kinetic energy coefficient; energy dissipation; friction factor; Manning's n; and the self-similarities of the normalized turbulent kinetic energy and its dissipation. Values for the exponent $1/N$ of the self-similar velocity distribution are also presented.

- For moderate slopes, expressions are proposed to estimate the equivalent clear-water depth, kinetic energy coefficient, and residual specific energy. Values for the exponent $1/N$ of the self-similar velocity distribution are also presented.

Regarding the inception point of air entrainment, experimental and numerical data presented in this dissertation allowed to present the following conclusions and novel contributions:

- Although different methodologies have been used to determine the inception point, some theoretically more accurate than others, due to the undulation of the free-surface and unsteadiness of the boundary layer thickness the results of the time-averaged inception point location present some scatter. Nevertheless, in general, it was observed that: i) L_i is higher when obtained from the balance between stabilizing and disturbing forces than from the intersection between the equivalent clear-water depth and the boundary layer thickness, which is in accordance with the literature for smooth channels; ii) visual observation returned up to 30% higher L_i than from the intersection between clear water depth and boundary layer thickness; iii) an overall proximity between results obtained considering different methodologies is observed.

- Different expressions are proposed to characterize the inception point of air entrainment in terms of location and equivalent clear-water depth for moderate and steep slopes, respectively. For steep slopes, a value of the mean air concentration is also suggested.

Focused on the aerated region of steep stepped channels, experimental data presented in this dissertation allowed to present the following conclusions and novel contributions:

- The mean air concentration and the bulked depth may be significantly influenced by the definition of the free-surface, contrarily to what happens with the clear-water depth.

- Empirical models were developed for estimating the maximum flow bulking as a function of the normalized critical depth.

Focused on a basin designed based on the recommendations for the design of USBR type III basins located downstream of a steep stepped channel, the experimental data presented in this dissertation allowed to present the following conclusions:

- At the entrance of the basin, the pressure head is much higher than both the flow depth and the respective hydrostatic pressure, as already observed by Meireles (2004) and Meireles et al. (2005) at the entrance of the type I stilling basin downstream of the same steep stepped channel.

- The proximity between flow depth profiles in the studied basin and a USBR type III basin located downstream of conventional spillways is acceptable.

- The pressure head profiles at the entrance of the basin show considerably larger values than those suggested by Peterka (1958) for USBR type III basins.

- As between USBR type I and III basins located downstream of conventional spillways, the hydraulic jump stabilizes much faster than in the type I basin downstream of a stepped channel of equal characteristics.

- The chute blocks located in the upstream end of the basin are observed to have negligible effect in the flow, possibly because the configuration of the steps along the chute already helps in the mixing of the flow, one of the main reasons for the existence of chute blocks in USBR type III basins, according to Peterka (1958).

At last, focused on the non-aerated region of steep stepped chutes, data obtained from a proposed 1D theoretical model of the main flow, derived directly from the Navier-Stokes equations, and presented in this dissertation, allowed to present the following conclusions:

- The proximity with experimental data indicates that the assumptions and simplifications considered in the model are adequate.

- Although capturing the overall behavior of the free-surface profile, the steady waves observed in both experiments and numerical simulations are not captured by the model.

In conclusion, this dissertation aims at providing an additional comprehension of the hydraulic characteristics of rough flows, specifically in stepped channels, and stepped spillways in particular. Empirical and theoretical expressions are intended to provide some assistance in the design of stepped spillways. The results presented in this dissertation are also an indication that numerical models can be used in order to improve the understanding of the skimming flow on stepped spillways, in general, or to help in practical specific cases. In fact, numerical methods start to provide practicing engineers with a complementary tool which can be used to help in the design, re-analysis and rehabilitation of stepped spillways, before performing physical model studies. This tool may be very useful in the re-evaluation of a dam spillway capacity for higher flows, for instance. At last, the proposed theoretical model shows that these type of flows, even if complex, can be characterized, until a certain extent, by theoretical approaches and not only by empirical expressions.

7.2 SUGGESTIONS FOR FUTURE RESEARCH

One of the main objectives of this Ph.D. dissertation was to study the hydraulics of skimming flow over stepped spillways from experimental observation. Although intense experimental investigation focused on stepped spillways has been performed in the last decades, the experimental facility of LNEC still has potential for future research, namely with the study of:

- converging stepped spillways;

- different crest configurations (e.g., labyrinth weir; gates) upstream of stepped spillway;

- energy dissipators downstream of stepped spillways;

- inception point characterization;

- turbulence statistics characterization of the skimming flow.

Future research should also be focused in the complementary numerical and theoretical investigations. In fact, although the results of this Ph.D. dissertation suggest that the theoretical model and the numerical integration used in the numerical simulations and the assumptions considered to the development of the presented theoretical model based in the Navier-Stokes equations are adequate for the non-aerated region of the skimming flow down stepped spillways, possible future research projects embrace the study of two-phase flow theories to include in the theoretical model; and LES (large eddy simulations).

REFERENCES

Amador, A., Sanchez-Juni, M., Dolz, J. (2006). “Characterization of the non-aerated flow region in a stepped spillway by PIV.” J. Fluid Eng., ASME, 138(6), 1266-1273.

Bombardelli, F. A. and García, M. H. (2003). “Hydraulic design of large-diameter pipes.” J. Hydr. Eng., ASCE, 129(11), 839-846.

Gioia, G., and Bombardelli, F. A. (2002). “Scaling and similarity in rough channel flows.” Phys. Rev. Lett., 88(1), 014501.

Hunt, S. L., and Kadavy, K. C. (2010). “Energy dissipation on flat-sloped stepped spillways: part 1. upstream of the inception point.” Transactions, ASABE, 53(1), 103-109.

Matos, J. (2000). “Hydraulic Design of Stepped Spillways over RCC Dams.” Proc. 1st Int. Workshop on Hydraulics of Stepped Spillway, Zurich, Switzerland, A. A. Balkema Publisher, Rotterdam, The Netherlands, 187-194.

Meireles, I., Matos, J., and Melo, J. F. (2005). "Pressure head and residual energy in skimming flow on steeply sloping stepped spillways." Proc. 31th IAHR Congress, Theme D, 2654-2663, Seoul, South Korea. (In CD.)

Meireles, M. (2004). “Emulsionamento de ar e dissipação de energia do escoamento em descarregadores em degraus.” M.Sc. thesis, IST, Lisbon, Portugal (in Portuguese).

Nezu, I., and Nakagawa, H., (1993). “Turbulence in open-channel flows.” AA Balkema, Rotterdam, The Netherlands.

Nikora V. and Smart G. M. (1997). "Turbulence characteristics of New Zealand gravel-bed rivers.", J. Hydr. Eng., 123(9), 764-773.

Peterka, A. J. (1958). "Hydraulic design of stilling basins and energy dissipators" in Engineering Monograph Nr. 25, 8th Edition, U.S. Department of the Interior, Water and Power Resources Service, Denver, USA.

Appendix

A.1 PREDICTION OF THE ASYMPTOTIC WATER DEPTH IN ROUGH COMPOUND CHANNELS

Appendix A.1 was published in the Journal of Irrigation and Drainage Engineering in April 2009. The authors are B. A. Younis, V. Sousa and I. Meireles.

This paper was developed in the framework of the course *Computational River Mechanics* of Prof. Bassam Younis, at UCDavis, USA, during the academic year 2007/2008, and concerns to the computation of the asymptotic water depth in rough compound channels by one dimensional approaches. Such approaches, which are widely used in practice, utilize one of a number of well-established methods for estimating the equivalent composite/compound roughness. It was found that many of these methods yield predictions of the asymptotic water depth which erroneously depend on the initial, control, depth. Only one of the methods examined was found not to exhibit this unsatisfactory behavior. The results are explained by analysis of the governing equations.

Prediction of the Asymptotic Water Depth in Rough Compound Channels

B. A. Younis[1]; V. Sousa[2]; and I. Meireles[3]

Abstract: We report on a curious result related to the computation of the asymptotic depth in rough compound channels by one-dimensional approaches. Such approaches, which are widely used in practice, utilize one of a number of well-established methods for estimating the equivalent composite/compound roughness. It was found that many of these methods yield predictions of the asymptotic water depth which erroneously depend on the initial, control, depth. Only one of the methods examined was found not to exhibit this unsatisfactory behavior. We explain the results by analysis of the governing equations.

DOI: 10.1061/(ASCE)0733-9437(2009)135:2(231)

CE Database subject headings: Open channel flow; Gradually varied flow; Roughness; Flood plains.

Introduction

A channel where the wall roughness is not constant along the wetted perimeter is referred to as a composite channel while a compound channel is one whose cross section is composed of several subsections which may be of different shape. When the wall roughness is not constant along the compound channel it is, in fact, a compound-composite channel. The most common example of a compound channel in nature is that of a river where the flow is usually confined to the main channel, except in flood events when it overflows over adjacent floodplains. In this case it is usual for the roughness to vary along the section perimeter.

We are concerned here with the computation of the asymptotic water depth attained in the subcritical flow in a long, straight, compound channel far upstream of a given control depth. Fig. 1 shows a representative cross section of the geometry under consideration and also defines the test problem used to illustrate the analysis. The dimensions and flow conditions are the same as those studied experimentally by Atabay (2001).

The conventional approach to predicting the variation of water depth in a channel when this is different from the asymptotic (normal) depth is to treat the flow as being one-dimensional and then solve the St. Venant equations or, if the flow is steady and the rate of change of depth with flow direction is small, the equations for gradually varied flows. In compound and/or composite channels, to maintain the one-dimensional character of the equations, an equivalent composite/compound value of Manning's n (n_c) is used. This parameter is obtained by appropriate aggregation of the values of the Manning's n for each subsection over the flow area (A), the wetted perimeter (P), and the hydraulic radius (R). Several alternative formulas for achieving this have been reported in the literature and are in use today in engineering applications. A review of the main proposals was conducted by Chow (1959) and, more recently, by Yen (1991, 2002) who made a further proposal for estimating n_c. The differences between these proposals stem from the assumptions made in order to relate the total value of a particular parameter (e.g., the friction slope S_f) to the sum of its constituents. In all cases, however, the result of the aggregation is a unique value for n_c which may be a function of flow depth even when the values of n for the various subsections are uniform. Among the widely used formulas for composite channels are those of Pavlovskii (1931), Lotter (1933), Einstein and Banks (1950), and Cox (1973). These divide the channel by subsections according to the different roughness along the channel perimeter (roughness division). In compound channels, the channel is normally divided in subsections of different geometry (geometrical division) and the total discharge is obtained by summing the discharges in each subsection (Chow 1959). Several options to divide the cross section into subsections have been suggested (Yen 2002), the most usual one being the vertical division shown in Fig. 1.

Yen (1991, 2002) has argued that composite and compound channels can be treated similarly. Consequently, it is common practice to consider the equations for composite channel as also applicable to compound channels. The writers show here that, in many of the alternative proposals, this feature produces results in the prediction of an asymptotic depth that is different from the normal depth. This is incorrect as there can only be a unique asymptotic depth, whose value is independent of the initial, control depth. While several previous studies have reported on the possibility that critical flow in a compound channel may occur at more than one depth (Petryk and Grant 1978; Blalock and Sturm 1981; Chaudhry and Bhallamudi 1988; Lee et al. 2002), experiments (Myers and Brennan 1990; Knight 1992; Knight and Brown 2001; Atabay 2001) show that, for a given discharge, there can be only a single, unique value for the normal depth. Smart (1992) reported the observation of two normal depths in a compound channel with a narrow, deep central section and wide rough floodplains but these are not the conditions of interest here.

[1]Professor, Dept. of Civil and Environmental Engineering, Univ. of California–Davis, Davis, CA 95616 (corresponding author). E-mail: bayounis@ucdavis.edu

[2]Ph.D. Student, Dept. of Civil Engineering and Architecture, Instituto Superior Técnico, Technical Univ. of Lisbon, Av. Rovisco Pais, 1049-001 Lisbon, Portugal.

[3]Ph.D. Student, Dept. de Engenharia Civil, Univ. de Aveiro, Campos Universitário de Santiago, 3810-193 Aveiro, Portugal.

Note. Discussion open until September 1, 2009. Separate discussions must be submitted for individual papers. The manuscript for this paper was submitted for review and possible publication on February 9, 2008; approved on September 2, 2008. This paper is part of the ***Journal of Irrigation and Drainage Engineering***, Vol. 135, No. 2, April 1, 2009. ©ASCE, ISSN 0733-9437/2009/2-231–234/$25.00.

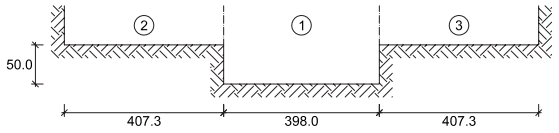

Fig. 1. Channel cross section (dimensions in mm)

Analysis

To illustrate the problem, the writers consider the case of flow in the compound channel studied experimentally by Atabay (2001) and which is depicted in Fig. 1. The roughness was uniform over the main channel and the floodplains with $n=0.0092$. The flow rate was $Q=8.92$ L/s and the longitudinal slope $S_0=0.002024$.

The normal depth, calculated from the iterative solution of Manning's equation, is $y_n=42.74$ mm. This compares favorably with the measured value of 42.83 mm. Thus, for the given conditions, the entire flow is contained within the main channel and the water depth, if displaced from this value at a particular location, will revert to this depth sufficiently far upstream from that location.

The flow is assumed to be steady and the water depth (y) is obtainable from the solution of the equations for gradually varied flows

$$\frac{dy}{dx}=\frac{S_0-S_f}{1-\dfrac{Q^2}{gA^3}\dfrac{dA}{dy}} \tag{1}$$

with

$$S_f=\left(\frac{Q}{K}\right)^2 \tag{2}$$

$$K=\frac{c_m}{n_c}AR^{2/3} \tag{3}$$

where K=channel conveyance; and c_m=units conversion constant.

The composite/compound n_c is determined using the following formulas:

1. Pavlovskii (1931). The assumption underlying this method is that the total resistance force is equal to the sum of subarea resistance forces. The method was initially proposed for use in composite channels and has the following form:

$$n_c=\left(\frac{1}{P}\sum_{i=1}^{N}P_i n_i^2\right)^{1/2} \tag{4}$$

2. Lotter (1933). This is based on the assumptions that the friction slope is the same for all the subsections and the total discharge equals the sum of the constituent discharges. It was first proposed as a formula for composite channels, but if the geometrical division matches the roughness division, which is usual in channels with floodplains, it is equivalent to the procedure presented by Chow (1959) for compound channels. The method gives

$$n_c=PR^{5/3}\left(\sum_{i=1}^{N}\frac{P_iR_i^{5/3}}{n_i}\right)^{-1}=AR^{5/3}\left(\sum_{i=1}^{N}\frac{A_iR_i^{5/3}}{n_i}\right)^{-1} \tag{5}$$

3. Einstein and Banks (1950). Here, it is assumed that the friction slope is the same for all the subsections and the velocities are equal in all subsections. This method was intended for use for composite channels, and has the following form:

$$n_c=\left(\frac{1}{P}\sum_{i=1}^{N}P_i n_i^{3/2}\right)^{2/3} \tag{6}$$

4. Cox (1973). This assumes that the total shear force equals the sum of the constituent subsection shear forces and the friction slope is the same for all subsections. Moreover, the subsection velocities are assumed to vary in proportion to the depth to a one sixth power law. This method was originally proposed for composite channels and has the following form:

$$n_c=\frac{1}{A}\sum_{i=1}^{N}A_i n_i \tag{7}$$

5. Yen (1991). This assumes that the total shear velocity is the weighted sum of subarea shear velocities. This method was proposed to be used in composite/compound channels and has the following form:

$$n_c=\frac{1}{PR^{1/3}}\sum_{i=1}^{N}P_iR_i^{1/3}n_i \tag{8}$$

The methods listed above were applied to the compound-channel problem of Fig. 1 for the values of flow rate, slope, and Manning's n given above. The solution of Eqs. (1)–(3) was achieved iteratively, using the Newton–Raphson method. Values of the step size Δx were chosen to ensure that the results are independent of the step size. Results were obtained for two values for the control depth (which was specified at $x=0$) viz. 60 and 38 mm corresponding to overbank and in-bank flows. The resulting plots of the variation of the water depth with upstream distance are presented in Fig. 2. In this figure, h is the depth of the main channel.

It is evident from this figure that all the methods tested, except that of Lotter, yield two different asymptotic values for the water depth depending on whether the initial, control depth was located above or below the banks of the floodplains. The Lotter method yields a unique asymptotic depth which corresponds exactly to the correct value of the normal depth for the given flow rate. The other methods also asymptote to the correct value provided that the initial depth is located below the banks.

The predicted stage-discharge relations close to the junction between the main channel and the floodplains obtained with the different methods are presented in Fig. 3. It can be seen that, except for the Lotter method, there exists a range of discharge values where the other methods for composite roughness yield two different asymptotic water depths for the same value of Q with one being below the bankfull depth and the other above it.

This anomalous behavior can be explained as follows. In a compound channel, R is not a single-valued function of y but rather increases in the main channel, decreases sharply on transition over the floodplains, and increases monotonically thereafter. In contrast, the flow area A varies monotonically with y. Thus, for a certain range of values of $AR^{2/3}$ (in this particular example, this range is $0.5<AR^{2/3}/(A_{\mathrm{BF}}R_{\mathrm{BF}}^{2/3})<1.0$ where BF refers to bankfull), the same value of $AR^{2/3}$ is associated with two different depths—one above the bankfull depth and the other below it. This can be seen from Fig. 4. When the control depth is greater than the bankfull depth (as indicated by the circle in Fig. 4), the iterative solution of Eq. (1) proceeds along the path shown with the flow

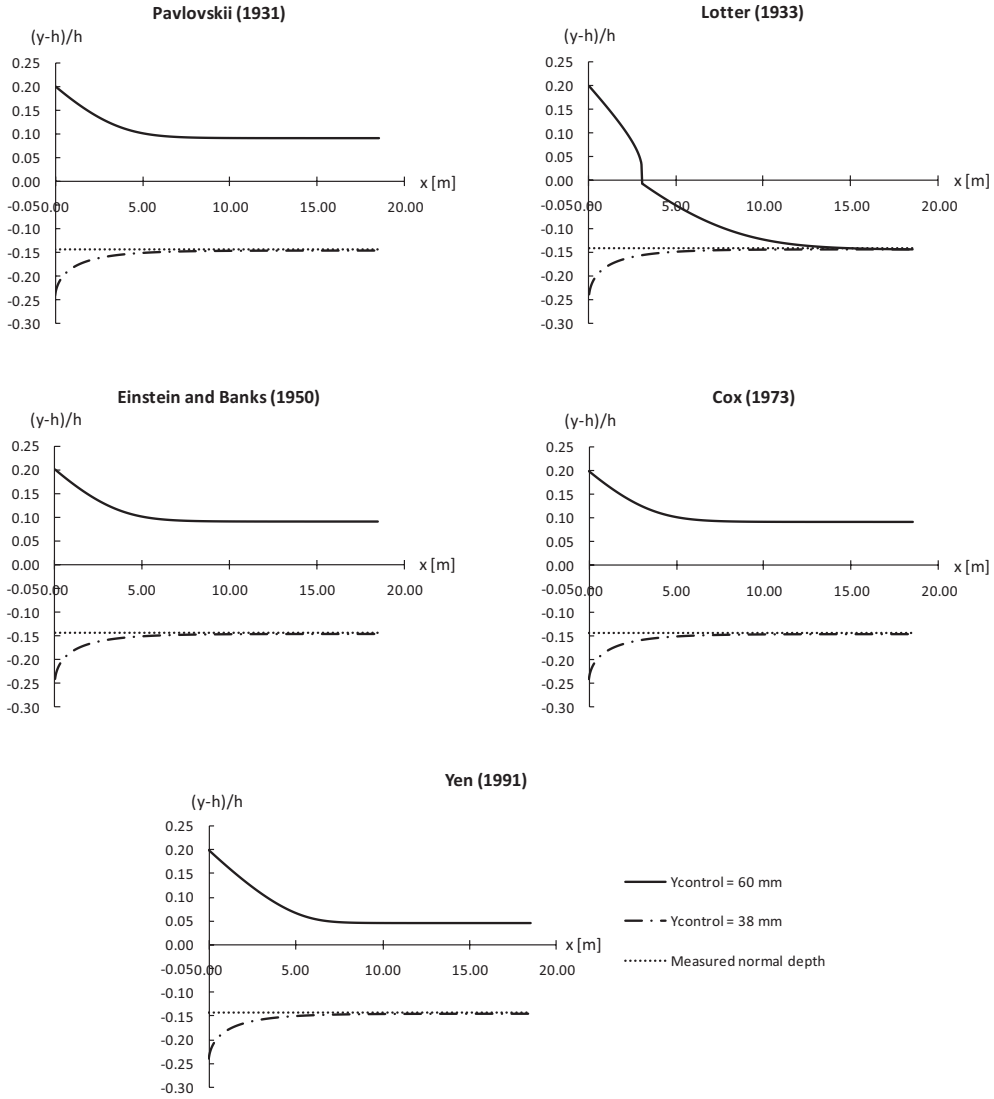

Fig. 2. Actual and normal water depths calculated with different methods

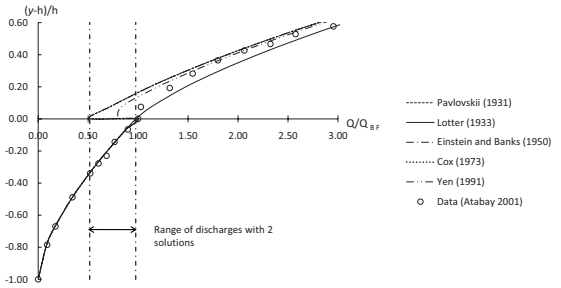

Fig. 3. Stage-discharge predictions

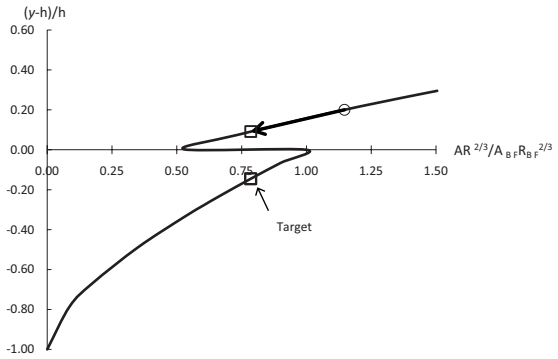

Fig. 4. Variation of $AR^{2/3}$ with depth

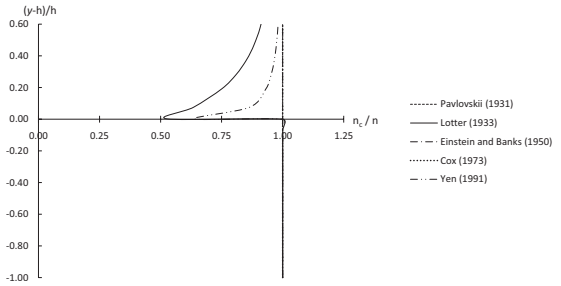

Fig. 5. Variation of n_c/n with depth

depth decreasing and with it both A and R. Eventually, the "correct" value of $AR^{2/3}$ is reached but with a flow depth which is greater than the asymptotic value. It is here that the ratio of $AR^{2/3}$ to n_c [i.e., the channel conveyance K of Eq. (3)] comes into play. If the method for composite/compound roughness does not allow for the variation of n_c with depth, then the ratio of $AR^{2/3}$ to n_c satisfies Manning's equation for the given slope and flow rate. When this occurs, S_f becomes identically equal to S_0. It then follows from Eq. (1) that dy/dx becomes zero and an erroneous asymptotic depth would thus be obtained. Fig. 5 shows the different methods' results for the variation of n_c/n with depth. The Lotter method obtains the greatest reduction in n_c with depth such that equilibrium is not reached at values of the water depth above bankfull and the integration is continued until the correct asymptotic depth is obtained. Interestingly, the shapes of the curves R/R_{BF} and n_c/n obtained with this method are very closely correlated as can be seen from Figs. 4 and 5. The method of Yen (1991) also obtains a reduction with depth, albeit to a much lesser extent than Lotter's. Not surprisingly, therefore, the Yen method returns an asymptotic depth which lies in between the correct value obtained by Lotter and those of the others.

Closure

When applied to compound channels, various methods for estimating the composite/compound value of Manning's n yield two values for the asymptotic depth: one located above the floodplain and another below. Since the correct asymptotic depth is the normal depth, which is unique for a given discharge in a wide compound channel with uniform roughness, one of the solutions obtained is in error. This is attributed here to the fact that some of these methods, when used for compound channels where n has the same value in the main channel and floodplains, yield either a small or no variation of n_c with depth. This result, coupled with the fact that $AR^{2/3}$ is a not single-valued function of depth, means that the asymptotic value of $AR^{2/3}$ can be obtained with the incorrect depth. Of the methods tested, only that of Lotter obtains a variation in n_c with depth which is sufficient to continue the integration until the correct value of the asymptotic water depth is obtained. Here, we do not make the claim that the Lotter method for determining composite roughness is superior to any of the others but merely that, for the conditions examined, it alone yielded the correct asymptotic depth irrespective of the starting conditions.

Acknowledgments

V. S. thankfully acknowledges the support of the ICIST Research Institute from IST, Technical University of Lisbon and of FCT (Foundation for Science and Technology). L. M. thanks the Fulbright Commission for the award of a Fulbright/FLAD research grant.

Notation

The following symbols are used in this paper:

A = flow area;
h = depth of main channel;
K = channel conveyance;
n, n_c = Manning's n, composite/compound n;
P = wetted perimeter;
Q = flow rate;
R = hydraulic radius;
S_0, S_f = channel slope, friction slope;
x = coordinate in flow direction; and
y, y_n = actual flow depth, normal depth.

References

Atabay, S. (2001). "Stage-discharge, resistance and sediment transport relationships for flow in straight compound channels." Ph.D. thesis, The Univ. of Birmingham, Birmingham, U.K.

Blalock, M. E., and Sturm, T. W. (1981). "Minimum specific energy in compound channel." *J. Hydr. Div.*, 107(6), 699–717.

Chaudhry, M. H., and Bhallamudi, S. M. (1988). "Computation of critical depth in compound channels." *J. Hydraul. Res.*, 26(4), 377–395.

Chow, V. T. (1959). *Open-channel hydraulics*, McGraw-Hill, New York.

Cox, R. G. (1973). "Effective hydraulic roughness for channels having bed roughness different from bank roughness." *Misc. Paper H-73–2*, U.S. Army Corps of Engineers Waterways Experiment Station, Vicksburg, Miss.

Einstein, H. A., and Banks, R. B. (1950). "Fluid resistance of composite roughness." *Trans., Am. Geophys. Union*, 31(4), 603–610.

Knight, D., ed. (1992). "SERC flood channel facility: Experimental data—Phase A." *Rep. No. SR 314*. HR Wallingford, Wallingford, U.K.

Knight, D., and Brown, F. (2001). "Resistance studies of overbank flow in rivers with sediment using the flood channel facility." *J. Hydraul. Res.*, 39(3), 283–301.

Lee, P., Lambert, M., and Simpson, A. (2002). "Critical depth prediction in straight compound channels." *Proc. Institution of Civil Engineers, Water Management*, 154(4), 317–332.

Lotter, G. K. (1933). "Considerations on hydraulic design of channels with different roughness of walls." *Transactions, All-Union Scientific Research Institute of Hydraulic Engineering, Leningrad*, 9, 238–241.

Myers, W., and Brennan, E. (1990). "Flow resistance in compound channels." *J. Hydraul. Res.*, 28(1), 141–155.

Pavlovskii, N. N. (1931). "On a design formula for uniform flow in channels with non-homogeneous walls." *Transactions, All-Union Scientific Research Institute of Hydraulic Engineering, Leningrad*, 3, 157–164.

Petryk, S., and Grant, E. (1978). "Critical flow in rivers with flood plains." *J. Hydr. Div.*, 104(5), 583–594.

Smart, G. (1992). "Stage-discharge discontinuity in composite flood channels." *J. Hydraul. Res.*, 30(6), 817–833.

Yen, B., ed. (1991). *Channel flow resistance: Centennial of Manning's formula*, Water Resource Publications, Highlands Ranch, Colo.

Yen, B. (2002). "Open channel flow resistance." *J. Hydraul. Eng.*, 128(1), 20–39.